Development and application of linked hydrodynamic-water quality models for small lakes, reservoirs, and tidal inlets

by

V. Chandy John

A Thesis Submitted to the
Faculty of Engineering
in Partial Fulfilment of the Requirements
for the Degree of

DOCTOR OF PHILOSOPHY

Major Subject: Civil Engineering

TECHNICAL UNIVERSITY OF NOVA SCOTIA

Halifax, Nova Scotia

1996

DEDICATION

in memory of my parents for their encouragement, inspiration, and support.

TABLE OF CONTENTS

LIST OF TABLES

LIST OF FIGURES

LIST OF SYMBOLS AND ABBREVIATIONS

V	lake's volume
C	concentration of the substance.
$W(t)$	rate of mass loading
Q	rate of flow of water through the volume
k	reaction coefficient
t	time
S	sources or sinks of a substance within the lake.
$U(t)$	a unit step function
C_p	pollutant concentration in the lake
Θ	phase shift (radians or degrees).
t_m	time of occurrence of the peak or maximum loading
ω	frequency of the oscillation
T_p	period of time over which a complete oscillation occurs
x, y	horizontal co-ordinates
Z	upward displacement of the free surface from a mean water level;
H	depth of the basin from mean water level
b	segment width
B	bottom stress coefficient;
f	Coriolis parameter
ω	angular velocity of the earth's rotation
ϕ	latitude;
g	gravitational acceleration;
τ_s	wind stress at the surface
C_D	drag coefficient
W	wind velocity
ρ_a	density of the air
ρ	density of water

DS	space step
H_{max}	maximum lake depth
B_{max}	maximum bottom stress coefficient
R	hydraulic radius
n	Manning roughness coefficient
A	cross-sectional area
L_i	length of segment i;
y_i	mean depth of segment i
U_i	velocity in segment i
Δt	computational time step
u,v, and w	components of currents in the x,y, and z directions,;
ζ (x,y,t)	height of the free surface above the xy-plane
N (x,y,z)	vertical eddy viscosity;
P_a	atmospheric pressure
P	fluid pressure.
γ	dimensionless drag coefficient.
V_i	phase of the equilibrium constituent i at Greenwich at t=o,
σ_i	speed of constituent i ,
C	concentration of the water quality constituent
E_x, E_y, E_z	longitudinal, lateral, and vertical diffusion coefficients
S_L	direct and diffused loading rate
S_B	boundary loading rate
S_K	total kinetic transformation rate.
S^T	total source/sink rate
Q	volumetric flow
V_j	volume of segment j
R	dispersive flow
L_c	characteristic length.

υ	numerical weighing factor (advection factor)
$P_i(t)$	precipitation velocity time function for segment i
A_i	surface area of segment i
$C_{oi}(t)$	concentration of pollutant in precipitation.
$E_i(t)$	evaporation velocity time function for segment i
$\omega 1$	settling velocity, m sec-1
V	cell volume, m^3
C_2	suspended solids concentration, g m^{-3}
K_c	death rate, sec^{-1}

ACKNOWLEDGMENTS

The author wishes to express his sincere appreciation and gratitude to Dr. D.H. Waller and Dr. M.G. Satish for their guidance, support and continued interest throughout the duration of this research. The author also extends his sincere appreciation to the other members of the guiding committee, Drs. M. Rahman and Jim Warner, for their valuable help and assistance.

Thanks are due also to Dr. Charles Rowney whose advice was instrumental during the initial stages of this thesis. Jean Heroux awarded a contract to develop a hydrodynamic and water quality model for a tidal inlet (Parr Inlet, NWT) during the first year of this research that laid the foundation of this research work. The author also wishes to express his gratitude to Rick Scott, Mark King, and Gordon Balcombe for their help in the field investigations. I thank also my family for their support.

The author gained considerable knowledge and experience on this thesis topic during 1986 to 1991 while working at King Fahd University of Petroleum and Minerals Research Institute, Saudi Arabia, as an Oceanographic Program Leader in the Environmental Monitoring and Modelling Program of the Arabian Gulf. He also obtained valuable modelling practical experience at SNC-Lavalin during 1991 to 1996 in several receiving water pollution control projects by application of hydrodynamic and water quality models as an environmental assessment tool. I am thankful to both these organizations for giving me the opportunity to work on these environmental protection projects.

Finally, the author gratefully acknowledges the financial assistance provided through TUNS graduate scholarship, 1990 Fund scholarship and teaching assistantships and through NSERC research funds allocated to Dr. D.H. Waller and Dr. M.G. Satish.

ABSTRACT

The main objective of this research is the development and application of a linked hydrodynamic-water quality model that can simulate the unique characteristics of small lakes, reservoirs, and tidal inlets and to study the mixing and transport of piped wastewater discharges. These discharges have been a major area of concern in recent years and government regulations and guidelines are in place for compliance monitoring and environmental effects monitoring. There are hardly any existing models that address the unique hydrodynamics and water quality processes in small lakes and reservoirs both in the near and far field. Two and three-dimensional linked hydrodynamic-water quality models developed in this thesis form a useful management tool for environmental impact assessment, evaluation of effluent treatment strategy, and optimum outfall siting. In addition, these models are also useful for study of sediment transport and coastal erosion, design of offshore and coastal structures, and the management of harbour operations.

This thesis describes the hydrodynamic and water quality model formulations, and documents the equations and assumptions underlying the model development. The hydrodynamic model simulates the circulation in the water body and the water quality model mimics the constituent water quality variations such as dye, bacterial, and suspended solids concentrations. These models developed were applied to simulate advective and diffusive transports of conservative and non-conservative pollutants in a typical small lake, such as, Long Lake (Nova Scotia) and a typical small tidal inlet, such as, Parr Inlet (North West Territories).

Long Lake has a complicated coastal configuration, and seven major streams of noticeably different water quality, empty into this lake. Many of these streams are on opposite sides of the lake and lateral averaging would combine them and therefore water quality changes will not be properly represented. Preliminary field measurements and initial simulations showed that wind driven currents have a major influence in small water bodies. Water quality measurements in Long Lake show effects of significant reduction in currents

with depth. The need for better representation of the vertical structure of wind driven currents and advancement of personal computers resulted in the development of a fully non-linear three dimensional hydrodynamic model. This model mimics the unique characteristics of small lakes, reservoirs and tidal inlets and uses an alternating direction implicit scheme and vertically varying eddy viscosity (VVEV) scheme to compute vertical profiles of currents. This personal computer based three-dimensional model provides a computationally feasible and reasonably accurate alternative to other layered three-dimensional models.

The three-dimensional hydrodynamic model developed is computationally intensive and takes one hour of real time for simulation of 6 hours of model time on a 486 DX2-100 personal computer. Therefore, a two-dimensional depth averaged segment-node model was developed for long term simulations (several months to one year). This model runs much faster on a the above mentioned personal computer and requires one hour of real time for simulation of two months of model time.

The main mass transport in Long Lake is due to wind, and the circulation caused by stream inflow/outflow contributes to a relatively small fraction of the total mass transport. The linked hydrodynamic-water quality model responses were studied for generation of currents, seiches, wind set up, and to contaminant loading. Both theoretical and experimental methods were used to evaluate the reliability of these models in predicting the hydrodynamics and water quality behavior. The theoretical methods developed were validated using both comparisons with analytical solutions (impulse, step and sinusoidal loading), and the experimental data gathered from the field. Drogue, water level, and water quality measurements were made at several locations in Long Lake as part of the experimental program. The linked hydrodynamic-water quality model was applied to Long Lake and Parr Inlet and the results of the simulations of water level/tidal elevations, streamflow/tidal/wind driven currents, and water quality variations are presented.

Chapter 1

INTRODUCTION

1.1 General

The numerical modelling of physical and bio-chemical processes in lakes, reservoirs, and tidal inlets has advanced significantly over the last decade due to the rapid development in the computer industry. This has resulted in considerable improvement in hydrodynamic and water quality modelling in surface waters. Development of computer technology has minimized most computational constraints and there is an increasing emphasis on principles of modelling, and accuracy of numerical schemes. This has enabled one to use more realistic model structures and model calibration/verification procedures. These models are built upon hydrodynamic, thermodynamic, and water quality/reaction principles as expressed by appropriate mathematical equations. One can get more insight into these processes from the analytical solutions of these equations. Generally, one can attempt quantitative simulation of the relatively complicated processes observed in nature only by numerical methods.

One may use water quality models to describe present water quality conditions, and to provide generic and site-specific predictions. Monitoring of physical and bio-chemical parameters in lakes, reservoirs, and tidal inlets is expensive and therefore, these measurements seldom have the spatial and temporal resolution needed to fully characterize the water body. A water quality simulation model can be used to interpolate between

observed data and can be used to guide future monitoring efforts. Descriptive models can also be used to infer the important processes controlling the present water quality, and to guide monitoring and model development efforts.

Providing generic predictions is another type of modelling task. Site-specific data may not be needed if the goal is to predict the types of water bodies at risk from a new chemical. A crude set of data may be adequate to screen a list of chemicals for potential risk to a particular water body. Generic predictions may sufficiently address the management problem to be solved, or they may be a preliminary step that will lead to a more detailed site-specific analysis.

The modelling work undertaken in this research provides site-specific prediction that is the most rigorous modelling task and includes model calibrations with a reliable set of monitoring data to provide credible predictions. These models developed can be used to extrapolate beyond the available data base and can be used in waste load allocation to protect water quality and to conduct feasibility analysis for remedial actions.

1.2 Outline of Present Research

As indicated by Waller et al. (1983), mathematical modelling of water quantity and quality is an integral part of the Halifax Urban Watershed Program (HUWP). This study was undertaken since the existing hydrodynamic/water quality models do not adequately represent the dynamics of small lakes, reservoirs, and tidal inlets. This thesis also stresses

the objectives of mathematical modelling under the umbrella of this program as the "systematic representation and understanding of the system behaviour; identification of data needs for model calibration, verification, and application; evaluation of model capability and limitations; and applications that might predict potential consequences of watershed management alternatives." The objectives of this research falls well within the scope of this broad objective of the HUWP.

The main objective of this research is to develop and validate a linked hydrodynamic-water quality model that is capable of simulating the unique characteristics of small lakes, reservoirs and tidal inlets described below:

- quick response to wind speed and direction changes and since wind driven currents decrease rapidly with depth a 3-D circulation model is required.
- water level variations are important for mass balance (ie. model should be very sensitive to water level changes and mimic seiches and wind setup)
- lateral boundaries, bottom topography, and bed roughness are important in circulation.
- near and far-field hydrodynamics are important.

Specific objectives of this research are:

- to study physical processes affecting water quality variations in small lakes, reservoirs, and tidal inlets and obtain model input data;
- to measure circulation patterns in Long Lake due to through flow and wind forcing;
- to measure variation of stratification and water quality in Long Lake;
- to develop a hydrodynamic model that represents unique near and far-filed characteristics of small lakes, reservoirs, and tidal inlets;
- to develop a water quality model that represents unique characteristics of small lakes, reservoirs, and tidal inlets;
- to study dispersion of contaminant plumes;
- to do sensitivity analysis, calibration and verification of the hydrodynamic and water quality models;
- to identify and discuss capabilities and weaknesses of models developed; and
- to optimize the computer source code to economically run on a micro computer, thus providing a broader use since most existing models are written for large mainframe computers and are expensive to run.

The fundamental physical laws and corresponding mathematical equations governing the motions of the lake waters and other physical parameters are discussed in this thesis. In principle, the problem is solved by numerical solution of the hydrodynamical differential

equations, once certain numerical problems such as computational instability and truncation errors have been considered. Since the problem of computing the water circulation of surface waters is a boundary-initial value problem, the models developed require a specification of the boundary conditions, shoreline configuration, depth, and initial values of the flow parameters. However, much of the behaviour of the lake is a direct consequence of external forces such as the wind stress which reduces the effect of the initial conditions. The mass circulation of the lake is mainly governed by the topography of the basin.

A common first step in hydrodynamic model development is a homogenous model where the lake is represented by one layer of fluid of constant temperature and density. Such models have been used to study the wind driven circulation and storm surge problems in the ocean and Great Lakes. In several hydrodynamic models of Great Lakes, the surface displacements may not be of interest since their effects on the internal mass distributions are unimportant. Thus the internal structure of the flow in such models is computed in such a fashion that the effects of the free surface waves are filtered out.

The hydrodynamic model developed in this research include displacements of the free surface. Since vertical displacements of the lake surface are included, the hydrodynamic model allows for external gravity waves. The speed of these waves is much greater than the internal wave speed and consequently puts restrictions on the computational time step. Nonlinear inertial accelerations are generally discarded in lake models, however, these are included in the three dimensional hydrodynamic model developed in this research. A more detailed discussion of the model development stages is given below.

The objective of the circulation modelling was initially the simulation of the storm driven currents (ie duration of 3 to 4 days). Therefore, the finite difference model based on the linearized Navier-Stokes equation was developed, using an explicit numerical scheme. The explicit scheme facilitated the running of the model on an IBM 286 personal computer, without the need for special Fortran compilers which use extended memory or virtual memory system. However, because of the small grid sizes used, the explicit numerical scheme requires time steps of a few seconds, so that the numerical stability condition is satisfied. This model when run on an IBM 386 personal computer required approximately one hour of real time, for simulation of one hour of model time.

Later it was found necessary to model seasonal water quality changes in the lake (periods of 6 months to 1 year). The explicit scheme was found not feasible, due to the long computing time that is required for this simulation. Therefore, the segment-node hydraulic modelling scheme was developed for long term simulations. This scheme runs much faster on a personal computer and requires one hour of real time for simulation of two months of model time.

Preliminary field measurements and initial simulations showed that wind driven currents have a major influence in small water bodies. Water quality measurements in Long Lake show effects of significant reduction in currents with depth. The need for better representation of the vertical structure of wind driven currents and advancement of computers facilitated the development of a fully non-linear three dimensional hydrodynamic model that mimics the physical processes in small lakes and reservoirs and tidal inlets. This

model uses a alternating direction implicit scheme and vertically varying eddy viscosity (VVEV) scheme to compute vertical profiles of currents. Analytical solutions for a rectangular basin and results from other well accepted three-dimensional numerical coastal models were used to verify the results of the proposed model which showed very good agreement. Field experiments were conducted to monitor circulation and water quality in Long Lake and used in the verification of the model.

Three-dimensional water quality model has been visualized as a superposition of layers of fluid. The reason for this approach is that, during summer period a lake may become stratified to the extent that apparent density discontinuities can be traced. Therefore water quality model consists of layers of water of different densities. Box models that have simple analytical solutions are used for reliability analysis and field data is used for verification of the water quality model. Several existing one, two, and three-dimensional hydrodynamic/water quality models were reviewed for this research. Various approaches used to model surface water bodies are described in Chapter 2. Simple analytical box models that describe the water body as internally homogenous or well mixed are discussed in Chapter 3. Mathematical formulations of hydrodynamic and water quality models are presented in chapters 4 and 5. Near-field and the far field hydrodynamics and distributions of the contaminants are discussed in chapters 6 to 8. Applications of these models to small lakes, reservoirs, and tidal inlets requiring three-dimensional representation (such as, Long Lake in Halifax urban watershed and Parr Inlet in North West Territories) are also presented in chapter 8.

Chapter 2
LITERATURE SURVEY

2.1 General

The physical transport of pollutants is governed by water movements. This motion covers a broad range of scales, from lake and ocean wide circulation to molecular motion. The spreading (dispersion) of a passive contaminant is influenced by advection and mixing (diffusion). A knowledge of the processes in boundary layers coupled with the surface and solid boundaries, processes occurring along ocean fronts, processes in the interior of the lake or ocean related to mesoscale eddies, spreading along isopycnic surfaces and small scale instabilities and molecular effects is required to understand water quality variations (Kullenberg, et.al. 1983; Csanady 1973).

2.2 Hydrodynamic Models

Hydrodynamic modelling is a basic requirement for studying transport processes that control the movement of sewage discharges, nutrients, toxic chemicals, spilled oil, heat, and dredge spoil. For such a modelling effort, it is essential to accurately represent water level and flow variations in the study area. The dynamics of some tidal inlets is complicated especially, where the entrance is restricted by a sill, complicated coastal configuration and bathymetry. The water column in the inlet was assumed to consist of two layers separated by the halocline that inhibit the exchange between these two layers.

In the past, many finite difference models that solve the hydrodynamic equations have been applied to the Great Lakes area (Simons 1976; Lam and Jaquet 1976; Lam and Halfon 1978; Lam and Simons 1976; Lam (Personal Communication)). The Canada Centre for Inland Waters (CCIW) model uses a multi layer wind driven circulation model to determine transient advective transport. This model uses a finite difference technique to

solve the equations of motion on a square mesh grid. The grid size ranges from 5 km on Lake Ontario to 6.7 km on Lake Erie. Selection of the spatial discretization of hydrodynamic models varies for different lakes. For Lake Erie, the grids used for both circulation and water quality were concurrent.

The hydrodynamic numerical circulation models used in the early years for surface waters were two dimensional and linearized. These were based on the depth-averaged momentum and continuity equations. A variety of computational methods have been used to obtain numerical solutions to these equations, including finite difference schemes (Duff 1983; Flather and Heaps 1975; Heaps 1983; Leendertse 1967; Leendertse and Liu 1975; Mathews and Mungall 1972), finite elements (Brebbia, C.A. and Partridge, P.W. 1976; Cheng, Powell and Dilloin 1976; Connor and Brebbia 1976; Connor and Wang 1973; Pinder and Gray 1977; Tee 1979; Wang 1978), harmonic analysis in time plus finite elements in space (Davies 1985, Le Provost and Poncet 1978; Le Provost, Rougier and Poncet 1981, Pearson and Winter 1977), and the method of characteristics (Lai 1976; Townson 1974). A review is given by Liu and Leendertse (1978).

Most three-dimensional models used in the early years were based on vertically integrated two-dimensional models. The three-dimensional model was composed of a vertical stack of two-dimensional models, separated by an impermeable interface and connected through interfacial friction. Vertical resolution in this model is enhanced by increasing the number of layers. The principal difficulty with this type of model is that in upwelling or downwelling regions the layers may impinge on the sea surface or sea bed. In later models, this problem is overcome by using a fixed finite difference grid in the vertical through which the fluid is free to move (a grid box model). With a fixed finite difference grid in the vertical, the number of vertical grid boxes increases as depth increases, but reduces in shallow water. However, this has the effect of reducing vertical resolution in a shallow region where, usually, high shears occur in the vertical.

The latter problem can be overcome by transforming the hydrodynamic equations into depth-following coordinates (sigma coordinates, see Freeman et al. 1972) and then

applying a finite difference grid in the vertical. This method ensures that a constant number of grid boxes are used through the vertical at each horizontal grid point. In this type of model, care must be taken to accurately resolve severe changes in bottom topography. This is because horizontal gradients of depth appear in the sigma transformation of the equations describing stratified flows, Davies (1982). A recent example of the use of this method with enhanced grid resolution in surface and sea bed boundary layers is given in Johns et al. (1983). Recent reviews of the various methods used to formulate three-dimensional layered or grid box models are given by Cheng et al. (1976) and Simons (1980).

2.3 Dispersion and Mixing

In order to design waste disposal sites or remediate contaminated sites, one must be able to predict the dispersion and fate of contaminants, both under existing conditions and following a variety of proposed remedial actions. Mass transport along lake or estuarine coastlines is governed by two processes: lateral turbulent dispersion and net longitudinal transport caused by density gradients. Dimensional analysis was used to determine characteristics of horizontal mixing, while vertical eddy viscosity and diffusivity coefficients are estimated by modelling (Tolmanzini, 1983).

Nielsen (1987) produced Puff and Particle dispersion models to assess the dilution of effluents continuously released to coastal areas. The Limfjord connected to the North Sea in Denmark was used as a study area. Devine (1987) suggested that wake mixing is effective in diluting liquid wastes at the ocean surface by a factor of 5×10^3 or more. Initial dispersion is by horizontal eddy diffusion in the deep ocean, but shear becomes dominant after several hours. Large particles sank rapidly out of the surface layer. Medium term processes diluted liquid wastes by a factor of 10^5 within 1-2 days. Long-term processes dilute the wastes further but slowly. Most particulate matter settles over an area of a few thousand square kilometres within a few weeks depending on currents. Many questions remain concerning movement of waste over the long-term and how particles move through

the water column and settle on the bottom.

2.4 Fate and Effect

Waldichuk (1975) suggested that we need to obtain more bioassay data in parallel with experiments with freshwater and marine systems. This should be carried out preferably using the same species acclimatized to the particular water, to compare marine and fresh water pollution results. More information is required on the mechanisms of increased seawater toxicity, since we may have higher toxicity for some substances in seawater due to some peculiar mode of toxic action.

He has also suggested that differences between the toxicity of a material in freshwater and seawater may be due to the differences in the form and bioavailability of the material in fresh water verses seawater, and the physiological differences between fresh and seawater species, or physiological differences within an indicator species in fresh or seawater. Kenega (1978), Klaplov and Lewis (1979) have suggested that the differences in toxicity detected by bioassays are usually small, except when the toxicant influences osmoregulatory functions of the test organisms.

2.5 Water Quality Models

Water circulation in the receiving waters is a basic parameter to the water quality models. A list of the different kinds of one, two and three dimensional and box model for water quality is presented in Table 2.2. As shown in these tables various approaches can be used to study hydrodynamics and water quality of receiving waters. The types of the hydrodynamic and water quality models range from simple uncoupled kinematic and dynamic box models to three-dimensional time-dependent dynamic transport dispersion models.

Pollutant transport modelling can be separated into an event (short term) or long term

modelling. Investigations of long term phenomena may be carried out using simple box models that have analytical solutions. Because of their simplicity, such models provide easily calculated estimates of marine water quality, which are often useful in broad planning and management. The lack of complexity of box models makes them an ideal starting point before developing linked hydrodynamic-water quality models. This detailed water quality modelling requires inclusion of actual geometric configuration and bathymetry, wind, diffusion coefficients and time dependant stream flow boundary conditions, etc.

Most of the lake or ocean water quality models are based on the advection-diffusion equation and are solved using three basic methods (finite difference method (FDM), finite element method (FEM) and finite section method (FSM)). Many researchers in Canada Centre for Inland Waters (CCIW) have used FDM (Lam and Halfon 1978, Lam and Jaquet 1976, Lam and Simons 1976). Ditoro and Conolly (1980), Murthy and Okubo (1977), Richardson (1976), Simons (1976),Chen J. (1975) have used this method for developing models for The Great Lakes . For example, circulation models for Lake Erie and Lake Ontario use a finite difference grid to solve the equations of motion on a square grid mesh. Application of this method to small surface water bodies is not attempted so far.

The second method is the finite section method (Thomann, 1972) which treats the water body as a series of completely mixed volume of segments. Mass balances are written for each segment, resulting in a set of equations solved simultaneously for their concentrations. This approach has been used for estuaries as well as lake by many researchers (Shanahan and Harelman 1982, Stefan and Demetracopoulos 1981, Thomann et al. 1975, Thomann et al. 1979, Uchrin 1980, Uchrin and Weber 1982).

Selection of the spatial discretization of water quality models varies for different inlets. For Lake Erie, grids employed for both circulation and water quality are concurrent. Advective transport in the water quality model is taken directly from the daily average circulation model results. Sensitivity to the diffusion coefficient for these large lakes was tested by the Canada Centre for Inland Waters (CCIW) and found moderate. A water quality model developed for Lake Superior was a four-layer model and was formulated as a square

finite difference grid, but with a grid spacing twice that of a circulation model. Horizontal advective transport for the water quality model was computed by summing the mass flow computed in the circulation model. Canada Centre for Inland Waters (CCIW) has also developed a four-layer model (Boyce 1979) for Lake Ontario using an irregular mesh, unlike the previous ones. For the calculation of advection and diffusion, the results are summed up over the faces of the water quality elements. For diffusion, sub grid-scale water diffusivities are used.

The ecological, limnological and environmental features of a Norwegian Lake (Rorslett 1988) and two Ethiopian reservoirs (Mesfin 1988), used for hydroelectric power generation were reported. Changes in water quality and biotic communities of streams below three reservoirs in southern Poland were found to depend on the quality of the water flowing into the reservoir and the type of reservoir (Dumnicka 1988). A flood control, low flow augmentation reservoir was found to dramatically decrease downstream suspended solids (SS) and total phosphate concentrations (Okereke 1988a), while also decreasing biological oxygen demand (BOD) and chemical oxygen demand (COD) loading rates. (Okereke 1988b). A one dimensional model was developed to predict the mixing of stratified reservoirs using buoyant jets, created by pumping water from a thermal layer to another (Gu and Stefan 1988). Dissolved oxygen (DO) dynamics upstream and downstream of a hydroelectric power facility were found controlled primarily by meteorological factors, and were independent of the method of hydrostatic operation (Mathur et al. 1988).

Seasonal and spatial fluctuations in the DO regime of Lake Surisar, India were reported by Sehgal and Jyoti (1986). Areal rates of hypolimnetic oxygen depletion were found to correlate with the maximum storage of DO at the onset of thermal stratification, suggesting that prediction of oxygen depletion rates can be improved if maximum oxygen storage after mixing is considered along with other factors known to influence oxygen depletion rates (Trimbee and Prepas 1988). An ecological model of Lake Yunoko, a dimictic lake was developed by Hosomi et al. (1991) to assess various programs for eutrophication control. A multi-component dynamic model for nutrients in the bottom

sediment-water system was incorporated into the model, a one-dimensional water temperature-water quality-ecological model. Several earlier studies of hydrodynamic mixing processes of plumes (Fan, 1967; French, 1972; Jirka, 1982; Lee, 1980; Jirka and Donekar, 1991) depict the behaviour of outfall plumes under various ambient current and stratification conditions.

Modelling of horizontal diffusion with sigma coordinate system has been investigated by Blumberg and Mellor 1987, Swanson and Spaulding (1985), Haney (1991), and Sheng (1987). The difficulty of modelling horizontal diffusion in sloping topography using sigma coordinate transformation is the introduction of spurious diffusion transport. Mellor and Blumberg (1985) noted that the full transformation formula for horizontal diffusion behaved poorly on sloping bottoms. Paul (1994) discussed spurious diffusion over irregular bathymetry induced by the full transformation diffusion formula and a simplified expression similar to Mellor and Blumberg's (1985) formula. Huang and Spaulding (1996) have presented a new formula to provide a more realistic calculation of horizontal diffusion.

2.6 **Monitoring Studies**

Cross and Boesch (1983) developed a generic risk assessment protocol for ocean waste disposal in which physical, chemical and biological processes, target organisms, critical pathways and food webs must be integrated to predict the actual levels of exposure to organisms or to a population and the subsequent effects. Champ, Conti and Park (1989) proposed a scheme for a rational, pragmatic and scientific approach to the use of a medium (lake or ocean) for waste disposal. They stressed that it would work only if the evaluation and use of disposal options were approached in an experimental manner as through a hypothesis to be tested.

Bierman et al (1985) proposed a research strategy for ocean disposal that supports a rational decision based upon a predictive hazard assessment approach. Several components

are established, each involving acquisition and synthesis of information leading to a regulatory decision. Lahey (1989) described a regulatory approach to ocean waste disposal based upon a charge system. The fees levied would generate revenue for important functions like research, monitoring and site studies.

An effective data-acquisition system for dispersion and transport measurement of contaminants in coastal areas has been developed by the Danish Isotope Centre (Appelquist and Nielsen, 1989). Fischer (1989) has suggested that biological monitoring of metals that accumulate in molluscan soft tissues is highly dependent upon the nutritional state of the molluscs. He proposes relating molluscan body burdens to shell weight to alleviate this problem. He has calculated a Cd/shell-weight index for body burdens of the blue mussel (Mytilus edulis) from Kiel fjord in the western Baltic Sea. The index is then compared with conventional calculations that relate Cd to soft tissue weight. He claims that Cd levels slightly above background levels are more precisely detectable by this index than through conventional systems.

Bokuniewicz (1989) has discussed the capping of contaminated muds with sand at subaqueous sites as a method of isolating contaminants from the aquatic environment. The U.S. Army Corps of Engineers has conducted testing of capping procedures for marine waste management for two decades.

Studies by Stebbing and Cleary (1989) using sensitive bioassay techniques to access the impact of wastes on marine waters, suggest that the correlative approach is unlikely to yield results upon which pollution control measures should be based and that a new approach is necessary to establish casual relationships with certainty.

Shellfish pathologies, as indicators of early impact stages may suggest single species die-offs and species-associated changes (Bright, 1987). Pelletier (1982) suggests a fourfold approach to the design of sampling stations for parameter assessment using test and reference stations and before and after sampling should be included. This requires deploying a pattern of stations that provide samples from an impacted area for comparison with a non-impacted area.

2.7 Model Calibration and Verification

Importance of model confirmation has been discussed in general by Caswell 1977, Davis et al 1976, Mihram 1973, Naylor and Finger 1971 and Van Horn 1969. A symposium on this topic was sponsored by USEPA (Hydroscience 1980). Many researchers (Mihram 1973, Shaeffer 1980, Thomann 1980, Thomann and Segna 1980, Thomann and Winfield 1976) have suggested various statistics useful for model confirmation. Thomann's publications stress the need for use of statistical tools for confirmation of water quality simulation models.

2.8 Previous Halifax Urban Watershed Studies

Most of the early modelling work conducted under the HUWP has been to study the whole Halifax Urban Watershed, rather than, focus on a detailed analysis of the Long Lake system behaviour. The earliest modelling effort of the Halifax Urban Watersheds was by Pinhey (1984) and he used a single event model, OTTHYMO (Ottawa Hydrologic Model) to simulate the quantity of surface runoff from rural or urban watersheds. Pinhey's (1984) study showed that OTTHYMO is applicable to this watershed. However, his study showed that the applicability is more significant in cases of individual watersheds than in complete watershed system modelling. The later modelling efforts of Salah (1986) and Rowney (1984) were directed to the application of QUALHYMO model to Halifax Urban Watersheds representing the complete system. Rowney's (1984) application of QUALHYMO model to the Long Lake watershed used the same data that had been used by Pinhey (1984). Rowney (1984) investigated the effect of different gate settings on Long Lake volume for 1983 and made model simulations with the uncalibrated model to demonstrate the use of the model in analyzing the impact of gate operation policy on lake volume.

A groundwater monitoring and model study was conducted by Attanayake (1986)

and applied to a simulation model to represent ground water-lake interaction. The main objective of his study was to determine water and chemical mass balances for Long Lake and its watershed. The results of Attanayake's (1986) study showed a net inflow of groundwater into the watershed area from neighbouring watersheds which also agrees with the estimates made by Waller et al. (1984). The study by Attanayake (1986) also showed that the external input doesn't significantly affect the groundwater storage since fractured rock aquifers exist in the area and act as underground hydraulic connections between the study area and the surrounding watersheds.

Several other studies deal with stream and lake morphometry, cross-sections, elevations, and drainage areas for Halifax Urban Watersheds (Haebler 1983; Scott 1984; Haebler 1984; Sheppard, 1982). Sheppard (1982) compiled all available Halifax Urban Watershed hydrological data, the data sources, and nature and location of data. Another study by Sheppard et al. (1984) describe the design and establishment of an effective and economical system for acquisition and management of hydro-meteorological data by means of an automated system utilizing microcomputer technology. The main objective of the study was the establishment of an integrated data base and data handling with an interpretation system. This thesis also investigated different aspects of the watershed monitoring system including protection against vandalism and unattended cold weather operation.

Haebler (1983) mapped detailed cross-sections on two streams, Beaverdam Brook and MacIntosh Run of Long Lake. The objective of this study was to study changes that might occur in the structure of the stream due to urbanization and development. Haebler (1984) established fourteen reference elevation marks in Halifax Urban watersheds by standard levelling techniques. This established absolute elevations of various weirs and lakes in the watershed area. A series of studies concerning water quantity analysis and stream discharges in the Halifax Urban Watershed were conducted by Haebler (1983, 1984 and 1985). A hydrologic study of the Beaverdam Brook watershed was conducted by Haebler (1983). He prepared rating curves for the stream. These rating curves have been

used in this hydrodynamic model study. Rainfall and runoff records from two storms were used to develop a unit hydrograph for the stream. Haebler (1984) collected discharge data relating to weir overflow and stream flow in the Halifax Urban Watersheds and developed stage-discharge curves for the two largest streams in Long Lake watersheds, Beaverdam Brook and Tracers brook (Figure 1.1). Rainfall, lake level, stream discharge and water quality data for the storm event of the 26th of June 1984, were analyzed in the report by Haebler (1985). The rainfall hyetographs for this storm and hydrographs on Bayers, Beaverdam and Traces Brooks were all plotted. Water quality samples were analyzed for fifteen different chemicals and showed the differences in water quality of these three streams.

Waller et al. (1984) prepared a preliminary water balance for Long Lake based on data available for 1983. An apparent discrepancy in the water balance was noticed in this study and explained the discrepancy by ground water inflow to the system. Pinhey and Waller (1984) extended the preliminary work done by Waller et al. (1984) by means of computer simulations that included the ground water effects and established a relationship between theoretical groundwater flow and storage. The relationship was used to predict watershed yield for a period other than that for which the relationship was developed which was found more reliable during the dry weather season. Scott (1984) investigated nine lakes and ponds in the Halifax Urban Watersheds. Scott's report (1984) also provides revised estimates of morphometric features, such as, bathymetric maps of Long, Chain and Chocolate Lakes and lake area and volumes.

The early modelling work to study the whole Halifax Urban Watershed (Pinhey 1984, Rowney 1984), lead into a more detailed study of the lake system behaviour in the Halifax Urban Watersheds (John 1985). The first mathematical modelling of circulation and pollutant variations in one of the HUWP lakes, Chain Lake, was undertaken during 1984-85 (John 1985; John and Waller 1990). Later two numerical hydrodynamic models, one based on a linearized finite difference approach and the other on a link-node approach were developed and applied to Long Lake (John, Satish and Waller 1995).

TABLE 2.1 TYPES OF HYDRODYNAMIC MODELS

References	Dimensions	Solution Technique	Equations	Forcing	Application
Liu and Leendertse (1978)	x, y, z, t	Finite differences Semi-implicit	Continuity u&v-momentum Salt conservation Turbulent energy	Tide Wind Riverflow	Long Island Sound San Francisco Bay Chesapeake Bay
Elliott (1975)	x (2 layer)	Uncoupled kinematic & dynamic box model	Continuity Salt balance u-momentum	Riverflow	Potomac Estuary
Hamilton (1979) Blumberg (1975) Wang and Kraviz (1979)	x,z,t	Explicit Finite differences semi-implicit	Continuity u-momentum Salt conservation	Riverflow and tide + wind	Rotterdam Waterway Potomac Estuary
Hodgins (1979)	x,t (2 layer)	Finite differences semi-implicit	Continuity u-momentum Salt conservation	Wind Riverflow	Alberni Inlet, British Columbia
ASA (1991)	x,y,t	Finite difference	Continuity u&v-momentum		Halifax Harbour
Reid et al (1977a)	x,y,t	Explicit Finite differences (subgrid scale)	Continuity $\bar{u}$ & $\bar{v}$-momentum	Tide & wind	Sabine-Caleasieu area of gulf coast
Pearson and Winter (1977)	x,y,t	Finite elements (time decomposed into tidal harmonies ω)	Continuity $\bar{u}$ & $\bar{v}$-momentum	Tide	Hood Can

TABLE 2.2 TYPES OF WATER QUALITY MODELS

References	Hydrodynamic Circulation Submodel	Variables	Kinetics	Forcing	Application
Leendertse and Gritton (1971) Leendertse and Liu (1975)	2-D (horizontal) time-dependent dynamic transport-dispersion model	Coliforms, salinity (chlorides), DO-BOD	Linear	Tide, fresh and storm drainage, BOD load, wind	Jamaica Bay (N.Y.)
Barrett and Mollowney (1972)	1-D tidally averaged box model	Organic carbon, organic nitrogen, ammonia, nitrate, DO	Linear Anaerobic kinetics included when DO < 5% saturation	Tide riverflow, wind, temperature	Thames Estuary (U.K.)
Nihoul et al. (1979)	1-D time-dependent dynamic transport dispersion model	DO, nitrate, ammonia, iron, manganese	Redox potentials control reaction rates assumed to be due to bacterial activity.	Tide, riverflow	Scheldt (The Netherlands)
Chen and Orlob (1972)	1-D time-dependent link-node dynamic transport-dispersion model	Temperature, salinity, nitrogen, phosphorus, DO-BOD,	Linear and Monod	Tide, riverflow, wind, light	San Francisco Bay Delta System
DiToro et al. (1977)	1-D tidally averaged transport-dispersion model	DO-BOD, phosphorus, silica, nitrogen	Linear and Monod	Tide, riverflow, wind, temperature, light	San Francisco Bay - Delta System Potomac Estuary
EPA (FOAM)	NONE	PAH	Linear		
EPA (1982) (EXAMS)	NONE	PAH	Linear		Sydney Harbor
EPA (WASP)	2-D (horizontal) residual current model	DO, nutrients	Linear		Sydney Harbor
ASA (1991)	2-D (horizontal) dynamic transport - dispersion	Coliform, DO	Linear	Tide, fresh and storm drainage	Halifax Harbor

Chapter 3

ANALYTICAL MODELS

The application of mathematical modelling techniques to hydrodynamics and water quality variations in surface waters allows a reasonable representation of a highly complex real world. The modeller attempts to identify both natural and manmade causes that are relevant to the water quality problem under consideration. Mathematical models can be used as a predictive tool and permit the forecasting and evaluation of the effects of changes in water quality in the surrounding environment. Some water quality problems are very complex and the only practical and economical way of screening several management alternatives is by using predictive numerical models. This Chapter presents simple analytical models and Chapters 4 and 5 present the development of hydrodynamic and water quality models.

Analytical box models describe the water body as being internally homogenous or well mixed and a single mass balance equation is used to characterize its dynamics. They provide easily calculated estimates of lake water quality that often are quite useful for broad planning and management. Box models are also useful to predict the state of a surface water body by determining the flows of matter across its boundaries. In this simple modelling approach, the internal structure or resolution of the water body is only important if it influences inputs and outputs.

In this section, a discussion on the application of box models to a lake is presented. However, this procedure is also applicable to reservoirs and tidal inlets. Temperature, chloride, sodium, and dissolved oxygen data collected for Long Lake during 1983-84 show that strong vertical mixing during fall, winter and spring cause these parameters to be fairly uniform in the vertical direction. For the simple modelling procedure discussed in this section the horizontal variation will be neglected. However, the horizontal variation will be considered in the more detailed models discussed in Chapters 4 and 5. Horizontal variations

can be also included by using multiple boxes to represent the water body. Generally, the inputs or loadings may consist of substances carried by tributary streams, bulk precipitation (wet and dry fall out) from sediment feedback etc. Output could be by sedimentation, vaporization or by flow through outlet or by reaction (ie. transformed into another compound).

Variation of the loadings with time may be assumed as sinusoidal loading, step loading, exponential loading or linear loading. As for inputs of chloride, it may be realistic to assume that it varies sinusoidally, with the maximum in January and minimum in May. Another approach is to examine it as a step loading. The mathematical formulations are described in the following paragraphs. Thus the approach in this study is to assume each load separately by using a simple loading function, and then study the response of the lake to each loading. Later, responses to individual loading may be added to get the total loadings.

Assuming that the prototype lake has constant volume and lake inflow equals the lake outflow, the rate of change of mass is given by:

$$\frac{dm}{dt} = V \frac{dC}{dt} \qquad (3.1)$$

where,

m is the mass of the substance;

$\frac{dm}{dt}$ is the rate of change of mass with respect to time;

V is the lake's volume and C is the concentration of the substance.

Mass carried by tributary streams enter the lake at its periphery and is dependant on the

following parameters:

- magnitude of stream flow,

- drainage basin characteristics,

- soil types,

- land use.

Atmospheric sources such as precipitation and dry fall out, enter across the air-water interface. These sources are dependant on the size of the lake's surface area and the amount of rainfall. Feedback of material from the bottom sediments may also enter the lake on an areal basis. Since complete mixing is assumed, the inputs change only temporarily and the variation in concentration with time can be represented as:

$$V \frac{dC}{dt} = W(t) \qquad (3.2)$$

where,

W(t) is the rate of mass loading,

$\frac{dc}{dt}$ is the change of concentration with respect to time, and

V is the lake volume.

The mass balance equation for a completely mixed lake can be written as:

$$V \frac{dC}{dt} = W(t) - QC \pm reactions \qquad (3.3)$$

where,

Q = the rate of flow of water through the volume

For this simple model, mass loadings of the lake is conceptualized by periodic functions, for which analytical solutions are available.

The assumed loading functions are :

1. Impulse loading

2. Step loading

3. Sinusoidal loading

These three cases discussed here have exact or closed form solutions since input is represented exactly by an idealized function of time. However, in reality, input and other model parameters vary non uniformly in time. In such cases, approximate numerical solution techniques can be used. These numerical techniques are discussed in chapters 4 & 5. The exact solution results will be used for comparison with the numerical model that represents variation with space and time.

3.1 Impulse Loading

The effect of an accidental spill of chemical waste can be modelled as an impulse, or a delta function representing a discharge over a short time period. If the spill occurs at time zero, ie. t=0, then the expression for pollutant concentration in the lake at any time may be derived as follows:

$$\frac{dC_p}{dt} + \frac{Q}{V} C_p = \frac{W(t)}{V} \qquad (3.4)$$

$$\frac{dC_p}{dt} + \alpha C_p = \frac{W(t)}{V} = \frac{m\,\delta(t)}{V} \qquad (3.5)$$

$W(t) = m\delta(t)$

Assume an initial condition $Cp(0) = 0$

Laplace transform of (3.5) yields

$$s\,\mathcal{L}\{C_p\} + \alpha\,\mathcal{L}\{C_p\} = \frac{m}{V} \qquad (3.6)$$

which reduces to

$$\mathcal{L}\{C_p\} = \frac{m}{V(s+\alpha)} \qquad (3.7)$$

Finding the inverse of the above, the solution yields:

$$C_p = \frac{m}{V} e^{-\alpha t} \qquad (3.8)$$

where,

Cp is a particular solution of the concentration, m is the mass of the substance, and V is the lake's volume

$$\alpha = \frac{Q}{V} + k$$

where, Q is the inflow rate which is
equal to outflow rate, k is the reaction coefficient, t is the time, S is the sources or sinks of a substance within the lake.

If 2×10^7 g of a substance is accidently spilled into a rectangular lake, the response of the lake to the spill is shown for two cases depending on the reaction rates of the substance ie, k = 1.05, for a non-conservative constituent and k = 1.00, for a conservative constituent (Figure 3.1).

3.2 Step Loading

We consider two cases:

Case 1: Step Input (type 1)

Suppose at time t=0, the lake loading is changed from zero (Figure 3.2) loading to

a new constant level of 5 X 10^7 g/yr, the response of the prototype lake to such loading can be derived as follows:

The loading can be represented as:

$$W(t) = \overline{W}\, U(t) \tag{3.9}$$

where,

U(t) is a unit step function

assume an initial condition Cp(0) =0

$$\frac{dC_p}{dt} + \alpha C_p = \left(\frac{\overline{W}}{V}\right) U(t) \tag{3.10}$$

Taking Laplace transform of eq (3.10)

$$\mathcal{L}\{C_p\}(s + \alpha) = \frac{\overline{W}}{V s} \tag{3.11}$$

which reduces to

$$\mathcal{L}\{C_p\} = \frac{\overline{W}}{V(s + \alpha)s} \tag{3.12}$$

Finding the inverse of the equation,

$$C_p = \frac{\overline{W}\,(\,1 - e^{-\alpha t}\,)}{\alpha V} \qquad (3.13)$$

C_p is the pollutant concentration in the lake

$\overline{W}$ is the new constant level loading

The calculated pollutant concentration in the prototype lake at the end of each (k=1.05) month is shown in as case 1 and in Figure 3.1.

Case 2: Step Input (type 2)

An opposite type of response of the lake is to cut off the loading completely after a known time (Figure 3.2). This can be derived as a step function given by:

$$\frac{dC_p}{dt} + \alpha C_p = 0 \qquad (3.14)$$

where,

C_p is the mean lake concentration

C_o is the initial concentration of the pollutant

solving we obtain

$$C_p = A\, e^{-\alpha t} \tag{3.15}$$

For $t = t_o$, $C_p = C_o$ we have,

$$C_o = A\, e^{-\alpha t_o} \tag{3.16}$$

Therefore, we get the expression for pollutant concentration in lake as follows:

$$C_p = C_o\, e^{-\alpha (t - t_o)} \tag{3.17}$$

where, t is the time at the concentration to be evaluated, and t_o is the initial time.
The response to this loading is presented in Figure 3.2.

3.3 Sinusoidal Loading

The periodic input to the prototype lake can be expressed mathematically as:

$$W(t) = \overline{W} + W_o \sin(\omega t - \Theta) \tag{3.18}$$

where, W is the constant part of loading,

W_o is the amplitude, and Θ is the phase shift (radians or degrees).

$$\theta = \omega \left[t_m - \left(T_p / 4 \right) \right] \qquad (3.19)$$

t_m is the time of occurrence of the peak or maximum loading

ω is the frequency of the oscillation

$\omega = 2\pi/T_p$ or $360/T_p$ where,

T_p is the period of time over which a complete oscillation occurs.

The particular solution for the case is given below (Chapra and Reckhow 1983):

$$C_p = \frac{W}{\alpha V}\left(1 - e^{-\alpha t}\right) + \frac{W_o}{V\sqrt{\alpha^2 + \omega^2}} \sin\left(\omega t - \theta - \arctan\frac{\omega}{\alpha}\right) -$$

$$\frac{W_o}{\sqrt{\alpha^2 + \omega^2}} \sin\left(-\theta - \arctan\frac{\omega}{\alpha}\right) e^{-\alpha t} \qquad (3.20)$$

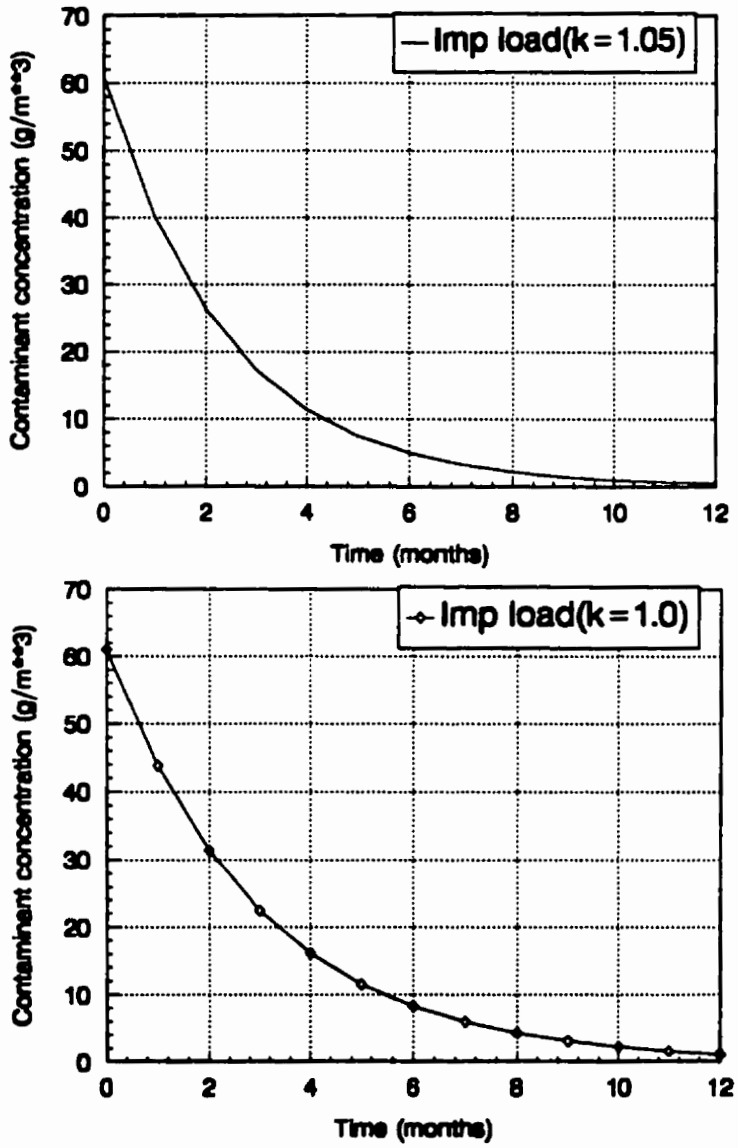

Figure 3.1 Response of a typical lake to impulse loading.

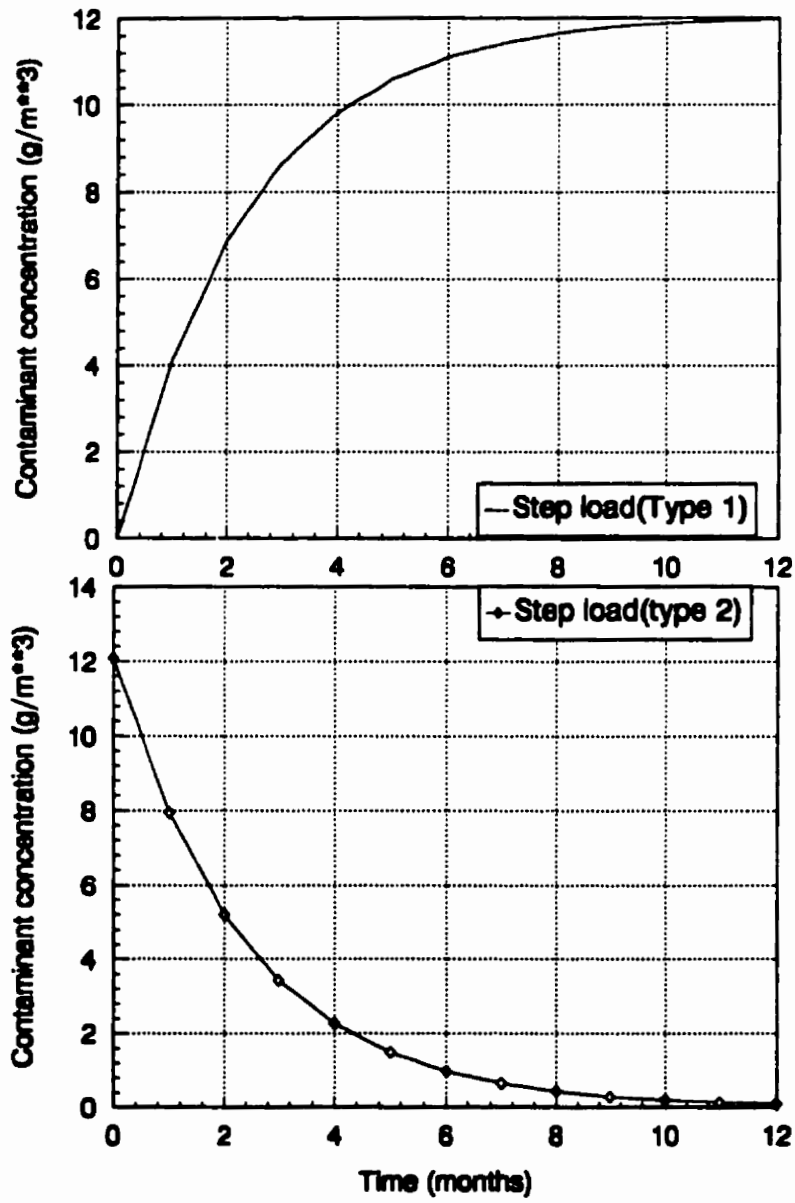

Figure 3.2 Response of a typical lake to step loading.

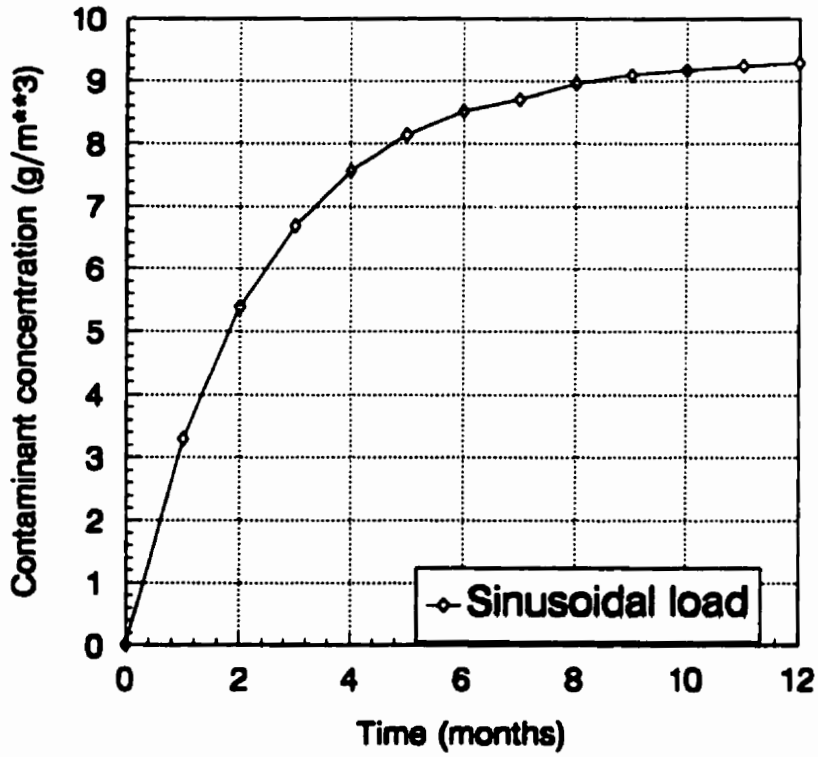

Figure 3.3 Response of a typical lake to sinusoidal loading

Chapter 4

DEVELOPMENT OF NUMERICAL HYDRODYNAMIC MODELS

4.1 General

Long Lake has a complicated coastal configuration, and seven major streams empty into this lake (Figure 4.1). Water quality of these streams varies considerably. Many of these streams are on opposite sides of the lake and lateral averaging would combine them and therefore water quality changes will not be properly represented. One of the interest of modelling in the present study was simulation of the summer period when these waters are stratified. However, other seasons can be also simulated using the model developed.

The objective of the circulation modelling was initially the simulation of the storm driven currents (storm duration of 3 to 4 days). Therefore, a finite difference 2-D depth averaged hydrodynamic model based on the linearized Navier-Stokes equation was developed, using an explicit numerical scheme. The explicit scheme facilitated the running of the model on an IBM 286 personal computer, without the need for special Fortran compilers which use extended memory or virtual memory systems. However, because of the small grid sizes used, the explicit numerical scheme requires time steps of a few seconds, so that the numerical stability condition is satisfied. This hydrodynamic model when run on an IBM 486 personal computer required approximately one hour of real time, for simulation of twelve hours of model time.

It is also necessary to model seasonal water quality changes in the lake (periods of 6 months to 1 year). The earlier mentioned scheme was found not feasible, due to the long computing time that is required for this simulation. Therefore, a 2-D depth averaged segment-node model was developed for long term simulations. This model runs much faster on a personal computer and requires one hour of real time for simulation of two months of model time.

Preliminary field measurements and initial simulations showed that wind driven currents have a major influence in small water bodies. Water quality measurements in Long Lake show effects of significant reduction in currents with depth. The need for better representation of the vertical structure of wind driven currents and advancement of personal computers resulted in the development of a third fully non-linear three dimensional hydrodynamic model. This model mimics the unique characteristics of small lakes, reservoirs and tidal inlets described in Section 1.2. This model uses an alternating direction implicit scheme and vertically varying eddy viscosity (VVEV) scheme to compute vertical profiles of currents. Analytical solutions for a rectangular basin and results from other available layered three-dimensional numerical model were used to verify the results of the model which showed good agreement. Field experiments were conducted to monitor circulation and water quality in Long Lake and used in the validation of the proposed models.

4.1.1 Modelling considerations

Analysis of the problem should dictate the spatial and temporal scales for the modelling analysis. For an adequate modelling exercise one needs to extend the network upstream and downstream beyond the influence of the waste loads being studied. One should also consider aligning the network so that sampling stations and points of interest (such as water withdrawals) fall near the centre of a model segment. If flows are to be input from the hydrodynamic model, then a water quality model segment must coincide with each hydrodynamic node. Once the model network was established, the modelling exercise proceeds to compute lake or reservoir hydrodynamics. To address this step a combination of in-situ drogue measurements, water level and seiche measurements, and hydrodynamic modelling were carried out as described in Chapter 6. The typical hydrodynamic model characteristics are shown in Table 4.1.

4.2 2-D Linear Hydrodynamic model

This numerical hydrodynamic model is based on the Navier-Stokes equation, and computes water levels and water transport components, using input values of depth array, inflows, outflows, and wind forcing. This model neglects the nonlinear accelerations and uses non-linear bottom friction. The co-ordinate system and variables used are shown in Figure 4.3. The horizontal components of currents in the lake and water surface elevation are represented by the following partial differential equations (Roesch et al. 1979):

$$\frac{\partial U}{\partial t} = fV - gH\frac{\partial z}{\partial x} - BU + \tau_{sx} \tag{4.1}$$

$$\frac{\partial V}{\partial t} = -fU - gH\frac{\partial z}{\partial y} - BV + \tau_{sy} \tag{4.2}$$

$$\frac{\partial Z}{\partial t} = -\frac{\partial U}{\partial x} - \frac{\partial V}{\partial y} \tag{4.3}$$

where,

t is the time; x, y are horizontal co-ordinates (x clockwise from y); U,V are components of vertically integrated currents; Z is the upward displacement of the free surface from a mean water level; H is the depth of the basin from mean water level; B is the bottom stress coefficient; f is the Coriolis parameter ($f = 2\,\omega \sin \phi$); ω is the angular velocity of the earth's rotation and ϕ is the latitude; g is the gravitational acceleration; τ_s is the wind stress at the surface.

The bottom stress coefficient is calculated using a variable non-linear bottom friction (Lam, 1982) given by the following equation:

$$B = (C_D (U^2 + V^2)^{1/2})/H^2 \qquad (4.4)$$

where,

C_D is the drag coefficient, selected as 0.002 for this study based on the bottom roughness.

The wind stress (τ_s) has been computed using the following general equation (Chow 1976)

$$\overline{\tau_s} = C_D \frac{\rho_a}{\rho} \mid \overline{w} \mid w \qquad (4.5)$$

where, τ_s is the wind stress, ρ_a is the density of air, ρ is the density of water, and w is the wind velocity.

Time dependent water level variations and horizontal velocity components were calculated using the model with the inputs described above. The selection of a suitable time step is necessary for stability of the model results. The stability condition is satisfied by the following criteria and is a necessary condition for convergence of the governing equations.

$$t < DS\sqrt{(2gH_{max})}$$

and

$$t < \frac{1}{B_{max}} \qquad (4.6)$$

where,

t is the time step, DS is the space step, g is the gravitational acceleration , H_{max} is the maximum lake depth and B_{max} is the maximum bottom stress coefficient.

Hydrodynamic models were applied to both Long Lake and Parr Inlet (Figures 4.1 and 4.2). The hydrodynamic model grids for Long lake and Parr Inlet are presented in Figures 4.3 and 4.4.

4.3 2-D Segment-node model

One dimensional models were successfully applied to Delaware Estuary (Harleman et al. 1968; Aydin and Ahlert 1978), however, these models assumed that the flow in the side reaches had negligible momentum. The lake model developed for long-term hydrodynamic simulations (several months to one year) in this thesis uses a new segment-node approach, in that it essentially uses a one-dimensional formulation to provide two dimensional flows and water level variations considering a three segment cross sectional approach (one main channel and two side reaches). This model that uses the segment-node approach, illustrates the propagation of a long wave through a shallow water system while conserving both momentum and volume. The equation of motion, based on the conservation of momentum, predicts water velocities and flows. The equation of continuity, based on the conservation of volume, predicts water heights and volumes. In this model, Coriolis Force and accelerations normal to the direction of flow are considered negligible.

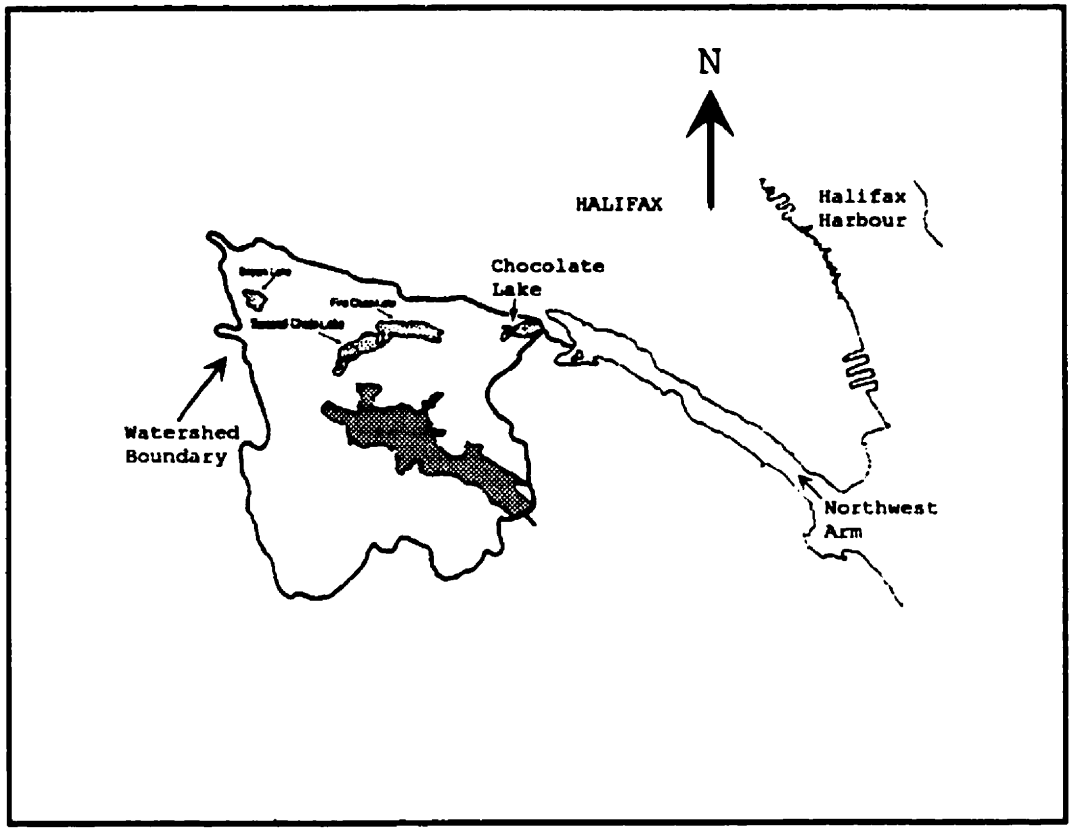

Figure 4.1 Long Lake study area

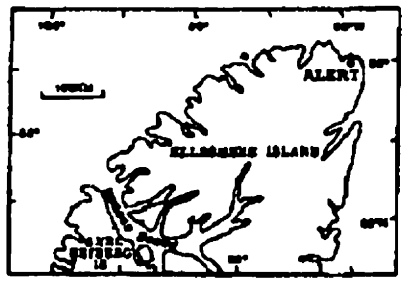

Figure 4.2a Parr Inlet Location.

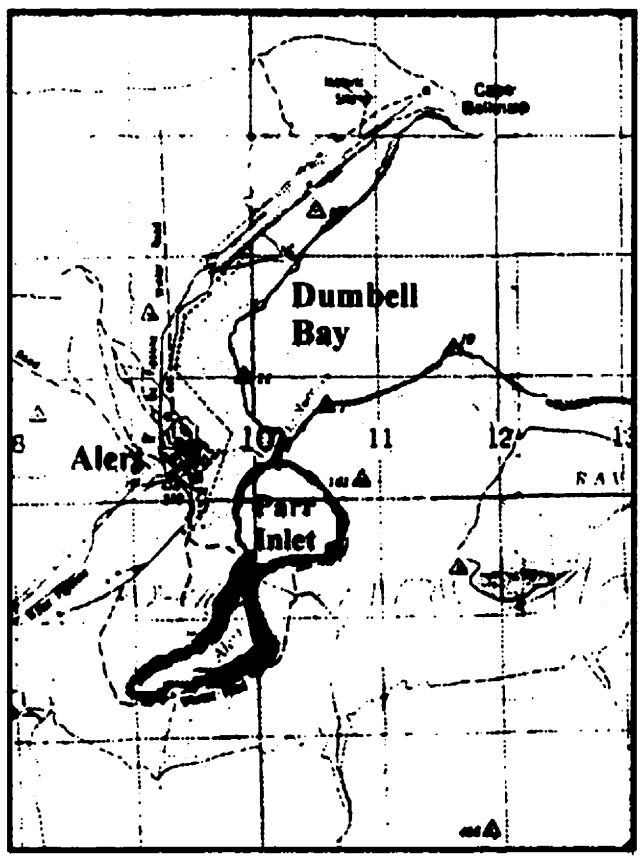

Figure 4.2b Parr Inlet study area

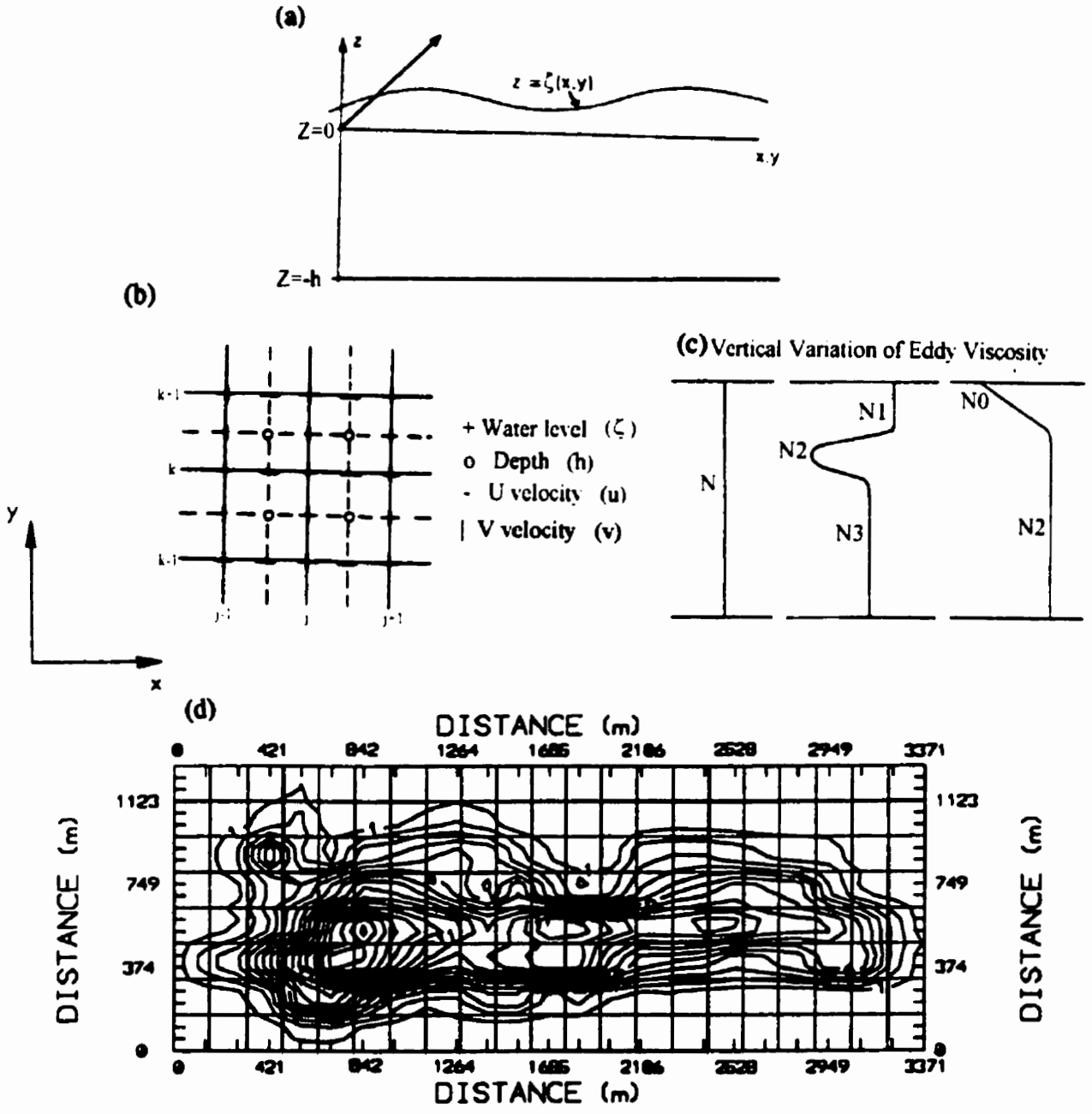

Figure 4.3 Details of the model (a) co-ordinate system, (b) finite difference scheme, (c) VVEV schemes used, and (d) model grid of Long Lake.

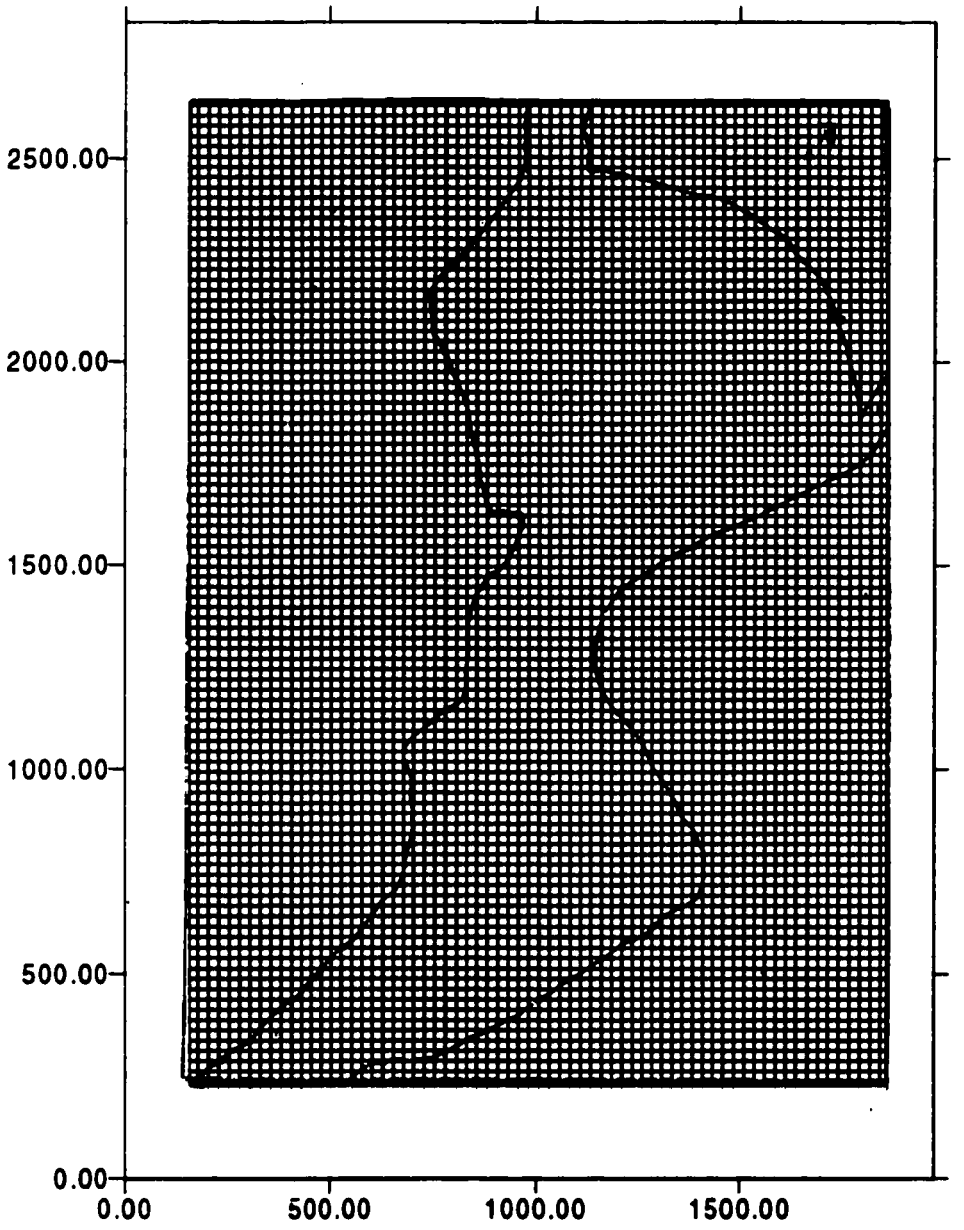

Figure 4.4 Hydrodynamic model grid - Parr Inlet

The segment-node model solves the equations of continuity and momentum for a branching or segment-node, computational network (Roesch et al., 1979, Ambrose et al, 198, Feigner and Harris, 1970). Variable upstream flows and downstream heads drives this model. The resulting unsteady hydrodynamics are averaged over larger time intervals and stored for later use by the water-quality program.

The equation of motion in one dimension is given by:

$$\frac{\partial U}{\partial t} = - U\frac{\partial U}{\partial x} - g\frac{\partial H}{\partial x} - \frac{gn^2}{R^{4/3}} \mid U \mid U + \frac{C_d}{R}\frac{\rho_a}{\rho_w}w^2\cos\psi \qquad (4.7)$$

where,

$\frac{\partial U}{\partial t}$ = the local inertia term, or the velocity rate of change with respect to time;

$U\frac{\partial U}{\partial x}$ = the Bernoulli acceleration, or the rate of momentum change by mass transfer; also defined as the convective inertia term from Newton's second law;

H is the water surface elevation, or head (height above an arbitrary datum); g is gravitational acceleration; C_d is the drag coefficient; R is the hydraulic radius (approximately equal to the depth for wide segments); n is the Manning roughness coefficient (usually between 0.01 and

0.10); x is the distance along the axis of a segment; t is the time; U is the velocity along the axis of a segment; and λ is the longitudinal axis.

The second term on the r.h.s. of eq. (4.7) is the gravitational acceleration that is driven by the slope of the water surface.

The equation of continuity is given by:

$$\frac{\partial A}{\partial t} = -\frac{\partial Q}{\partial x} \tag{4.8}$$

where:
A = cross-sectional area; Q = flow.

For rectangular segments of constant width b:

$$\frac{\partial H}{\partial t} = -\frac{1}{b}\frac{\partial Q}{\partial x} \tag{4.9}$$

where:

b = width; H = water surface elevation (head); $\frac{\partial H}{\partial t}$ = rate of water surface elevation change with respect to time; $\frac{1}{b}\frac{\partial Q}{\partial x}$ = rate of water volume change with respect to distance per unit width.

The greater degree of mixing in the epilimnion allows adequate aeration of the water, whereas, the water in the hypolimnion will often be depleted of oxygen as shown in the case of Long Lake for the summer period (see Chapter 6). Therefore, it is of importance to determine the origin of the water withdrawn since this determines the quality of the outflowing water. The thermocline in Long Lake (see Chapter 6), during summer starts below about a 5m depth and therefore the possibility of drawing water from below the thermocline in the case of Long Lake is minimal.

The outflow in Long Lake was estimated for minimum, mean, and maximum cases using the discharge curves drawn by Rowney (1984) for the outflow weir. These three discharge curves were adjusted to the model's zero reference level. Any of these three relationships established between the depth above model reference and Long Lake outflow may be used in the segment-node model.

4.3.1 Segmentation Scheme

Basically most cross-sections of Long Lake may be represented by one deep channel and two side reaches (Figure 4.3_a). However, these deep channels occasionally swing to one side at many cross-sections (Figure 4.3_b). The partition of the lake's cross section to three channels is carried out by dividing the cross-section into three areas of equal width. The depth of each channel is represented by the mean depth along that channel width. Therefore, the three cross sectional areas when added provide the lake's true cross sectional area. The selected segment-node network scheme for Long Lake is shown in Figure 4.6.

The construction of the three-segment model was made to account for the momentum of the flow within the side reaches, and to approximate the changes in the lateral position of the deep channel. Long Lake is modelled as a series of segments in the longitudinal direction of the lake with up to three open channels running side by side. The downstream velocity in each segment is calculated by solving [4.7].

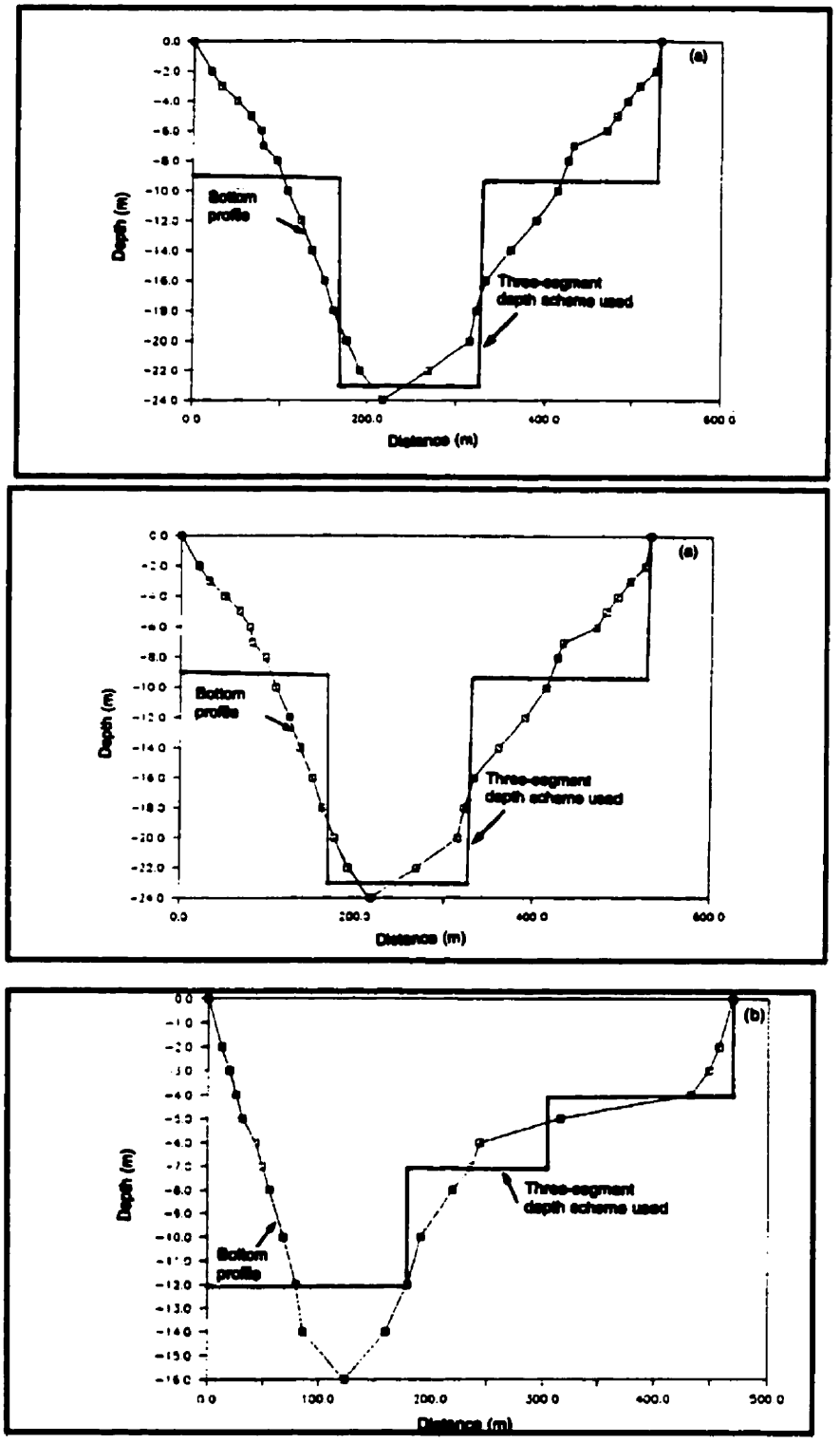

Figure 4.5 Selected cross sections for Long lake

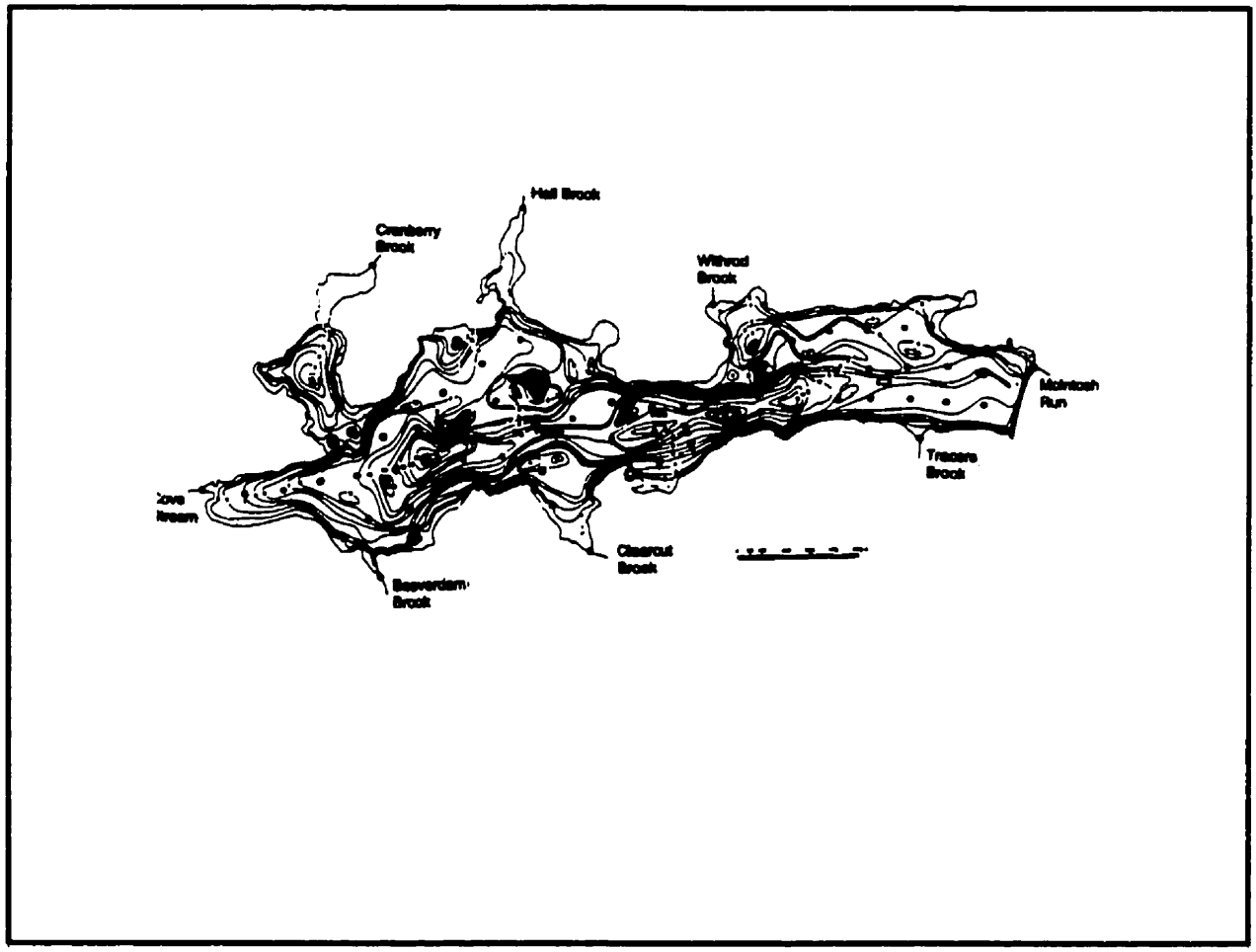

Figure 4.6 Segment-node network scheme for Long Lake

The segment-node model was thus laid out by a network of interconnected segments and nodes that represent the lake system. Manning's roughness coefficient (n) was used as the primary calibration parameter in the model simulations. The value of n can be highly variable, depending on such factors as bed roughness, vegetation, segment irregularities in cross-section or shape, obstructions, and depth. Values of n can potentially vary from less than 0.01 to greater than 0.08. Deeper, straighter reaches have lower roughness coefficients. In general, the value of n increases upstream as segments become more constricted and shallow.

4.3.2 Model Input Parameters

Input parameters used to solve the equations of motion and continuity and other parameters calculated by the segment-node model are:

Node Parameters: The input parameters associated with nodes are initial surface elevation (head), surface area, and bottom elevation. Volumes and mean depths are calculated internally.

Segment Parameters: The input parameters associated with segments are length, width, hydraulic radius or depth, segment orientation, initial velocity, and Manning's roughness coefficient.

The segment length is generally dependent on a computational stability criteria given by:

$$L_i \geq (\sqrt{gy_i} \pm U_i)\ \Delta t \tag{4.10}$$

where:

L_i = length of segment i; y_i = mean depth of segment i; U_i = velocity in segment i; Δt = computational time step; g =gravitational acceleration.

Boundary Parameters: The downstream boundaries can be defined by either specifying outflows or surface elevations. Surface elevations at each downstream boundary can be specified. Inflows and outflows can be specified as constant or time variable. Inflows at an upstream boundary are represented by negative flows(i.e.: to introduce a flow across a boundary into the network it must be negative); outflows are represented by positive flows.

Wind Parameters: The input parameters associated with wind acceleration are wind speed, wind direction, segment orientation, and segment hydraulic radius. Wind speed and direction are measured at a point 10 meters above the water surface. This wind is to be representative for the entire water body. Values of wind speed and direction may vary with time.

4.3.3 Model Network

Equations (4.7) and (4.9) form the basis of the hydrodynamic model. Their solution gives velocities (U) and heads (H) throughout the water body over the duration of the simulation. Because closed-form analytical solutions are unavailable, the solution of equations (4.7) and (4.9) requires numerical integration on a computational network, where values of U and H are calculated at discrete points in space and time. A flexible, computationally efficient type of network has been developed for these equations by Feigner and Harris, 1970. The "segment-node" network solves the equations of motion and continuity at alternating grid points. At each time step, the equation of motion is solved at the segments, giving velocities for mass transport calculations, and the equation of continuity is solved at the nodes, giving heads for pollutant concentration calculations.

A physical interpretation of this computational network can be developed by picturing the segments conveying water and the nodes as nodes storing water. Each node is a volumetric unit that acts as a receptacle for the water transported through its connecting segments. Taken together, the nodes account for all the water volume in the lake or tidal inlet. Parameters influencing the storage of water are defined within this node network.

Each segment is an idealized rectangular conveyor that transports water between two nodes, whose midpoints are at each end. Taken together, the segments account for all the water movement in the lake or tidal inlet. Parameters influencing the motion of water are defined within this segment network. The segment-node computational network, then, can be viewed as the overlapping of two closely related physical networks of segments and nodes.

4.3.4 Implementation of the Equations

To apply differential equations 4.7 and 4.9 to a segment-node computational network, they must first be written in a finite difference form. The equation of motion becomes:

$$\frac{U_i^t - U_i}{\Delta t} = - U_i \frac{\Delta U_i}{\Delta x_i} - g\frac{\Delta H_i}{\Delta x_i} - \frac{g\, n_i^2}{R_i^{4/3}} U_i|U_i|$$

$$+ \frac{C_d}{R_i}\frac{\rho_a}{\rho_w} W_i^2 \cos \Psi_i \qquad (4.11)$$

where:

U_i^t is the velocity in segment i at time t

Δx_i is the segment length

Δt is the time step

i is the segment number

$\frac{\Delta U_i}{\Delta x_i}$ is the velocity gradient in segment i with respect to distance

$\frac{\Delta H_i}{\Delta x_i}$ is the water surface gradient in segment i with respect to distance

All values on the right hand side of equation (4.11) are referenced to the previous time step (t-Δt).

The water surface gradient, $\Delta H_i/\Delta x_i$, can be computed from the node heads at either end of the segment. The velocity gradient, however, can not be computed directly from upstream and downstream segment velocities because of possible branching in the network. If branching does occur, there would be several upstream and downstream segments, and any computed velocity gradients would be ambiguous. An expression for the velocity gradient within a segment can be derived by applying the continuity equation (4.8) to the segment and substituting U A for Q:

$$\frac{\partial A}{\partial t} = -\frac{\partial Q}{\partial x} = -U\frac{\partial A}{\partial x} - A\frac{\partial U}{\partial x} \qquad (4.12)$$

Rearranging terms:

$$\frac{\partial U}{\partial x} = -\frac{1}{A}\frac{\partial A}{\partial t} - \frac{U}{A}\frac{\partial A}{\partial x} \qquad (4.13)$$

Writing this in finite difference form and substituting bR for A and bΔH for ∂A gives the following expression for the velocity gradient:

$$\frac{\Delta U_i}{\Delta x_i} = -\frac{1}{R_i}\frac{\Delta H_i}{\Delta t} - \frac{U_i}{R_i}\frac{\Delta H_i}{\Delta x_i} \tag{4.14}$$

The term $\Delta Hi/\Delta t$ is computed as the average water surface elevation change between the nodes at each end of segment i during time step t. Substituting equation (4.14) into (4.11) and rearranging gives the explicit finite difference equation of motion applied to each segment i:

$$U_i^t = U_i + \Delta t \left[\frac{U_i}{R_i}\frac{\Delta H_i}{\Delta t} + \left(\frac{U_i^2}{R_i} - g\right)\frac{\Delta H_i}{\Delta x_i}\right.$$

$$\left. - \frac{g\, n_i^2}{R_i^{4/3}}\, U_i |U_i| + \frac{C_d}{R_i}\frac{\rho_a}{\rho_w}\, W_i^2 \cos\psi_i\right] \tag{4.15}$$

Writing the equation of continuity (4.9) in finite difference form gives:

$$\frac{H_j^t - H_j}{\Delta t} = -\frac{\Delta Q_j}{B_j\, \Delta x_j} \tag{4.16}$$

where:

j = node number

The numerator ΔQ_j is given by the summation of all flows entering and leaving the node. The denominator $b_j\, \Delta x_j$ can be expressed directly as the surface area A_j^s of the node.

Substituting these identities into equation (4.17) and rearranging gives the explicit finite difference equation of continuity applied to each node j:

$$H_j^t = H_j - \Delta t \frac{\sum_i Q_{ij}}{A_j^s} \tag{4.17}$$

At this point, one equation for each segment and each node, in the computational network exists. Given input parameters describing the network configuration and geometry, initial values for segment velocities and node heads, boundary conditions for downstream heads, and forcing functions for freshwater inflow and wind stress, equations (4.15) and (4.17) are solved using Runge-Kutta procedure.

4.4 3-D Non-Linear Hydrodynamic Model

4.4.1 General

The 3-D hydrodynamic model computes stream flow or tidal and wind-driven circulation in a lake, reservoir or tidal inlet by solving the depth-averaged Navier-Stokes equations using finite differences. Dynamic vertical velocity profiles are computed using the VVEV algorithm. A two block variable grid system can be used with finer mesh for a selected area of the lake if required.

The model requires the stream inflows and outflows at the model open boundaries and the wind speed and direction over the lake as input. Model outputs include water heights, depth-averaged velocities, and vertical velocity profiles.

4.4.2 The Mathematical Formulations

4.4.2.1 The Governing Equations

This numerical hydrodynamic model is based on the Navier-Stokes equation, and computes water levels and water transport components, using input values of depth array, inflows, outflows, and wind forcing. This model includes the nonlinear accelerations and uses non-linear bottom friction. It is common in models of lake, tidal, and wind-driven currents to make a number of simplifying assumptions in the equations of fluid dynamics. The fluid is assumed to be incompressible and of uniform density, horizontal eddy viscosity is neglected, and the vertical momentum equation is approximated by the hydrostatic pressure equation. The horizontal components of currents in the lake and water surface elevation are represented by the following differential equations of horizontal momentum, continuity, and pressure (Leendertse 1967):

$$\frac{\partial u}{\partial t} + u\frac{\partial u}{\partial x} + v\frac{\partial u}{\partial y} + w\frac{\partial u}{\partial z} = fv - g\frac{\partial \zeta}{\partial x} - \frac{1}{\rho}\frac{\partial P}{\partial x} + \frac{\partial}{\partial z}\left[N\frac{\partial u}{\partial z}\right] \quad (4.18)$$

$$\frac{\partial v}{\partial t} + u\frac{\partial v}{\partial x} + v\frac{\partial v}{\partial y} + w\frac{\partial v}{\partial z} = -fu - g\frac{\partial \zeta}{\partial y} - \frac{1}{\rho}\frac{\partial P}{\partial y} + \frac{\partial}{\partial z}\left[N\frac{\partial v}{\partial z}\right] \quad (4.19)$$

$$\frac{\partial u}{\partial x} + \frac{\partial v}{\partial y} + \frac{\partial w}{\partial z} = 0 \quad (4.20)$$

$$P = P_a + g\rho(\zeta - z) \qquad (4.21)$$

where,

t is the time; x, y are horizontal co-ordinates; with the z-axis points vertically upwards u,v, and w are components of currents in the x, y, and z directions, respectively; ζ (x, y, t) is the height of the free surface above the xy-plane; h is the depth of the lake from the mean water level; f is the Coriolis parameter ($f = 2\,\omega \sin \phi$); ω is the angular velocity of the earth's rotation and ϕ is the latitude; g is the gravitational acceleration; N (x, y, z) is the vertical eddy viscosity; ρ is the fluid density which is assumed to be uniform in this case; P_a is the atmospheric pressure, and; P is the fluid pressure.

4.4.2.2 Boundary and Initial Conditions

In addition to the differential equations (4.18) to (4.20) there are a number of kinematic and dynamic initial and boundary conditions.

On the water surface, $z = \zeta$

$$\rho N \frac{\partial U}{\partial z} = \tau^s_x \qquad \text{and}$$

$$\rho N \frac{\partial v}{\partial z} = \tau^s_y \qquad (4.22)$$

On the sea bottom, z= -h:

$$\rho N \frac{\partial u}{\partial z} = \tau^b_x \qquad \text{and}$$

$$\rho N \frac{\partial v}{\partial z} = \tau_y^b \qquad (4.23)$$

where (τ^s_x, τ^s_y) are the components of shear stress on the water surface, and (τ^b_x, τ^b_y) are the components of bottom friction stress.

For the surface shear stress it is usual to take:

$$(\tau_x^s , \tau_y^s) = \gamma \rho_a \sqrt{(W_x^2 + W_y^2)}\,(W_x, W_y) \qquad (4.24)$$

where, ρ_a is the density of air, (W_x, W_y) are the components of wind velocity, and γ is a dimensionless drag coefficient. Several of the forms proposed for γ are discussed and compared by Mathison (1983)

For bottom friction we take:

$$\tau_x^b = -\frac{g\rho}{c^2}\sqrt{(u^2 + v^2)}\; u \qquad (4.25)$$

at z = -h, and

$$\tau_y^b = -\frac{g\rho}{c^2}\sqrt{(u^2 + v^2)}\; v \qquad (4.26)$$

at z=-h

where c is the Chezy coefficient. This coefficient depends on the nature of the bottom and also to some extent on the depth of water. An expression of the following type is used by Leendertse (1967) for these coefficients:

$c = C_1 \ln (C_2 H + C_3)$

C_1, C_2, C_3 are constants. Hen and Hunter (1988) and Hunter (1975) provide a theoretical description of bottom friction formulation.

On coastal boundaries, the component of the current velocity along the outward normal to the boundary is set at zero. On open boundaries, the most appropriate condition, especially for shallow seas, is to specify water elevation at the open boundaries (Bills and Woye 1986). Thus, for the open boundary we express the elevation in a standard harmonic form:

$$\zeta = Z_0 + \sum_i^n f_i A_i \cos (V_i + U_i + \sigma_i^c + g_i) \qquad (4.27)$$

where, Z_o is the mean value; A_i is the amplitude of constituent i, g_i is the phase lag behind the equilibrium constituent i on the Greenwich meridian; f_i ,U_i are the nodal factors accounting for the 18.6 year period variation in amplitude and phase of constituent, V_i the phase of the equilibrium constituent i at Greenwich at t=o, σ_i is the speed of constituent i, and n is the number of streamflow constituents being considered.

Other types of open boundary conditions have been reviewed and tested by many, including Blumberg and Kantha (1985).

4.4.2.3 The VVEV Scheme

In this thesis, a Vertically Varying Eddy Viscosity (VVEV) scheme is used for the computation of vertical velocity profiles. In the VVEV scheme, the depth-averaged equations are first solved at each time step. Then the surface heights and depth averaged velocities computed from this part of the algorithm are used as part of the input to the horizontal

momentum equations which are solved at each horizontal grid point for the vertical profiles of the velocity. A finite difference scheme is used to solve the depth averaged equations and a generalized Crank-Nicholson finite difference scheme is used to solve the one-dimensional time-dependent vertical momentum equations.

The VVEV algorithm was developed as an alternative to the full three-dimensional hydrodynamic model given by equations (4.18) to (4.21). The VVEV simulation algorithm consists of two parts. In the first part, the surface elevation and depth-averaged velocity components are obtained from the two-dimensional depth-averaged hydrodynamic equations. In the second part, the vertical velocity profiles are computed by solving the one-dimensional time-dependent vertical momentum equations, which form a coupled parabolic system of equations. These equations use the depth-averaged velocity components computed in part one as input.

The so-called shallow-water approximation forms the basis for the depth-averaged hydrodynamic equations. According to this approximation, equations (4.18) to (4.21) are replaced by their averaged versions over the vertical dimension. This leads to a two-dimensional system of equations rather than the full three-dimensional system given by equations (4.18) to (4.21), Pinder and Gray (1977).

In integrating the model equations, we introduce the depth-averaged horizontal velocity components, u and v defined as follows:

$$\bar{u} = \frac{1}{H}\int_{-h}^{\zeta} u\,dz \qquad \text{and} \qquad (4.28)$$

$$\bar{v} = \frac{1}{H}\int_{-h}^{\zeta} v\,dz \qquad (4.29)$$

where, $H = \zeta + h$ is the total water depth.

The governing equations may then be written as follows:

$$\frac{\partial \zeta}{\partial t} + \frac{\partial}{\partial x}(H\bar{u}) + \frac{\partial}{\partial y}(H\bar{v}) = 0 \qquad (4.30)$$

$$\frac{\partial}{\partial t}(H\bar{u}) + \frac{\partial}{\partial x}(H\overline{uu}) + \frac{\partial}{\partial y}(H\overline{uv}) + gH\frac{\partial \zeta}{\partial x} = Hf\bar{v} - \frac{H\partial P}{\rho \partial x} + \frac{\tau_x^s - \tau_x^b}{\rho} \qquad (4.31)$$

$$\frac{\partial}{\partial t}(H\bar{v}) + \frac{\partial}{\partial x}(H\overline{uv}) + \frac{\partial}{\partial y}(H\overline{vv}) + gH\frac{\partial \zeta}{\partial y} = -Hf\bar{u} - \frac{H\partial P}{\rho \partial y} + \frac{\tau_y^s - \tau_y^b}{\rho} \qquad (4.32)$$

where the following notation is used:

$$\overline{uu} = \frac{1}{H}\int_{-h}^{\zeta} u^2 dz; \quad \overline{uv} = \frac{1}{H}\int_{-h}^{\zeta} uv dz; \quad \overline{vv} = \frac{1}{H}\int_{-h}^{\zeta} v^2 dz \qquad (4.33)$$

which represent the mean squares and the mean product of the velocity components averaged over the water column.

By neglecting the advective terms, which in most cases are small, Nihoul (1975), equations (4.18) and (4.19) reduce to:

$$\frac{\partial u}{\partial t} = fv - g\frac{\partial \zeta}{\partial x} + \frac{\partial}{\partial z}\left[N\frac{\partial u}{\partial z}\right] - \frac{1}{\rho}\frac{\partial p}{\partial y} \qquad (4.34)$$

$$\frac{\partial v}{\partial t} = -fu - g\frac{\partial \zeta}{\partial y} + \frac{\partial}{\partial z}\left[N\frac{\partial v}{\partial z}\right] - \frac{1}{\rho}\frac{\partial p}{\partial y} \qquad (4.35)$$

Equations (4.34) and (4.35) form a coupled parabolic system, and these equations can be

solved by a finite difference scheme as proposed. Note that it is feasible to retain the advective terms; however, in this research the approximation given in (4.34) and (4.35), which is adequate for most cases is used (Nihoul and Jamart 1987).

4.4.2.4 The Simulation Algorithm

The proposed simulation scheme consists of two parts. In the first part, the system of hyperbolic equations for $\vec{u}$, $\vec{v}$, and ζ given by equations (4.30) to (4.32) are solved using a finite difference scheme. In the second part, the parabolic system of equations given by equations (4.34) and (4.35) are solved using a generalized Crank-Nicholson finite difference scheme.

Schematic representations of various VVEV schemes used are presented in Figure 4.3c. For a weakly stratified season, a constant eddy viscosity as shown in Figure 4.3c was used. However, since strongly stratified conditions occur during summer season (Figures 6.5 to 6.8), a more complex VVEV scheme as shown in Figure 4.3c was required. During summer stratified season, high shear occur across the pycnocline. Above the pycnocline, wind-induced turbulence produces a well mixed top layer of thickness 4 to 6 m in the case of Long Lake (Figure 6.5 to 6.8). Within the pycnocline the turbulence is reduced by stable stratification. Below the pycnocline the turbulence increases to a certain value that is determined by ambient currents. A detailed description of the solution scheme used for vertical momentum equations including the effect of stratification is presented in Appendix A.

4.4.3 Model Configuration

The model domain shown in Figure 4.1 was selected to adequately model the Long Lake and Parr Inlet. For this application, the model grid geometry and water depths were obtained from CWRS (Scott, personal communication) (Tables 4.2 and 4.3). A 62.5 m grid spacing (Δx or Δy) and the corresponding time step (Δt) of 2 seconds were used. Wind records from Shearwater weather station were used for providing model wind forcing.

4.4.3.1 Model Setup

The first step in model setup is the selection of the model grid for an optimum geographic area to adequately represent the area of interest.

Model Grid and Water Depths

The study area of interest to setup the hydrodynamic model for Long Lake and Parr Inlet was determined from charts for the area.

The following are the sequence of steps:

(1) selection of grid size and overlay of the grid on the chart;
(2) approximation of land and open sea boundaries;
(3) selection of coordinate axis and defining grid points;
(4) digitization of water depths from the chart; and
(5) selecting time step.

The region is overlaid by a single grid block in Cartesian coordinates. The grid comprises of multiple boxes with equal grid sizes in both x and y directions. A proper grid size is chosen for the region to adequately represent the space and time scales of the variables considered in the model. The smaller the grid size selected, the better the region is represented . However, it should be noted that smaller grid sizes lead to smaller time steps and a larger number of grid points, thus greatly increasing computational time. Coordinate axes are drawn in suitable directions; for example the x-axis in this application extends in the longitudinal direction and the y-axis is taken along the transverse direction. The axes were selected in such a way that the long stretches of coastline, are as closely parallel as possible to the x- coordinate direction. However, the angle between x-axis and north which describes the grid orientation can be easily changed by changing the rotation parameter in the hydrodynamic model input file.

The land and open sea boundaries are approximated by sides of grid boxes. The grid points along the x-axis are designated by subscript M and the grid points along the y-axis by N. M runs from 1 to MMAX and N runs from 1 to NMAX to cover the given water area. A maximum grid size of 50 x 50 is allowed due to memory limitations. The applications to Long Lake and Parr Inlet use a 50 X 26 grid.

Depths are digitized (in meters) from the chart and assigned at all grid points. The depth at the grid point (N,M) is taken as the average value of the depths within the grid box which the grid point (N,M) represents. Note that the grid points which lie on land and on the grid lines N=1, N=NMAX, M=1 and M=MMAX have zero depth values, which represent model domain borders.

A quantity H_{mean} is added to all depths to represent Mean Water Level (MWL) since the depth charts used are referenced to a chart datum. Note that H_{mean} equals zero if the chart from which the depths are read is referenced to MWL.

As shown in Figure 3.3, water depths are used in meters for all "active" water grid points (designated by code #1 in input file); code #0 are entered at the grid points lying on land; the open boundary grid points are designated by code #2, where as the model domain borders are given code #9.

The time step selected is smaller than the maximum time step allowed for stable computations. The maximum time step is computed as described below.

Model Time Step

It is necessary that the following numerical stability condition is satisfied

$$\frac{\Delta x}{\Delta t} < \sqrt{(2gH_{max})} \tag{4.36}$$

where,

Δx= mesh or grid size

Δt = model time step

g = gravitational acceleration

H_{max} = maximum water depth in the model domain

The maximum water depth in the model domain for Parr Inlet is 30 meters and for a grid size of 62.5 m, the required model time step is 2.5 seconds or less. Lower grid size would require a smaller time step and a larger number of grid points to cover the same domain, and the model run time would increase considerably. Therefore a 62.5 m X 62.5 m grid size and two seconds time step were selected for the simulations. The hydrodynamic model computes the maximum time step and checks it with the selected time step. If the selected time step is larger than the maximum time step, the program will not run.

4.4.3.2 Initial and Open Boundary Conditions

The 3 dimensional hydrodynamic model starts performing the computations from initially flat condition. Therefore, all velocity components are initially set to zero and water heights are given a small constant initial value. The program runs spinup = 24 hours of real time to

reach approximately steady conditions for tidal flow predictions. However, the wind-driven flow computations start at time zero.

The three-dimensional hydrodynamic model accepts water heights at boundary points as open boundary conditions. Water heights at open boundary points are computed in the program by linearly interpolating the water heights with respect to time and space. This hydrodynamic model requires that the wind velocity distribution is specified at all grid points for wind driven current simulation.

Surface Drag Coefficient

The dimensionless surface drag coefficient is an important parameter in computing surface shear stresses due to wind. A value between 0.0024-0.0028 is chosen for this area. However, selection of this value requires adequate field data so that best fit between computed and observed values of water height and current velocity is achieved. In the simulations presented an average value of 0.0026 is assumed.

Chezy Coefficients (Bottom Roughness)

The three-dimensional hydrodynamic model computes the values of the Chezy coefficient at each point from the given values of depth according to the formula given in Section 4.4.2.2. It is required that the coefficients used in calculation of Chezy coefficient (CHEZ1, CHEZ2 and CHEZ3) are selected according to sea bottom type in the specific area of interest and water depth in the study area in order to give the best fit between computed and observed values of water height and current velocity.

A default value of CHEZ1=25, CHEZ2 = 1 and CHEZ3 = 1 is assumed in the present application. The coefficient CHEZ2 is depth dependent and the selected Chezy coefficient ranges from 60 to 115, for water depths varying from 10 m to 100 m respectively. This corresponds to a Manning n of 0.02 to 0.03.

Dispersion and Eddy Viscosity Coefficients

The dispersion of contaminants (e.g. suspended solids, bacteria) in Long Lake or Parr Inlet contributed by mixing and transport processes are included in the water quality model through solution of mass balance equations discussed in Chapter 5. The hydrodynamic model explicitly includes dispersive processes due to general circulation, tidal and wind driven circulations. However, the dispersion processes not explicitly included in hydrodynamic model can be included implicitly through horizontal diffusions coefficients. This eddy diffusion coefficient was chosen to be $5m^2/s$ for the application of water quality model to Parr Inlet. It should be noted that an eddy diffusion coefficient of $30m^2/s$ was chosen for Halifax Inlet water quality simulations.

The eddy-viscosity coefficients are important parameters which control the vertical velocity profiles in a 3-D model. Schematic representations of various VVEV schemes used are presented in Figure 4.3c. For a weakly stratified season, a constant eddy viscosity as shown in Figure 4.3c was used. However, since strongly stratified conditions occur during summer season, and a more complex VVEV scheme as shown in Figure 4.3c was required. During summer stratified season, high shear occur across the pycnocline. Above the pycnocline, wind-induced turbulence produces a well mixed top layer of thickness 4 to 6 m in the case of Long Lake (Figure 6.5 to 6.8). Within the pycnocline the turbulence is reduced by stable stratification. Below the pycnocline the turbulence increases to a certain value that is determined by ambient currents. A detailed description of the solution scheme used for vertical momentum equations is presented in Appendix A. The above coefficients (i.e. surface drag, bottom friction and eddy viscosity) are used as tuning parameters.

4.4.4 Tidal and Wind Forcing Parameters

Surface elevations at each grid point on the model open boundary were specified by predicted tidal elevations for several tidal constituents as shown in Figure 6.14. Tidal height (referenced to the model datum) was specified at equally spaced intervals throughout the

tidal cycle. The input parameters associated with wind acceleration (wind speed, wind direction) were specified from measured data. The hydrodynamic results generated by the model simulations were stored for use as input to the water quality model.

4.5 Model Testing, Sensitivity Analysis and Validation

Sensitivity analysis provides a better understanding of the correspondence between the model and the physical processes being modelled. In this study, a series of model simulations were performed to determine the response of the receiving waters to changes in model input parameters. Details of this sensitivity analysis carried out are presented in Section 7.2. The hydrodynamic/water quality models developed were validated using drogue and moored current measurements and water quality (chlorides) profile data. The linked hydrodynamic-water quality model was tuned using Chezy, drag and diffusion coefficients. Further details of model validation are presented in Section 7.3.

TABLE 4.1

Typical Hydrodynamic Model Characteristics

Water body	Small lakes, reservoirs, and tidal inlets with strong response to wind.
Computer	IBM386/486 or better personal computer with math co-processor.
Model type	event or long term depending on the capacity of the computer.
Time step	Few seconds for hydrodynamic model and few minutes for the segment-node model.
Cell structure	Square grid for hydrodynamic model and flexible grid for segment-node model.
Input parameters	Streamflow, tide, wind, bathymetry, precipitation, evaporation, drag coefficient, and eddy viscosity coefficient.
Representation of stratification	By two or more layers with false bottom at thermocline or by selection of appropriate VVEV scheme.
Outflow	The segment-node model will route the outflow based on the weir hydraulics.

Table 4.2 Long Lake model depth grid

0	1	2	3	4	5	6	7	8	9	10	11	12	13	14	15	16	17	18	19	20	21	22	23	24	25	26	27
1	0	0	0	0	0	0	0	0	0	0	0	0	0	0	0	0	0	0	0	0	0	0	0	0	0	0	0
2	0	0	0	0	0	0	2.0	4.5	5.0	0.5	0	0	0	0	0	0	0	0	0	0	0	0	0	0	0	0	0
3	0	0	0	0	0	0	2.0	5.0	5.3	0.5	0	0	0	0	0.1	1.5	0	0	0	0	0	0	0	0	0	0	0
4	0	0	0	0	0	0	1.5	5.0	6.5	0.4	0	0	0	0	2.2	3.8	0	0	0	0	0	0	0	0	0	0	0
5	0	0	0	0	0	0.5	3.0	6.3	7.8	2.0	0	0	0	1.8	4.5	5.0	1.5	0	0	0	0	0	0	0	0	0	0
6	0	0	0	0	1.0	3.5	5.3	7.8	7.8	2.0	0.2	1.8	1.7	6.0	7.3	6.5	3.0	0.3	0	0	0	0	0	0	0	0	0
7	0	0	0	1.2	3.5	5.8	7.5	8.0	7.9	5.0	1.0	3.5	4.5	5.5	6.5	6.0	5.0	1.5	0	0	0	0	0	0	0	0	0
8	0	0	1.0	2.0	4.5	7.0	7.3	8.0	8.0	4.0	1.8	3.0	3.5	3.5	2.0	3.0	4.0	2.0	0.8	0.8	0.3	0	0	0	0	0	0
9	0	0	0.5	3.0	6.0	7.8	8.5	11.0	11.0	7.0	3.0	3.0	1.0	0	0	0.1	1.5	0.1	0	1.0	1.0	0	0	0	0	0	0
10	0	0	0	4.0	7.0	12.0	13.0	13.0	13.0	9.0	7.0	5.0	1.0	0	0	0	0	0	0	0.8	0.8	0	0	0	0	0	0
11	0	0	0.1	3.0	7.2	12.0	14.0	15.0	16.0	12.0	8.2	7.0	2.0	0	0	0	0	0	0	0.7	0.7	0	0	0	0	0	0
12	0	0	0.1	0.5	6.5	8.0	14.0	19.0	19.5	16.0	12.0	6.0	4.6	2.0	0	0	0	0	0	0	0	0	0	0	0	0	0
13	0	0	0	0.1	1.0	4.0	11.0	20.0	23.0	19.0	13.0	6.0	5.8	5.0	1.0	0	0	0	0	0	0	0	0	0	0	0	0
14	0	0	0	0	0.1	3.5	8.0	16.0	22.0	14.0	7.0	7.5	6.0	5.8	6.5	2.0	0	0	0	0	0	0	0	0	0	0	0
15	0	0	0	0	0.1	2.0	5.5	14.0	19.0	10.0	5.0	6.8	6.0	5.0	6.0	4.0	0.1	0	0	0	0	0	0	0	0	0	0
16	0	0	0	0	0	0.1	6.0	13.0	18.0	7.8	3.0	6.0	5.6	4.5	3.0	0.5	0.1	0	0	0	0	0	0	0	0	0	0
17	0	0	0	0	0	2.0	8.0	13.0	13.5	8.0	6.0	6.6	6.0	5.5	6.0	2.0	0.1	0	0	0	0	0	0	0	0	0	0
18	0	0	0	0	0	2.0	7.5	13.0	13.0	7.5	5.8	6.0	5.8	6.0	5.8	3.5	0	0	0.1	0.1	0	0	0	0	0	0	0
19	0	0	0	0	0	0.3	6.5	10.0	13.0	8.0	5.3	3.7	6.5	5.8	6.0	5.0	1.5	0.1	1.5	0.1	0	0	0	0	0	0	0
20	0	0	0	0.1	1.5	4.5	6.5	7.0	11.0	8.0	6.3	2.5	2.0	5.5	6.0	3.5	3.0	1.8	1.0	1.0	0.8	0	0	0	0	0	0
21	0	0.1	0.8	1.5	3.3	5.0	5.0	7.0	12.0	7.5	2.0	0.1	3.5	5.3	5.8	3.5	0.1	0	0.5	0.8	0.8	0	0	0	0	0	0
22	0	0.8	1.0	2.5	3.8	4.0	6.5	7.5	12.0	7.5	6.0	3.0	5.0	6.0	3.8	0.5	0	0	0	0	0	0	0	0	0	0	0
23	0	0.5	6.0	2.0	3.8	6.8	7.3	8.0	11.5	9.0	7.5	6.0	6.0	6.5	2.0	0	0	0	0	0	0	0	0	0	0	0	0
24	0	0	0	0.1	0.1	3.0	9.0	11.0	11.5	9.0	7.8	6.5	3.8	2.0	0.1	0	0	0	0	0	0	0	0	0	0	0	0
25	0	0	0	0	0	1.5	10.0	13.0	11.5	9.0	7.5	6.0	1.5	1.5	1.5	0	0	0	0	0	0	0	0	0	0	0	0
26	0	0	0	0	0.3	3.5	10.0	16.0	11.5	13.0	6.3	1.5	0	0.8	0.8	0	0	0	0	0	0	0	0	0	0	0	0
27	0	0	0	0.1	1.0	5.0	10.0	17.0	13.0	12.5	3.0	0	0	0.1	0.1	0	0	0	0	0	0	0	0	0	0	0	0
28	0	0	0	0.5	2.5	5.0	10.0	17.0	15.0	10.5	2.0	0	0	0	0	0	0	0	0	0	0	0	0	0	0	0	0
29	0	0	0	0.1	2.0	5.0	8.0	15.0	15.0	9.0	10.0	0	0	0	0	0	0	0	0	0	0	0	0	0	0	0	0
30	0	0	0	0	0.6	4.5	8.5	12.5	12.0	5.0	0.5	0	0	0	0	0	0	0	0	0	0	0	0	0	0	0	0
31	0	0	0	0	0	2.0	7.5	12.0	13.0	6.0	0.1	0	0	0	0	0	0	0	0	0	0	0	0	0	0	0	0
32	0	0	0	0	0	0.1	5.0	13.5	12.5	3.0	0.2	0	0	0	0	0	0	0	0	0	0	0	0	0	0	0	0
33	0	0	0	0	0	0	2.5	14.0	12.0	4.0	2.0	0.1	1.1	1.0	1.0	0	0	0	0	0	0	0	0	0	0	0	0
34	0	0	0	0	0	0	1.8	9.0	11.5	6.0	4.0	4.5	4.0	3.5	2.0	0	0	0	0	0	0	0	0	0	0	0	0
35	0	0	0	0	0	0	1.5	10.0	13.0	3.0	15.0	6.0	6.0	3.5	2.8	0.1	0	0	0	0	0	0	0	0	0	0	0
36	0	0	0	0	0	0.1	3.5	11.0	13.0	6.5	2.5	3.5	5.0	3.5	2.0	0.5	0	0	0	0	0	0	0	0	0	0	0
37	0	0	0	0	0	0	4.0	13.0	13.3	7.0	3.5	3.0	5.0	2.0	0	0	0	0	0	0	0	0	0	0	0	0	0
38	0	0	0	0	0	0	2.0	10.5	13.0	8.0	6.5	6.5	3.8	0.8	0	0	0	0	0	0	0	0	0	0	0	0	0
39	0	0	0	0	0	0	1.8	9.0	10.5	7.0	5.5	4.8	3.5	0.8	0	0	0	0	0	0	0	0	0	0	0	0	0
40	0	0	0	0	0	0	1.8	8.0	9.0	6.8	4.5	5.0	3.8	0.8	0	0	0	0	0	0	0	0	0	0	0	0	0
41	0	0	0	0	0	0	1.8	7.0	7.5	5.8	6.5	4.5	4.0	0.5	0	0	0	0	0	0	0	0	0	0	0	0	0
42	0	0	0	0	0	0	3.0	7.0	7.5	5.0	6.5	6.8	3.0	0	0	0	0	0	0	0	0	0	0	0	0	0	0
43	0	0	0	0	0	0	6.0	6.5	7.0	5.0	5.0	6.8	3.0	0	0	0	0	0	0	0	0	0	0	0	0	0	0
44	0	0	0	0	0	1.0	5.8	6.5	6.5	5.0	5.0	6.5	3.2	0	0	0	0	0	0	0	0	0	0	0	0	0	0
45	0	0	0	0	0.3	2.5	6.0	6.0	6.5	6.0	6.0	6.0	3.5	0	0	0	0	0	0	0	0	0	0	0	0	0	0
46	0	0	0	0	0	3.0	6.0	6.5	6.0	3.5	6.0	6.3	3.5	0.1	0	0	0	0	0	0	0	0	0	0	0	0	0
47	0	0	0	0	0.3	6.5	6.5	6.0	5.8	6.5	3.0	2.0	2.5	0	0	0	0	0	0	0	0	0	0	0	0	0	0
48	0	0	0	0	0.5	5.5	6.5	7.0	6.0	3.0	0.3	0.1	2.0	0	0	0	0	0	0	0	0	0	0	0	0	0	0
49	0	0	0	0	1.5	5.5	6.5	7.3	6.5	2.0	0	0	0.8	0	0	0	0	0	0	0	0	0	0	0	0	0	0
50	0	0	0	0	0	0	0	0	0	0	0	0	0	0	0	0	0	0	0	0	0	0	0	0	0	0	0

Table 4.3 Parr Inlet model depth grid

Water depths (decimetres)

M/N	1	2	3	4	5	6	7	8	9	10	11	12	13	14	15	16	17	18	19	20	21	22	23	24	25	26	27	
1	0	0	0	0	0	0	0	0	0	0	0	0	14	28	14	0	0	0	0	0	0	0	0	0	0	0	0	1
2	0	0	0	0	0	0	0	0	0	0	0	0	28	55	28	0	0	0	0	0	0	0	0	0	0	0	0	2
3	0	0	0	0	0	0	0	0	0	0	0	0	28	55	31	4	0	0	0	0	0	0	0	0	0	0	0	3
4	0	0	0	0	0	0	0	0	0	0	0	8	40	65	56	38	25	19	13	5	0	0	0	0	0	0	0	4
5	0	0	0	0	0	0	0	0	0	5	25	59	91	105	136	101	90	76	60	48	40	26	8	0	0	0	0	5
6	0	0	0	0	0	0	0	0	0	10	46	99	130	138	138	135	133	115	95	85	78	50	15	0	0	0	0	6
7	0	0	0	0	0	0	0	0	0	19	66	125	161	173	168	160	150	133	118	105	88	61	29	5	0	0	0	7
8	0	0	0	0	0	0	0	0	5	44	114	178	218	210	223	213	200	178	158	143	121	95	59	23	4	0	0	8
9	0	0	0	0	0	0	0	0	10	56	129	198	250	273	270	261	255	230	198	178	160	133	93	44	9	0	0	9
10	0	0	0	0	0	0	0	0	5	43	125	195	265	298	298	295	290	263	225	200	183	163	123	66	19	0	0	10
11	0	0	0	0	0	0	0	0	0	30	103	190	270	305	305	305	298	268	230	205	190	178	145	95	35	0	0	11
12	0	0	0	0	0	0	0	0	0	19	79	170	263	305	305	305	288	255	225	200	183	173	153	110	41	0	0	12
13	0	0	0	0	0	0	0	0	0	5	51	149	248	290	290	285	255	220	203	183	163	153	135	98	38	0	0	13
14	0	0	0	0	0	0	0	0	0	0	40	138	228	260	265	215	185	160	148	115	123	108	84	54	23	0	0	14
15	0	0	0	0	0	0	0	0	0	0	14	114	205	245	235	155	130	113	97	88	76	56	27	11	4	0	0	15
16	0	0	0	0	0	0	0	0	0	0	19	66	175	245	185	128	108	88	68	49	15	19	5	0	0	0	0	16
17	0	0	0	0	0	0	0	0	0	0	5	19	121	213	160	100	74	45	24	11	4	0	0	0	0	0	0	17
18	0	0	0	0	0	0	0	0	0	0	8	21	89	148	113	59	26	8	0	0	0	0	0	0	0	0	0	18
19	0	0	0	0	0	0	0	0	0	0	13	40	96	36	48	14	0	0	0	0	0	0	0	0	0	0	0	19
20	0	0	0	0	0	0	0	0	0	0	13	43	81	73	21	0	0	0	0	0	0	0	0	0	0	0	0	20
21	0	0	0	0	0	0	0	0	0	0	21	51	64	61	28	0	0	0	0	0	0	0	0	0	0	0	0	21
22	0	0	0	0	0	0	0	0	0	0	28	55	55	58	35	5	0	0	0	0	0	0	0	0	0	0	0	22
23	0	0	0	0	0	0	0	0	0	6	14	59	63	68	54	23	5	0	0	0	0	0	0	0	0	0	0	23
24	0	0	0	0	0	0	0	0	5	23	58	75	83	90	83	46	13	0	0	0	0	0	0	0	0	0	0	24
25	0	0	0	0	0	0	0	6	29	64	73	109	113	120	120	84	36	8	0	0	0	0	0	0	0	0	0	25
26	0	0	0	0	0	0	0	11	53	74	128	150	153	163	168	135	79	29	5	0	0	0	0	0	0	0	0	26
27	0	0	0	0	0	0	0	10	45	93	143	178	175	218	223	193	135	69	19	0	0	0	0	0	0	0	0	27
28	0	0	0	0	0	0	0	9	30	68	126	175	213	243	248	233	195	125	44	4	0	0	0	0	0	0	0	28
29	0	0	0	0	0	0	0	9	28	60	111	163	205	225	210	233	213	158	68	8	0	0	0	0	0	0	0	29
30	0	0	0	0	0	0	0	10	33	64	109	155	188	190	185	185	158	101	38	4	0	0	0	0	0	0	0	30
31	0	0	0	0	0	0	4	16	38	65	108	148	165	144	111	94	68	26	0	0	0	0	0	0	0	0	0	31
32	0	0	0	0	0	5	14	28	53	80	116	138	133	93	46	26	13	5	0	0	0	0	0	0	0	0	0	32
33	0	0	0	0	5	18	31	50	75	96	115	113	90	51	16	5	2	0	0	0	0	0	0	0	0	0	0	33
34	0	0	5	13	26	46	65	84	96	98	88	69	43	18	4	0	0	0	0	0	0	0	0	0	0	0	0	34
35	0	5	18	36	58	78	88	89	85	66	40	21	8	0	0	0	0	0	0	0	0	0	0	0	0	0	0	35
36	0	13	14	53	65	71	63	49	38	13	5	0	0	0	0	0	0	0	0	0	0	0	0	0	0	0	0	36
37	0	21	54	61	51	35	13	10	5	0	0	0	0	0	0	0	0	0	0	0	0	0	0	0	0	0	0	37
38	5	35	63	55	30	8	0	0	0	0	0	0	0	0	0	0	0	0	0	0	0	0	0	0	0	0	0	38
39	10	33	45	30	8	0	0	0	0	0	0	0	0	0	0	0	0	0	0	0	0	0	0	0	0	0	0	39
40	10	25	30	15	0	0	0	0	0	0	0	0	0	0	0	0	0	0	0	0	0	0	0	0	0	0	0	40
41	13	28	23	8	0	0	0	0	0	0	0	0	0	0	0	0	0	0	0	0	0	0	0	0	0	0	0	41
42	15	23	8	0	0	0	0	0	0	0	0	0	0	0	0	0	0	0	0	0	0	0	0	0	0	0	0	42
43	8	8	0	0	0	0	0	0	0	0	0	0	0	0	0	0	0	0	0	0	0	0	0	0	0	0	0	43
44	0	0	0	0	0	0	0	0	0	0	0	0	0	0	0	0	0	0	0	0	0	0	0	0	0	0	0	44
45	0	0	0	0	0	0	0	0	0	0	0	0	0	0	0	0	0	0	0	0	0	0	0	0	0	0	0	45
46	0	0	0	0	0	0	0	0	0	0	0	0	0	0	0	0	0	0	0	0	0	0	0	0	0	0	0	46
47	0	0	0	0	0	0	0	0	0	0	0	0	0	0	0	0	0	0	0	0	0	0	0	0	0	0	0	47
48	0	0	0	0	0	0	0	0	0	0	0	0	0	0	0	0	0	0	0	0	0	0	0	0	0	0	0	48
49	0	0	0	0	0	0	0	0	0	0	0	0	0	0	0	0	0	0	0	0	0	0	0	0	0	0	0	49
50	0	0	0	0	0	0	0	0	0	0	0	0	0	0	0	0	0	0	0	0	0	0	0	0	0	0	0	50
	1	2	3	4	5	6	7	8	9	10	11	12	13	14	15	16	17	18	19	20	21	22	23	24	25	26	27	

Chapter 5

DEVELOPMENT OF NUMERICAL WATER QUALITY MODEL

5.1 General

The water quality model developed as part of this study for small lakes, reservoirs and tidal inlets is a three-dimensional (multi-layer) model intended to simulate the impact of storm loads or effluent spills on Long Lake's water quality. This model is intended to simulate transient distribution of dye, bacteria, and suspended solids. Pollutant concentrations in the lake prior to the storm runoff must be specified as an initial condition in the water quality model. The water quality model is based on the mass balance approach and uses predicted or measured velocity fields. Since detailed current and circulation measurements are not available for Long Lake, the alternative was to look for a suitable hydrodynamic model instead of carrying out long term measurements. The hydrodynamic model simulation results are used as input to the water quality model.

Most pollutants enter the water body at its periphery, and therefore, gradients in pollutant concentration exist between the near field and interior regions. In addition, water quality is also influenced by shoreline configuration, circulation pattern, bathymetry, and the reaction rate of the substances being modeled. Transport of the material within a lake or inlet system is controlled mainly by advection and diffusion. Wind energy, water level variations, and density differences cause motion of water and mass transport of contaminants. The water quality model uses the input of water levels, circulation, eddy viscosity variations and diffusion coefficients. Diffusion coefficients may be measured or estimated from field measurements. This model can be used to assess the different water management alternatives and to study alternate locations of waste outfalls to enhance the water quality. For example, the developments in the vicinity of Long Lake include a regional park, two industrial parks, an agricultural fair, and residential land use. Some of

these developments, such as, Atlantic Winter Fair and Park development, may require onsite waste water disposal or disposal of treated waste water into the adjacent Long Lake. This thesis examines the impact of a hypothetical waste water flow into the lake.

The water quality model characteristics are shown in Table 5.1. The segmentation of the lake for the water quality model is the same as that of the hydrodynamic model. However, the difference is in the variables representing the model. The mass transport of contaminants in the water is studied in this thesis using numerical tracer studies, and model validation by using chloride as a tracer. The fate of the material forms the main focus of this study. This was carried out by a combination of numerical studies, field monitoring, parameter estimation, model testing, and validation. This will ensure the development of a model which is validated or verified. In this study, the hydrodynamic and water quality models were validated independently.

5.2 Mathematical Formulations

5.2.1 Mass Balance Equation

A mass balance equation for dissolved constituents in small water bodies under consideration here, must account for all the material entering and leaving through direct and diffuse loading; advective and dispersive transport; and physical, chemical, and biological transformation, if applicable. Consider a coordinate system, where the x- and y-coordinates are in the horizontal plane, and the z-coordinate is in the vertical plane. The mass balance equation around an infinitesimally small fluid volume can be written as (Leendertse 1967):

$$\frac{\partial C}{\partial t} + \frac{\partial}{\partial x}(U_x C) + \frac{\partial}{\partial y}(U_y C) + \frac{\partial}{\partial z}(U_z C) =$$

$$\frac{\partial}{\partial x}\left(E_x\frac{\partial C}{\partial x}\right) + \frac{\partial}{\partial y}\left(E_y\frac{\partial C}{\partial y}\right) + \frac{\partial}{\partial z}\left(E_z\frac{\partial C}{\partial z}\right)$$

$$+ S_L + S_B + S_K \qquad (5.1)$$

where:

C is the concentration of the water quality constituent; t is the time; U_x, U_y, U_z are longitudinal, lateral, and vertical advective velocities; E_x, E_y, E_z are longitudinal, lateral, and vertical diffusion coefficients; S_L is the direct and diffused loading rate; S_B is the boundary loading rate (including upstream, downstream, and atmospheric etc.); S_K is the total kinetic transformation rate.

The water quality model solves a finite-difference form of equation 5.1 by specifying appropriate transport, loading, and transformation parameters. For brevity and clarity, however, the derivation of the finite-difference form of the mass balance equation will be for a one-dimensional case. Assuming vertical and lateral homogeneity, we can integrate equation 5.1 over y and z to obtain

$$\frac{\partial}{\partial t}(AC) = \frac{\partial}{\partial x}\left(-U_x AC + E_x A\frac{\partial C}{\partial x}\right) + A(S_L + S_B) + AS_K \qquad (5.2)$$

where:

A = cross-sectional area

5.2.2 Finite Difference Formulation and Implementation of the Mass Balance Equation

The water quality model solves a finite difference approximation of equation 5.1 for the model that represents the important characteristics of small lakes, reservoirs, and tidal inlets. This section explains the derivation of the model's finite difference mass balance equation using the one-dimensional form for convenience. Regrouping the terms in 5.2 for mathematical convenience gives:

$$\frac{\partial}{\partial t}(AC) = -\frac{\partial}{\partial x}(QC) + \frac{\partial}{\partial x}(E_x A \frac{\partial C}{\partial x}) + AS^T \qquad (5.3)$$

where:

S^T =total source/sink rate $= S_L + S_B + S_K$; Q = volumetric flow = A U_x.

Assuming that derivatives of C are single-valued, finite, continuous functions of x, then the Taylor's series expansion gives:

$$C|_{x_o+\Delta x} = C|_{x_o} + (\Delta x)\frac{\partial C}{\partial x}|_{x_o} + \frac{1}{2}(\Delta x)^2\frac{\partial^2 C}{\partial x^2}|_{x_o} + \frac{1}{6}(\Delta x)^3\frac{\partial^3 C}{\partial x^3}|_{x_o} + \cdots \qquad (5.4)$$

$$C|_{x_o-\Delta x} = C|_{x_o} - (\Delta x)\frac{\partial C}{\partial x}|_{x_o} + \frac{1}{2}(\Delta x)^2\frac{\partial^2 C}{\partial x^2}|_{x_o} - \frac{1}{6}(\Delta x)^3\frac{\partial^3 C}{\partial x^3}|_{x_o} + \cdots \qquad (5.5)$$

Assuming that terms containing the third and higher powers of Δx are negligible in comparison with the lower powers of Δx, then equations 5.4 and 5.5 can be subtracted to give:

$$\frac{\partial C}{\partial x}\Big|_{x_o} = \frac{C\|_{x_o + \Delta x} - C\|_{x_o - \Delta x}}{2\Delta x} \qquad (5.6)$$

with an error term of order Δx^2, using the central-difference approximation. The forward-difference formula is given by:

$$\frac{\partial C}{\partial x}\Big|_{x_o} = \frac{C\|_{x_o + \Delta x} - C\|_{x_o}}{\Delta x} \qquad (5.7)$$

Similarly, the backward-difference formula is given by:

$$\frac{\partial C}{\partial x}\Big|_{x_o} = \frac{C\|_{x_o} - C\|_{x_o - \Delta x}}{\Delta x} \qquad (5.8)$$

Equations 5.6 and 5.8 can be obtained from 5.4 and 5.5 respectively, by assuming that the second and higher order powers of Δx are negligible. The error term for both the forward difference and the backward difference approximation is of order Δx.

Substituting the central difference approximation into the advection term of 5.3 gives:

$$\frac{\partial}{\partial x}(QC) = \frac{Q\|_{x_o + \Delta x} C\|_{x_o + \Delta x} - Q\|_{x_o - \Delta x} C\|_{x_o - \Delta x}}{2\Delta x} \qquad (5.9)$$

Similarly, the dispersion term becomes:

$$\frac{\partial}{\partial x}\left(E_x A\frac{\partial C}{\partial x}\right) = \frac{(E.A)\|_{x_o+\Delta x}\cdot\frac{\partial C}{\partial x}\|_{x_o+\Delta x} - (E.A)\|_{x_o-\Delta x}\cdot\frac{\partial C}{\partial x}\|_{x_o-\Delta x}}{2\Delta x} \qquad (5.10)$$

Substituting the central difference approximation into $\frac{\partial C}{\partial x}\|_{x_o+\Delta x}$ in equation 5.10 gives:

$$\frac{\partial}{\partial x}\left(E_x A\frac{\partial C}{\partial x}\right) = \frac{(E.A)\|_{x_o+\Delta x}\frac{C\|_{x_o+2\Delta x} - C\|_{x_o}}{2\Delta x}}{2\Delta x} - \frac{(E.A)\|_{x_o-\Delta x}\frac{C\|_{x_o} - C\|_{x_o-2\Delta x}}{2\Delta x}}{2\Delta x} \qquad (5.11)$$

When applying the difference approximations to segment "j", x_o corresponds to the centre of j, $x_o + \Delta x$ to the interface j, j+1, $x_o - \Delta x$ to the interface j-1, j, $x_o + 2\,\Delta x$ to the centre of j+1, and $x_o - 2\,\Delta x$ to the centre of j-1. The mass balance equation for segment j can be written:

$$\frac{\partial}{\partial t}(A_j C_j) = -\frac{Q_{j,j+1}}{\lambda_j} C_{j,j+1} + \frac{Q_{j-1,j}}{\lambda_j} C_{j-1,j}$$

$$+ A_j \cdot S_j^T \qquad (5.12)$$

Multiplying through by λ_j gives:

$$\frac{\partial}{\partial t}(V_j\ C_j) = -\ Q_{j,j+1}\ C_{j,j+1} + Q_{j-1,j}\ C_{j-1,j}$$

$$+\ R_{j,j+1}\ (C_{j+1} - C_j) - R_{j-1,j}\ (C_j - C_{j-1})$$

$$+\ V_j\ S_j^T \qquad (5.13)$$

where:

V_j is the volume of segment j = A_j λj; R is the dispersive flow = E A/L_c; L_c is the characteristic length.

Interface concentrations C_{jj+1} and C_{j-1j} must be expressed in terms of the segment concentrations:

$$C_{j,j+1} = \nu C_{j+1} + (1 - \nu)\ C_j \qquad (5.14)$$

$$C_{j-1,j} = \nu C_j + (1 - \nu)\ C_{j-1} \qquad (5.15)$$

where:

υ = numerical weighing factor (advection factor) between 0 and 1

Specifying υ = 0 gives a backward difference approximation for the advective term, whereas

$\upsilon = 1/2$ gives a central difference approximation.

Equation 5.13 can be extended to the multi-dimensional form actually employed by the water quality model. Consider "i" segments adjoining segment j and interfaces denoted "ij." The general equation becomes:

$$\frac{\partial}{\partial t}(V_j C_j) = -\sum_I Q_{ij} C_{ij} + \sum_I R_{ij}(C_i - C_j)$$

$$+ \sum_L V_j S_{Lj} + \sum_B V_j S_{B_j} + \sum_k V_j S_{K_j} \qquad (5.16)$$

where:

Q_{ij} = flow, defined as positive when leaving segment j, and negative when entering j

Equation 5.16 is the general expression used in the water quality model to evaluate the mass derivatives for every segment "j" during each time step "t" between initial time t_o and final time t_F. Given concentrations and volumes at t, The water quality model calculates new masses at $t + \Delta t$ using the one-step Euler scheme:

$$(V_j C_j)_{t+\Delta t} = (V_j C_j)_t + \frac{\partial}{\partial t}(V_j C_j)_{t+\Delta t} \Delta t \qquad (5.17)$$

where:

Δt=the time step.

Given new masses at time t + Δt, The water quality model finds the new concentrations by dividing by the new volumes:

$$C_{j,t+\Delta t} = (V_j\ C_j)_{t+\Delta t} / V_{j,t+\Delta t} \qquad (5.18)$$

The new volumes are calculated internally from the computed flow fields using the principle of continuity.

5.2.3 Advective Transports

Advective water column flows directly control the transport of dissolved and particulate pollutants in small water bodies. In addition, changes in velocity and depth resulting from variable flows can affect such kinetic processes. An important early step in any water quality modelling study is to simulate water column advection properly by the hydrodynamic model and to use it as an input to the water quality model. Dispersive transports are discussed in Section 5.2.5.

5.2.4 Evaporation and Precipitation

In small lakes and reservoirs, evaporation and precipitation play a significant role in the overall water balance. Precipitation may be a low level source of some pollutants. Evaporation concentrates pollutants in the body of water. Therefore in the water quality model, evaporation and precipitation are used as input parameters. Evaporation or precipitation rates may be defined as varying with time. The precipitation input to segment i, at time t, is given by:

$$\frac{\partial M_i}{\partial t} = P_i(t)\ A_i\ C_{oi}(t) \qquad (5.19)$$

where, $P_i(t)$ is the precipitation time function for segment i, A_i is the surface area of segment i, $C_{oi}(t)$ concentration of pollutant in precipitation.

In addition, segment volumes are adjusted:

$$\frac{\partial V_i}{\partial t} = A_i\ (P_i(t) - E_i(t)) \qquad (5.20)$$

where:

$E_i(t)$ = evaporation time function for segment i

5.2.5 Formulation of Vertical Exchanges

In lakes and reservoirs, the concentration can change over a short distance in the vertical direction. Consequently they require a grid size that is much smaller in the vertical direction than in the horizontal direction. The set up can be visualized by considering the fluid motion in horizontal slices, with an exchange between these slices for the mass.

Since considerable variation in concentrations can exist in the vertical direction, it is useful to compute momentum and mass fluxes in the different layers of the system. This requires integration of equations 5.1 through 5.5 over the height of the layer. The layout of the depth grid used is shown in Figure 4.1. Modelling of Long Lake requires vertical resolution in the flow field. In particular it is desirable to separate the dynamics of the euphotic mixed layer from that below it. To provide this resolution, a subroutine was constructed to compute the 0 to 5m flow, the 5m to bottom depth flow, and the vertical flow

between them. The formulation is described in detail in Appendix B.

The degree of vertical mixing between two layers in Long Lake is an important parameter that determines the vertical gradients of water quality as shown in eqs. (5.21) and (5.22) (Thomann and Mueller 1987).

$$s_1 = \frac{(W_1 + \beta W_2)/Q}{1 + (1-\beta)E_{12}/Q + V_1 K_1/Q} \qquad (5.21)$$

$$s_2 = \beta \left(s_1 + \frac{W_2}{E_{12}} \right) \qquad (5.22)$$

where, s_1 and s_2 are the concentrations of a substance in layer 1 and layer 2 respectively, W is the load, Q is the flow (Appendix B), E is the vertical dispersion coefficient, K is the first order decay rate, V is the volume of the layer, and

$$\beta = \frac{E_{12}}{E_{12} + V_2 K_2}$$

The temperature profile method was used for computation of vertical diffusion coefficient. Water temperature profiles have been used extensively and for many years for estimating vertical dispersion in lakes and reservoirs. For a steady state case the heat balance equation for hypolimnion with assumptions (1) heat entering the lake has been dissipated at the bottom of the first layer (2) "s" to represent the temperature with no sources, sinks or decay of heat, is given by:

$$V_2 \frac{\Delta T_2}{\Delta t} = \frac{E_{12} A_{12}}{\overline{z}_{12}} (T_1 - T_2) \qquad (5.23)$$

where the first term on the left is the time rate of change of temperature T_2 in layer 2 in ^{o}C, T_1 is the temperature of the upper layer. Equation (5.23) states that the change in temperature of the second layer is due entirely to the heat flux from the exchange between the two layers. If T_1 and T_2 are known from measurements, then equation (5.23) can be used to estimate E_{12}.

$$E_{12} = \frac{|T_2^{(t-1)} - T_2^{(t)}| V_2 \overline{Z_{12}}}{(T_1 - T_2) \Delta t A_{12}} \qquad (5.24)$$

A lotus spreadsheet was used to calculate the vertical diffusion coefficient variations for the whole year showing considerable seasonal variations as shown in Chapter 8.

5.2.6 **Water Quality Parameters**

The constituent transport relationships compute the transport of all constituents with their unit volume reaction rates expressed in the source and sink terms. Both internal and external sources and sinks are specified. All external boundary constituent sources and sinks and all internal sources and sinks due to reactions are computed for all nonconservative materials. The source and sink term, represents a mass rate of change (grams per second) of a constituent due to kinetic reactions.

5.2.6.1 **Conservative Tracer**

A conservative constituent has been modelled, which will mimic field experiments, such as, dye studies and movements of conservative materials through the water body. The conservative constituent has been used to aid in calibrating and testing flow regimes. As a conservative material, this constituent has no internal sources or sinks.

5.2.6.2 **Inorganic Suspended Solids**

Inorganic suspended solids are important in water quality simulations because of their influence on both density and light. Increased solids concentrations reduce light penetration in the water column affecting temperature distribution. Nearly all biological and chemical reactions are temperature dependent. Nutrient concentrations are also affected by solids through adsorption and settling. Light and nutrient availability largely control algal production.

The equation for the sources and sinks for inorganic suspended solids is given by (USEPA 1985):

$$C_{ss}(K, I, 2) = \omega_1 V C_2 / \Delta z \qquad (5.21)$$

where; ω_1 is the settling velocity, m sec^{-1}; V is the cell volume, m^3; C_2 is the suspended solids concentration, g m^{-3}; Δz is the cell thickness, m.

In the finite difference representation of suspended solid concentrations, the solids settled from layer K-1 of segment I serve as a source for the layer below it, K. However, only a fraction (F) is allowed to settle to the K layer as determined by the ratio of their widths,

B(K,I)/B(K-1,I). The remaining portion (1-F) is lost to the sediments. No provision is made to accumulate inorganic solids or allow resuspension in the sediments. In reality, concentrations generally decrease with distance away from the dominant flow path. This effect is not included.

5.2.6.3 **Coliform Bacteria**

Coliform bacteria is commonly used as an indicator of pathogen contamination. Safety standards and criteria for drinking and recreational purposes are based upon coliform concentrations. Predictions of coliform bacteria are important because of their impact on recreation and water supply.

The equation for the sources and sinks for coliforms is given by: (USEPA 1985, Zison et al 1978):

$$C_{cb}(K,I,3) = -K_c\theta^{(T-20)}VC_3 \qquad (5.22)$$

where; K_c is the death rate, sec^{-1}; θ is the temperature correction factor; T is the water temperature, °C; V is the cell volume, m^3; C_3 is the coliform concentration, g m^{-3}.

The Q10 formulation arises from a doubling of the reaction rate with each 10°C increase in temperature. This doubling rate has not been found at lower temperatures (Hargrave 1972b) and is quite variable for various reactions (Giese 1968).

5.3 Physical processes controlling near field plume dispersion:

Near-field constitutes the region of a receiving water where the initial jet characteristic of

momentum flux, buoyancy flux and outfall geometry influence the jet trajectory and mixing of an effluent discharge. The near-field stability depends on the amount of local recirculation and re-entrainment of already mixed water back into the buoyant jet region. Stable discharge conditions are associated with weak momentum and deep water and are also sometimes called deep water conditions. Unstable discharge conditions have localized recirculation patterns and are also called shallow water conditions. Far-field is the region of the receiving water where buoyant spreading motions and passive diffusion control the trajectory and dilution of the effluent discharge plume. Far-field Processes that affect the sewage - physical mixing mechanisms that are dominated by the ambient receiving water conditions particularly ambient current velocity and density differences between the mixed flow and the ambient receiving water. Far-field mixing processes (buoyant spreading) which arise due to the buoyant forces caused by the density difference between the mixed flow and the ambient receiving water.

The geometric and dynamic characteristics of a receiving water body (ambient conditions) that impact mixing zone processes include shape, vertical cross sections, bathymetry, ambient velocity, and density distribution. The velocity field within the receiving water (ambient currents) which tends to deflect a buoyant jet into the current direction. In the example discussed in this thesis, the sewage effluent mixing is caused by a combination of initial momentum flux and buoyancy flux (buoyant jet) which is also called a forced plume. Pure Jet is a discharge where only the initial momentum flux in the form of a high velocity injection causes turbulent mixing. It is also called momentum jet or non-buoyant jet. However, a pure plume is a discharge where only the initial buoyancy flux leads to local vertical accelerations which then lead to turbulent mixing. Buoyant surface discharge is the release of a positively or neutrally buoyant effluent into a receiving water through a canal, channel, or near-surface pipe. The discharge conditions, such as, the geometric and flux characteristics of an outfall installation affect the mixing processes. These geometric and flux characteristics include port area, elevation above the bottom and orientation, effluent discharge flow rate, momentum flux, and buoyancy flux.

Hydrodynamic mixing processes constitute the physical processes that determine the fate and distribution of effluent once it is discharged and the hydrodynamic mixing zone that represent the zone of strong initial mixing where the so called near-field processes occur. It is the region of the receiving water where outfall design conditions are most likely to have an impact on in-stream concentrations. We also need to consider intermediate-field effects where induced flows in shallow waters extend beyond the strictly near-field region of outfall.

TABLE 5.1

Water quality model characteristics

Water body	Small lakes, reservoirs and tidal inlets of area of few sq Km, strong response to wind, inflow and outflow.
Computer	IBM 486 or compatible with math co-processor or mainframe.
Model type	event or long term depending on the capacity of the computer.
Time step	Few seconds to several minutes depending on the modelling strategy.
Cell structure	Square grid, dimensions of the grid according to the details of representation of the model.
Input parameters	inflow/outflow, wind, bathymetry, precipitation and evaporation and diffusion coefficients.
Representation of stratification	By two or more layers, the top layer accounts for water level variation. The bottom layer takes into account any high density flows such as road salt and for vertical diffusion rates.

Chapter 6

FIELD EXPERIMENTS AND RESULTS

Field measurements were made for the purposes of the validation of the models developed during this study and the details are as follows:

6.1 Long Lake

6.1.1 Description of the Study Area

Long Lake has an area of about 204.8 ha, watershed land area of about 1066 ha, and maximum depth of 30.2 m (Table 6.1). The dam at the south east end of Long Lake is provided with a sluice gate and a spillway section. The Long Lake watershed can be represented by twenty subwatershed units, representing all drainage systems within this area. The area of each unit, along with the lake into which the unit drains, with the soil type, slopes and vegetation were reported by Sunderland, Preston & Simrad (1974). The three larger subwatersheds constitute nearly 65 % of total watershed area and have defined collector and tributary streams.

The climate of the area is humid and characterized by cold winters and mild summers. The mean annual air temperature in Halifax is 6.8°C. Distribution of rainfall throughout the year ranges from a low of 6.2 % of the year's precipitation in June, to a high of 11 % in November, based on mean monthly records of precipitation in the Halifax area for the period 1941-1971. The mean annual rainfall in the Long Lake area is 1380 mm (Sutherland et al. 1975).

Long Lake has been studied for over a decade (Waller *et al.* 1983) as part of the Halifax Urban Watershed Program (HUWP). Currents in the lake are produced mainly by

wind and flow-through. However, the width of Long Lake is much greater than the width of the inlet and the outlet and the flow-through gradient currents are small in comparison to currents produced by external forces such as wind, particularly during periods of strong wind.

Halifax Urban Watersheds (Figure 1.1) which constitute Long Lake, Chain Lakes, Chocolate Lake and their watersheds, were the water supply source for the city of Halifax, until May 1977. In May 1977, when Pockwock treatment plant was commissioned, the supply was changed. This resulted in the release of the Halifax Urban Watersheds for development. The largest lake (Long Lake) was released for development, Chain Lake is being retained and protected from development and Chocolate Lake is surrounded by a completely developed watershed (Waller et al.1983). The Centre for Water Resource Studies started the Halifax Urban Watershed Program using this unique situation to carry out

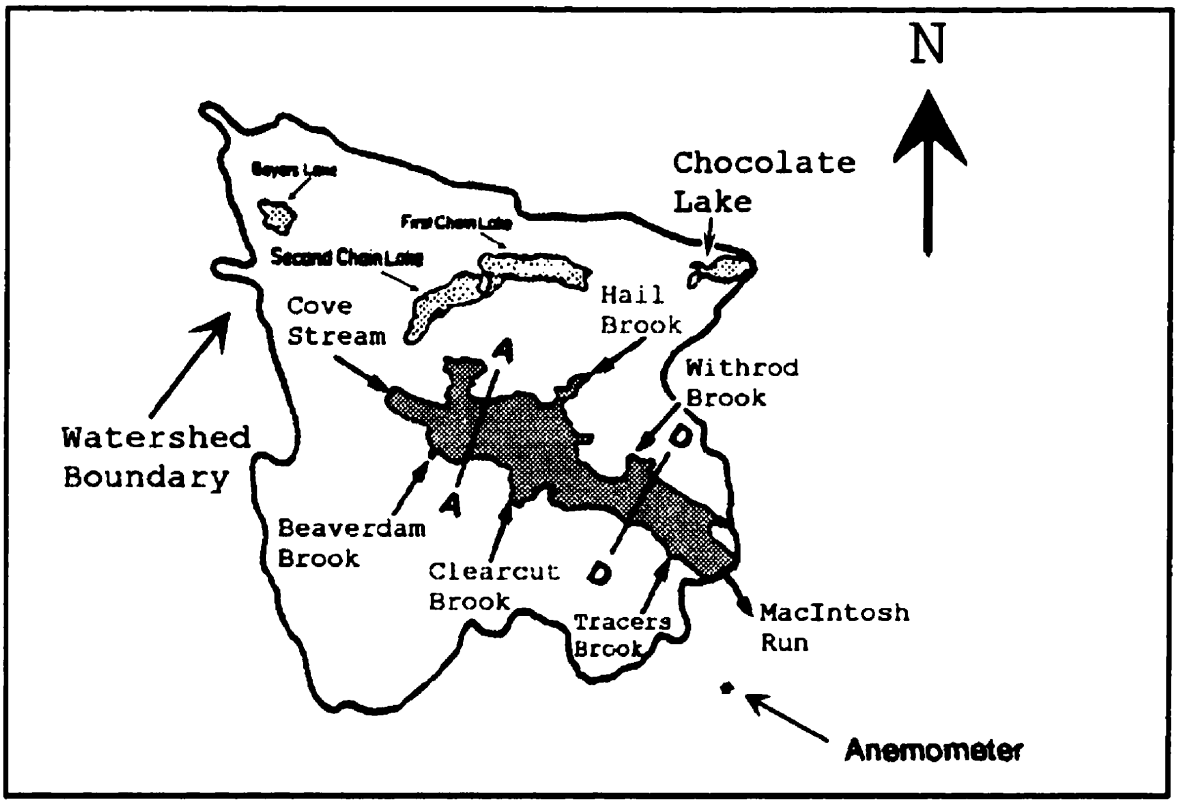

Figure 6.1 Long Lake inflows and outflow

research to monitor lake water quality, hydrological and meteorological parameters, land use as well as to study the response of the watershed and lakes to these causal factors.

Long Lake is the largest lake in the watershed and has two major inflows (Cove Stream and Beaverdam Brook) and five minor inflows (Tracers Brook, Clearcut Brook, Cranberry Pond inflow, Hail Brook and Withrod Brook). The outflow from Long Lake is at the end opposite to where cove stream discharges into Long Lake. This outflow, known as MacIntosh Run flows a distance of approximately 4.1 km before it flows into the Atlantic Ocean. During 1977 to 1984, a pipe discharged via a blow off into Beaverdam Brook, one of the perennial streams discharging into Long Lake. This pipeline originates from Spruce Hill Lake (a lake located outside the watershed area) and provided the high pressure gravity supply directly to the City distribution system. This blow off pipe discharges into the Beaverdam Brook. In the southeastern end of Long Lake, a dam with a controlled sluice gate and overflow provides the control for lake level.

The chemical loadings into the lakes within the Halifax Urban Watersheds are a result of direct precipitation, watershed runoff and groundwater effects. The factors influencing the loadings are particulates in the air, residence time of water in the watershed, land slopes, soil types and vegetal cover.

The major types of bedrock found in the watersheds are granite and shale, with granite underlying about 90 % of the watershed lands west of the Chain Lakes. An extensive system of faults and fractures criss-crosses the watershed area, and this may have considerable effect on water quality (Sunderland *et al.* 1975, MacDougall *et al.* 1963, Fraser J. 1986). These faults and fractures may enhance the entry of pollutants from the watershed lands to lakes without being absorbed by the soil.

Soil cover in the watersheds in most areas is shallow being only a few inches deep. The soil consist primarily of Gibraltar, Wolfville and Halifax soils and are similar through out the watershed area (MacDougall *et al.* 1963). Soil types such as Aspotogen, Bayswater

and Rockland are also found in the watersheds. The vegetation in the watershed area is in an early stage of regeneration following logging or burning that took place several decades ago. The largest specimens found in the watersheds are Spruce, Hemlock and White Pine. Long Lake watershed is divided into twenty subwatershed units representing all drainage systems within this area. The larger subwatersheds constitute nearly 65 % of total watershed area and have defined collector and tributary streams. Average annual precipitation is 1630 mm approximately based on 1971 to 1975 data (Byers 1983). Distribution of rainfall throughout the year ranges from a low of 6.2 % of the year's precipitation in June, to a high of 11 % in November, based on mean monthly records of precipitation in the Halifax area for the period 1941-1971. A large parcel of land west of the watershed, including some watershed land was acquired by the city of Halifax for industrial, residential and recreational purposes. These developments are expected to have some effects on the chemical characteristics of the water flowing into Long Lake, both as overland flow and ground water seepage. The physical characteristics of Long Lake is presented in Table 6.1.

6.1.2 **Field Measurements**

Field measurements were conducted to obtain the required data on water levels, lake circulation, wind speed and direction, temperature and chloride distributions, so that the numerical models could be validated. Measured lake level data was used to verify the seiches and wind set up predicted by the numerical hydrodynamic model. Surface currents were measured using drogues and used to verify model predictions of circulation. Chloride measurements were used for verification of water quality model predictions. These field measurements required several equipment, such as, an aluminum boat, paddles, life jackets, anchor, stop watch, drogues, theodolite, electronic distance meter (EDM), Temperature-chloride recorder, water sampler, etc.

6.1.2.1 **Wind speed and direction**

Wind speed and direction were measured on an hourly basis at CJCH site (Figure 6.1) using the existing data acquisition system. An anemometer was connected to the data acquisition system which measured wind speed and direction. The wind measurements were made at about 7 m height above ground level for 2 min every hour along with the maximum wind speed that occurred during the last 10 min of the hour. The vectorial average of this 2-minute record was the representative average wind for that hour. Wind data was recorded for the period from 1400 hr. of August 4, 1989 to 1100 hr of August 11,1989 (Figure 6.2).

6.1.2.2 **Temperature, Conductivity and Dissolved Oxygen**

To understand the spatial distribution of thermal stratification in Long Lake, temperature profiles were measured at 11 lake locations (Figures 6.3) and the lake inflow and outflow locations. Monthly measurements (June to August 1983) were carried out at all 11 locations, to decide on periods during which multi-layer modelling is required (Figures 6.4 to 6.8). Temperature was measured using a portable direct reading temperature probe at every one meter depth intervals. Water depth at the sampling location during the period of measurements was also noted. Measured dissolved oxygen profiles at the deepest location (Figure 6.9) obtained from CWRS was used to evaluate the effect of stratification on Long Lake waters.

6.1.2.3 **Water level and seiches**

For the verification of seiche amplitude and its period, water levels were recorded (Figure 6.10) every 1 min. Measurements of water levels at cove stream end and outlet end for different wind conditions (Figure 6.11) were used to verify wind set up.

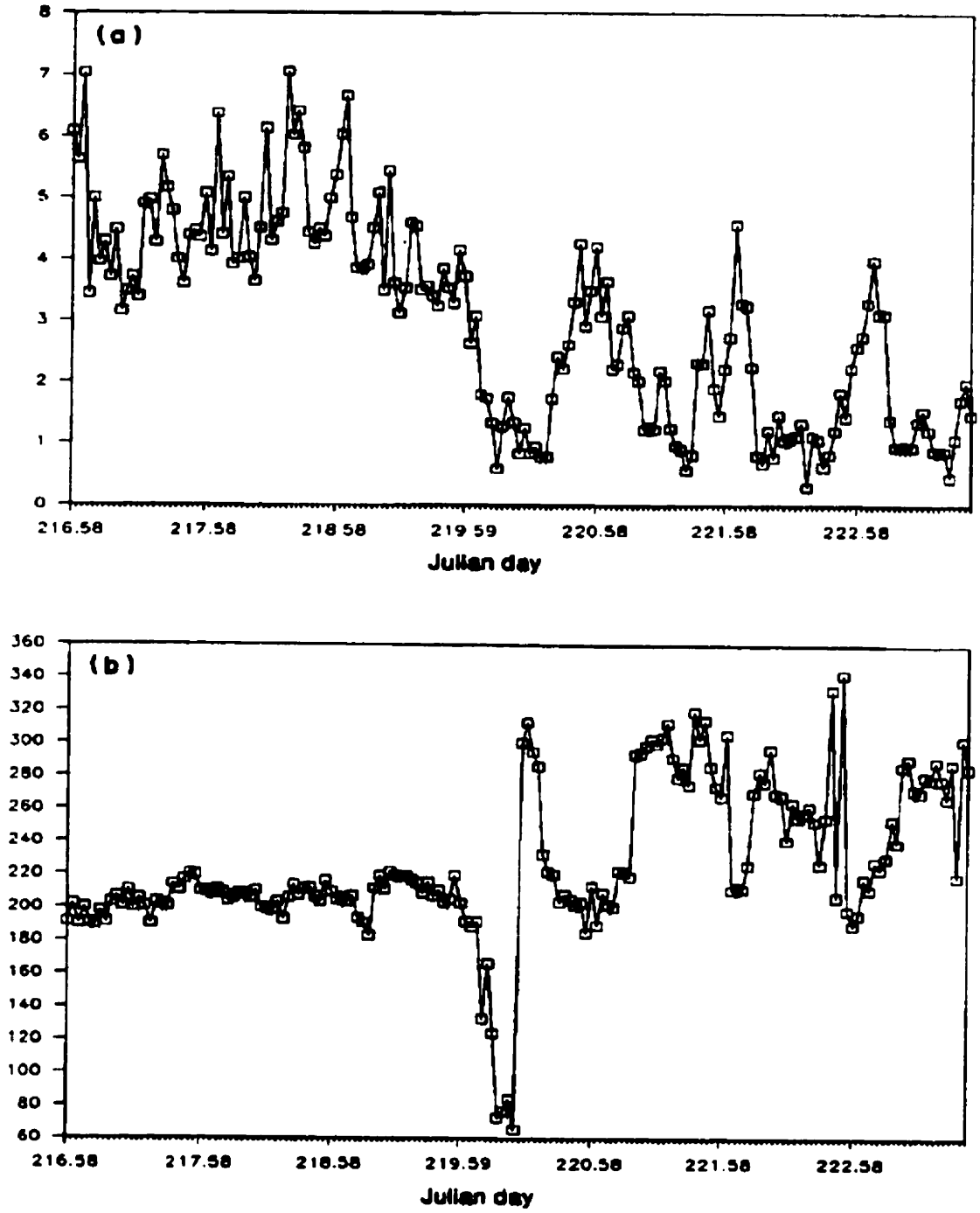

Figure 6.2 Recorded wind speed (m/s) [(a)] and wind direction (°N) [(b)]

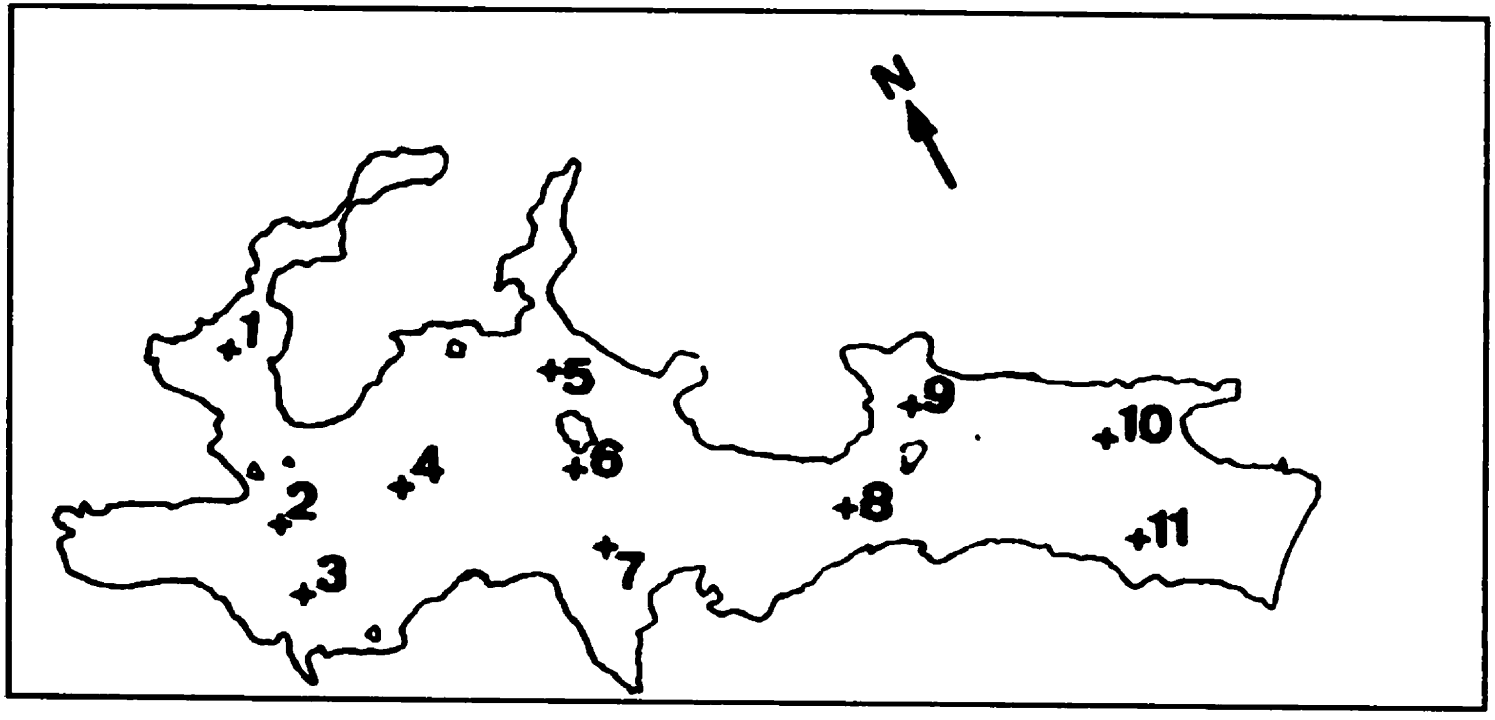

Figure 6.3 Long Lake profiling stations

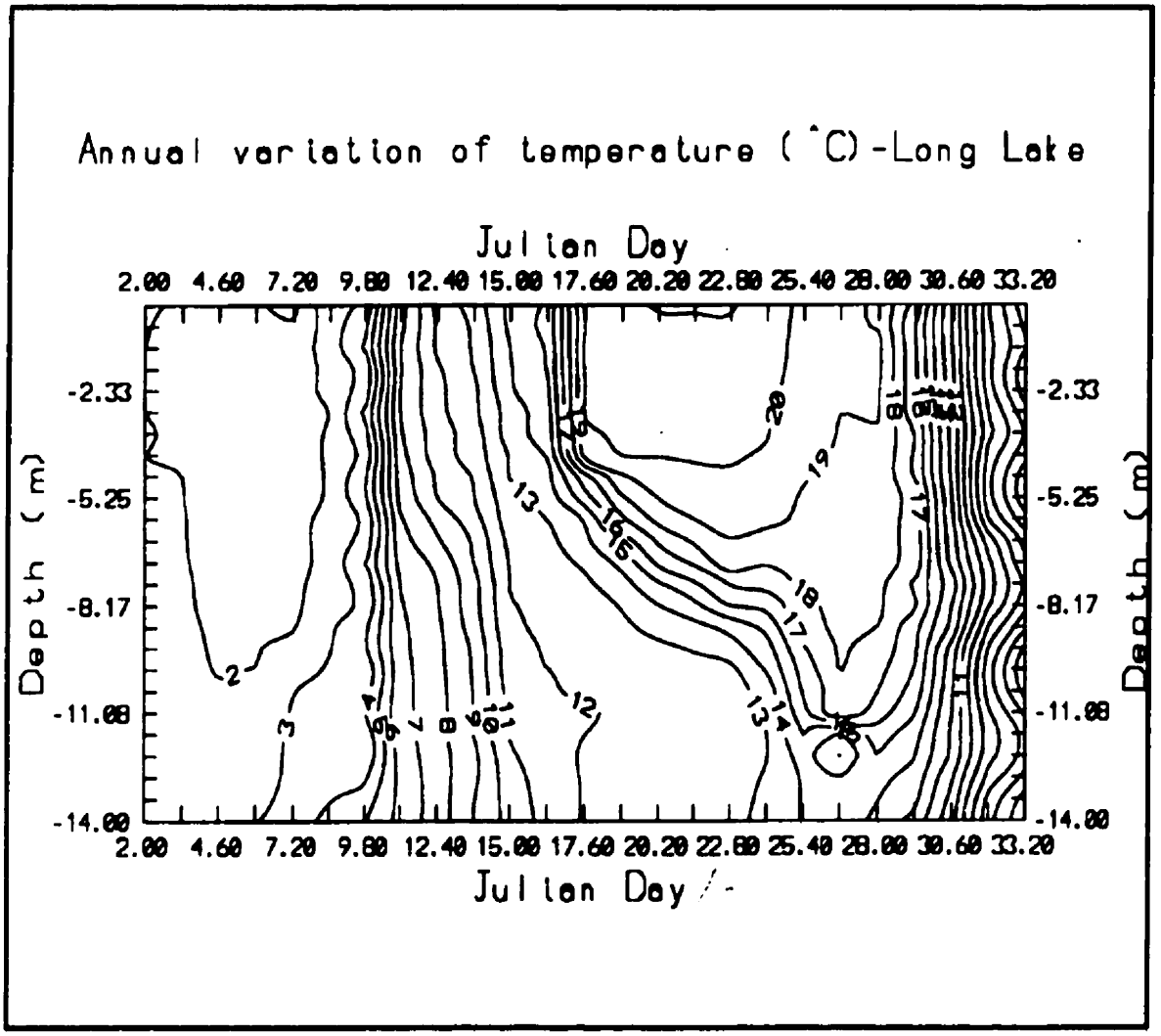

Figure 6.4 Temperature variations at the deepest location in Long Lake with depth and time for year 1983 (Based on CWRS Long Lake data)

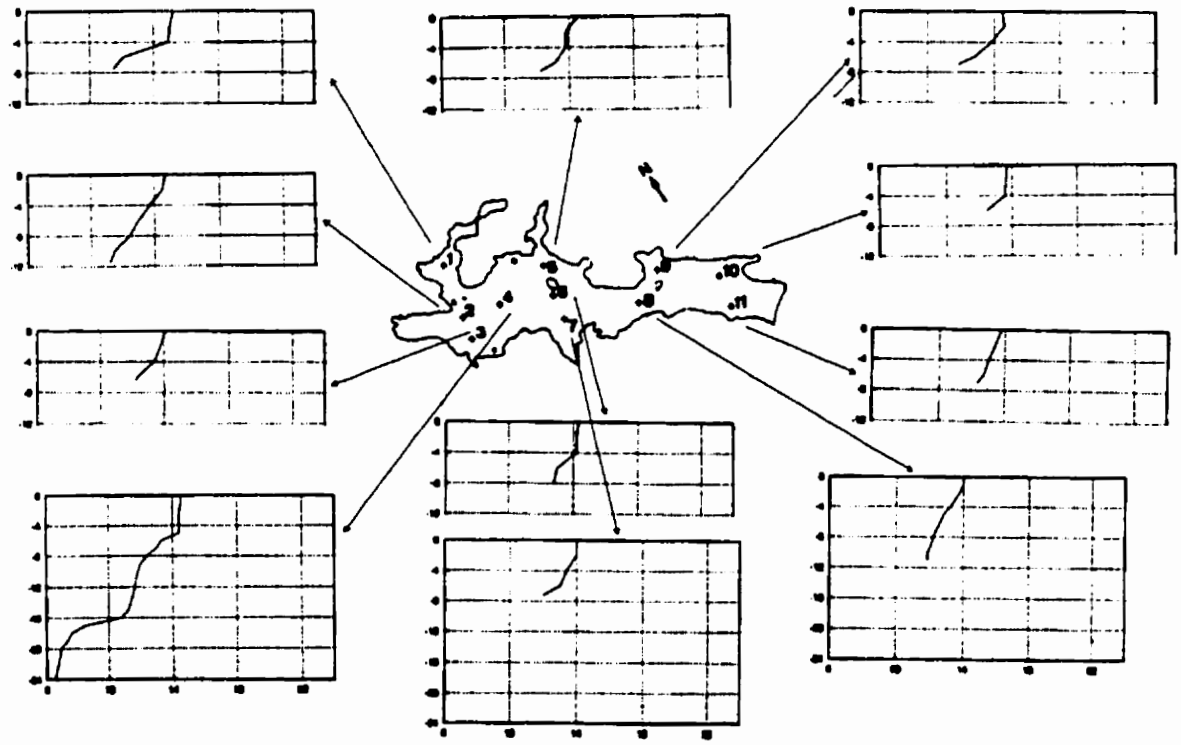

Figure 6.5 Vertical profile of temperature in Long Lake - June 7, 1983

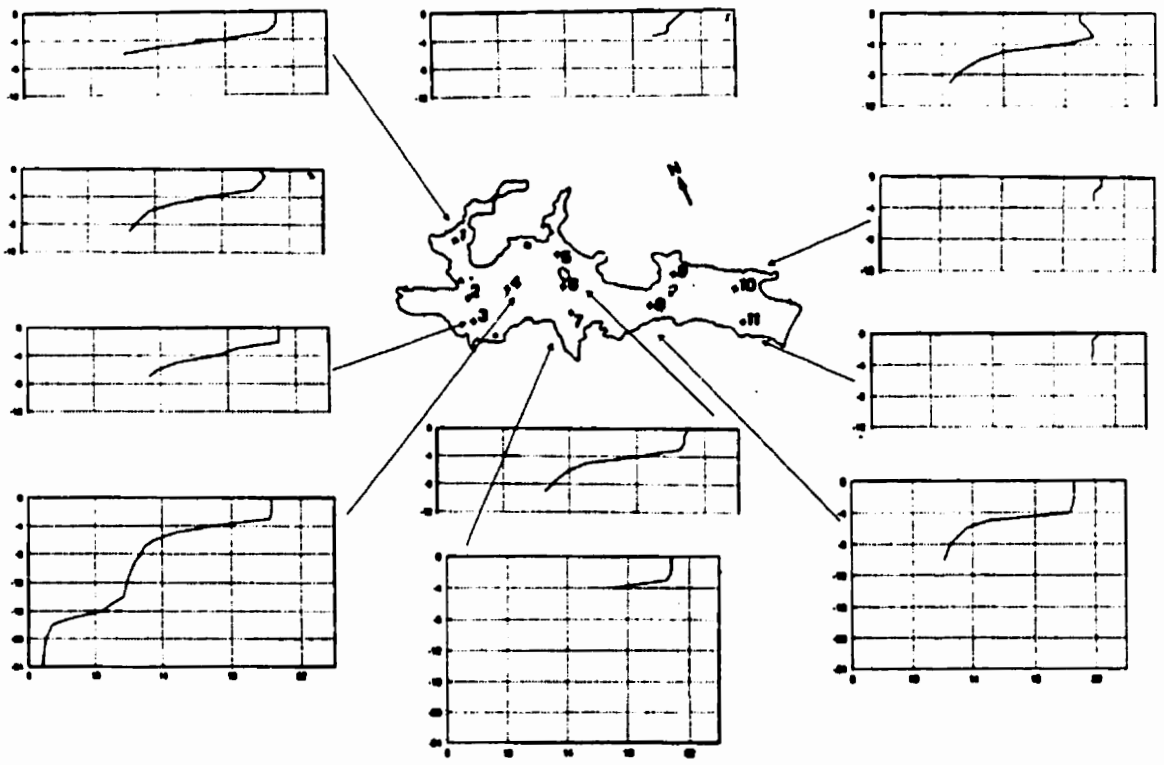

Figure 6.6 Vertical temperature profile in Long Lake - June 28, 1983

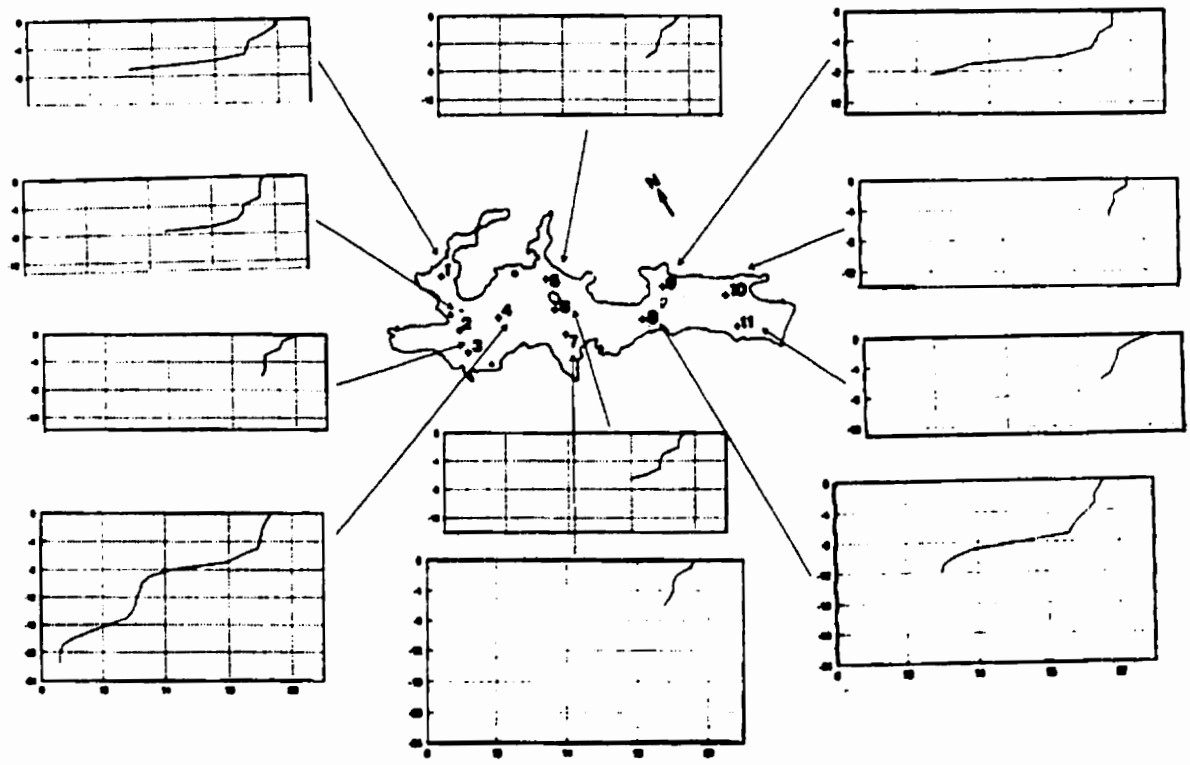

Figure 6.7 Vertical temperature profiles in Long Lake - July 27, 1983

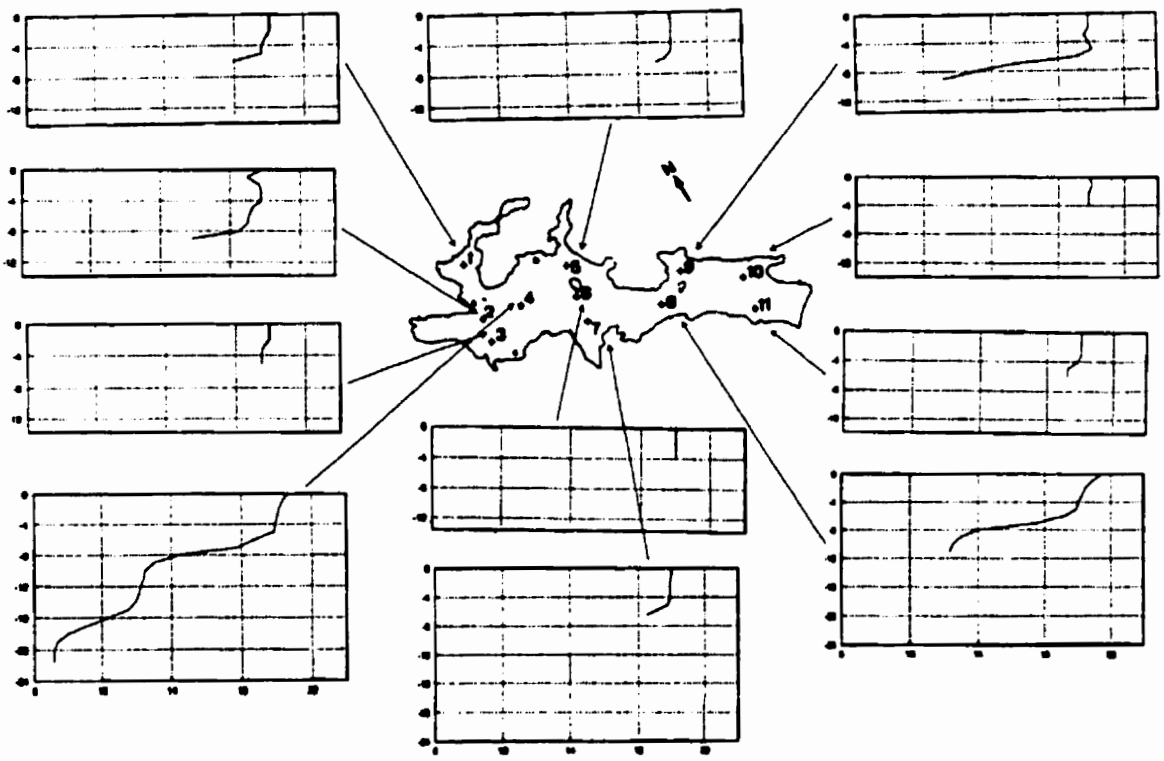

Figure 6.8 Vertical temperature profiles in Long Lake - July 27, 1983

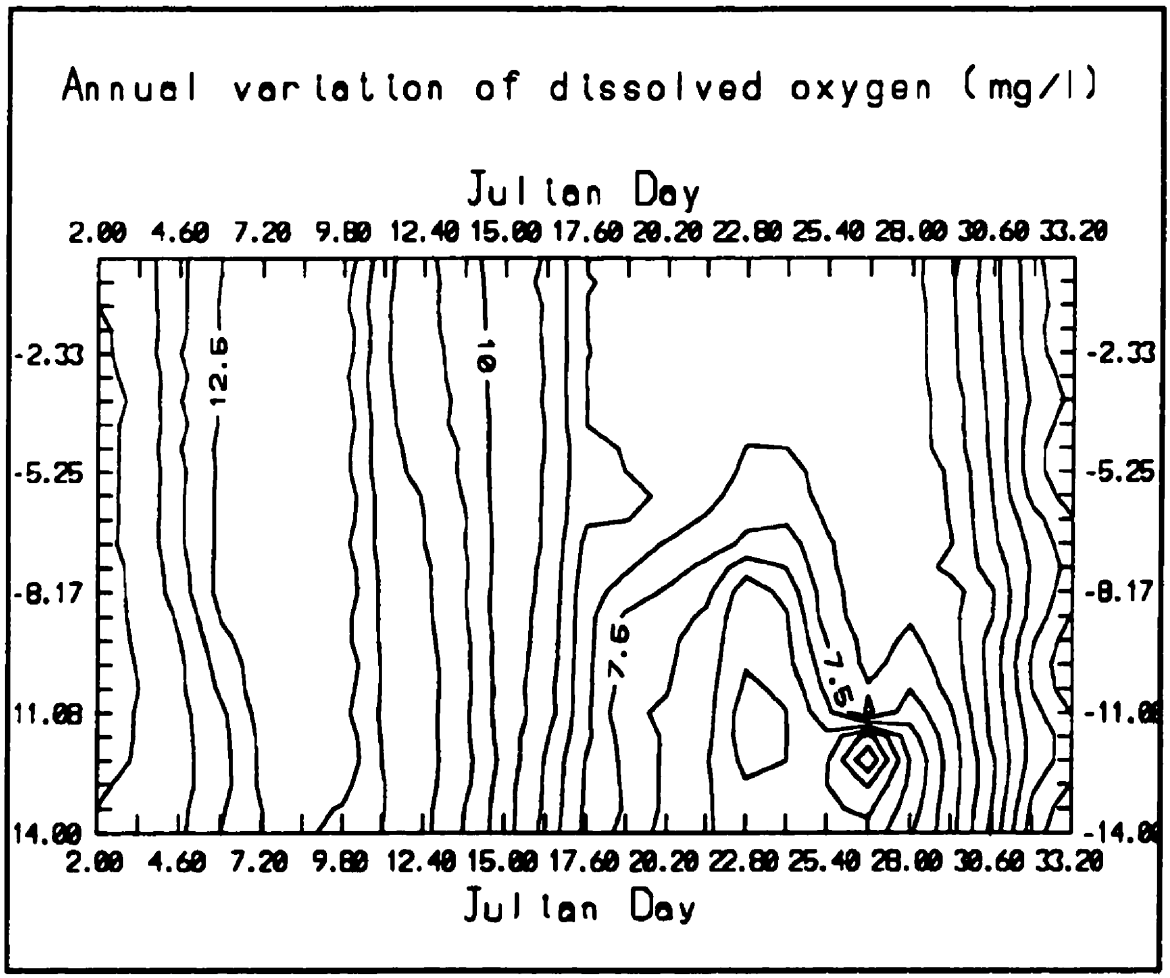

Figure 6.9 Dissolved oxygen variations at the deepest location in Long Lake with depth and time for year 1983 (Based on CWRS Long Lake data)

6.1.2.4 **Drogue tracking**

Current meters presently available cannot measure with sufficient accuracy low velocity currents in small lakes and reservoirs. Therefore, drogue measurements which are more suitable for low velocity measurements were conducted for obtaining the required circulation data for Long Lake. The drogue used in this study was designed (Figure 6.10b) such that only a minimum portion of the drogue was above water, to reduce the errors in measurements due to wind drag effects. Drogue measurements were carried out at many locations in the lake on August 25, 1988, and August 9 and 11, 1989 (Figure 6.13). Relatively strong wind conditions persisted on August 9, 1989 during which period field measurements were made using drogues.

The data collected were corrected for the effect of wind on the drogue. Tracking of the float was carried out using two theodolite stations and by triangulation. The distance between theodolites was measured using Electronic Distance Measuring System (EDM). Simultaneous measurement of wind was also carried out as explained earlier. The drogue consists of two underwater sails made of canvas in a vertical plane intersecting at right angles. On the upper and lower edges, the sails are fastened by wooden battens 1.2 m long. The drogue was attached to a small surface buoy to provide the surface flotation. The weight of the drogue was adjusted to make it slightly positively buoyant. The drogue aligned itself at right angles to the flow after travelling a couple of meters, maintained the orientation of the flow. The drogues were weighted so that the surface area exposed to the wind is kept to a minimum and hence truly follows the water flow. A few surface current measurements due to streamflow during calm winds were carried out using surface drifters at stations near major streamflow locations. The drogue was released from a aluminum boat fitted with an outboard motor at a number of locations and was continuously tracked with theodolites.

6.1.2.5 Circulation and Water Quality

Wind plays a major part in the lake mixing processes and varies significantly both in speed and direction (Figure 6.2). Assessments of lake stratification and circulation were made using the measured data collected from Long Lake. A strong thermocline developed around mid-June in Long Lake and continued to exist until mid-October. The effect of this thermocline (Figure 6.4) in restricting the mixing is quite visible from the vertical distribution of dissolved oxygen (Figure 6.9) during the summer months. Measured annual temperature distribution in Long Lake for the deepest location shows that strong vertical mixing takes place in the lake during all seasons except summer (Figures 6.4). Measurements of temperatures at 11 lake stations carried out at monthly intervals during summer show that strong thermocline persist even in the embayments (6.5 to 6.8). Strong thermal stratification during summer restricts the quantity of water available for circulation and mixing, and hence the dilution of pollutants introduced into the lake. During summer, thermocline starts at a depth of about 6m and the lake volume available for circulation and mixing is limited to the upper 0-6m, which was about 65% of the total lake volume. Presence of two to three separate layers were identified during this period in Long lake. Epilimnion generally occurs from 0 to 6 m and hypolimnion from 8 to 32 m. They are separated by a zone of rapidly changing temperatures, ie. thermocline or metalimnion which are about 2 m in thickness during summer.

The seasonal variation of dissolved oxygen shows gradual decrease of dissolved oxygen with increase in water temperature. The dissolved oxygen concentration shows strong vertical mixing during fall, winter and spring seasons (Figure 6.9). During summer, the hypolimnetic (below about 7 m water depth) oxygen shows depletion with a lowest value of about 5 mg/l (Figure 6.9). This indicates that vertical mixing of the oxygen rich surface layer to the bottom layer is inhibited by the thermocline. This reduces the dissolved oxygen content in the deeper waters, during summer, to a minimum of 5 mg/l (in comparison to 8

mg/l in the surface waters). This according to environmental guidelines (Halifax Harbour Task Force, 1990) is the minimum necessary for fish propagation. It drops even below this value in fall and is probably related to the two well defined thermal discontinuities present during the summer period. This shows that, even during fall, the vertical mixing was not large enough to penetrate the lower thermocline and was probably the cause for the continued low dissolved oxygen content in the bottom layer. This justifies the two layer system representation for Long Lake. Vertical distribution of temperature was used to compute the vertical diffusion coefficient used as an input to the water quality model. The computed seasonal variation of vertical diffusion coefficient shows that it is minimum during summer showing that a two layer modelling scheme is required for the summer period.

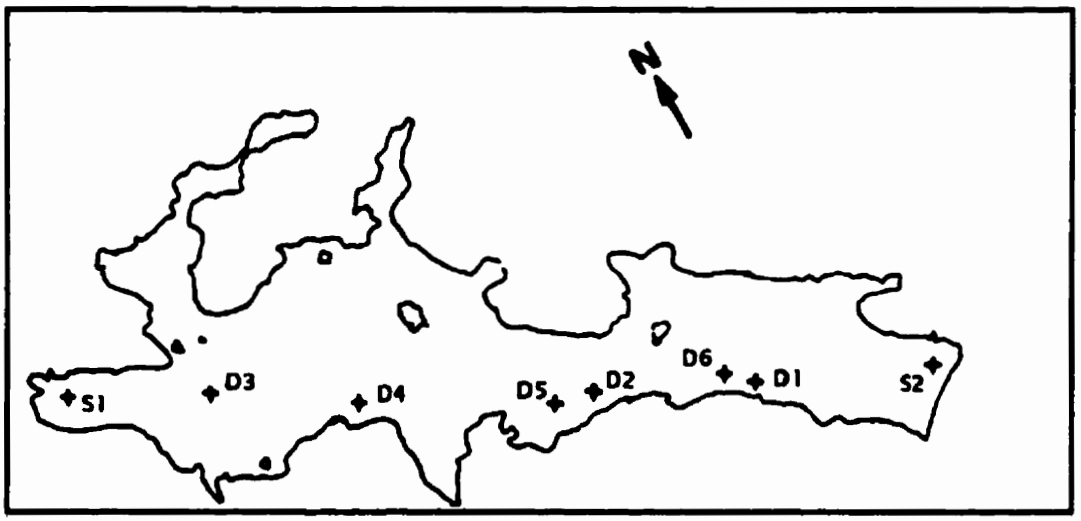

Figure 6.10 Long Lake drogue and seiches measurement stations.

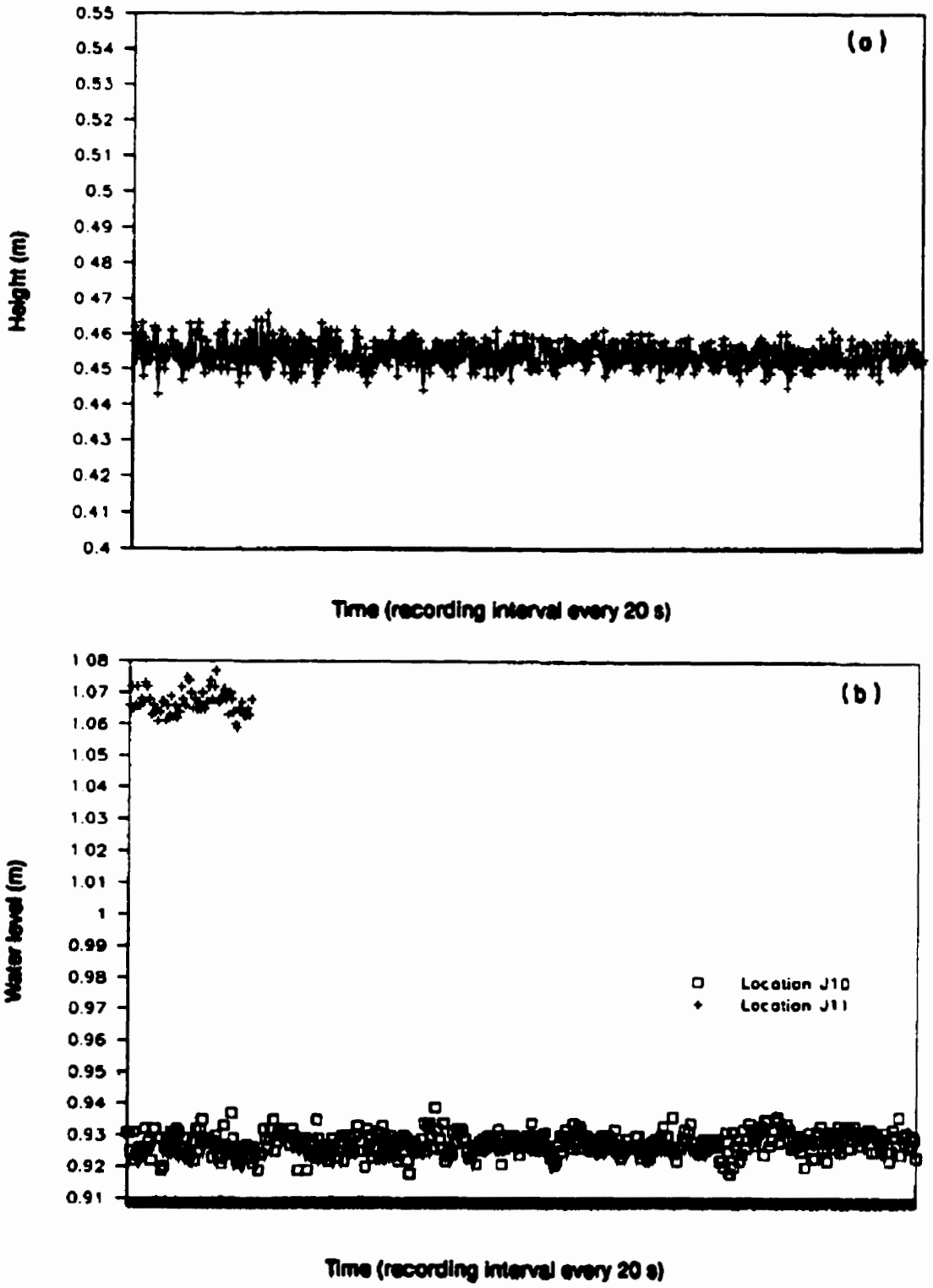

Figure 6.11 Measured seiches (a) at cove stream end and (b) outlet end.

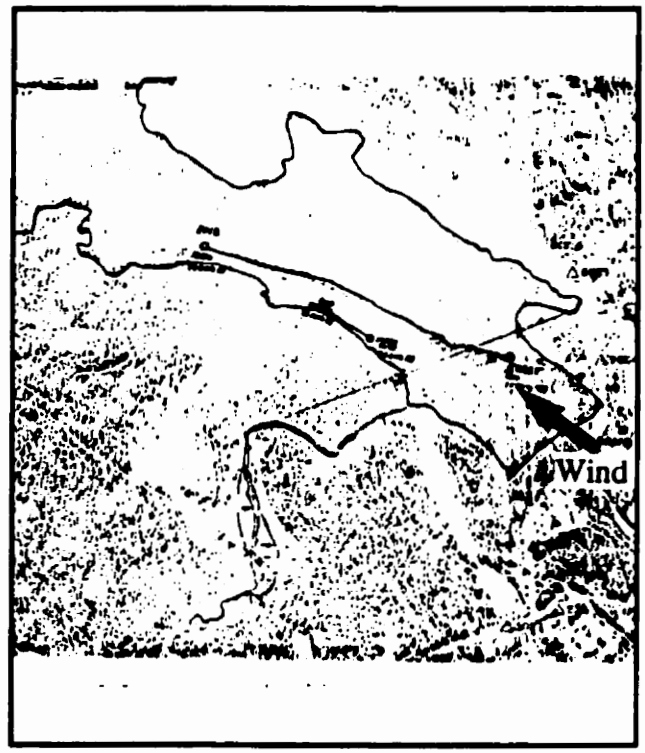

Figure 6.12 Observed drogue tracks for southeast wind - 1988

The recorded maximum wind speed was 2.7 m/s from northwest, on 9 August 1989. Measured drogue tracks are presented in Figures 6.12 and 6.13. Measured seiches at two end of Long Lake (cove stream end and outlet end) are presented in Figure 6.12. Model simulations were made for the corresponding days of drogue measurement with the existing boundary and initial conditions and the results were compared in Chapter 7.

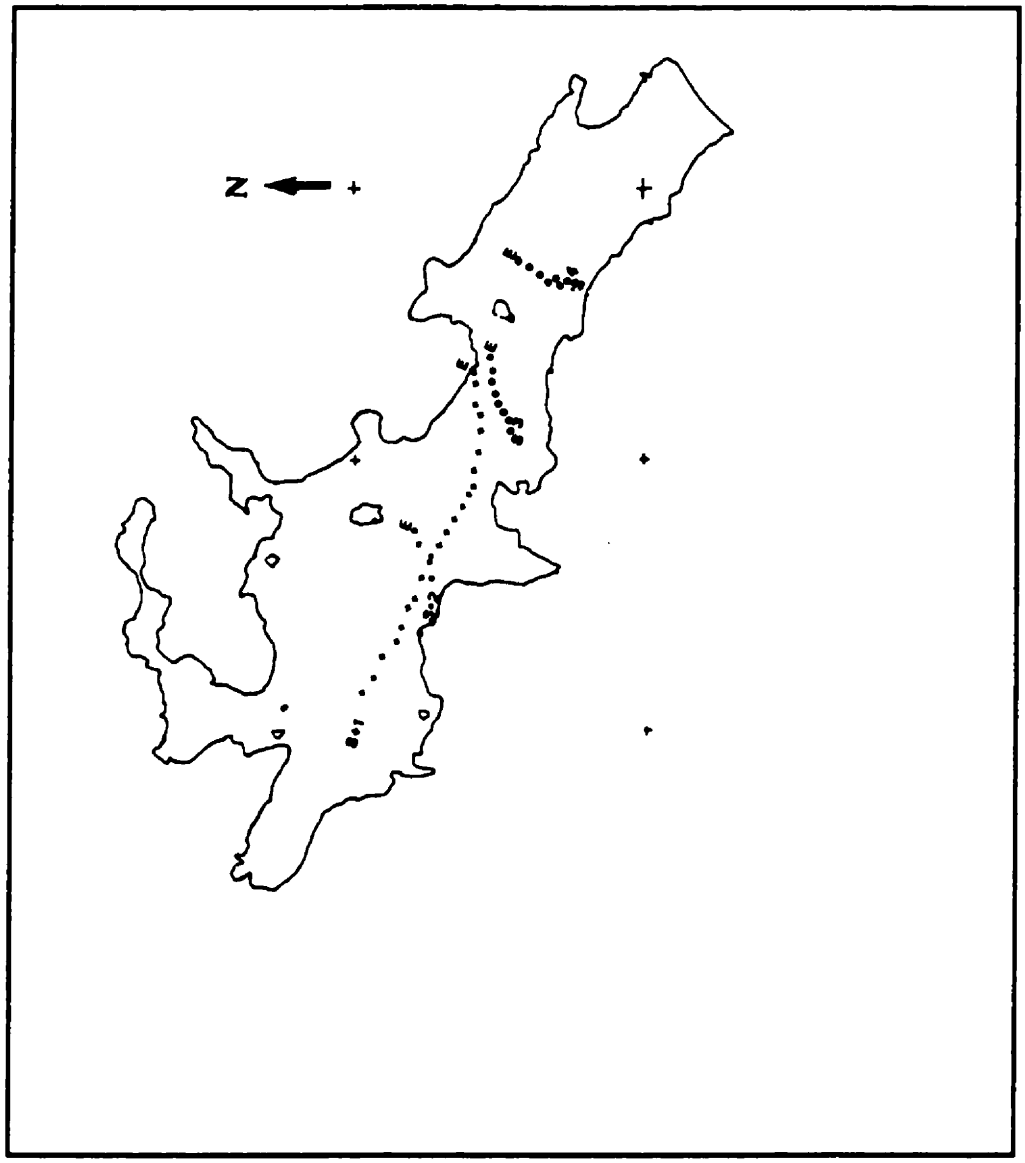

Figure 6.13 Observed drogue tracks for wind from NW (s1) and SW (s2, s3 and s4)- 1989

6.2 Parr Inlet

6.2.1 General

Parr Inlet is located on the northern tip of Ellesmere Island and is the most remote Arctic community in the Northern Hemisphere (Heroux, J.A. 1985). The physical features of Parr Inlet are presented in Table 6.2. The annual average air temperature in the Parr Inlet area is -18°C. July and August have mean temperatures above the freezing point. The annual precipitation is 160 mm of which 20 mm is rain. The average wind speed is 10 km/h from a predominant westerly direction. The physical characteristics of Parr Inlet are presented in Table 6.2.

As indicated earlier, the Parr Inlet is approximately 2 km long, has an average width of 0.4 km and an average depth of approximately 10.6 m. The bottom of the inlet has relatively steep slopes on both sides extending to the shoreline. The bathymetry of Parr Inlet has two prominent circular depressions on the Inlet floor. There is a very shallow connection between these depressions which are approximately 150m long and have an average water depth of about 5.0 m below chart datum. This narrow channel has the strongest tidal currents in Parr Inlet.

6.2.2 Freshwater Flow

The major source of fresh water flowing into the Parr Inlet is by snow melt. There are no rivers flowing into Parr Inlet. Because of the presence of large quantities of fresh water, in agreement with the definition of Pritchard (1967), Parr Inlet can be classified as an estuary.

6.2.3 Tides

The tides in Parr Inlet are of a mixed, mainly semi-diurnal type with diurnal inequality (Figure 6.14). This diurnal inequality depends upon the relative magnitudes of their semi-diurnal and diurnal components and upon the time these components reach their maxima. The effect of having a small diurnal tide super-imposed on a large semi-diurnal tide is that it increases the heights of alternate high and low waters and it decreases the heights of the intermediate waters. The maximum expected tidal range for the Parr Inlet is approximately 1.0 m (Table 6.2).

6.2.4 Water Column Structure and Physical Properties

Temperature, conductivity, salinity and dissolved oxygen profiles for Parr Inlet were obtained (Heroux, 1985) from 8 locations in August 1983 (Figure 6.15) representing the different grid locations in the hydrodynamic and transport model to understand the spatial and temporal variations of stratification. The sampling locations, temperature, and salinity profiles for Parr Inlet are presented in Tables 6.3 to 6.5.

Parr Inlet is a fjord type estuary with a well defined two layer system; a top fresh water layer of 0 to 3 m (salinities ranging from 0 to 7 $^{0}/_{00}$) overlaying the saline seawater layer. There is very little mixing of the fresh top layer with the saline bottom layer because mixing is inhibited by a strong halocline (difference in density between top and bottom layer could reach 18 $kg \cdot m^{-3}$), draw density profiles between these two layers. As a result of this feature, the mill and sewage effluents released to the surface are generally confined to the surface freshwater layer of 0 - 3 m, thus restricting the available ambient dilution. The saline water below 3 m essentially has a salinity greater than 23 ‰ and forms a relatively stable layer with limited vertical mixing. Vertical mixing of inlet waters due to strong winds is limited since Parr Inlet surface waters arefrozen except during the hottest summer month.

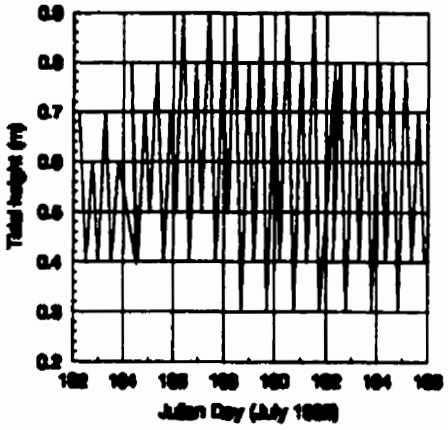

Figure 6.14 Predicted tidal variations in Parr Inlet

The results presented here show that the bottom layer in Parr Inlet has salinity values ranging from 23 ‰ to 32 ‰. The mean value of the salinity in the top 2 m was found to be 3 ‰. These measurements showed that salinity values could range from 0 ‰ to 32 ‰, depending on the location in the Inlet. The salinity values measured during the flood tide were slightly higher than during ebb tides. Numerical model results and discussions are presented in Chapter 8.

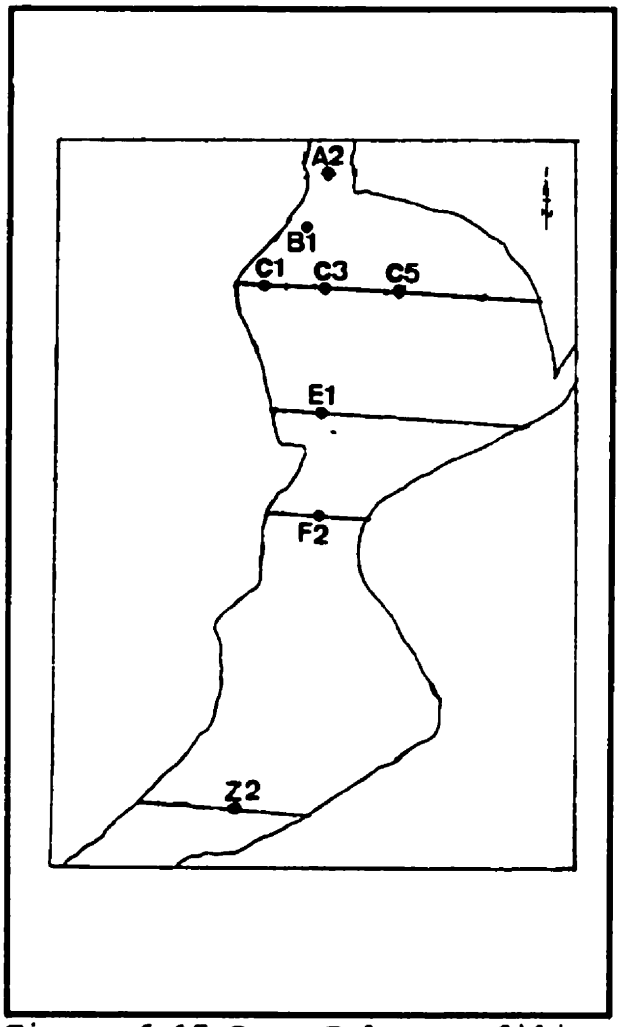

Figure 6.15 Parr Inlet profiling stations.

Table 6.1

Physical features of Long Lake

Location	44°37'30"N, 63°40'00"W
Elevation above sea level	62.8 m
Area of the lake	204.8 ha
Watershed area (land)	1066.2 ha
Watershed area (total)	1271 ha
Maximum length	3371 m
Width	670.7 m
Maximum depth	30.2 m
Mean Depth	7.4 m
Volume	14.37×10^6 m^3
Flushing time	11.91 years
Turn over time	1 year

Table 6.2

Physical features of Parr Inlet

Location	82.30 °N, 62.0 °W
Area of the inlet	0.81 km^2
Maximum length	2.05 km
Mean width	0.395 km
Maximum depth	30.2 m
Mean Depth	10.6 m
Volume	1.085 X 10^6 m^3
Mean High High Water	1.04 m
Maximum High High Water	1.25 m
Mean Lower Low Water	0.15 m
Maximum Low Low water	0.06 m

Tidal information at Alert** (Position: 82.3°N, 62.2°W)

**Source: Canadian Hydrographic Service

Table 6.3 Measured water temperature in Parr Inlet - 7 -11 August 1983

Station and maximum depth	Depth (m)	7	8	9	10	11	Station and maximum depth	Depth (m)	7	8	9	10	11
A-2 (11.5 m)	0	-	2.5	3.0	3.0	3.0	C-3 (16.5m)	0	2.0	2.0	3.0	3.0	3.0
	1	1.0	2.5	2.0	3.0	3.0		1	1.5	2.5	3.0	3.0	3.0
	2	-	-	2.0	2.0	2.0		2	-	-	3.0	2.0	2.5
	3	0.0	1.0	0.0	-	1.0		3	-1.5	2.0	0.0	0.0	0.0
	5	-2.0	-0.5	- 1.0	-	- 1.0		5	-2.0	-2.0	-1.0	-1.0	-1.0
	7	-	-	- 1.5	-	- 1.5		7	-	-	-2.0	-2.0	-2.0
	10	-	-	-	-			10	-	-1.5	-	-	-
B-1 (10.0 m)	0	2.0	2.0	3.0	2.0	3.0	C-5 (30.0 m)	0	2.0	2.0	2.0	3.0	3.0
	1	1.5	2.0	3.0	2.0	3.0		1	-	3.0	2.0	3.0	3.0
	2	-	-	3.0	2.0	2.0		2	-	-	-	2.5	0.5
	3	0.0	1.0	1.0	-	-		3	-	2.0	0.0	0.0	0.0
	5	-1.0	-2.0	- 1.0	-	-		5	-1.0	0.5	-1.5	-1.0	-1.0
	7	-	-	- 1.5	-	-		7	-	-	-2.0	-1.5	-1.5
	10	-	-1.5	-	-	-		10	-	-1.0	-	-	-
C-1 (3.8 m)	0	2.0	2.0	3.0	3.0	3.0	E-1 (11.5 m)	0	1.0	3.0	3.0	3.0	3.0
	1	2.0	2.5	3.0	3.0	2.5		1	-	2.5	3.0	2.5	3.0
	2	1.5	2.1	-	2.0	-		2	1.0	-	3.0	2.0	2.0
	3	0.5	-	-	0.5	2.0		3	-	1.5	1.0	0.0	0.0
	5	-	-	-	-	-		5	-3.0	-0.5	-	-1.0	-1.0
F-2 (5.0 m)	0	2.0	-	-	-	-	Z-2 (13.0 m)	0	2.0	2.0	3.0	3.0	3.0
	1	2.0	-	-	-	-		1	-	2.0	3.0	3.0	3.0
	2	2.0	-	-	-	-		2	-1.0	-	3.0	2.0	2.5
	3	-1.0	-	-	-	-		3	-	2.0	0.0	0.0	0.0
	5	-	-	-	-	-		5	-	0.0	-1.0	-1.0	-0.5
	7	-	-	-	-	-		7	-	-	-1.5	-1.0	-1.5
	10	-	-	-	-	-		10	-	-1.0	-	-	-

Table 6.4 Measured dissolved oxygen in Parr Inlet - 7 -11 August 1983

Station and maximum depth	Depth (m)	7	8	9	10	11	Station and maximum depth	Depth (m)	7	8	9	10	11
A-2 (11.5 m)	0	-	11.8	12.6	-	-	C-3 (16.5m)	0	11.8	11.8	13.8	10.8	9.0
	1	11.9	11.6	12.2	-	-		1	-	11.8	13.1	11.0	8.6
	2	-	-	12.8	-	-		2	-	-	-	10.8	8.6
	3	11.6	12.8	12.0	-	-		3	-	12.2	13.6	9.8	6.4
	5	12.0	12.0	10.8	-	-		5	12.5	10.0	12.2	9.8	7.0
	7	-	-	11.0	-	-		7	-	-	-	10.0	6.0
	10	-	-	-	-	-		10	11.8	-	11.8	-	-
B-1 (10.0 m)	0	11.8	12.4	11.0	10.5	-	C-5 (30.0 m)	0	-	12.5	13.8	9.5	-
	1	11.6	12.0	11.2	9.6	-		1	12.0	-	13.0	9.3	-
	2	-	-	10.8	11.0	-		2	-	-	-	-	-
	3	10.2	13.2	10.0	-	-		3	13.4	-	13.5	8.3	-
	5	9.8	12.0	10.4	-	-		5	10.8	10.8	12.5	8.5	-
	7	-	-	9.7	-	-		7	10.0	-	-	8.5	-
	10	-	11.5	-	-	-		10	-	-	11.8	-	-
C-1 (3.8 m)	0	9.8	11.8	-	12.0	12.0	E-1 (11.5 m)	0	13.0	14.0	12.0	-	-
	1	10.2	11.8	-	11.6	12.0		1	-	13.8	11.8	-	-
	2	-	11.8	-	-	11.6		2	13.0	-	11.7	-	-
	3	10.4	12.0	-	-	9.0		3	-	14.2	10.4	-	-
	5	-	-	-	-	-		5	11.6	11.8	-	-	-
F-2 (5.0 m)	0	12.0	-	-	-	-	Z-2 (13.0 m)	0	9.5	13.2	10.1	-	-
	1	12.0	-	-	-	-		1	-	12.8	10.0	-	-
	2	12.0	-	-	-	-		2	10.0	-	9.6	-	-
	3	10.0	-	-	-	-		3	-	12.8	8.6	-	-
	5	-	-	-	-	-		5	9.6	12.4	-	-	-
	7	-	-	-	-	-		7	-	-	9.0	-	-
	10	-	-	-	-	-		10	9.9	11.8	-	-	-

Table 6.5 Measured salinity in Parr Inlet - 7 -11 August 1983

Station and maximum depth	Depth (m)	7	8	9	10	11	Station and maximum depth	Depth (m)	7	8	9	10	11
A-2 (11.5 m)	0	-	1.0	1.0	1.0	1.0	C-3 (16.5m)	0	0.5	0.8	0.5	1.0	1.0
	1	0.5	0.8	2.0	2.5	2.0		1	0.5	1.0	0.5	1.0	2.0
	2	-	-	3.5	4.5	7.0		2	-	-	1.0	4.0	4.0
	3	3.0	3.8	23.0	-	24.5		3	4.0	6.7	28.0	26.0	25.0
	5	29.0	25.2	29.0	-	28.0		5	30.0	28.2	29.0	29.0	28.5
	7	-	-	29.0	-	28.5		7	-	28.2	30.0	29.5	29.5
	10	-	-	-	-			10	-	-	-	-	-
B-1 (10.0 m)	0	<0.5	0.8	1.0	2.5	1.0	C-5 (30.0 m)	0	-	1.0	1.5	1.0	1.0
	1	0.5	0.9	1.0	3.0	2.0		1	1.0	1.0	1.5	1.0	1.0
	2	-	-	1.0	4.5	4.0		2	-	-	-	3.0	25.0
	3	3.0	4.0	27.0	-	-		3	4.0	6.5	28.0	26.5	25.0
	5	28.0	28.5	29.0	-	-		5	31.5	25.5	28.0	29.0	28.5
	7	-	-	29.0	-	-		7	32.0	-	28.0	29.5	29.5
	10	-	28.5	-	-	-		10	-	29.0	-	-	-
C-1 (3.8 m)	0	-	0.5	0.8	1.0	1.0	E-1 (11.5 m)	0	1.0	0.8	1.0	1.0	-
	1	0.5	0.9	1.0	1.0	2.0		1	-	0.9	1.0	1.0	-
	2	1.0	2.0	-	4.0	4.5		2	1.0	-	1.0	4.0	-
	3	2.5	-	-	22.0	-		3	-	4.5	27.5	25.0	-
	5	-	-	-	-	-		5	30.0	27.2	-	29.0	-
F-2 (5.0 m)	0	0.0	-	-	-	-	Z-2 (13.0 m)	0	0.5	0.8	0.5	0.5	0.5
	1	0.0	-	-	-	-		1	-	0.8	0.5	0.5	0.5
	2	0.0	-	-	-	-		2	1.0	-	3.0	3.0	4.5
	3	28.0	-	-	-	-		3	-	16.5	25.5	28.0	28.0
	5	-	-	-	-	-		5	32.0	26.2	25.5	29.0	28.0
	7	-	-	-	-	-		7	-	-	-	-	-
	10	-	-	-	-	-		10	-	-	-	-	-

Chapter 7

SENSITIVITY ANALYSIS AND VERIFICATION OF MODELS

7.1 Numerical Diffusion and Stability

For detailed representation of circulation, a nonlinear finite difference model was set up for Long Lake, which divides it into 495 grid squares of 62.5 m X 62.5 m each. The average depth at each grid square or segment was then computed using a planimeter/digitizer (Figure 4.2). The input parameters are, wind stress, inflows and outflows, bottom friction, rainfall, and evaporation. For the summer period the system was conceptualized as a layer system separated by a thermocline in the case of water quality model.

In this study, the non-linear hydrodynamic model is solved by using an ADI technique, and the segment-node model and water quality model with an explicit solution technique. In an implicit solution, the variables and their derivatives are both considered as unknowns and are determined simultaneously. A commonly used implicit solution technique is based on the Thomas algorithm, an adaptation of Gaussian elimination (Tetra Tech, 1975; Beca and Arnett, 1976). In an implicit method, the derivatives are evaluated before the projections of concentrations are made. An explicit method requires short time steps to ensure stability as well as conservation of mass. Another problem associated with the finite difference scheme is numerical diffusion. However, numerical diffusion is relatively small for the type of simulations carried out in this study. Numerical diffusion has been minimized by (1) reducing the grid size and (2) substracting the numerical diffusion from the actual diffusion coefficient using the method described in Chapra and Reckhow (1983). A description of the horizontal and vertical eddy diffusivities used is presented in Section 8.1.

Both forward difference and central difference schemes, were tried for the solution of the advection-diffusion equation of the water quality model. The forward difference scheme was used for all simulations carried out for the sensitivity analysis and storm simulations.

7.2 Sensitivity Analysis

7.2.1 Hydrodynamic and Segment-node Models

Sensitivity analyses of both hydrodynamic and segment-node models were also carried out to understand the rate of change of one input variable with respect to change in the model response. The results of the sensitivity analysis also show any imperfection in the model structure and solution methods. The sensitivity analysis also provides a better understanding of the correspondence between the model and the physical processes being modeled. The sensitivity response of the hydrodynamic model and segment-node model for (1) the response of the lake to various wind speeds from both the Cove stream end and outlet end (2) the oscillations of the lake surface (seiches) after the wind was stopped and the rate at which the oscillation dies down was investigated. The period of measured seiches was compared with empirical relationships established. Seiches and wind set up computed from the 2-D hydrodynamic model for different wind conditions in the lake are shown in Figures 7.1 and 7.2. The segment-node modelling approach was found more suitable for micro-computer application and therefore easily interfaced with existing Long Lake watershed models. Therefore, a more detailed sensitivity analysis was carried out using this modelling approach (Figures 7.1 to 7.6). Results of the simulation, such as cross-sectional velocity and hydraulic head for Long Lake were compared for various segments and presented in Figures 7.7 and 7.8.

A series of runs were performed to determine the response of the lake to changes in model input parameters to provide a better understanding of the correspondence between the

model and the physical processes being modeled (John, Satish, and Waller 1995). These tests showed that the models are sensitive to variable winds and stream flows as shown in Figures 7.1 to 7.9. The 3-D hydrodynamic model developed was tested for wind-driven circulation, using a rectangular basin test problem introduced by Davies and Owen (1979). Hydrodynamic parameters used to tune the model are Chezy, drag coefficients and vertical eddy viscosity.

Seiches in the lake were investigated by imposing a strong wind, namely 15 m/s and then suddenly cutting off the wind and computing the water level variations. The seiche pattern for a wind speed of 15 m/s shows the period of oscillation to be about 14.4 min. The maximum height of seiches simulated by an average wind of 15 m/s was found to be 8 cm at the outlet end and 4 cm at the cove stream end. The maximum change in water level due to wind set up by persistent winds of 20 m/s was about 12 cm and 8 cm at the mouth and head of the lake respectively.

It was also found that an increase of wind speed from 15 m/s to 20 m/s would almost double the wind set up on either end of the lake, with wind blowing along the lake (Figure 7.2). The nodal point of the seiche oscillation has been found to be near the centre of the lake. Wind setup has an effect in increasing or decreasing the outflow. For example, a wind setup of 7 cm at the outlet end of Long Lake (as discussed above) would result in an increase in outflow from 0.2 m^3/s to 1.7 m^3/s (Figure 7.9).

7.3 Verification of Numerical Models

The development of a model (or models) has to take into account various parameters or factors, such as time scales (e.g. from short duration of a few seconds, to few hours, to longer duration in order of days/weeks to seasonal/annual variations); space scale (e.g. near field versus far field transport); characteristics of receiving waters (e.g. well mixed or stratified); relative importance of the driving forces (e.g. stream flow versus meteorological forcing, large scale circulation, etc.); feasibility of field data collection for model

calibration/validation and input; and to a large extent, the objective of this research and the degree of details required.

The performances of the hydrodynamic and water quality models are to be compared with a set of in situ field data to establish the model's suitability to make predictions. Reckhow *et al.* (1990) have discussed model verification techniques and have commented on the tendency of verification tests to control the risk of mistakenly rejecting a valid model as opposed to controlling the risk of mistakenly accepting an invalid model. Reckhow *et al.* (1990) note that a model that generates a highly variable response characteristic may not be distinguished as significantly different from a sample of highly uncertain field observations.

In this research, the model verifications were carried out using two methods:

(1) by comparison with analytical model results for which complete solutions are available.

(2) by comparison with field data.

7.3.1 Verification Evaluation procedure

A quantitative statistical analysis is carried out to provide an overall evaluation basis for the model. The statistical parameters considered in this evaluation are defined below.

Letting x_j and y_j represent the observed and modeled variables respectively at time j, we may define for each station the following quantities:

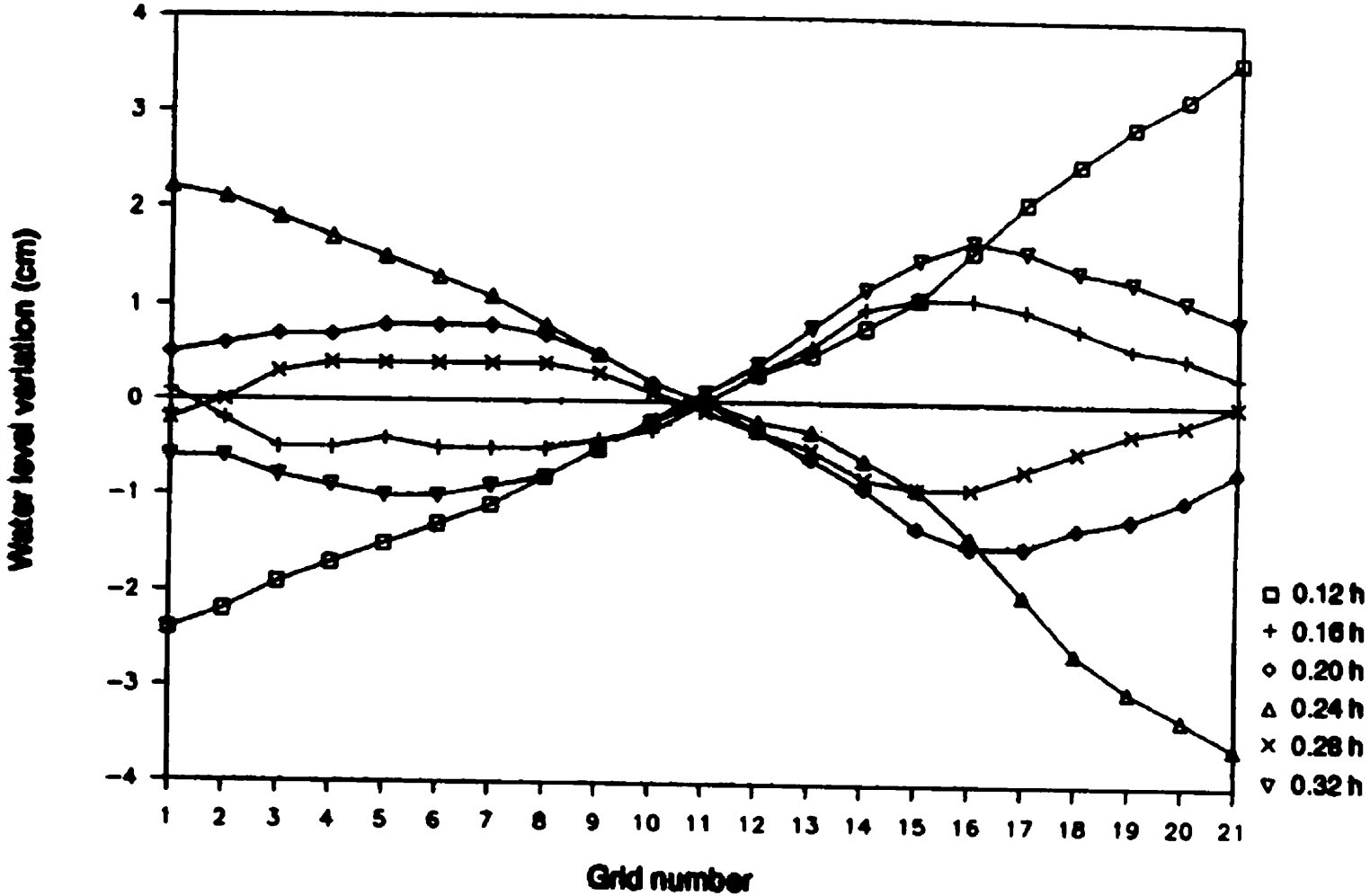

Figure 7.1 Seiches in Long Lake

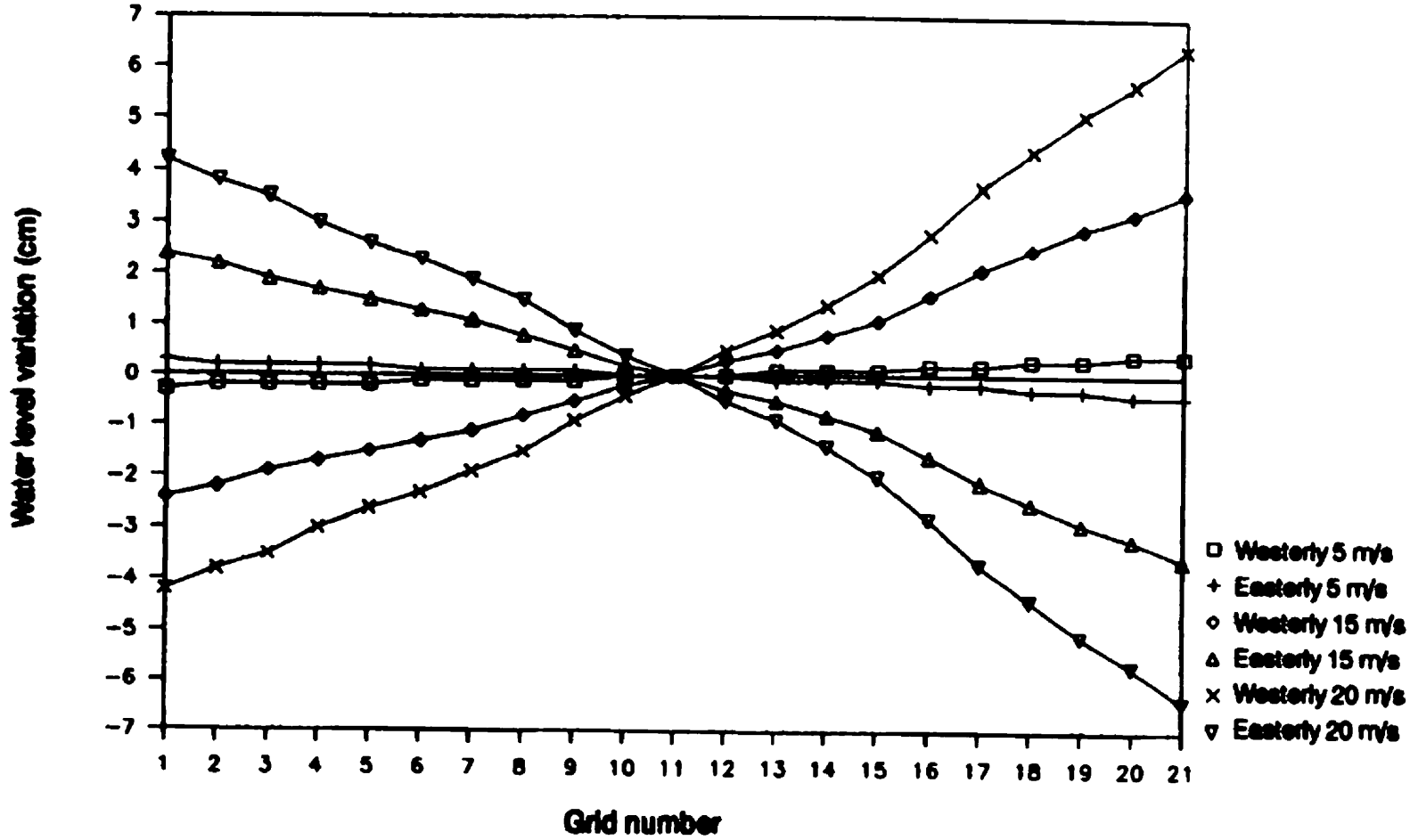

Figure 7.2 Wind set up in Long Lake

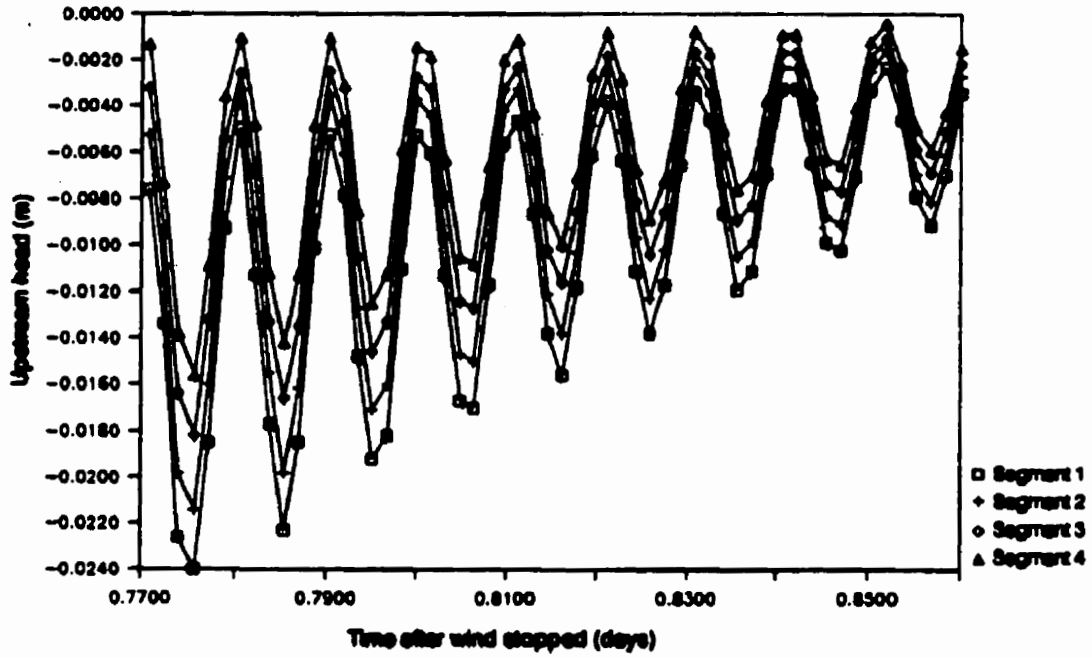

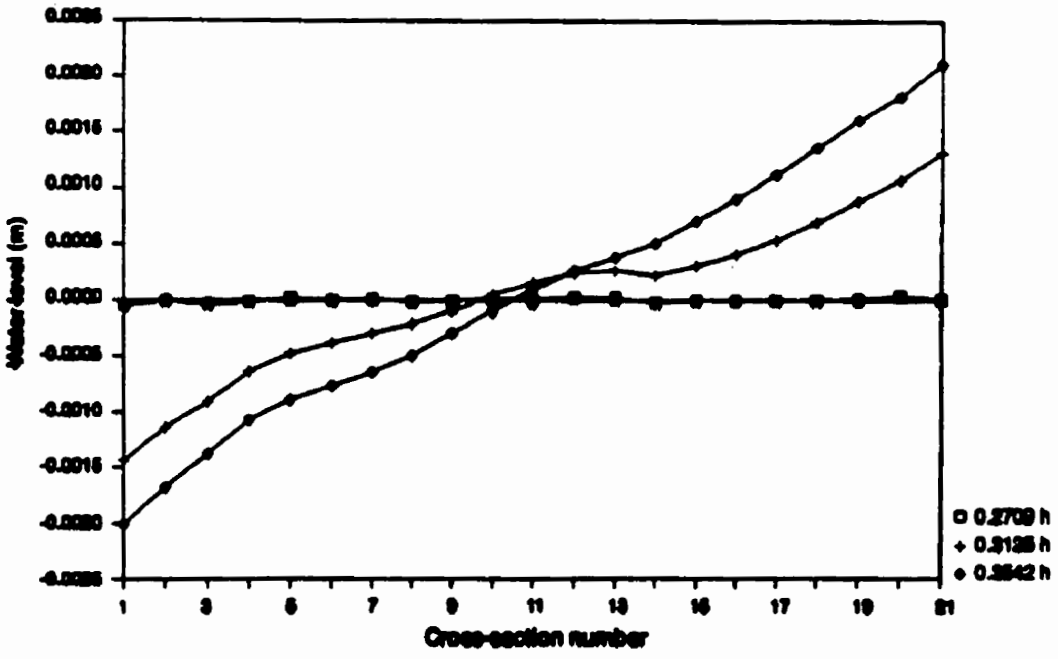

Figure 7.3 Water level changes due to seiches generated by 15 m/s wind at selected segments.

Figure 7.4 Wind setup for westerly wind of 5 m/s.

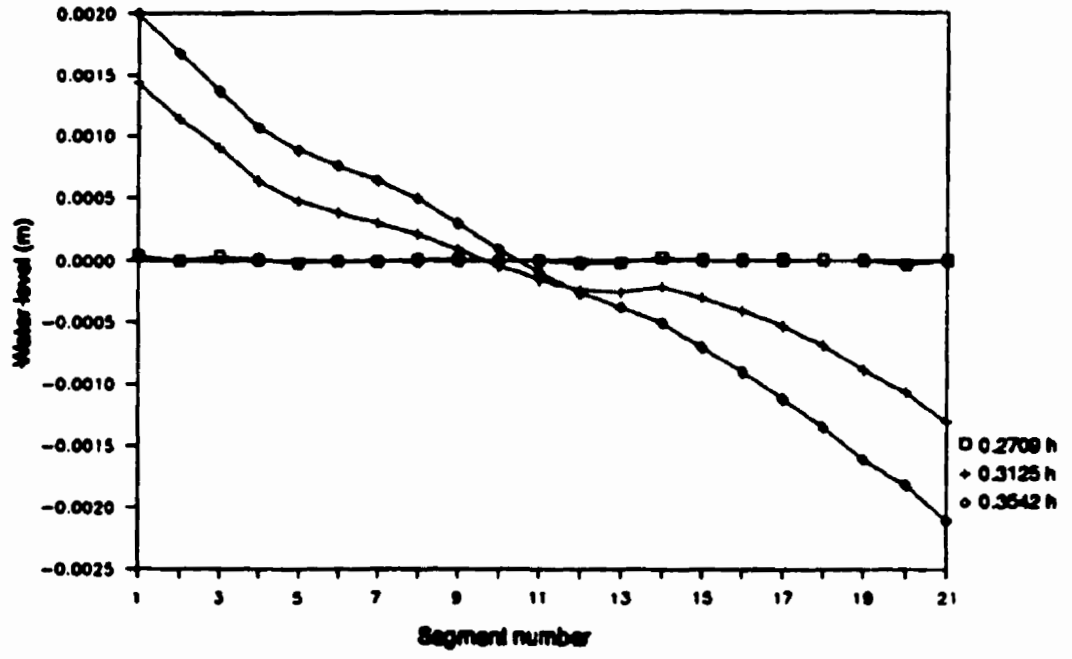

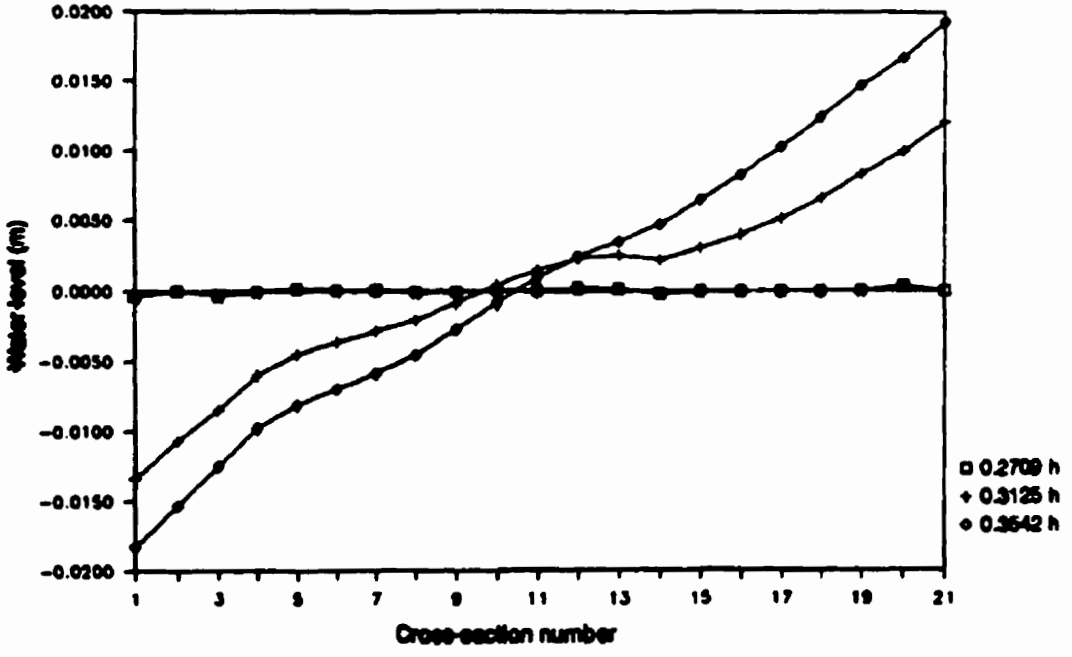

Figure 7.5 Wind setup computed-segment-node model-easterly wind of 15 m/s

Figure 7.6 Wind setup computed-segment-node model-westerly wind of 15 m/s

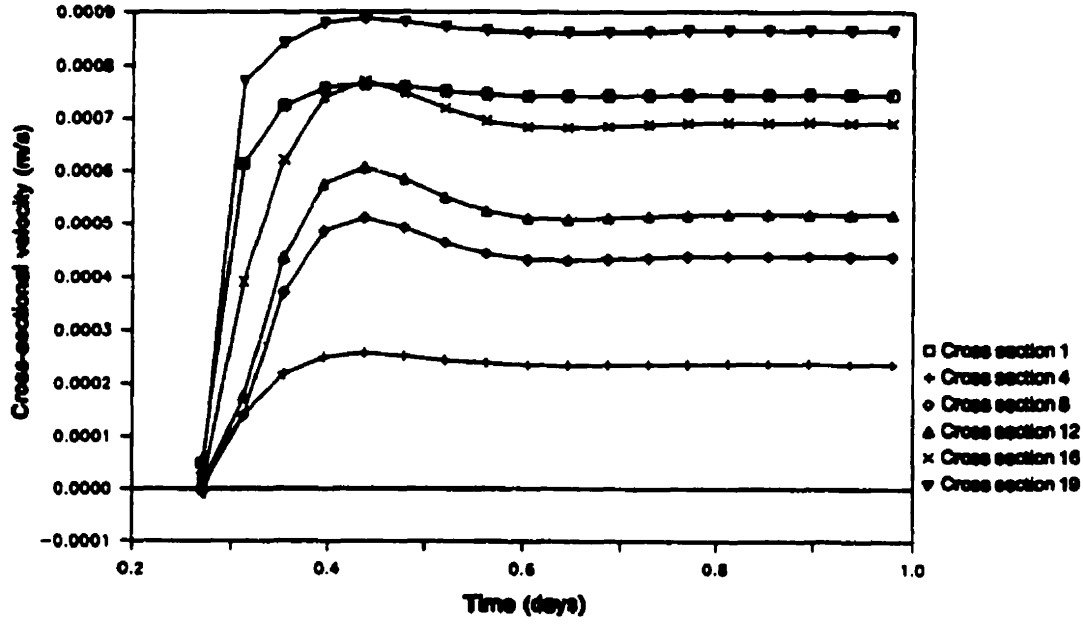

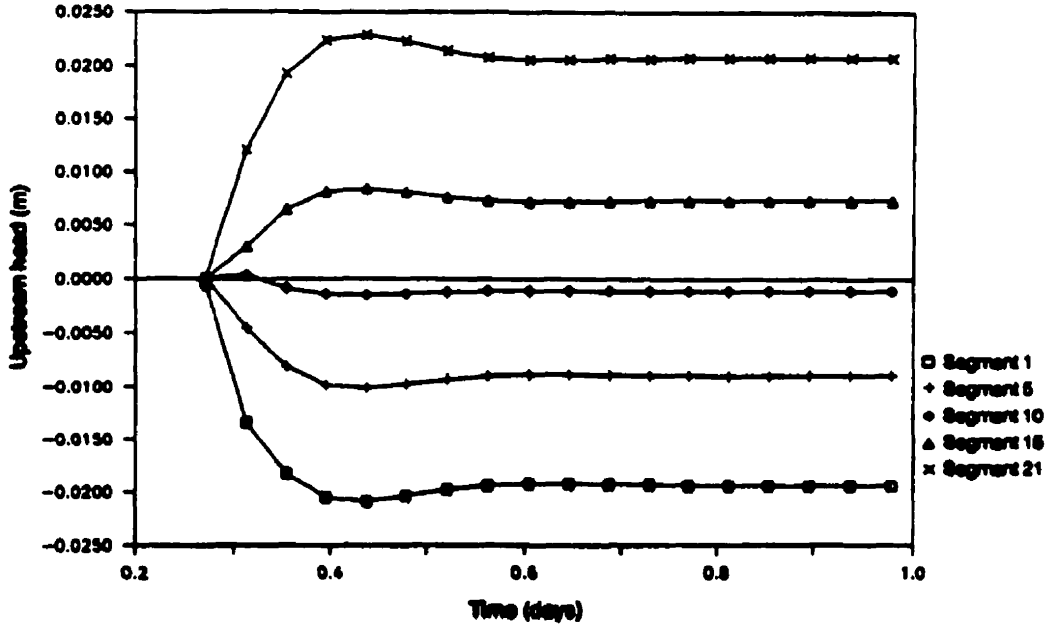

Figure 7.7 Stream flow currents for rain storm 1984 summer
Figure 7.8 Water level changes due to wind for westerly wind of 15 m/s

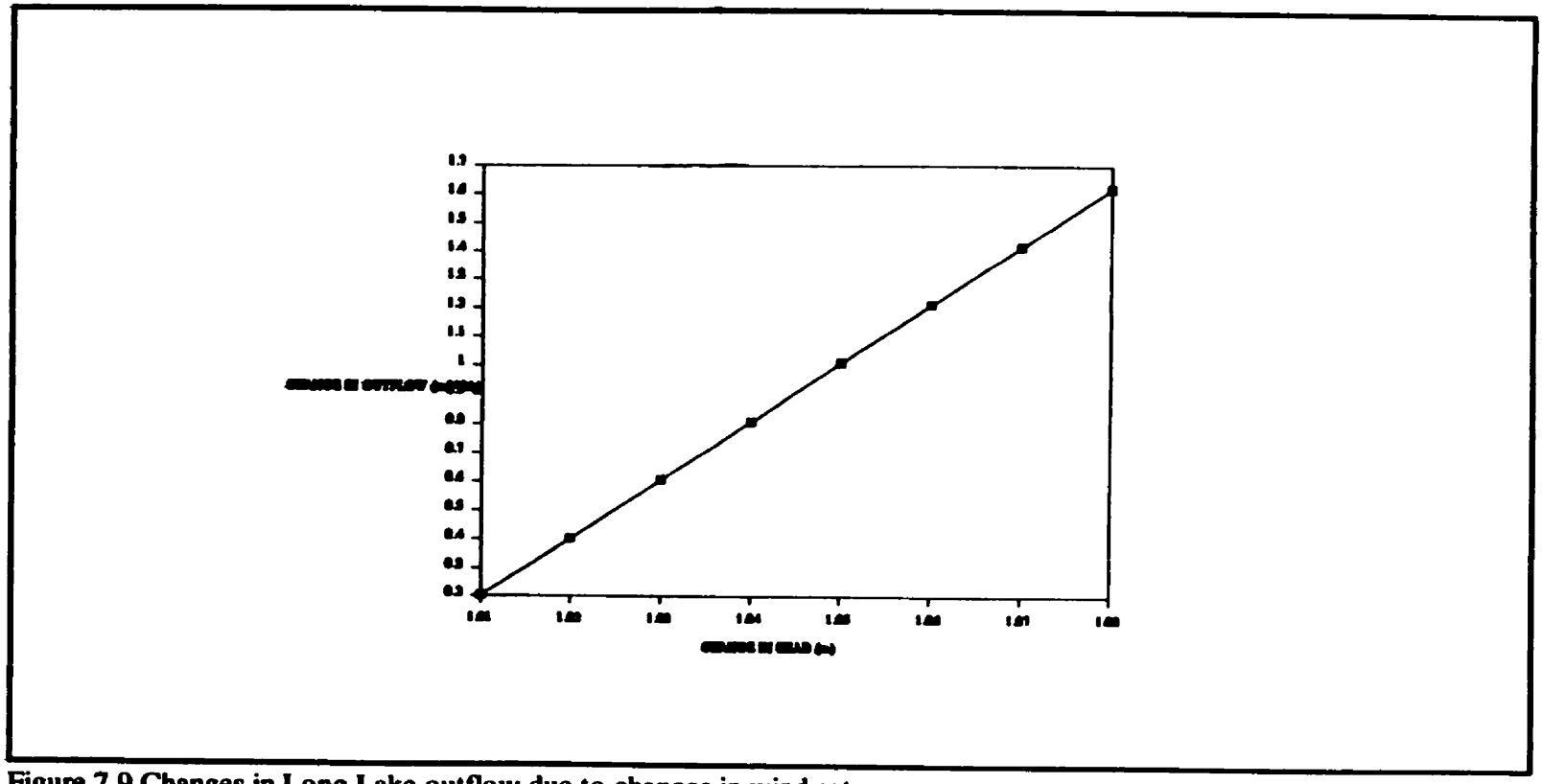

Figure 7.9 Changes in Long Lake outflow due to changes in wind setup.

A) Mean error (or Bias):

$$Mean\ Error = \sum_{i=1}^{N} \frac{(x_i - y_i)}{N} \quad , \tag{7.1}$$

B) Absolute Mean Error:

$$Absolute\ Mean\ Error = \sum_{i=1}^{N} \frac{|x_i - y_i|}{N} \quad , \tag{7.2}$$

C) Root Mean Square Error (RMSE):

$$RMSE = \left(\sum_{i=1}^{N} \frac{(x_i - y_i)^2}{N} \right)^{\frac{1}{2}} \quad , \ and \tag{7.3}$$

D) Scatter Index (SI):

$$SI = \frac{RMSE}{\overline{x}} \cdot 100\% \quad ; \tag{7.4}$$

with $\overline{x} = \sum_{i=1}^{N} \frac{x_i}{N}$ and N = number of data points. A correlation coefficient is also

calculated, by the least squares linear regression method.

The terms are interpreted as follows. Positive (negative) mean error indicates that the model over (under) estimates the observed value on average. The absolute mean error is a measure of the total average difference between the two variables. The root mean square error is a measure of the deviation of the variable y_j about x_j for all j. The Scatter Index indicates the relative strength of the deviation of the variable y_j about x_j. The correlation coefficient, program developed for evaluations, and scatter plots are provided in Appendix D. Appendix D also includes the goodness of fit of a linear least squares regression analysis of the data.

The statistics themselves do not provide a definitive measure of the model's performance, however they do provide insight into model behavior, and give a prediction of the suitability of the predicted data. It must be emphasized that care should be taken when using the statistics. The statistics calculated make no allowance for a time lead, or lag in the model; therefore, interpretation requires both a statistical and physical analysis.

7.3.2 Verification statistics

The verification statistics displaying mean, standard deviation and the number of data points calculated and comparison statistics calculated for various verification sites are presented in Tables 7.1 and 7.2. These Tables also present the statistics for the overall comparison period, at each verification site and the error statistics calculated, to describe the difference between the model and coincident measured data.

A comparison of predicted current field and chloride concentrations, with the measured current components and chloride concentrations is presented. The results of the statistical analysis including the time series of predicted and observed data sets are presented in Tables 7.1 and 7.2.

Table 7.1. Comparison of Measured and Predicted Current Statistics .

Location	Current	Mean	SD (%)	Mean Error	Absolute Mean Error	RMSE	Scatter Index (%)	Linear Correlation
Halifax Harbour	U-Comp (m/s)							
	Measured	0.31	3.37	0.09	0.59	0.75		0.98
	Predicted	0.22	3.41					
Halifax Harbour	V-comp (m/s)							
	Measured	-0.49	5.13	-0.27	1.85	2.08		0.98
	Predicted	-0.21	3.26					
Long Lake	Wind currents (cm/s)							
	Drogue	8.37	4.06	1.51	2.06	2.93	35.0	0.86
	Predicted	6.86	2.06				42.7	

Table 7.2. Comparison of Measured/Analytical and Predicted Concentrations.

Location	Pollutant Loading	Mean	SD	Mean Error	Absolute Mean Error	RMSE	Scatter Index (%)	Linear Correlation
Long Lake	Impulse							
	Analytical	1.11	0.03	-0.03	0.03	0.03	2.98	0.97
	Numerical	1.14	0.01				2.90	
Long Lake	Step (Type 1)							
	Analytical	2.20	1.27	0.008	0.08	0.009	0.427	1.00
	Numerical	2.19	1.26				0.429	
Long Lake	Step (Type 2)							
	Analytical	9.90	1.27	-0.008	0.008	0.010	0.098	1.00
	Numerical	9.91	1.26				0.098	
Long Lake	Chloride (mg/l)							
	Measured	53.91	12.54	2.59	8.49	9.60	17.8	0.93
	Predicted	51.33	19.65				18.7	

7.3.3 Hydrodynamic and Segment-node Model Verification Results

The segment-node and 2-D depth averaged hydrodynamic model results were verified against current measurements carried out in Long Lake using floats and drogues. The 2-D depth averaged hydrodynamic model was also applied to Halifax Harbour to predict the tidal and wind-driven current fields. The predicted currents were also verified with measured tidal current data, using Acoustic Doppler Current Profiler (ADCP) (Figure 7.10). Both model predictions and current measurements were carried out as part of the Halifax Harbour Clean up Program. Detailed descriptions of the tidal and wind driven currents in Halifax Harbour along with changes in the flow regime due to the construction of the Ives Island (STP site) were also studied using the 2-D non-linear hydrodynamic model as part of the Halifax Harbour Clean up Program. From these simulations, M2 tidal currents were extracted and compared with ADCP measured currents for M2 tidal current constituent (Table 7.1). The results show very good agreement of predicted and measured values.

The segment-node and 2D depth averaged hydrodynamic model simulation results and limited surface flow measurements using surface drifters during periods of calm winds show that, the streamflow generated currents range from about .01-.1 cm/s. These measurements show slightly larger currents than actually predicted by both the above mentioned models (Figure 7.10). Simulations carried out during the period of drogue measurements show good agreement between results predicted between the above mentioned models and in-situ current measurements (Figures 7.11 to 7.13). A regression analysis of segment-node model results, with the measured data, shows good correlation, however, measured values are larger by about 15 percent (Figure 7.12).

As shown in Table 7.1 and Figure 7.11, the model predicted currents with measured current statistics for Halifax harbour show very good agreement. The root mean square error between measured data and model predictions is generally less than 2.9. The correlation coefficient of the predicted data with measured data was 0.98 indicating a high degree of

temporal and amplitude agreement.

Comparison of the drogue movements with currents predicted by the segment-node and 2D depth averaged hydrodynamic models shows good agreement, with a correlation coefficient of 0.86 (Table 7.1). It should be noted that drogue mostly measured currents in the top 1 m of the water column and the model predicts depth averaged currents and therefore measured currents were about 15 % higher than predicted.

7.3.4 Water Quality Model Verification Results

The comparisons of the numerical water quality model results with analytical results were carried out for both impulse and step loading. The results show good agreement between numerical and analytical model results. The water quality model results were initially verified with analytical model results for various types of pollutant loadings and later verified against measured chloride values for two deep locations in Long Lake.

As the next step the water quality model was tested for its response to variable wind driven currents, and variable stream flows and pollutant input loads. The results show that the model is sensitive to variable winds, stream flows and pollutant loads.

To test the water quality model sensitivity and performance, the model results have been studied for various simplified input chemical loadings such as, step loading and impulse loading (Figure 7.14). Since these types of loadings have analytical solutions, it is useful in carrying out comparisons with the model results. A comparison of the results obtained from the advection-diffusion model, with the results obtained for a prototype lake is given below.

Step loading

Advection-diffusion model results for a single grid, using a step loading (type 1) of the following characteristics, along with the analytical results, obtained by solving equation (3.3) are shown in Table 7.2.

Initial lake pollutant concentration = 0
Reaction coefficient (conservative constituent) = 1.0
pollution loading rate 1.6 g/sec
inflow rate = outflow rate = 0.132 m^3/sec
Similar runs are also carried out for step loading (type 2) with the following characteristics.
Initial lake pollutant concentration = 12.1 g/m^3
Reaction coefficient (conservative constituent) = 1.0
Pollutant loading rate = 0
inflow = outflow = 0.132 m^3/sec

Thirty days of simulation of the advection-diffusion model runs are compared with the results obtained from the solution of the equation (3.3) (Table 7.2 and Figure 7.14). The results show good correlation between analytical and model results.

The model predicted chloride distributions were also verified against measured chloride data for Long Lake. As shown in Figure 7.15 good agreement was found between measured and predicted chlorides, with a correlation coefficient of 0.93.

Impulse loading

The model is also tested for impulse loading for a 6-day period and are compared with results obtained from the advection-diffusion model (Table 7.2). The following characteristics are used in the simulation.

Initial lake pollutant concentration = 0

Reaction coefficient (conservative constituent) = 1.0

Pollutant loading for first two hours = 9.504 X 105 g

Volume of the lake = 8.209 X 105 m^3

Comparison of water quality simulations using numerical and analytical models show excellent agreement, with a correlation coefficient of 1.00 (Table 7.3). The absolute mean square error between analytical and numerical models is less than 0.01. The chloride concentrations predicted by the advection diffusion model were slightly lower than measured chloride concentrations with a correlation coefficient of 0.93 indicating good agreement (Figure 7.14). A more detailed discussion of the numerical model results are presented in Chapter 8.

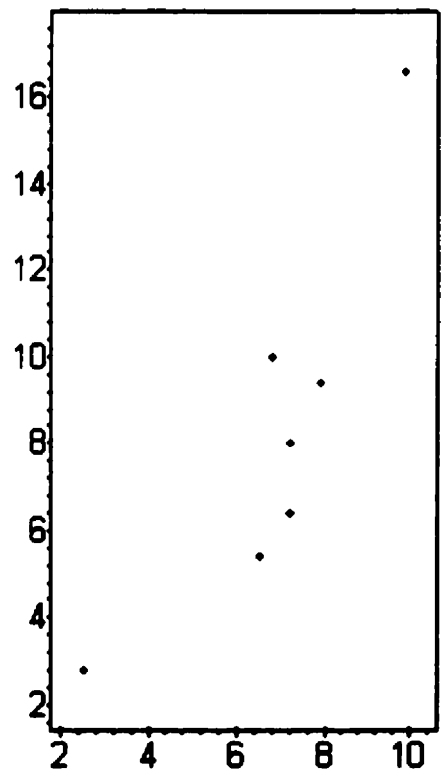

Figure 7.10 Comparison of measured drogue speed (x) and predicted current speed (y).

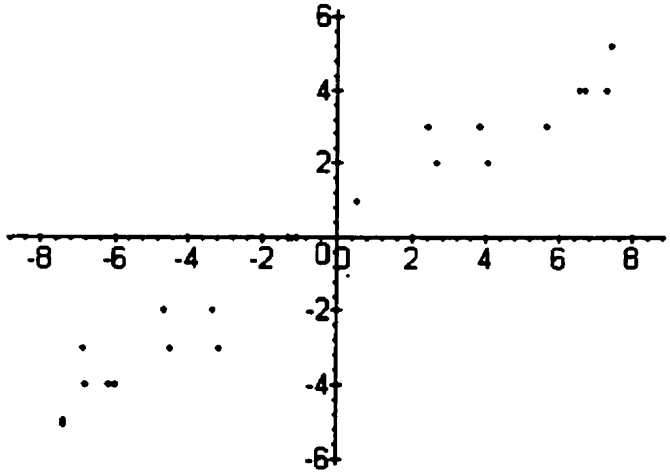

Figure 7.11a Measured (x) and predicted (y) U- component of currents

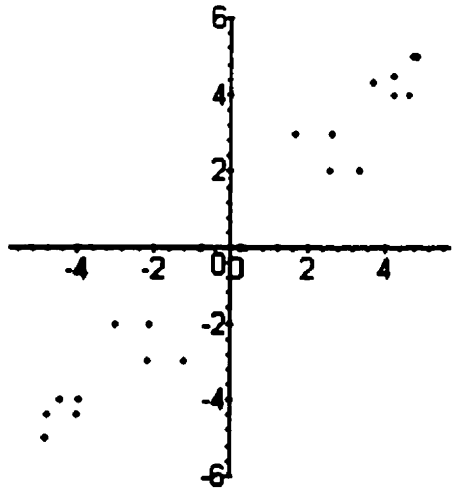

Figure 7.11b Measured (x) and predicted (y)V-component of currents

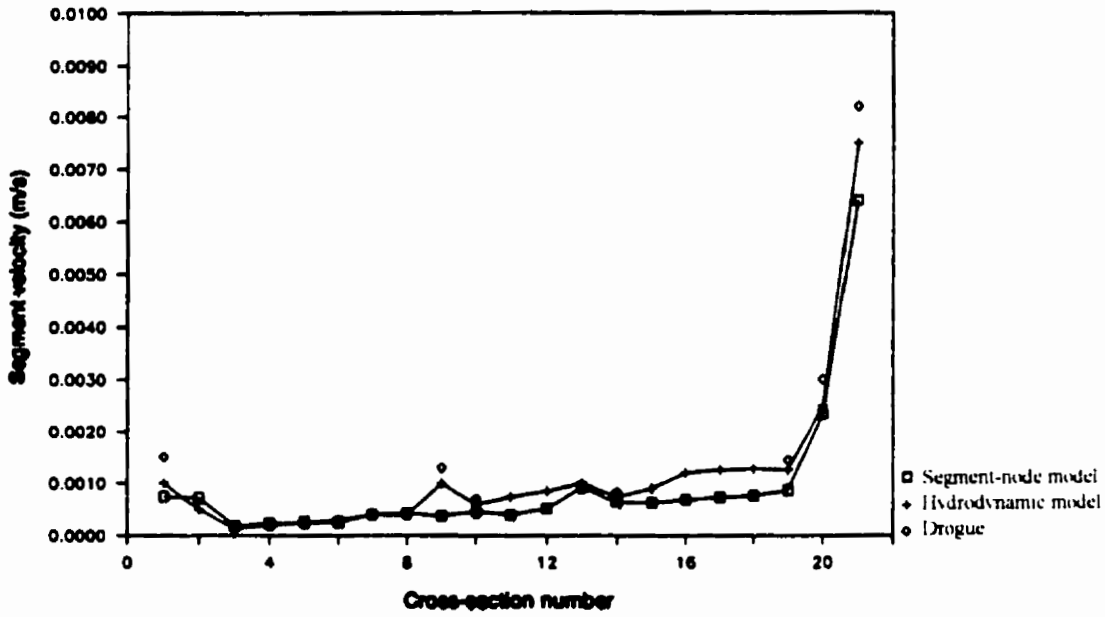

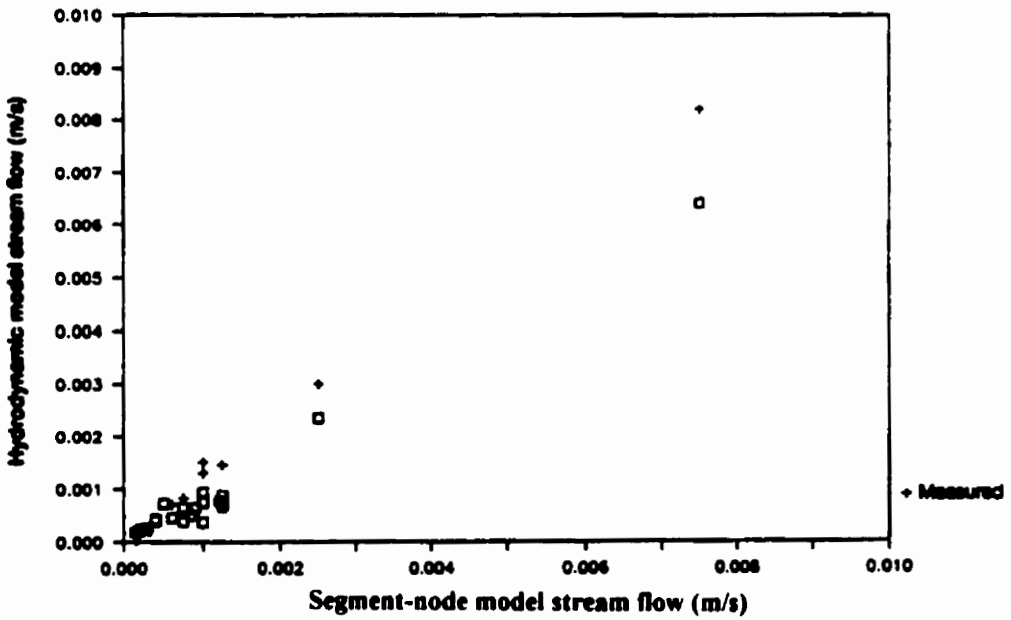

Figure 7.12 Streamflow generated currents - observed vs modelled.

Figure 7.13 Streamflow generated currents - observed vs segment-node results.

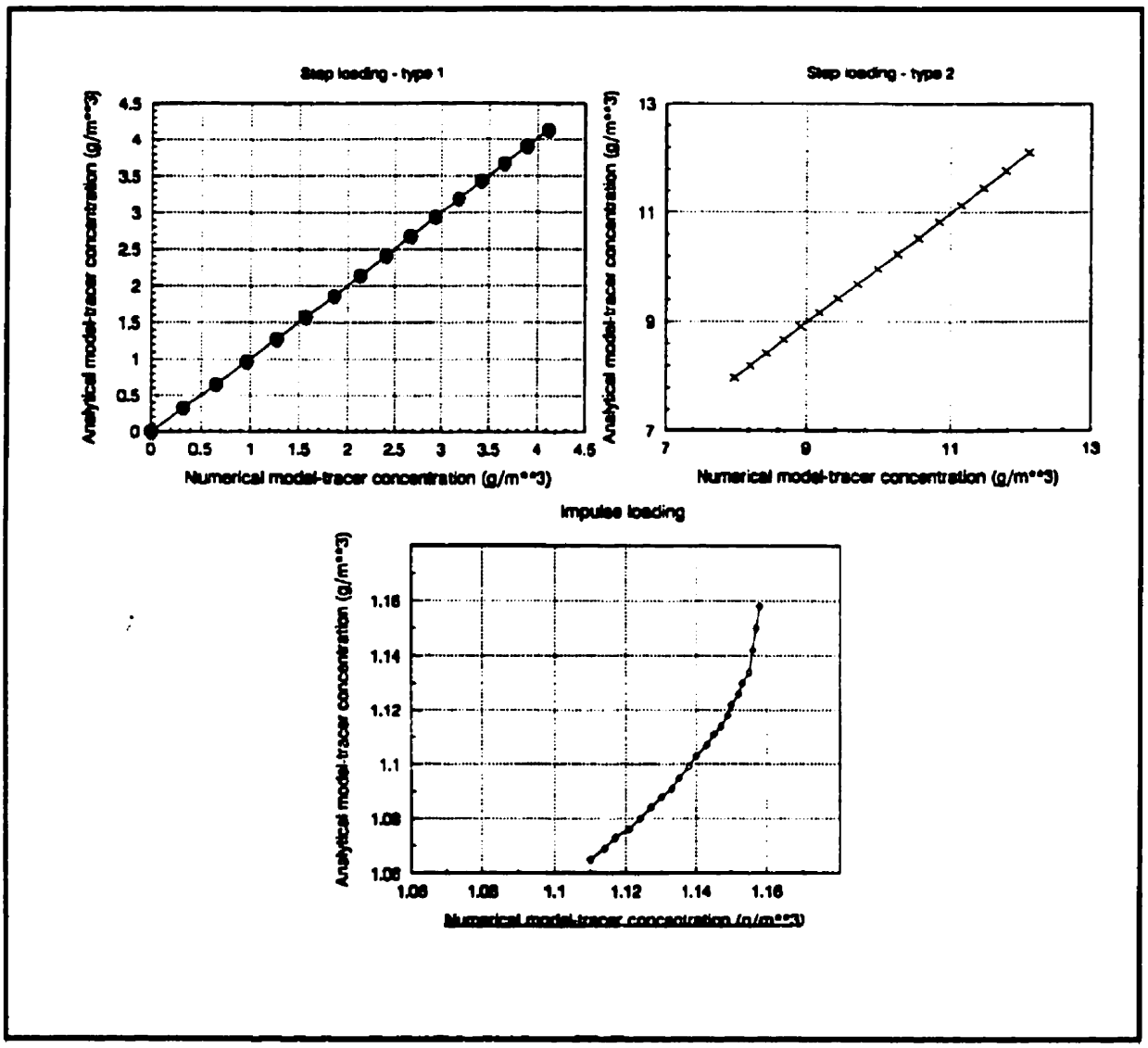

Figure 7.14 Comparison of numerical and analytical model results.

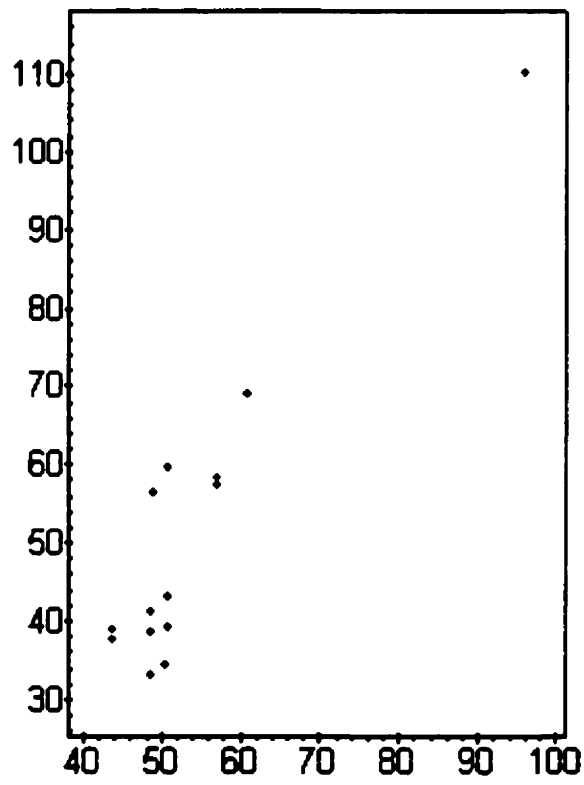

Figure 7.15 Comparison of measured (x) and predicted (y) chlorides

Chapter 8
NUMERICAL MODEL RESULTS AND DISCUSSIONS

8.1 Horizontal and Vertical Eddy Diffusion

Pollutants are transported by random molecular motion, and mixed by large-scale eddies in lakes or tidal inlets. If sufficiently long observational time and space scales are employed, this motion can be viewed as random and treated mathematically as diffusion processes. Eddies are much larger than the "random steps" of molecules, and mixing by turbulent diffusion is much greater than by molecular diffusion. Murthy (1976) and Okubo (1971) studied variation of horizontal turbulent diffusion with length scale in Lake Ontario and in the Oceans (Figure 8.1). Turbulent diffusion coefficients are several orders of magnitude greater than those on molecular scale. It should be also noted that horizontal diffusion in lakes is much greater than vertical diffusion.

Temperature measurements carried out in Long Lake (Chapter 6) were used to compute vertical eddy diffusion. Measured monthly temperatures for Long Lake for the upper layer (above thermocline) and the lower layer (below thermocline), diffusion coefficients and its monthly variation are presented in Figure 8.2. As shown in Figure 8.2 even the maximum vertical diffusion coefficient for Long Lake is very small (46×10^{-3} cm^2/s) in comparison to the horizontal diffusion coefficient for Long Lake (based on its length scale) of 10^3 to 5×10^3 cm^2/s. In contrast to molecular diffusion where the motion of the particle is assumed to be identical in scale, turbulence contains a wide range of eddy sizes. Thus, it would be expected that the resulting diffusion would be scale dependant. It has been shown that generally the horizontal turbulent diffusion coefficient varies with the 4/3 power of the scale of the phenomena (Murthy 1976, Okubo 1971) and is supported by observations in both lakes and oceans (Figure 8.1).

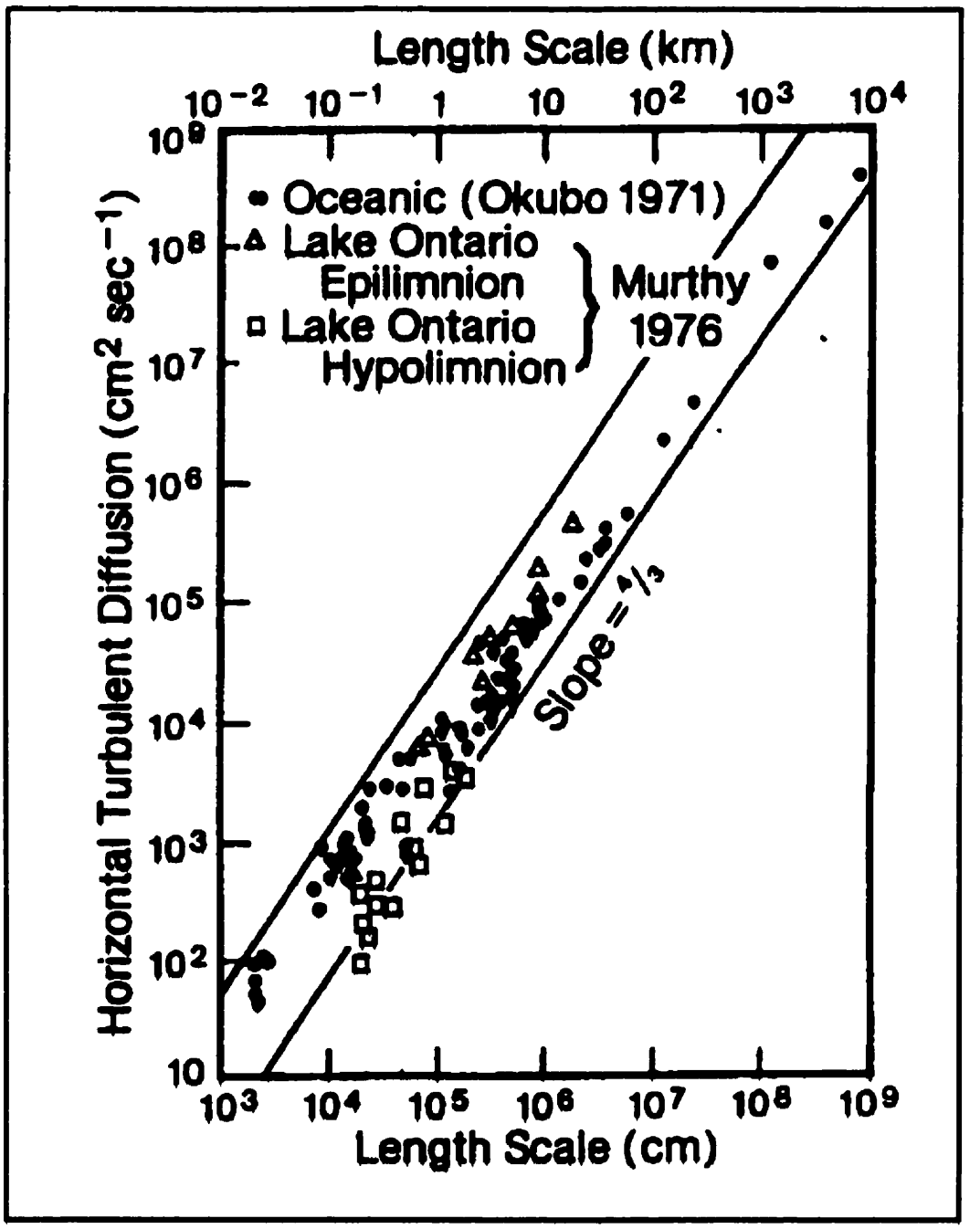

Figure 8.1 Horizontal turbulent diffusion in lakes and oceans.

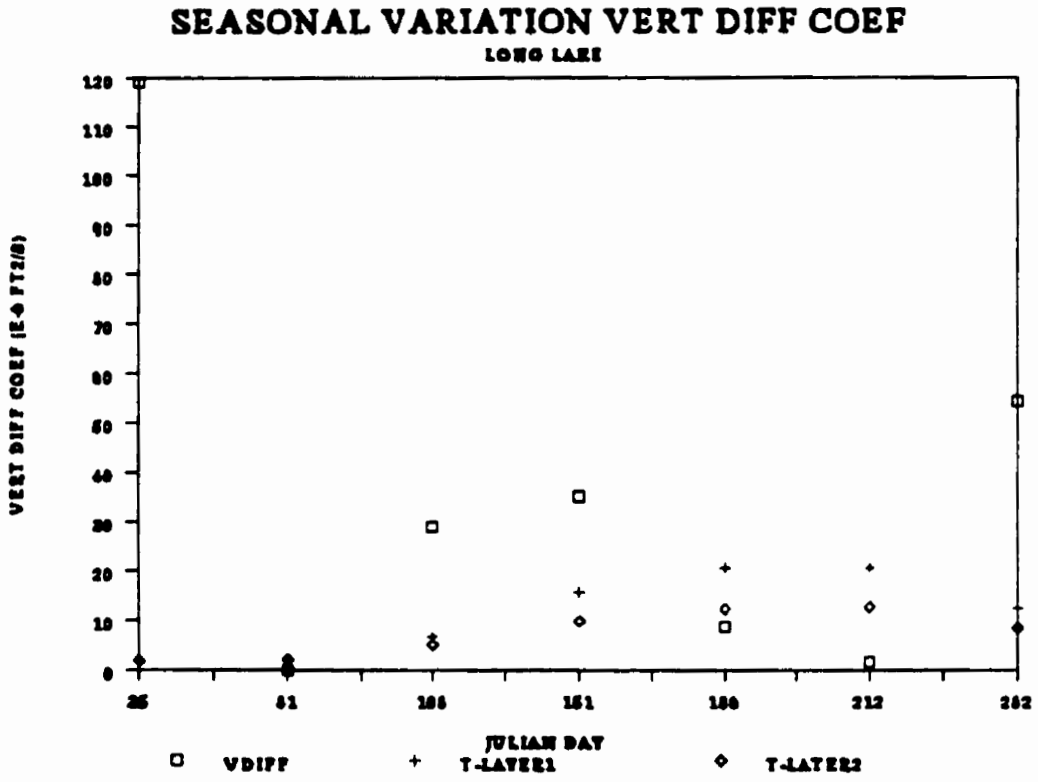

Figure 8.2 Seasonal variation of vertical diffusion coefficient computed

The scale-dependence of eddy diffusivity has great practical consequence to modelling pollutant transport in lakes. If the effluent is rapidly discharged into a small area such as a cove, as is the case for Clearcut Brook of Long Lake, the diffusion of the resulting cloud would accelerate as it grows in size. This happens because larger and larger eddies would play a role in its mixing as it spread. When the spill grows bigger than the largest eddy, a constant eddy diffusion coefficient model could be used to approximate further mixing.

One way to avoid the problem of scale-dependant diffusion is to limit the models to cases where the long-term distributions of pollutants are simulated. On a long enough time scale, we can account for the large scale circulation of a lake as an advective term and assume that all eddys of a small scale can be treated as random turbulent diffusion. A study by Lam and Jaquet (1976), about the range of horizontal eddy diffusivity values for lakes, shows that the values range from 10^4 to 10^6 cm^2/s. Thomann et al (1975), used 9000 cm^2 /s for horizontal diffusivity values. Using Okubo (1971), horizontal eddy diffusivity for Long Lake based on its length scale (Figure 8.1) could vary from a lower value of 1,000 cm^2/s to upper value of 5,000 cm^2/s.

8.2 Model Application to Long Lake

8.2.1 Segment-node and 2-D Depth Averaged Models

The two dimensional vertically averaged model was run during all seasons except summer. During summer, when stratification occurs density profiles based on measured data were used for near-field. However, for far-field, a false bottom at the thermocline was assumed, since the thermocline inhibits mixing below that level.

Lake model simulation carried out using both segment-node and 2-D depth averaged models showed that wind is a major source of currents in Long Lake during rain storms with associated strong wind. Flow measurements carried out using drogues (lagrangian method)

showed that surface speeds range from 0.01 to 0.1 cm/s due to through flow during calm winds in Long Lake. However, larger currents (2.6 to 12.5 cm/s) were also recorded during periods of moderate winds varying from 2.1 to 4.6 m/s (Figure 7.10). Computed circulation in the lake show that water currents in the lake are primarily due to wind effects. Hydrologic through flow contributes very little to the net water transport in the lake. Wind setup and seiches have an influence on water balance in Long Lake. As shown in Figure 7.9 a change in head of 7 cm due to wind setup could increase the Long Lake outflow by 1.4 m^3/s. Conversely, a wind setdown may reduce the outflow. This may be a factor to be considered in water and mass balance calculations.

8.2.2 **Non-linear 3D Hydrodynamic Model**

A three dimensional hydrodynamic model provides a better prediction of the surface currents and current profiles during summer stratified period in Long Lake. However, the model predictions in the two dimensional vertically averaged mode provides reasonably good results for most purposes during summer if false bottom at thermocline is used. The hydrodynamic model was tested for its response to variable wind speeds and then used to simulate mean wind driven circulation and current profiles in the lake. The results from the circulation model were later input to water quality model for predictions.

Wind-induced current structure involves the solution of the one-dimensional hydrodynamic equations describing currents through the vertical at a point. The work of Ekman is a classic example of this, however, eddy viscosity was assumed to be constant in his research. Subsequently solutions for several vertical eddy viscosity distributions have been computed as discussed in Chapter 2. The principal difficulty with a point model is that it considers the wind stress and bottom stress at a given position only. To overcome this problem, a three-dimensional model was developed for small lakes and reservoirs in this research. This model uses a two-dimensional hydrodynamic model to compute the total flow in a region. A current profile at a point is then extracted from the model by solving the

hydrodynamic equations in the vertical direction.

The method developed is computationally efficient in that only the two-dimensional equations have to be solved over the whole region of interest. This method is computationally economical when profiles at a selected number of points and times are required. However, this method would be computationally expensive if used to study the full three-dimensional wind-driven and stream flow circulation in a lake or reservoir. This three dimensional model developed has also an advantage over the three-dimensional layered or grid models of yielding continuous current profiles. Moreover, they provide a computationally feasible and reasonably accurate alternative to other three-dimensional models.

The above model computes wind-driven and/or stream flow/tidal circulation in any defined area of Long Lake. The program has a single block structure. The hydrodynamic model enables the detailed study in a specific region of interest in the Lake. The model also computes dynamic vertical velocity profiles for any specified area. Implementation and calibration/verification details of the models are discussed.

The results of the simulation for mean wind driven circulation in the Long Lake for winds blowing from two predominant directions, such as, southeast and northwest are presented in Figures 8.3, 8.4 and Appendix A. The vertical variation of wind driven currents for selected location presented in Figures 8.5 to 8.8 shows rapid reduction of wind-driven current with depth in the top two metres. The current speed reduction below 2 meters is gradual.

The hydrodynamic model in the steady state mode was run to simulate stream flow and wind-driven circulation using a northwesterly synthetic wind with a maximum wind speed of 10 m/s. Computations were carried out for 36 hours after reaching steady conditions. The results are presented at hourly intervals.

The water heights at the open boundary are generated from the hydrodynamic model. A linear interpolation scheme is used to compute intermediate values in both time and space.

The grid size is 62.5 meters with a maximum depth of 23 meters average over the grid. For stable computations, the time step must be equal to or less than 2 seconds. The time step selected for this case study was 1 second. Thus, 3600 time steps correspond to 1 hour of real time. The results are presented in Appendices D and E.

8.2.3 Near-Field Prediction of a Hypothetical Effluent Plume

8.2.3.1 General Principles of Mixing Zone Prediction and Environmental Analysis

For a reliable mixing zone prediction and environmental analysis, it is necessary to evaluate each scenario through several iterations. Small changes in ambient or discharge conditions can sometimes cause drastic shifts in the applicable flow configuration and the size or appearance of mixing zones. The plume analysis has been used to evaluate the size and shape of mixing zone, bottom impact of the discharge flow, water surface exposure, and bank attachment, and other factors. The plume mixing zone is generally sensitive to discharge geometry variations, ambient conditions, and discharge flow changes.

Actual process changes can result in variations of one or more of three parameters associated with the discharge: flow rate, density, or pollutant concentration. The total pollutant mass flux is the product of discharge flow times the discharge pollutant concentration. Thus, decreasing the pollutant mass flux will, in general, decrease the resulting pollutant concentration in the near-field and far-field. For a given pollutant mass flux, an increase in discharge flow implies an increase in discharge pollutant concentration, and vice versa. For the variety of flow classes there is no universal rule whether high or low volume discharges are preferable for optimizing near-field mixing. Mostly, the sensitivity is small, and even more so for far-field effects. A change in discharge flow will influence, in turn, the discharge velocity and hence the momentum flux.

The actual density of the discharge flow controls the buoyancy effects relative to the ambient water. Occasionally, the discharge density is controllable through the amount of

process heating or cooling occurring prior to discharge. Usually, near-field mixing is enhanced by maximizing the total density difference (positive or negative) between discharge flow and ambient water.

The turbulent mixing and dispersion processes when waste effluent is discharged from the outfall into receiving waters, are normally divided into three stages (1) jet-mixing stage in initial mixing field, or called near field, close to the discharge point. (2) spreading of wastefield in surface or submerged transition zone and (3) natural diffusion and advection stage in turbulent mixing zone, or called far field.

In stage 1, the buoyancy of discharge and momentum fluxes are dominant until at the end of the near field where the wastefield is established. The buoyant discharge rise to the water surface or to a intermediate equilibrium height of rise below the surface owing to the ambient density stratification and mix (entrain) with the ambient ocean water. In this stage 2, the momentum, buoyancy of discharge and ambient current are dominant. The established wastefield horizontally spreads and developments. In stage 3, mixing process is only dependent upon ambient ocean currents and turbulence. In moving water the horizontal velocity will govern the dilution. The wastewater is carried away by ambient ocean currents and further diluted by diffusion and advection.

The characteristics of the wastefield vary with the ambient current speed and direction. The dominant parameters of the established wastefield at the end of the initial mixing field typically are: the minimum initial dilution, S_m, the maximum rise height of the wastefield, z_{max}, and the thickness of the wastefield, h_c. The highest dilution exists at high ambient current, low discharge and weak ambient density stratification. Whereas, the lowest dilution occurs at low current, high discharge and strong density stratification. The rise height of the wastefield decreases with increase of dilution when the ambient current is perpendicular to the outfall axis and the rise height in the case of parallel to current direction is greater than that when normal to the current. As the ambient current speed increases, the thickness and rise height of the wastefield will generally reduce.

The physical transport of pollutants covers a broad range of scales, from lake and

ocean wide circulation to molecular motion. The spreading of a passive contaminant is influenced by advection and diffusion. To understand water quality variations, we need to have a through knowledge of the processes in boundary layers coupled to the surface and the solid boundaries. These processes include that occurring along ocean fronts, processes occurring in the interior of the lake or ocean related to eddies, spreading along isopycnic surfaces and small scale instabilities and molecular effects.

Bottom-generated turbulence mixes properties such as temperature and salinity to produce a homogeneous layer a few metres thick. The physical structure of the benthic layer influences biological, chemical and geological processes at or near the lake or ocean floor and how these processes communicate with the lake and ocean interior.

8.2.3.2 Near Field Predictions

In the present analysis, simulations were carried out taking into account the size and orientation of the outfall for different current regimes, stratification and effluent flows. The near-field analysis was carried out using the plume model. Far field mixing and transport computations were carried out using the advection diffusion model. The initial dilution represented in this study is the maximum concentration (not the mean concentration across plume) observable at the water surface. It is to be expected that the surface discharge plume for this situation will be quite variable in appearance and mixing characteristics since both ambient velocity conditions change and the discharge exit velocity will vary depending on lake water level variations. Therefore, several applications of the model were performed to assess the behaviour at different ambient currents and stratification. These individual steady-state plume predictions have been combined to obtain a complete description of the actual unsteady plume behaviour.

The near-field effects were examined for a hypothrtical effluent outfall located near the Clearcut Brook, and the performance of the outfall is evaluated by the prediction of the fate of a hypothetical effluent flow in the water column. The outfall location is at bottom

125 m off shoreline, at 8.5 m water depth and ambient inlet flow plus wind current of 0.08 m/s. The emphasis for the study was placed on the geometry and dilution characteristics of the near-field. In this study the decay processes for bacteria are assumed to be of first-order. Nova Scotia Department of Environment guidelines specify a mixing zone of about 100 m extending in any direction from the discharge point. The limiting values for faecal coliform bacteria (fc) should be below 200 fc/100 ml for recreational activities and below 14 fc/100 ml for shell fish harvesting.

The following are the ambient and discharge data used in the model:

Type of Outfall:	submerged single port pipe outfall
Outfall pipe diameter:	0.2 m (8") dia
Distance from shoreline to outfall:	125 m
Water depth at outfall:	8.5 m
Position of outfall centre:	0.3 m above sea bottom
Assumed effluent faecal coliform conc:	5000/100 ml
Ambient stream flow plus wind current:	0.08 m/s.

Three-dimensional perspective plot of the plume centreline location for the hypothetical case study is shown in Figures 8.9. Plots of dilution and bacteria (faecal coliform) concentration (#/100 ml) with distance perpendicular to the outfall pipe are presented in Figures 8.10 and 8.11. Plume model results showing plume geometry, dilution rates, and bacteria concentrations are presented in Table 8.1 and in Appendix C.

8.2.3.3 Hydraulic Behaviour of Effluent Plume

The discharge configuration is hydrodynamically "stable", that is the discharge strength (measured by its momentum flux) is weak in relation to the layer depth and in relation to

the stabilizing effect of the discharge buoyancy (measured by its buoyancy flux).

In the first near-field zone, depending on the ratio of the jet to crossflow length scale to the plume to crossflow length scale the above zone may be replaced by a strongly deflected jet in crossflow. In the second near-filed zone, the plume is strongly deflected in the crossflow. The plume has been strongly deflected by the current and is slowly rising. The plume approaches the layer pycnocline boundary at about 3 m above lake bottom. The bent-over submerged jet/plume approaches the layer boundary ie, pycnocline. Within a short distance the concentration distribution becomes relatively uniform across the plume width and thickness.

8.2.3.4 **Far field Prediction**

The solution of the advection-diffusion equation was carried out using both forward difference and central difference schemes. The forward difference scheme was used for all simulations carried out for sensitivity analysis and all simulations. It was found that the numerical diffusion is relatively small for the simulations carried out in this study. An example of mass balance computations for a stratified lake is presented in Appendix B.

Based on the calculated residual flows the mass transport in the inlet was calculated for each grid location for 72 hours both for wind from southeast and from northwest (Figures 8.12 and 8.13) and the dye concentration at different time intervals were obtained. A continuous dye source of 484 mg/l was released at 132 m /day discharge rate which mimics contaminant loading. As it is noticed from the simulation, the dye concentration at the source location is increasing gradually. Proper mixing and circulation of inlet waters is important to maintain quality of Long Lake. Strong density stratification in Long Lake occurs due thermocline which restricts the quantity of the water available for circulation and mixing, and hence the dilution of pollutants introduced into Long Lake.

8.3 **Model application to Parr Inlet**

Parr Inlet (Figure 1.2) has a narrow and shallow connection between the oval shaped inner Inlet and circular shaped outer Inlet with a narrow mouth to Dumbell Bay. The maximum grid depth in the inlet is 30 m in the northern outer Inlet and 25 m in the southern inner Inlet. Currents generally are higher at the entrance and the narrow connection between the two portions of the Inlet. The Inlet is about 2.05 km long, a mean width of 0.395 km and has a maximum depth of about 30.2 metres and mean depth of 10.6 m. The connection between these two bays is shallow with a water depth of 5 m. The entrance to the Inlet is narrow and well protected from the ocean waves from the open ocean. The mean tidal range is about 0.15 m with large tidal range reaching about 0.27 m.

Effluent disposal in the ocean compared with the inland treatment of sewage has many benefits, such as, lower capital expenditure, reduced operation and maintenance costs; minimum land requirements; less energy and resource consumption; reduced noise, odour and visual control etc. For the coastal cities and towns, one of the best and ultimate means for disposal of sewage effluents which are economically and environmentally is through a properly designed and optimally sited submarine outfall.

One of the most essential and dominant environmental parameters in the design of ocean outfall system and environmental impact assessment (EIA) of disposal of wastewaters, is the minimum initial dilution. An ocean outfall system must meet the environmental and public health requirements such as water quality control standards, criteria, laws, acts or rules issued by federal, provincial and local regulatory authorities for receiving waters to reduce possible hazardous consequences of the wastewater to the local receiving water environment.

A number of data sources were used in the plume/hydrodynamic model input, and evaluation of the assimilative capacity, such as, oceanographic data supplied by Jean Heroux, Canadian Hydrographic Office (CHS) Bathymetry Charts, and CHS Tide Tables. Ambient density profiles have been computed for extreme conditions using the above

measured data. Taking this assumption, the modelling has been conducted and the dispersion and transport of bacteria investigated.

The equations considered here are, the momentum equation and equation of continuity and include, the advective, Coriolis force, wind stress, and non-linear friction terms. Classical definitions of estuaries do not fit the case of some inlets in the high latitudes, such as, Parr Inlet, where snow melt instead of a river that contribute a large quantity of fresh water. Therefore, we describe here mixing in a class of water bodies that do fit Pritchard's definition of estuary " an estuary is a semi enclosed coastal body of water that has a free connection with the open sea and within which seawater is measurably diluted with fresh water derived from land drainage ". Major difference is that the fresh water source is distributed instead of point source as in rivers and streams. The main objective of the computation of the hydrodynamics in a tidal inlet is to provide the necessary input to a pollutant transport model.

The verified hydrodynamic and water quality models developed for Long Lake were later applied also to Parr Inlet. These models responded well to variable wind speeds, variable stream flows, and pollutant input loads (Chapter 7). Results of the hydrodynamic model simulation for different stages of the tide and after superposition of wind forcing over tide forcing are shown in Figures 8.14 to 8.20. The flood and ebb reversals are realistically simulated by the model and current vectors are similar to currents observed in inlets of similar configuration. When a steady wind of 10 km/h is superimposed on the tide, this produces a coastal current of maximum speed of 5 cm/s.

Wind speed and direction and temperature and salinity profiles at a number of locations in the inlet were used as model input (Heroux Personal Communication). Predicted tidal elevation at the inlet entrance were used for model simulations. Wind speed and direction data from weather station at Alert, the nearest weather station to Parr Inlet were also used for simulation purposes. Temperature and salinity profiles available for some representative stations in Parr Inlet were used to confirm the thickness of the fresh water layer, its spatial variation and to decide on the layered inlet configuration.

Parr Inlet has been divided into about 379 square segments of 50 m X 50 m. The average depth at each segment was then computed using a planimeter from a most recent bathymetric chart. Typical dimensions of the inlet are length and width, 2.05 km and 0.90 km respectively. The tidal variation computed at the Parr Inlet open boundary is shown in Figure 6.14. Water levels at the open (ocean) boundary serve as the forcing for the water motion in the inlet, and wind stress is also included. The input parameters are, wind stress, bottom friction, precipitation, and evaporation. Since Parr Inlet is stratified during summer, a multi-layered three dimensional model would be required to compute the water levels and currents for the summer period. However, the model will also run in the two dimensional vertically averaged mode and this could be sufficient when stratification is negligible.

During summer period, strong stratification of the inlet waters restricts the quantity of the water available for circulation and mixing, and hence the dilution of pollutants introduced into the inlet. Halocline starts at a depth of about 3 m and the inlet volume available for circulation & mixing is limited to the upper 0-3 m, which is only 22% of the total inlet volume. To represent this situation it was assumed that a false bottom exists at 3 m depth and simulations were carried out accordingly. The bottom layer is stagnant except for the vertical diffusion of mass for the transport of pollutant. However, the vertical component of velocity may be assumed to be small.

To run the model, the input data were read and initial values set for all variables. All water surface elevations are initially set equal, and set to the initial tidal elevation at the mouth of the inlet, thus giving a level surface throughout the system. Then the tidal elevation at the open boundary of the inlet is varied according to the given tide, and then the flow in the system is computed. The flow in the inlet depends on the tidal elevation at the mouth, the geometry and the wind stress. The model calculates the time dependent water level variations and horizontal velocity components using the inputs described above. The selection of a suitable time step is necessary for stability of the model results. The hydrodynamic simulation was carried out continuously for a period of 48 hours to reach equilibrium conditions.

Physical, chemical and biological processes in Parr Inlet are complex due to the shoreline configuration, circulation pattern and tidal characteristics. The mixing is further complicated by vertical stratification of two markedly different density layers which inhibit the mixing between the upper and lower layers. A three dimensional model is required to represent the hydrodynamics of near-field, however, a three-dimensional model based on two layers is sufficient to represent Parr Inlet hydrodynamics and water quality. However, the two layer approach developed for the far-field model is applicable to many layers in the vertical. The model results would help us to understand response of the inlet to alternate locations of the sewage disposal site, changes of the pollutant concentration and freshwater sources.

The model application to Parr Inlet has been carried out using both nearfield and far field models to understand the behaviour of the effluent plume in the receiving waters under different environmental conditions; and evaluation of the receiving water quality in terms of its compliance with Nova Scotia Standards and Guidelines Manual for the Collection, Treatment and Disposal of Sanitary Sewage. The segmentation of the inlet for water quality model is the same as that of hydrodynamic model. However, the difference is in the variables representing the model. This far-field model is a three dimensional, two layer model, and requires the input parameters, such as, inlet current components in the horizontal plane, tidal characteristics and rainfall quantity and quality.

The purpose of this application of the models to Parr Inlet is to evaluate the impact of sewage outfall on water quality and evaluate the assimilative capacity of the receiving waters. The assimilative capacity depends on wastewater characteristics, ambient currents, stratification, outfall geometry etc. The Federal Standards and Guidelines Manual requires a recreational water quality criteria for faecal coliform (fc) bacteria of 200 fc/100 ml and shellfish harvesting criteria of 14 fc/100 ml. Federal guidelines also require that the effluent from the sewage treatment plant should not exceed a faecal coliform count of 5000 fc/100 ml depending on the sensitivity of the receiving waters.

8.3.1 Water level variations

Numerical simulations of the tidal and wind driven currents in an in an inlet are presented in Figures 8.14 to 8.20. The initial simulation is carried out with only tidal forcing and results are shown in Figures 8.14 and 8.18. Generally, larger currents are observed at the central region of the inlet and at the entrance. At high tide the flow reverses in the short channel faster than in the mainstream, because the momentum in the mainstream cause the flow to continue for some time after occurrence of the highest tidal elevation. This means that flow may be coming out of the side channel and flowing upstream in the main channel; a portion of a pollutant cloud may be stored temporarily in the side channel and then be redeposited in the main channel while the bulk of the cloud is some distance upstream.

8.3.2 Predicted Tidal Currents

Currents in the Inlet entrance and at the gut between north and south bay are strongly confined in the north-south direction. Predicted maximum flood and ebb currents near the Inlet entrance are 0.16 and 0.12 m/s respectively, thus showing slightly stronger flood currents (Figures 8.14 to 8.20). The tidal residual current distribution in the Parr Inlet shows the dominance of the flood currents and the presence of an anti-clockwise eddy in the North Bay (Figure 8.20). This would indicate a longer retention time for sewage disposed if trapped in this eddy.

The main criteria for selecting a suitable model are mixing and circulation in the lake. To represent a conservative parameter (eg. dye, salinity) in the system, all the water quality data collected from the inlet have been examined. Variables which act as indicators of mixing are selected to understand the inlet response to pollutant loading. From this data different density layers in the Parr Inlet were configured for the model simulation.

Wind could be a major mechanism for strong currents in the inlet especially during the slack period (Figure 8.20). As pointed out earlier the wind waves produced by the wind

action have little effect on large scale dispersion. Assuming a steady uniform wind of 10 km/hr, blowing for 5 hours the hydrodynamic model was run for 5 hours. A steady state of generated currents was reached at the end of 4 hours.

Computed circulation in the inlet show that water currents in the inlet is primarily due to tidal and wind effects.5.1 Water Level Variations and Tidal Currents.

8.3.3 **Predicted pollutant distribution**

Both forward difference and central difference schemes were tried for the solution of the advection-diffusion equation. The forward difference scheme was used for all simulations carried out for sensitivity analysis and storm simulations. It was found that the numerical diffusion is relatively small for the type of simulations carried out in this study.

Based on the residual flows the mass transport in the inlet was calculated by solving the advection-dispersion equation for each grid location and for 48 hours to obtain the dye concentration at different time intervals. A continuous dye source of 484 mg/l was released at 132 m /day discharge rate which simulates the mean sewage loading to the inlet. The results of the simulation after48, 96, and 168 hours are shown in Figures 8.21 to 8.23. As it is noticed from the simulation, the dye concentration at the source location is increasing gradually. This shows that flushing rate at the mouth of the inlet is not sufficient to cause equilibrium concentrations. Proper mixing and circulation of inlet waters is important to maintain quality of inlets. Strong density stratification in the inlet occurs due halocline which restricts the quantity of the water available for circulation and mixing, and hence the dilution of pollutants introduced into the inlet. The halocline during summer starts at a depth of about 3m, with a top layer of average density 1.001.7 kg/m3 and a denser bottom layer below 3m with an average density of 1023.25 kg/m3. Therefore the inlet volume available for circulation and mixing is limited to the upper 0-3m, which was about 22% of the total inlet volume. The dissolved oxygen content gradually reduces from 11.7 mg/l at surface to 9.6 mg/l at 7 m. Various conclusions of this research are presented in Chapter 9.

Table 8.1 PLUME GEOMETRY AND TRAJECTORY

Plume Centerline Position			Dilution Ratio	Conc.	Vertical plume depth	Horizontal plume half width	Plume upper boundary	Plume lower boundary
X (m)	Y (m)	Z (m)						
.00	.00	.50	1.0	.500E+04	.10			
.98	.13	.71	3.8	.131E+04	.14			
1.41	.16	.78	5.3	.936E+03	.16			
5.29	.36	1.34	23.0	.217E+03	.33			
6.15	.39	1.45	27.6	.181E+03	.36			
7.87	.45	1.64	37.4	.133E+03	.42			
8.30	.46	1.69	40.0	.125E+03	.43			
9.60	.49	1.83	47.9	.104E+03	.47			
10.03	.50	1.87	50.7	.986E+02	.48			
15.63	.62	2.40	89.0	.560E+02	.64			
21.66	.73	2.90	135.5	.368E+02	.79			
23.25	.73	3.50	230.4	.216E+02	1.48	1.48	3.51	2.02
24.11	.73	3.50	233.8	.213E+02	1.44	1.55	3.51	2.07
25.84	.73	3.50	240.4	.207E+02	1.37	1.68	3.51	2.14
26.71	.73	3.50	243.6	.205E+02	1.34	1.74	3.51	2.17
27.57	.73	3.50	246.9	.202E+02	1.31	1.80	3.51	2.20
28.44	.73	3.50	250.1	.199E+02	1.28	1.87	3.51	2.22
29.30	.73	3.50	253.4	.197E+02	1.26	1.93	3.51	2.25
30.17	.73	3.50	256.6	.194E+02	1.24	1.98	3.51	2.27
31.90	.73	3.50	263.3	.189E+02	1.20	2.10	3.51	2.31
32.76	.73	3.50	266.6	.187E+02	1.18	2.16	3.51	2.32
33.63	.73	3.50	270.0	.184E+02	1.17	2.21	3.51	2.34
34.49	.73	3.50	273.4	.182E+02	1.15	2.27	3.51	2.35
35.36	.73	3.50	276.9	.180E+02	1.14	2.32	3.50	2.36
36.23	.73	3.50	280.4	.177E+02	1.13	2.37	3.50	2.38
37.96	.73	3.50	287.7	.173E+02	1.11	2.48	3.50	2.40
38.82	.73	3.50	291.4	.171E+02	1.10	2.53	3.50	2.40
39.69	.73	3.50	295.2	.169E+02	1.09	2.58	3.50	2.41
40.55	.73	3.50	299.0	.166E+02	1.09	2.63	3.50	2.42
41.42	.73	3.50	302.9	.164E+02	1.08	2.68	3.50	2.43
42.28	.73	3.50	306.9	.162E+02	1.07	2.73	3.50	2.43
43.15	.73	3.50	311.0	.160E+02	1.07	2.78	3.50	2.44
44.88	.73	3.50	319.4	.156E+02	1.06	2.88	3.50	2.45
45.74	.73	3.50	323.7	.154E+02	1.06	2.93	3.50	2.45
46.61	.73	3.50	328.1	.152E+02	1.05	2.98	3.50	2.45
47.47	.73	3.50	332.6	.149E+02	1.05	3.03	3.50	2.45
48.34	.73	3.50	337.1	.147E+02	1.05	3.07	3.50	2.46
49.20	.73	3.50	341.8	.145E+02	1.05	3.12	3.50	2.46
50.93	.73	3.50	351.4	.141E+02	1.05	3.21	3.50	2.46
51.80	.73	3.50	356.3	.139E+02	1.05	3.26	3.50	2.46
52.67	.73	3.50	361.3	.137E+02	1.05	3.30	3.50	2.46
53.53	.73	3.50	366.5	.136E+02	1.05	3.35	3.50	2.46
54.40	.73	3.50	371.7	.134E+02	1.05	3.39	3.50	2.46
55.26	.73	3.50	377.0	.132E+02	1.05	3.44	3.50	2.46
56.13	.73	3.50	382.5	.130E+02	1.05	3.48	3.50	2.45
56.99	.73	3.50	388.0	.128E+02	1.05	3.52	3.50	2.45
57.86	.73	3.50	393.6	.126E+02	1.05	3.57	3.50	2.45
58.72	.73	3.50	399.4	.124E+02	1.06	3.61	3.50	2.45
59.59	.73	3.50	405.2	.122E+02	1.06	3.65	3.50	2.44
60.45	.73	3.50	411.2	.121E+02	1.06	3.70	3.50	2.44
65.64	.73	3.50	449.2	.110E+02	1.09	3.95	3.50	2.42
66.51	.73	3.50	455.9	.109E+02	1.09	3.99	3.50	2.41
66.51	.73	3.50	455.9	.109E+02	1.09	3.99	3.50	2.41

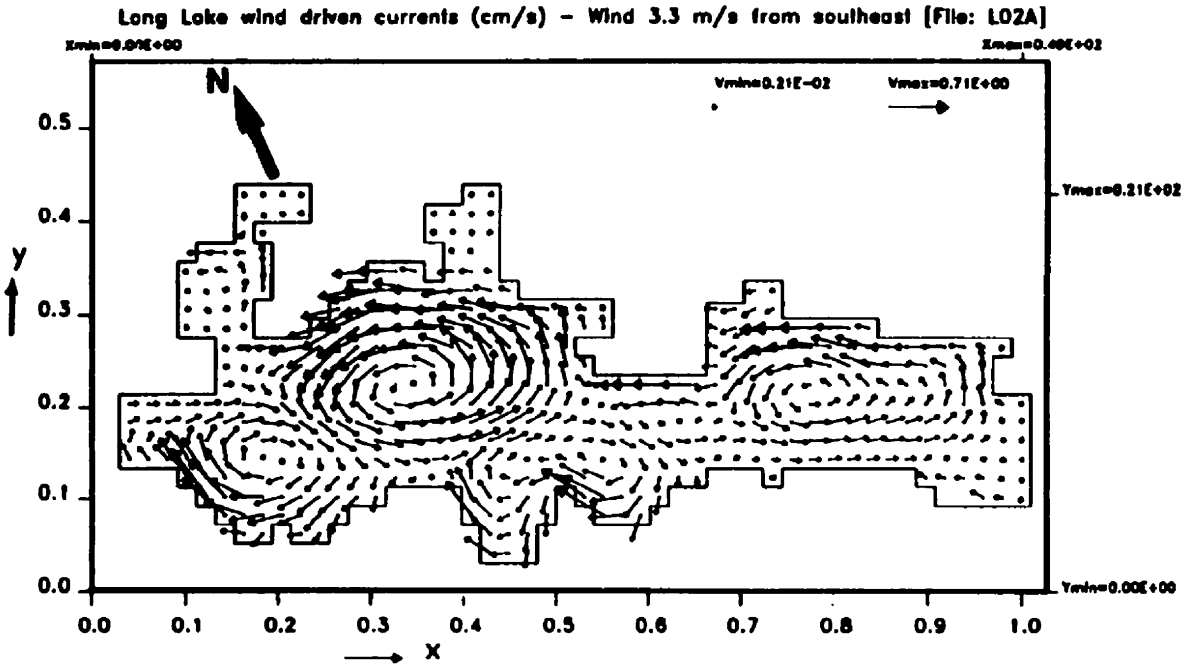

Figure 8.3 Long Lake wind driven currents (cm/s) for southeast wind3.3 m/s

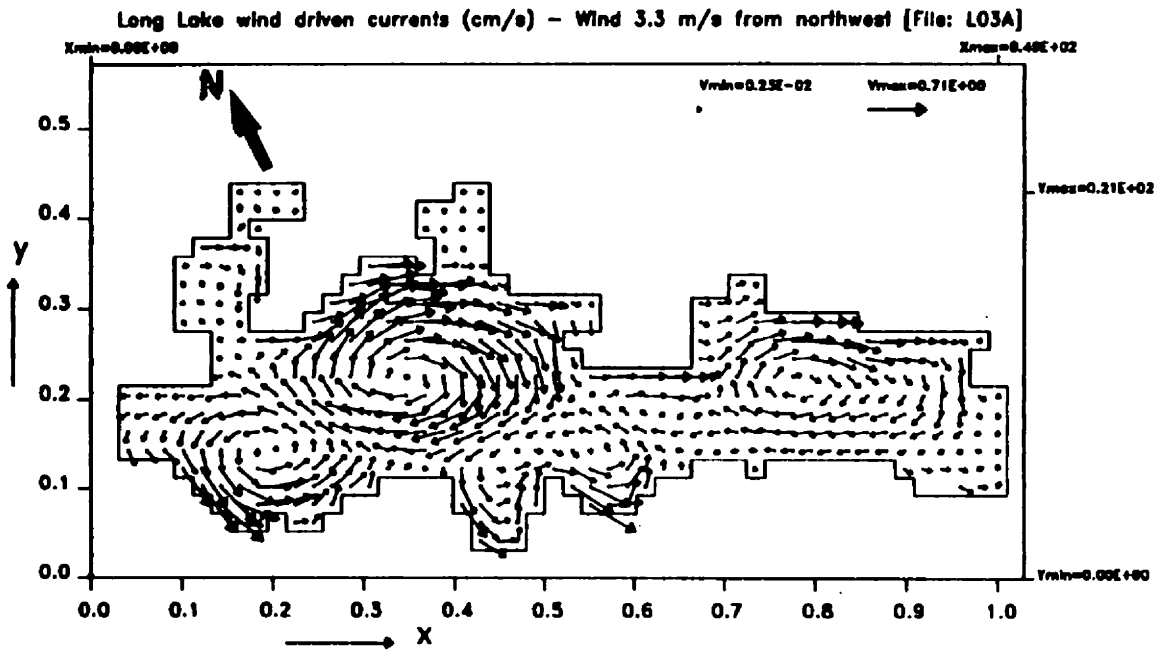

Figure 8.4 Long Lake wind driven currents (cm/s) - wind 3.3 m/s from northwest.

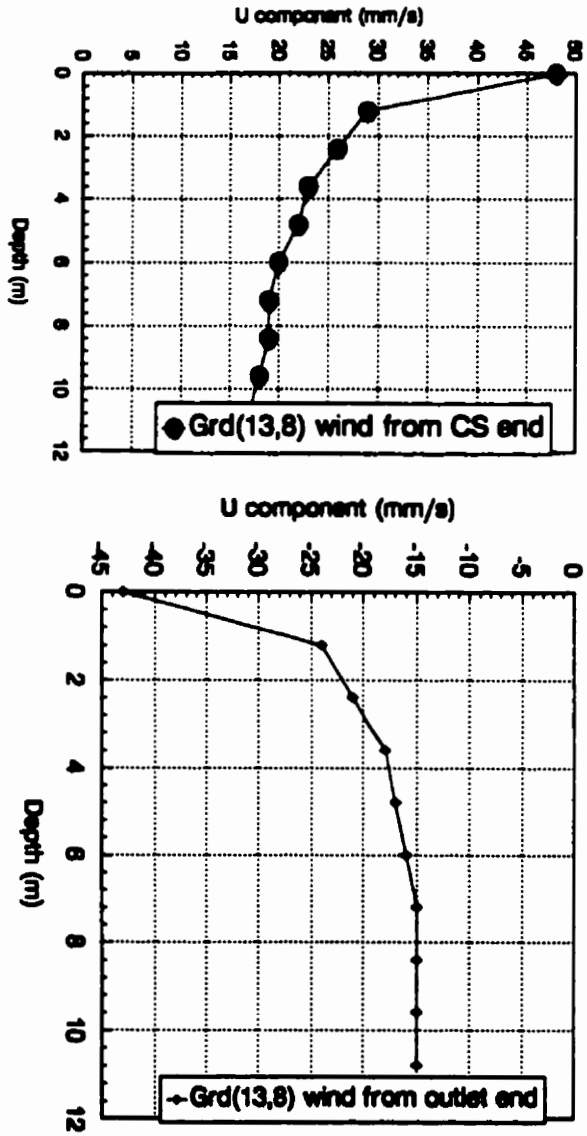

Figure 8.5 Long Lake wind driven currents - vertical profiles (grid location 1)

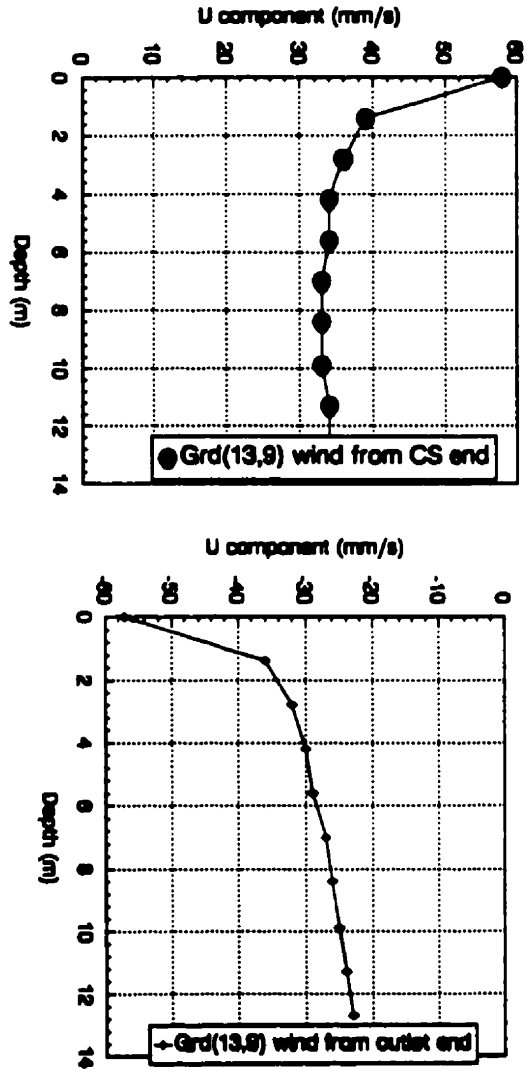

Figure 8.6 Long Lake wind driven currents - vertical profiles (grid location 2)

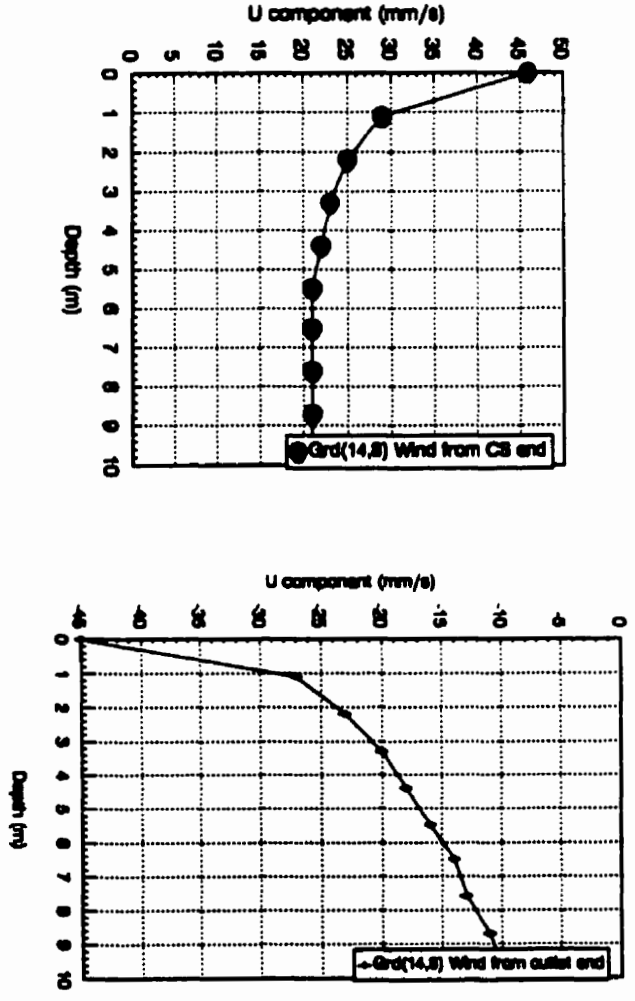

Figure 8.7 Long Lake wind driven currents - vertical profiles (grid location 3)

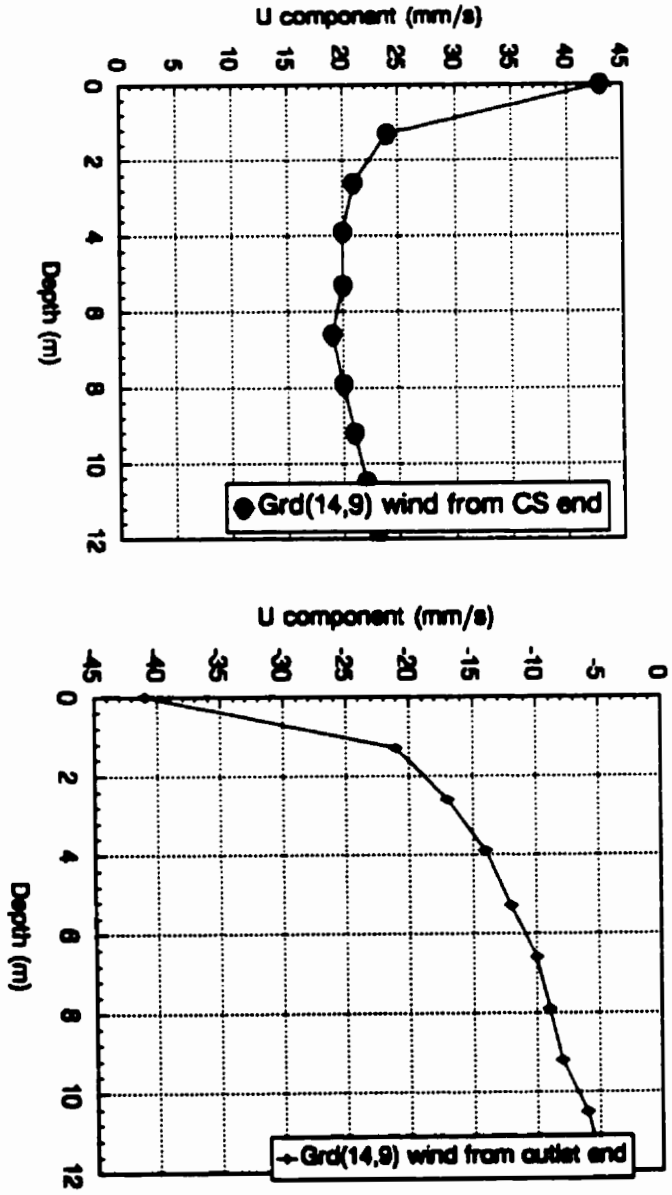

Figure 8.8 Long Lake wind driven currents - vertical profiles (grid location 4)

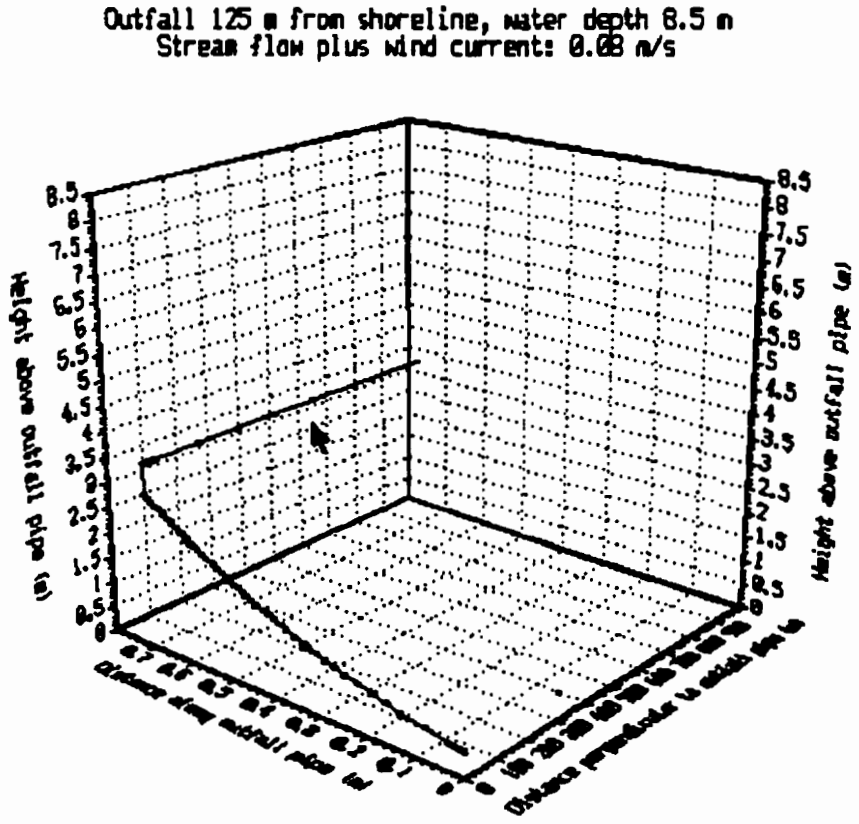

Figure 8.9 Three dimensional perspective plots of plume centerline location.

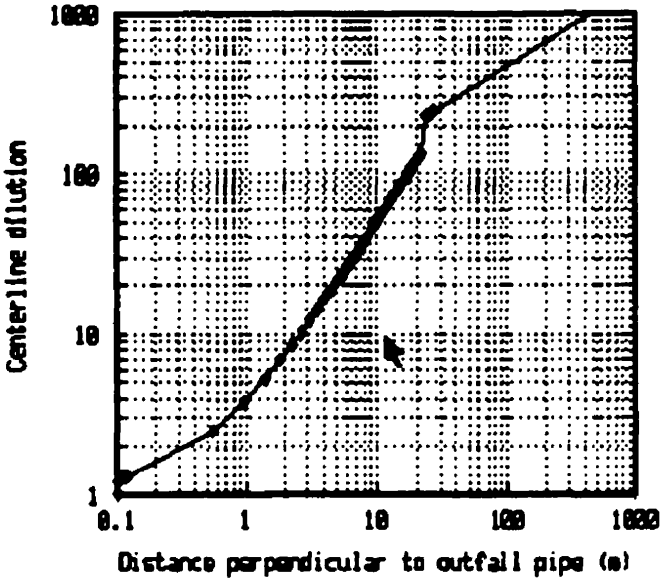

Figure 8.10 Near-field centerline dilution for a hypothetical pipe discharge.

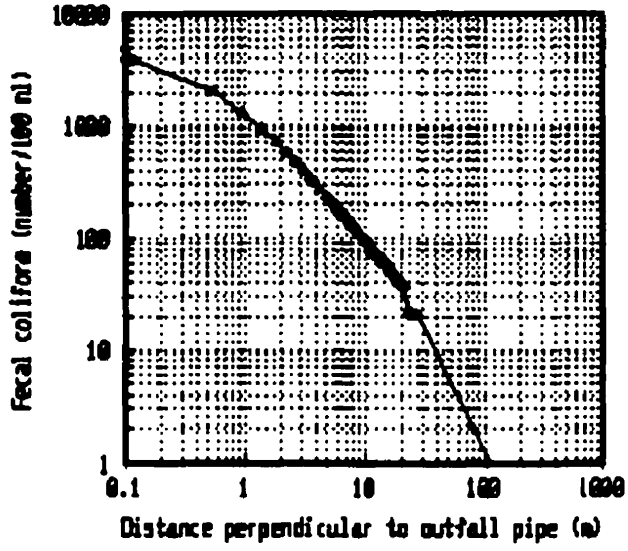

Figure 8.11 Near-field centerline faecal coliform concentration for a hypothetical pipe discharge.

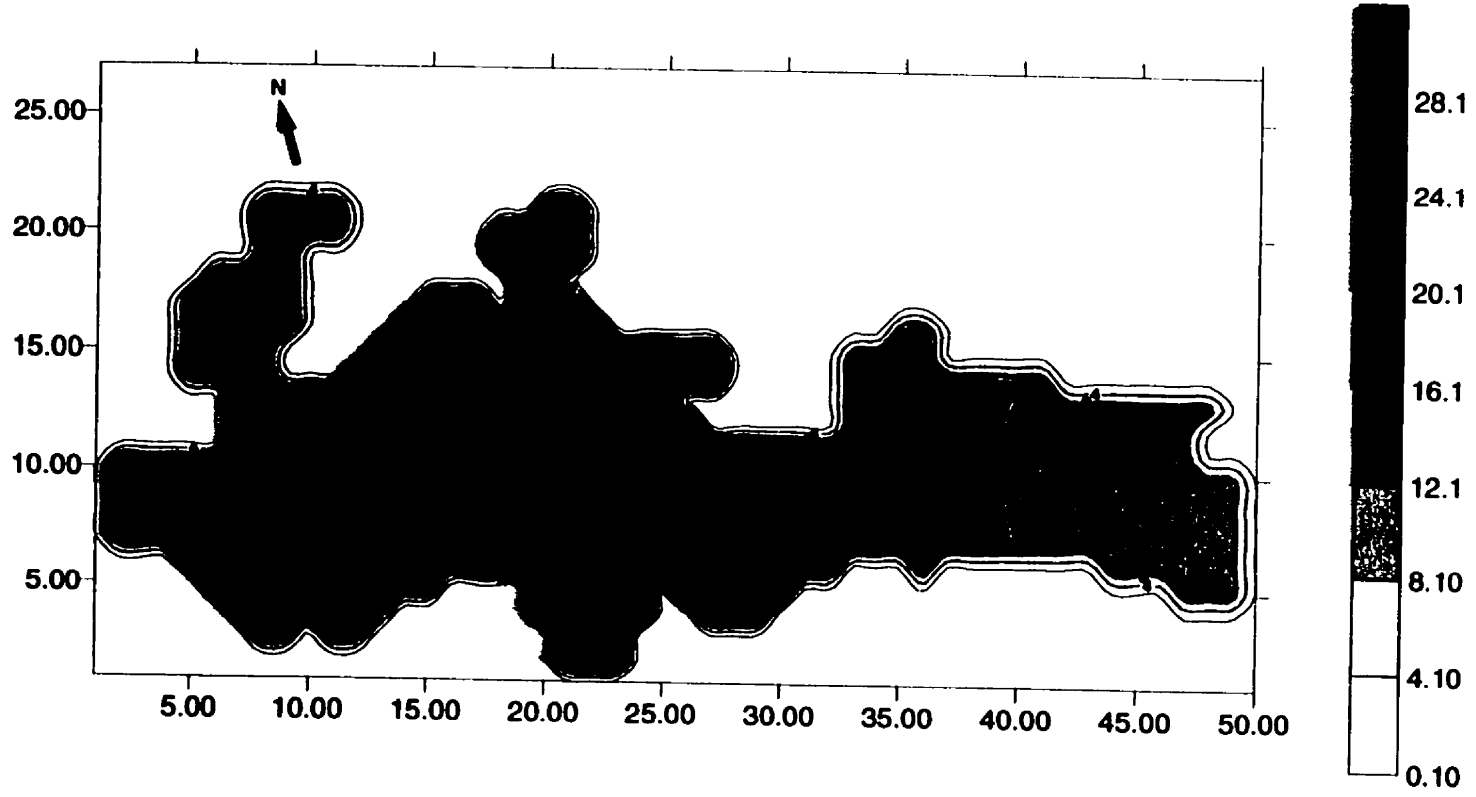

Figure 8.12 Long Lake dye concentration after 72 hours - wind from southeast.

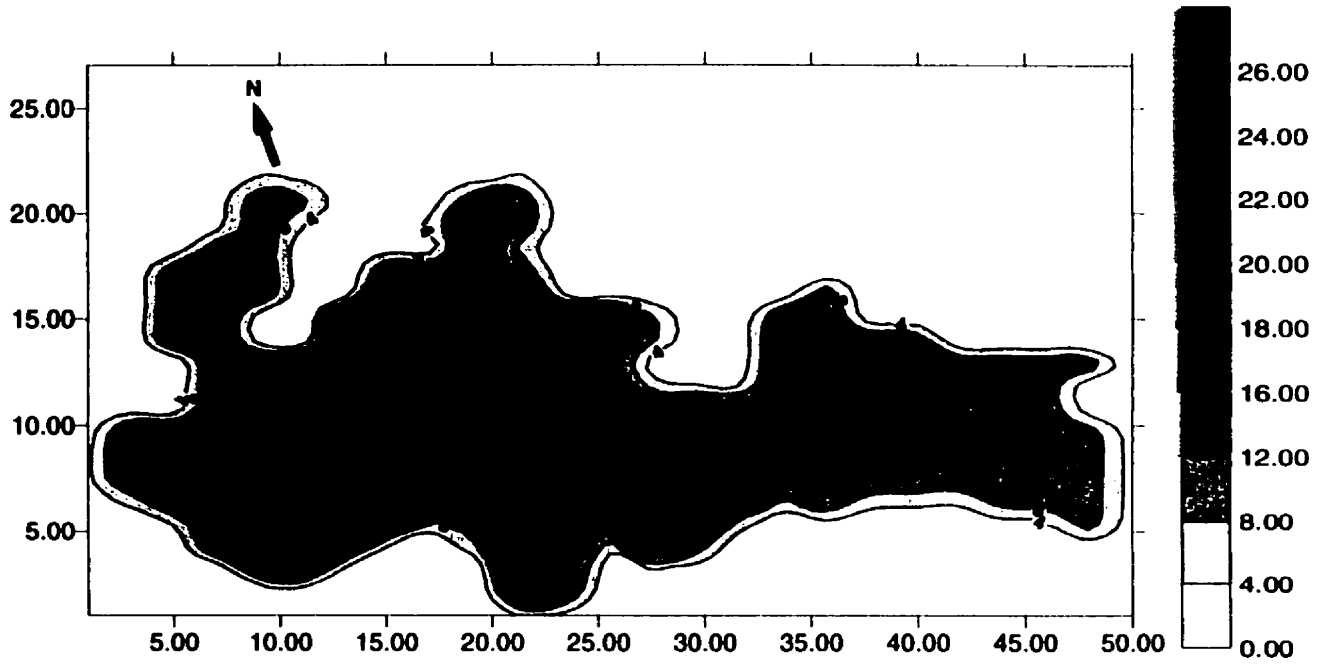

Figure 8.13 Long Lake dye concentration after 72 hours - wind from northwest.

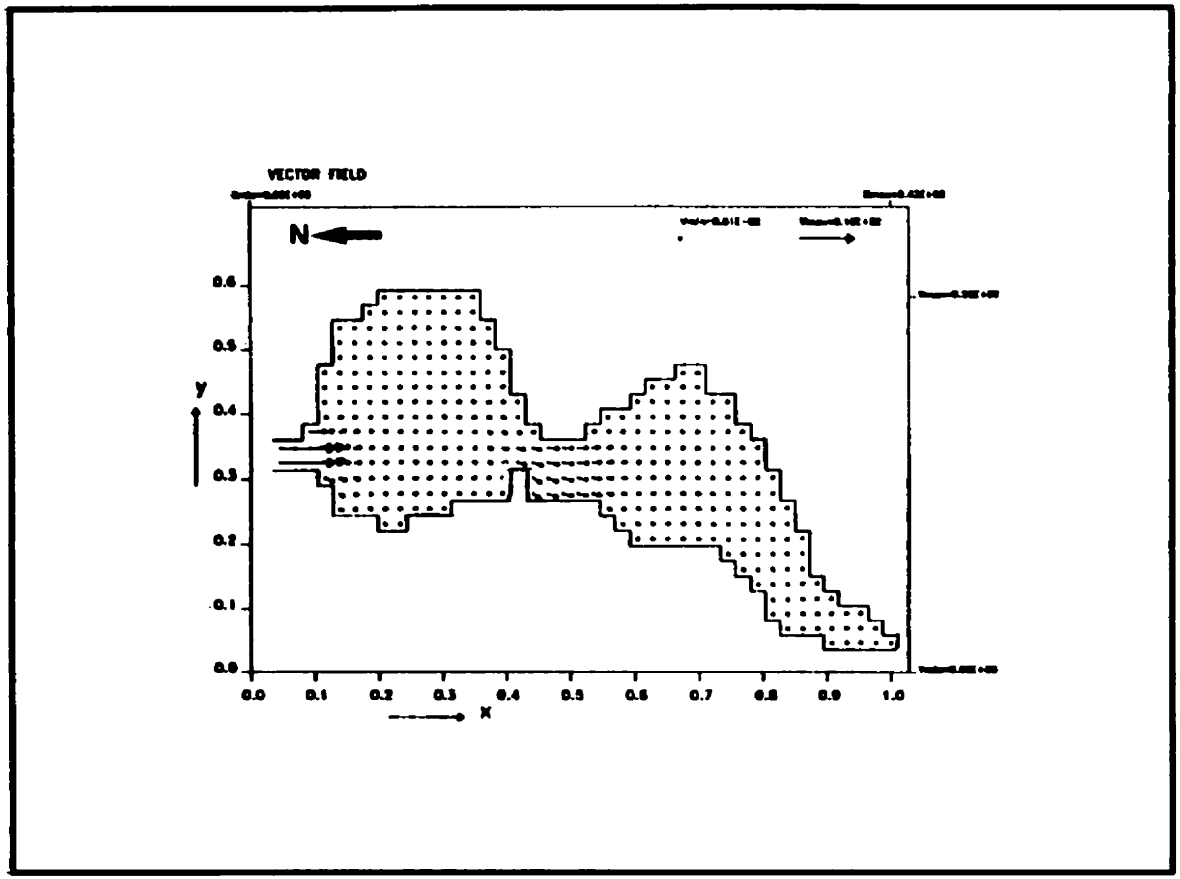

Figure 8.14 Parr Inlet tidal current field 0 hours after spin up

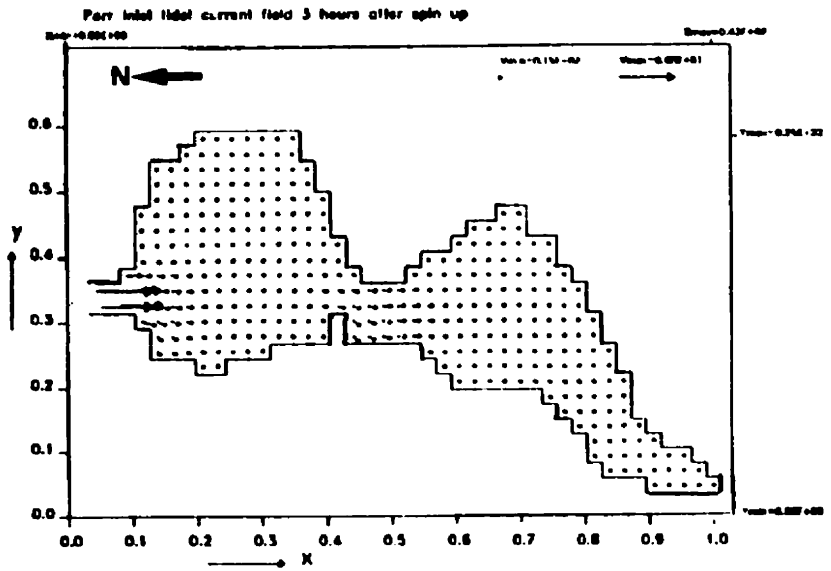

Figure 8.15Parr Inlet tidal current field 3 hours after spin up

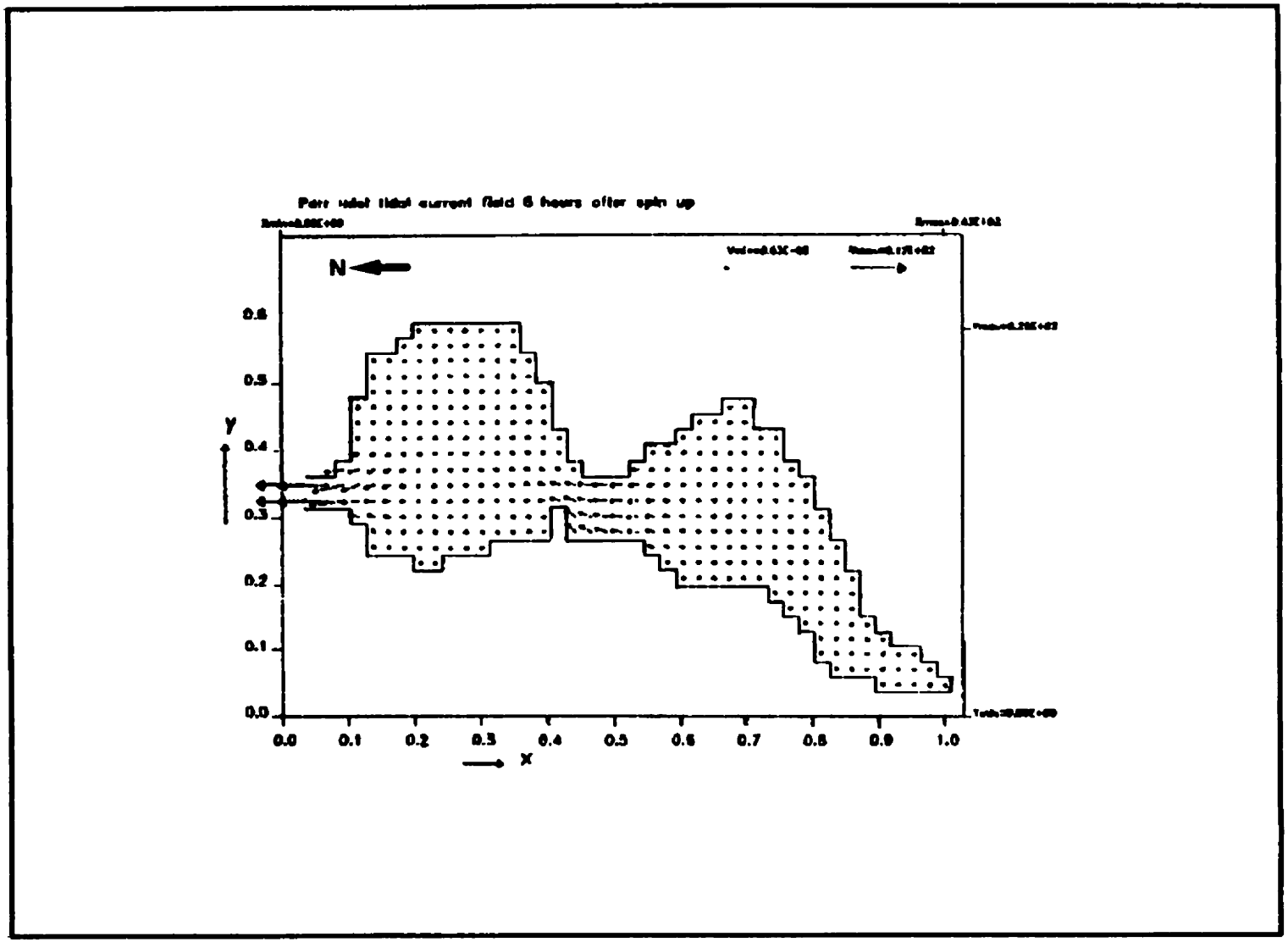

Figure 8.16 Parr Inlet tidal current field 6 hours after spin up.

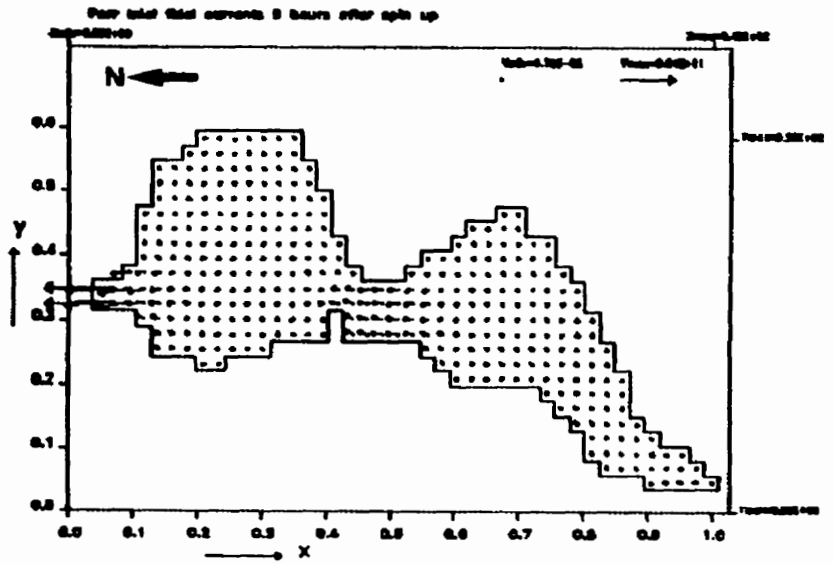

Figure 8.17 Parr Inlet tidal current field 9 hours after spin up.

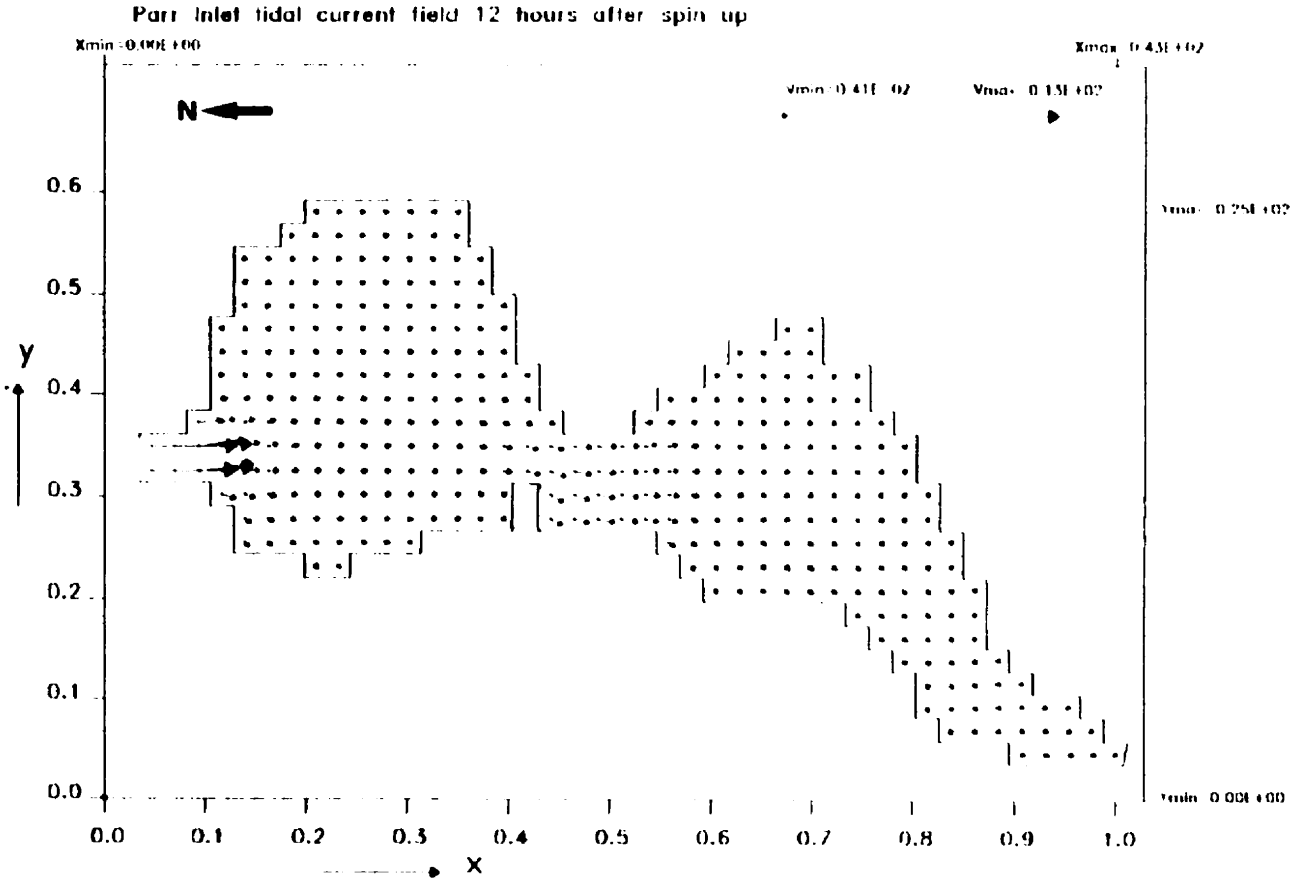

Figure 8.18 Parr Inlet tidal current field 12 hours after spin up.

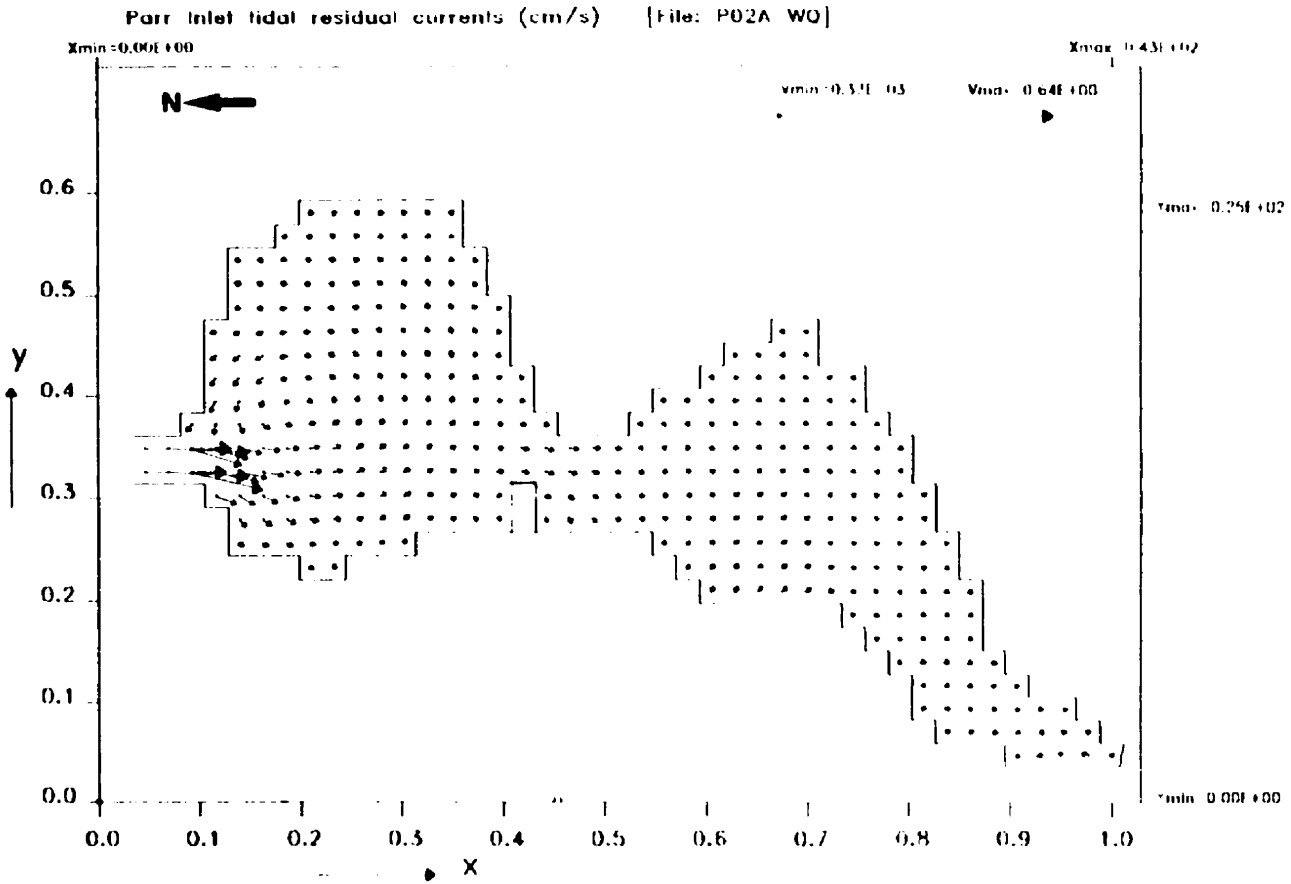

Figure 8.19 Parr Inlet tidal residual currents (cm/s)

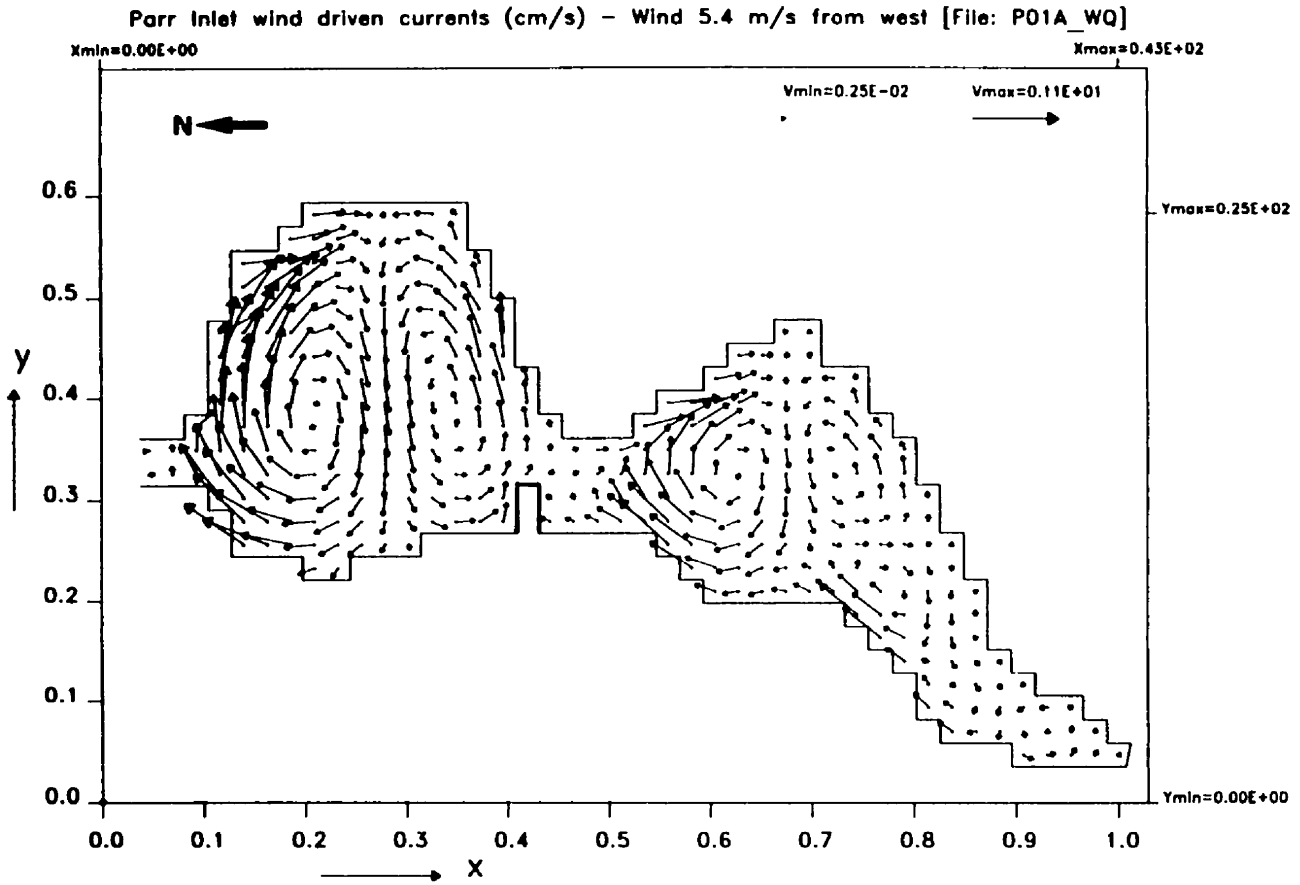

Figure 8.20 Parr Inlet wind driven currents (cm/s) - westerly wind 5.4 m/s.

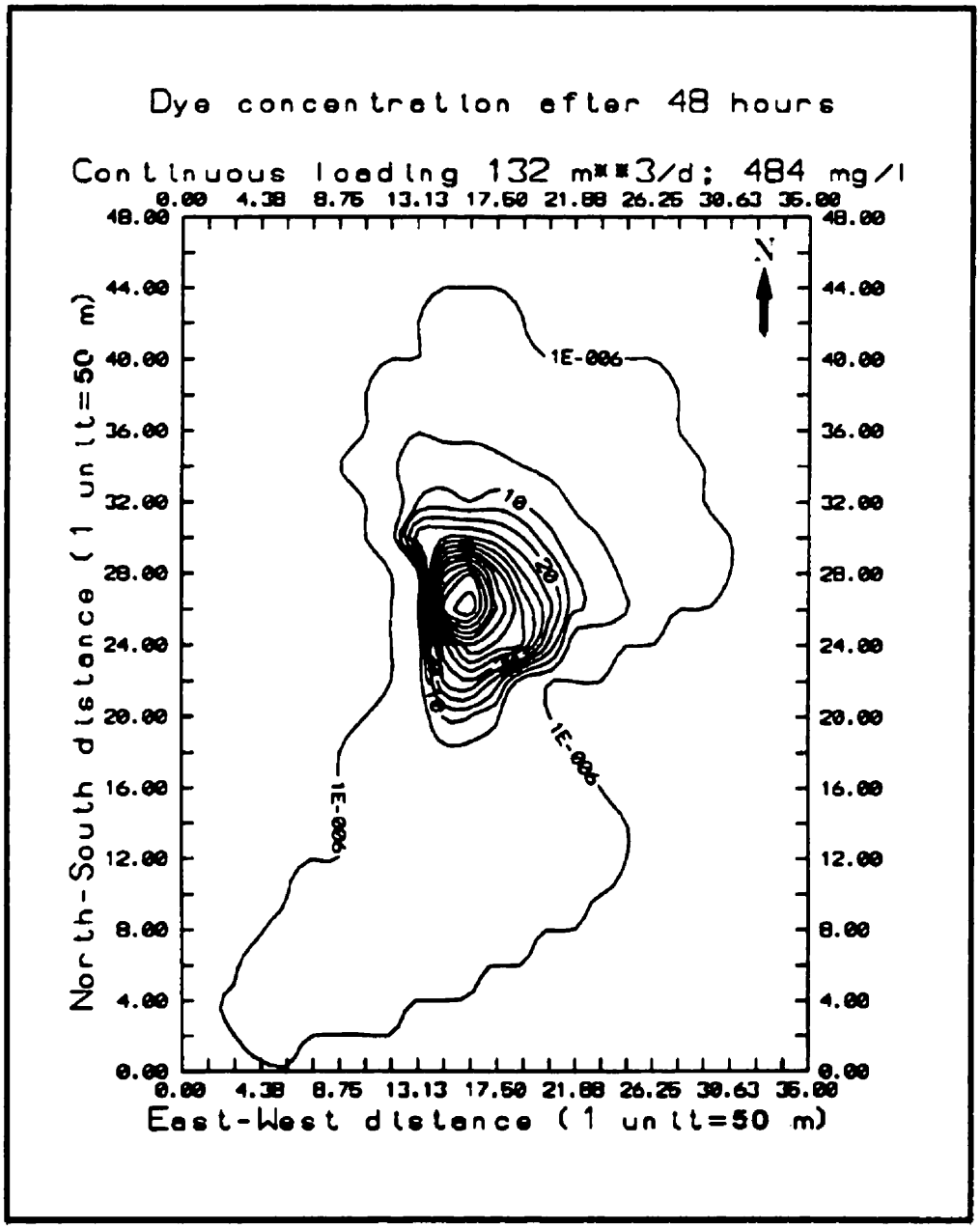

Figure 8.21 Dye concentrations in Parr Inlet after 48 hours.

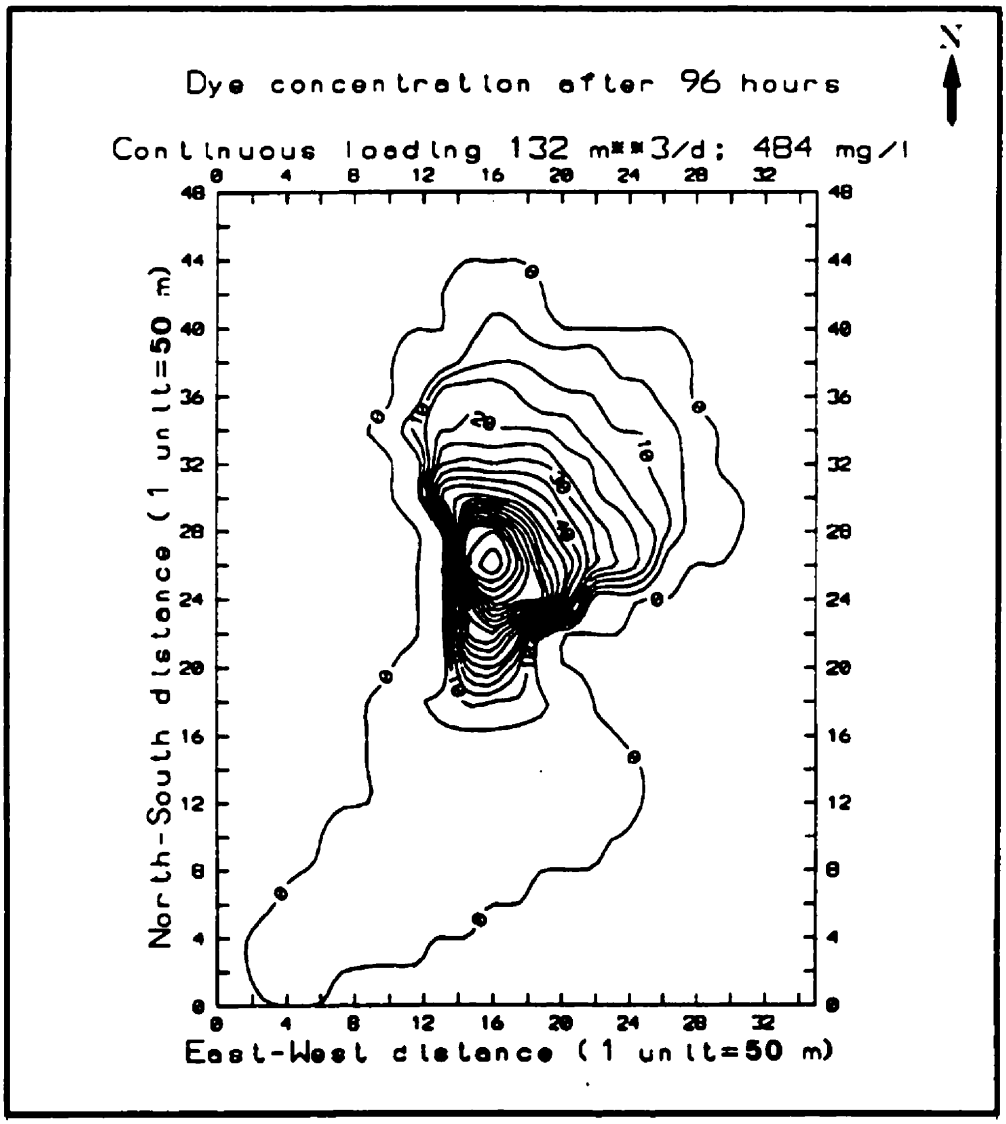

Figure 8.22 Parr Inlet dye concentration after 96 hours.

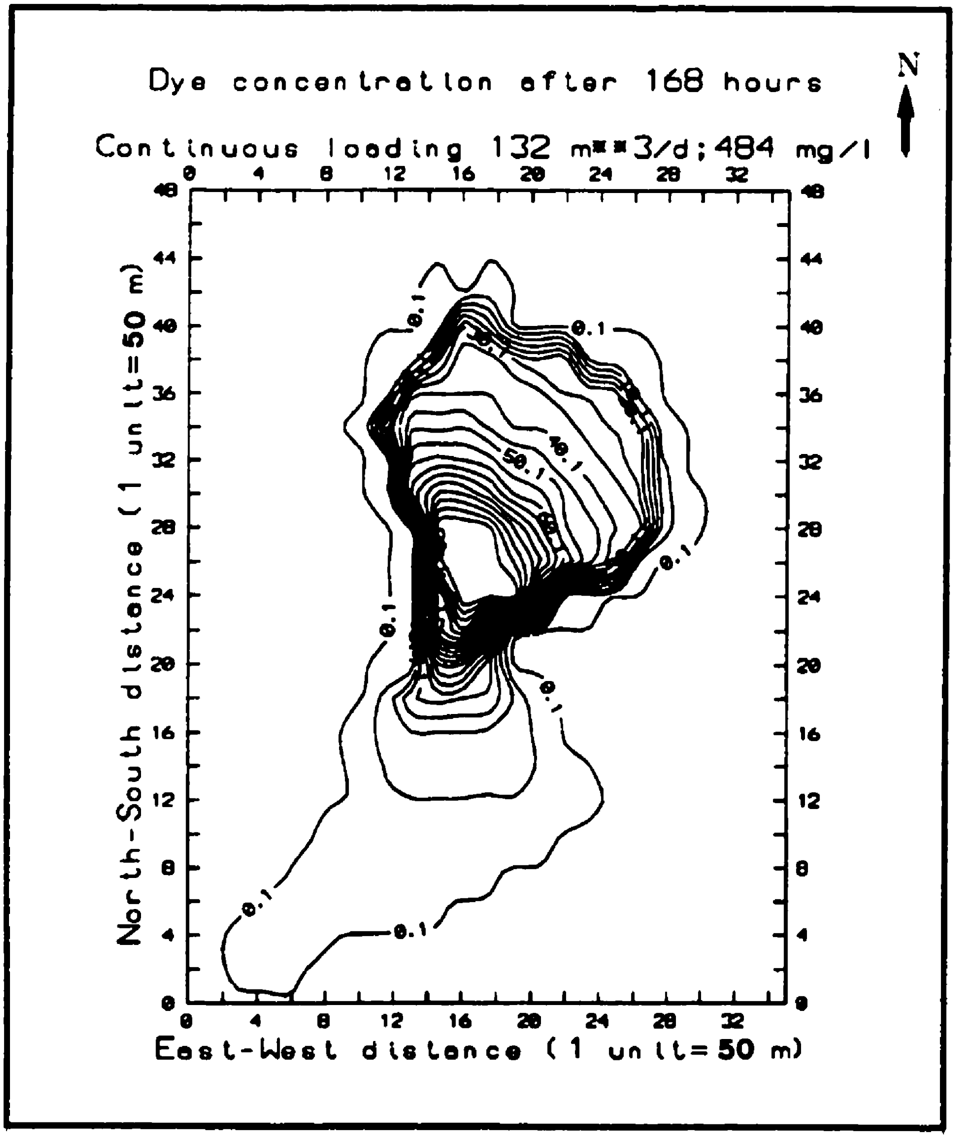

Figure 8.23 Dye concentrations in Parr Inlet after 168 hours

Chapter 9

CONCLUSIONS AND RECOMMENDATIONS

1. The three dimensional hydrodynamic model which utilizes a Vertically Varying Eddy Viscosity (VVEV) scheme developed in this thesis has the ability to simulate the unique characteristics of small lakes, reservoirs, and tidal inlets. It also provides a useful tool in monitoring and combatting pollution caused by municipal and industrial waste discharges, sediment transport studies, design of offshore and coastal structures, and the management of harbour operations.

2. This three dimensional model developed has an advantage over other three-dimensional layered or grid models of yielding continuous current profiles. Moreover, it provides a personal computer based 3-D model and a reasonably accurate alternative to other three-dimensional models. It also provides more accurate surface and near-bottom current predictions for reliable surface contaminant and bottom sediment transport predictions.

3. The three-dimensional hydrodynamic model has been validated using analytical models and results of an existing three-dimensional layered hydrodynamic model. 2-D depth averaged hydrodynamic model was validated with field data.

4. Non-linear convection terms in Navier-Stokes equation are important for simulation of wind-driven or tidal circulation in small lakes and tidal inlets and therefore are included in the three-dimensional hydrodynamic model.

5. Eddy viscosity variation with depth need to be considered in adequately describing wind driven currents especially in small deep lakes and variations of ambient current with depth are important.

6. The segment-node model initially developed in this thesis uses essentially a one-dimensional formulation to provide two dimensional flows and water level variations. This method uses a three segment cross sectional approach and is computationally efficient which makes it suitable for long term simulations. Applications of the segment-node model show good agreement with observed data.

7. Both the segment-node and the 3-D hydrodynamic model developed are very sensitive to head changes. Seiches with a period of oscillation of 14.4 min. was computed using both models for a constant wind speed of 15 m/s, causing elevation changes of 8 cm at the outlet end and 4 cm at the cove stream end.

8. Wind forcing was found to be the main causal factor for lake circulation especially during wind storms.

9. The linked hydrodynamic-water quality model simulates both near and far-field mixing and transport. The water quality model has been verified with analytical models. However, due to the limited variation of most water quality variables in Long Lake, the water quality model validation was limited to the chloride data.

10. Since thermocline exists below a depth of about 6m in Long Lake, the lake volume available for circulation and mixing is reduced to the upper 0-6m, which was about 65% of the total lake volume.

11. During summer, the hypolimnetic oxygen shows depletion with a lowest value of

11. During summer, the hypolimnetic oxygen shows depletion with a lowest value of about 5 mg/l (the minimum dissolved oxygen value necessary for fish propagation) and that suggests that vertical mixing of oxygen rich surface layer to the bottom layer is inhibited by the thermocline.

12. The greater degree of mixing in the epilimnion allows adequate aeration of the water, whereas, the water in the hypolimnion in Long Lake (during summer) will be some times depleted of oxygen. Therefore, it is of importance to determine the origin of the water withdrawn since this determines the quality of the outflowing water. The summer thermocline in Long Lake starts below about 5m depth and therefore the possibility of drawing water from below thermocline in the case of Long Lake is minimal.

13. Many existing lake water quality models neglect the water level variations in the mass balance computations. However, model applications to Long Lake show that water level variations affect mass balance distributions.

14. Recommendations for future work include:

- verification of the vertical profiles of currents predicted by the three-dimensional hydrodynamic model using moored current meters or Acoustic Doppler Current Profiler (ADCP) data.

- conduct moored current measurements using current meters of accuracy better than ±0.1 cm/s and obtain storm driven current profiles.

- modification of the water quality model to include resuspension of suspended solids to the water column from the lake bottom.

- conduct dye diffusion experiments and obtain in-situ horizontal and vertical eddy diffusion rates.

- detailed investigation of the internal and near-field hydraulics in the presence of a multi-port diffuser and prediction of the resulting concentration field.

Chapter 10

BIBLIOGRAPHY

Adams, E. Eric (1987) Vertical diffusion in a stratified cooling lake, Jour. Hyd. Div., ASCE, Vol 113, No. 3.

Allender, J.H. (1977) Comparison of model and observed currents in Lake Michigan., J. Phys. Oceanog. 7, 711-718.

Appelquist, H. and P.B. Nielsen (1989). A data-acquisition system for three-dimensional measurements of natural and artificial tracers in the sea, Danish Isotope Centre, Copenhagen, In: Oceanic Process. in Mar. Poll., vol.4, pp.31-38.

Attanayake, M.P. (1986). Application of Simulation Water Balance and Field Methods for Analysis of a Small Lake - Ground Water System. Ph.D. thesis, Department of Civil Engineering, Technical University of Nova Scotia, Halifax, N.S

Aydin, F. N. and Ahlert, R. C. (1978). A new view of dispersion in well-mixed estuaries. Ecological Modelling 15:301-326.

Beca and Arnett. (1976). A limnological model eutrophic lakes and impoundments, Battelle Pacific Northwest Laboratories. Prepared for Office of Research and Development U.S. Environmental Protection Agency.

Bhowmik, N.G. and Stall, J.B. (1978) Circulation pattern in the Fox Chain of lakes in Illinois. Water Resources Research 14, 633-642.

Biermann V.J. (1985). Research strategy for ocean disposal: Conceptual strategy and case study, In: Environmental Hazard Assessment of Effluents, H.L. Bergman, R.H. Kimerle, A.W. Maki (eds.), Pergamon Press, Elmsford N.Y., 25pp.

Blumberg, A.F., Kantha, L.H., (1985) Open boundary conditions for circulation methods, J. of Hydraulic Eng. Vol. 111, No. 2, pp. 237-255.

Blumberg, A.F. and Mellor, G.L. (1987) A description of a three dimensional coastal ocean model. Three Dimensional Coastal Ocean Models, N.S. Heaps, ed., Am. Geographical Union., Washington, D.C.

Bokuniewicz, H. (1989). Behaviour of sand caps at subaqueous dredged-sediment disposal sites, Marine Sciences Res. Centre, S.U.N.Y., In: Oceanic Process. in Mar. Poll., vol.4, pp. 221-229.

Boyce, F.M. (1979). Assessment of water quality simulation capability for Lake Ontario. Scientific Series Report No. 111. Inland Waters Directorate, National Water Research Institute, Canada Center for Inland Waters. Burlington, Ontario.

Brebbia, C.A. and Partridge, P.W., (1976) Finite element simulation of water circulation in the North Sea, Appl. Math. Modeling 1, pp. 101-107.

Bright, D.A.(1987). The Histology of Macoma Carlotlensis Whiteaves 1880 and Histopathology Related to Mine Tailings Discharge, U.Vic., MSc. thesis.

Byers, J.W. (1983). Report on hydrometeorological data in records of the Public Service Commission on Long and Chain Lakes watersheds. 1971-75, CWRS Contribution 1983-3.

Callaway, R. J. (1976). A brief assessment of estuarine modelling-recent developments and future trends. Pollution, Chapter 11.

Caswell, H. (1977). The validation problem, in systems analysis and simulation in ecology. Vol IV, B.C. Patten Ed. (New York: Academic Press). PP 313-325.

Champ, M.A.,Conti M.C. and P.K. Park (1989). Multimedia risk assessment and ocean waste management, U.S.E.P.A., Wash., In: Oceanic Process. in Mar. Poll., vol.3, pp. 3-24.

Chapra, S. C. and K. H. Reckhow (1983) Engineering Approaches for Lake Management, Vol. 1&2 Ann Arbor Science.

Chen, J. , (1975) A comprehensive water quality- ecological model for Lake Ontario. NTIS Report No. PB258064, Great Lakes Environmental Research Laboratory, USNOAA.

Cheng, R.T., T. M. Powell and T.M. Dilloin (1976) Numerical models of wind-driven circulation in lakes. Appl. Math. Modelling, 1, 141-158.

Chow, Ven Te (1976). Handbook of Applied Hydrology, McGraw Hill Book Company, N.Y.

Churchill, J.H. and Csanady, G.T. (1983) Near surface measurements of quasi-Lagrangian velocities in open water. J. Phys. Oceanog. 13, 1669-1680.

Connor, J.J. and Brebbia, C.A., (1976) Finite elements for fluid flow, Butterworth, London.

Connor, J.J. and Wang, J., (1973) Finite element modeling of hydrodynamic circulation, Numerical Methods in Fluid Mechanics ed. by C.A. Brebbia & J.J. Connor, Pendtech Press,

London. pp. 335-387.

Cross, F.A. and D.F. Boesch (1983). Assessment technologies workshop summary, In: Background Papers: IODS Spec. Sym. on Waste Mgmt. in the Ocean: Policies and Strategies, Intl. Ocean Disposal Sym., Florida Inst. of Technol., Melbourne, Florida, 11p.

Csanady G.T. (1967) Phys. Fluids Suppl. S76.

Csandy G.T. (1973) Turbulent Diffusion in the Environment. D. Reidel Publishing Company.

Davies, A.M., (1980) On formulating a three-dimensional hydrodynamic sea model with an arbitrary variation of vertical eddy-viscosity, Computer Methods in Appl. Mech. and Eng. 22, pp. 187-211.

Davies, A.M., (1980) Application of the Galerkin method to the formulation of a three-dimensional nonlinear hydrodynamic numerical sea model, Appl. Math. Modeling 4, pp. 245-255.

Davies, A.M., (1982) On computing the three dimensional flow in a stratified sea using the Galerkin method, Appl. Math. Modeling, 6, pp. 347-362.

Davies, A.M., (1985) Application of the DuFort-Frankel and Saul'ev methods with time splitting to the formulation of a three-dimensional hydrodynamical sea model, Int. J. Num. Methods in Fluids 5, pp. 405-425.

Davies, A.M., (1985) On determining the profile of steady wind-induced currents. Appl. Math. Modeling, 9, pp. 409-418.

Davies, A.M., and Furnes G.K., (1980) Observed and computed M2 tidal currents in the North Sea, J. Phys. Oceanogr., 10, pp. 237-257.

Davies, A.M. and Owen, A., (1979) Three dimensional numerical sea model using the Galerkin method with a polynomial basis set, Appl. Math. Modeling, 3, pp. 421-428.

Davies, A.M. and Stephens, C.V., (1983) Comparison of the finite difference and Galerkin methods as applied to the solution of the hydrodynamic equations, Appl. Math. Modeling, 7, pp. 226-240.

Delvigne G.A.L. (1987) A model for vertical diffusion in stratified shear flows , Jour. Hyd. Res. ASCE, V 112, #11

Devine M. (1987) Analysis of mixing and dispersion of individual wastes dumped into the deep sea., NOAA Oceanic Processes in Marine Pollution, Vol 2.

DiToro, D. M. and Conolly, J.P., (1980). Mathematical models of water quality in large lakes. Part 1: Lake Huron and Saginav bay. Report No. EPA-600/3-80-056. USEPA.

Dobroklonskiy, S.V., (1969) Drift currents in the sea with exponentially decaying eddy viscosity coefficient, Oceanology, 9, pp.19-25.

Duff, G.F.D., (1983) A special ADI model for the Laplace tidal equations, Comp. & Math. with Applics., 9, pp. 507-516.

Dumnicka, E. et al. (1988). Effects of regulated streams on the hydrochemistry and zoobenthos in differently polluted parts of the upper Vistula River (Southern Poland). Hydrobiologia (Den.), 169, 183.

Dyke, P.P., (1977) A simple ocean surface layer model, Riv. Ital. Geotis., 4, pp. 31-34.

Environmental Protection Agency (1978) Rates, constants and kinetics, formulations in surface water modelling. USEPA.

Environmental Protection Agency (1985) Rates, constants and kinetics, formulations in surface water modelling. USEPA.

Feigner and Harris (1970) Documentation report - FWQA dynamic estuary model, U.S. Department of the Interior, Federal Water Quality Administration.

Fisher, I.H. (1983) Field measurement of shallow lake circulation. Proc. Eighth Australian Fluid Mechanics Conference, Newcastle, NSW, (ed. R.A. Antonia), pp 6A.10-14.

Fischer ,H.B et al, (1979) Mixing in Inland and Coastal Waters, Academy Press, New York., Proc. 21st Congress, Int. Ass. for Hydraulic Res., Melbourne.

Fischer, H. (1989). An alternative approach to the biological monitoring of metals in the mussel Mytilus edulis, Kiel, F.R.G., In: Oceanic Process. in Mar. Poll., vol.4, pp. 94-99.

Flather, R.A. and Heaps, N.S., (1975) Tidal Computations for Morecambe Bay, Geophys. J.R. Astr. Soc. 42, pp. 489-517.

Forristall, G.Z., (1974) Three dimensional structure of storm-generated currents, J. Geophys. Res., 79, pp. 2721-2929.

Forristall, G.Z., (1980) A two-layer model for hurricane-driven currents on an irregular grid, J. Phys. Oceanogr. 9, pp. 1417-1438.

Freeman, N., G., Hale, A.M., and Danard, M.B., (1972) Modified sigma equation approach to the numerical modeling. Great Lakes Res. 77, 1050-1060.

Fraser, J. (1986)., Department of Civil Engineeing, TUNS, Halifax, N.S.M. A. Sc. Thesis.

Gardner, G.B. and D. W. Pritchard (1974) Verification and use of a numerical model of the Chesapeake and Delaware Canal. Tech. Rep. 87, Ref 74-7. Chesapeake Bay Institute, The Johns Hopkins University.

Godin, G. (1972). The Analysis of Tides. The University of Toronto Press.

Graf, W.H., Perrinjacquet, C., Bauer, S.W., Prost, J.P. and Girod, H. (1979). Measuring on Lake Geneva (Le Leman). In Hydrodynamics of Lakes (eds W.H. Graf and C.H. Mortimer), pp. 123-148, Elsevier, Amsterdam.

Gu R. and Stefan H. (1988) Mixing of temperature stratified lakes and reservoirs by buoyant jets. J. Environ. Eng. Div. Proc. Am. Soc. Civ. Eng., 114, 898.

Haebler, Roland.(1983). A hydrologic study of the Beaverdam Brook watershed, Halifax, Nova Scotia.,Centre for Water Resources Studies, Contribution No. 83-11, TUNS, Halifax, Canada.

Haebler, Roland. (1984). Stage discharge curves in the Halifax Urban Watershed. Centre for Water Resources Studies, Contribution No. 84-1, TUNS, Halifax, Canada.

Haebler, Roland. (1985). Complete rainfall, lake level, stream discharge and water quality data for the storm event of June 26, 1984. Center for Water Resources Studies Contribution No. 85-3. Technical University of Nova Scotia, Halifax, N.S

Halifax Harbour Task Force. (1990). Final Report, Ministry of Environment, Halifax, Nova Scotia.

Haney, R.L. (1991). On the pressure gradient force over steep topography in sigma coordinate ocean models. J. Phys. Oceanography, 21, 610-619.

Hansen, W., (1962) Hydrodynamical methods applied to oceanographic problems, Proc. Symp. Math. Hydrodyn. Phys. Ocean., Institute fur Meereskenude, Universtat Hamburg, pp. 24-34, 1962.

Harleman, D.R.F., Lee, C.H., and Hall L. (1968). Numerical studies of unsteady dispersion in estuaries. Journal Sanitary Engineering Division ASCE 94(SA5)

Heaps, N.S., Storm Surges, (1983) 1967-1982, Geophys. J., R. Astron. Soc., 74, pp. 331-376.

Heaps, N.S. (Ed.), (1987) Three Dimensional Coastal Ocean Models, American Geophysical Uni.

Hen, C.J. and Hunter J.R., (1988) A new method for describing bottom stress in two dimensional hydrodynamical models of shallow homogenous seas, estuaries and lakes, Appl. Math. Modeling, Vol. 12, pp. 573-580.

Henaidi, A.K., (1984) Preliminary report on drifting buoy movements, MEPA, Gulf Area Oil Companies Mutual Aid Organization, GAOGMAO, December No. GO-86/87-07.

Hood, D.W. (1989). Evolution of at sea scientific monitoring strategies, School of Ocean., U. of Wash., Seattle, In: Oceanic Process. in Mar. Poll., vol.4, pp. 3-28.

Huang, W. and M. Spaulding (1996) Modeling Horizontal Diffusion with Sigma Coordinate System. Journal of Hydraulic Engineering. Vol. 122, No. 6.

Hunter, S.C., (1975) A note on quadratic friction in the presence of tides, Estuarine and Coastal Marine Science 3, pp. 473-475.

Hydroscience Inc., (1970). Development of water quality model of Boston Harbour., Interim Report. Comm. Of Mass. Wat. Res. Comm., Boston. Mass., 18pp.

Jelesnianski, C.P., (1967) Numerical computations of storm surges with bottom stress, Mon. Weather Rev., 95, pp. 740-756.

Jirka G.H., and R.L. Donekar (1991) Hydrodynamic classification of submerged single port discharges. J. Hydraulic Engineering. ASCE. Vol. 117, HY9.

Jirka G.H. (1982) Multiport diffusers for heat disposal: a summary, J. Hydraulics Division. ASCE. Vol. 108, HY12. 1423-68.

John, V. Chandy (1985). Mathematical Modelling of the Response of First Chain Lake to Pollutant Loading. M.A.Sc. thesis. Department of Civil Engineering, Technical University of Nova Scotia. Halifax.

John, V. C. (1986) Numerical simulation of circulation due to wind and tidal forcing in a tidal inlet. Presented at 6th CSCE/CWRA Atlantic Region Hydrotechnical Conference, P.E.I., Canada.

John , V. Chandy and D. H. Waller (1990) Simulation of circulation and water levels in small lakes. HYDROSOFT 90, Hydraulic Engineering Software Conference, Massachusetts,

USA, 3-5 April 90.

John, V. Chandy, Stephen L. Coles and A. I. Abozed (1990) Seasonal cycles of temperature, salinity and water mass characteristics of Western Arabian Gulf. Oceanologica Acta, France, Vol. 13, No. 3, 273-281.

John, V. C., P. Kruss and Y. H. Fadlallah (1991) Oceanographic monitoring program of the western Arabian Gulf, Marine Technology Society Journal, USA, 25, 2, 22-28.

John, V. Chandy (1992) Circulation and mixing processes and its effect on pollutant distribution in the Arabian Gulf. Applied Ocean Research, U.S.A. 14, 59-64.

John, V. Chandy (1992) Harmonic tidal current constituents of the Western Arabian Gulf from moored current measurements. Coastal Engineering, Netherlands, 17 (1992) 145-151.

John, V. Chandy, M.G. Satish and D.H. Waller (1995) Development and evaluation of numerical hydrodynamic models for small lakes and reservoirs. Can. J. Civ. Eng. 22: 270-282.

John, V. Chandy, M.G. Satish and D.H. Waller (1996). Effluent plume behaviour in stratified surface waters, Coastal Zone Canada 96, Rimouski, Quebec, Canada.

John, V. Chandy (1996). Numerical simulation of three-dimensional wind driven lake currents. under preparation.

Johns, B., Sinha P.C., Duke S.K., Mohanty, V.C. and Rao, A.D., (1983) Simulation of storm surges using a three dimensional numerical model : An application to the 1977, Andhra Cyclone, Q.J.R. Metrol. Soc. 109, pp. 211-224 .

Kenega, E.E. (1978). Test organisms and methods useful for early assessment of acute toxicity of chemicals, Environ. Sci Technol., 12(12), pp. 1322-1329.

Kirwan, Jr., A. D. G. McNally (1975) The effect of wind and surface current on drifters. J. Phys. Oceanog. 5(2):361-368

Klaplov, L.A. and R.H. Lervis (1979). Analysis of toxicity data for California marine water quality standards, J. Water Poll. Control, Fed. 51(8), pp. 2054-2070.

Kullenberg, G. C.R. Murthy and H. Westerberg. (1973). An experimental study of diffusion characteristics in the thermocline and hypolimnion regions of Lake Ontario. Proceedings of the 16th Conference on the Great Lakes Research. International Association of Great Lakes Research. Pp. 774-790.

Lahey, W.L. (1989). Pricing mechanisms for ocean waste disposal; a viable regulatory tool, Ex. Office of Environ. Affairs, MA, Boston, In: vol.3, Oceanic Process. in Mar. Poll., pp.287-296.

Lam, D.C.L. and Jaquet, J.M. (1976). Computations of physical transport and regeneration of phosphorous in Lake Erie, Fall 1970. Jour. of the Fisheries Research Board of Canada, Vol. 33, No. 3, 550-563.

Lam, D.C.L. and Halfon, E. (1978). Model of primary production including circulation influences in Lake Superior. Applied Mathematical Modeling. Vol. 2 , No. 1, 34-40.

Lam, D.C.L. and Simons, T.J. (1976). Numerical computations of advective and diffusive transports of chloride in Lake Erie 1970, ibid, 537-549.

Lam, D.C.L. (1983). Personal Communication.

Lam D.C.L. and T.J. Simons (1970) Numerical computations of advective and diffusive transports of chloride in Lake Erie, Jour.of the Fisheries Research Board of Canada, Vol. 33, No. 3, March 1976 ,pp 537-549.

Laevastu, T., (1975) Multilyer hydrodynamical-numerical models, Proc. Symp. Modeling Tech. (ASCE) pp. 1010-1020.

Lai, C., (1976) Some computational aspects of one and two-dimensional unsteady flow simulation by the method of characteristics, Proc. Int. Symp. Unsteady Flow Open Channels, Int. Assoc. Hydraul. Res., Newcastle-upon-Tyne pp. 1-12.

Lai, R.Y.S., and Rao, D.B., (1976) Wind drift currents in deep sea with variable eddy viscosity, Arch. Metevrol. Geophys. Biolimatol., Ser. A, 25, pp. 131-140.

Le Provost, C. and Poncet, A., (1978) Finite-element method for spectral modeling of tides, Int. J. Num. Methods Eng. 12, pp. 853-871.

Lawrence, D.J. (1972). Oceanographic and water quality parameters in the Strait of Canso, 1968-1970. Atlantic Oceanographic Laboratory (Bedford Institute of Oceanography) Data Series BI-D-72-10.

Le Provost, C., Rougier, G. and Poncet, (1981) A., Numerical modeling of the harmonic constituents of the tides, with application to the English channel, J. Phys. Ocean. 11, pp. 1123-1138.

Leendertse, J.J., (1967) Aspects of a computational model for long period water-wave

propagation, Rand. Cor. Rep. RM-5294-PR.

Leendertse, J.J. and Liu, S.K., (1975) Modelling of three-dimensional flows in estuaries, in Modelling Techniques (publ. by ASCE) pp. 625-642.

Leendertse, J.J. and Liu, S.K., (1975) A three-dimensional model for estuaries and coastal seas, Rand Corp. Tech. Rep. Tech. Rep. R-1764-OWRT.

Limno- Tech Inc. (1978) Mathematical modeling of the impact of storms on water quality in Onondaga Lake, Ann Arbor, Mich.

Lions, J.L., (1972) Some methods of solving nonlinear boundary-value problems, (Paris, Dunod).

Liu, S.K. and Leendertse, J.J., (1978) Multidimensional numerical modeling of estuaries and coastal seas, Adv. Hydrosciences 11, pp. 95-164.

Loucks, R.H., D.J. Lawrence, D. Ingraham, and B. Flemming. (1973). A Technique for Estimating Extremes of Ocean Current Vectors. Atlantic Oceanographic Laboratory (Bedford Institute of Oceanography), Report Series BI-R-73-10.

MacLaren Plansearch (1991) Limited, (1991a). Physical oceanography of Halifax Harbour. submitted to Jacques Whitford Environment Limited, as part of Halifax Harbour Clean-up Project EAR.

MacLaren Plansearch (1991) Limited, (1991b). Sediment transport of Halifax Harbour. Submitted to Jacques Whitford Environment Limited, as part of Halifax Harbour Clean-up EAR.

MacLaren Plansearch (1991) Limited, (1992). Conceptual engineering on the outfall and diffuser. Report submitted to Metro Engineering Inc.

Madsen, O.S., (1977) A realistic model of wind-induced Ekman boundary layer, J. Phys. Oceanogr., 7, 248-255.

Mathews, J.B. and Mungall, J.C.H., (1972) A numerical tidal model and its application to Cook Inlet, Alaska, J. Mar. Res. 30, pp. 27-38.

Mathison, J.P., and Johansen, O., (1983) A numerical tidal and storm surge model for the North sea, Marine Geodesy, 6, pp. 267-291.

Mathur D. (1988) Effects of variable discharge schemes on dissolved oxygen at a hydroelectric station. Water Resour. Bull. 24, 159.

Mellor, G. and Blumberg, A. (1985). Modelling vertical and horizontal diffusivities with the sigma coordinate system. Monthly Weather Rev., 113, 1379-1383.

Mesfin M. et al. (1982). Some limnological observations on two Ethiopian hydroelectric reservoirs:Koka (Shewa Administrative District) and Finchaa (Welega Administrative District). Hydrobiologica (Den), 157, 47.

Mihram G.A. (1973). Some practical aspects of the verification and validation of simulation models. Op. Res. Q. 23:17-29.

Murray, J.W. (1987). Sources and fates of aquatic pollutants, Adv. Chem., Ser. no. 216, Hites, R.A. and S.J. Eisenreich (ed.), pp. 153-184.

Murthy, C.R., and Okubo, A., (1977). Interpretation of diffusion characteristics and lakes, October 1975. Marine Sciences Directorate, Canada Dept. Of Fisheries and Environmenta, Ottawa. Canada. Manual Report Series. No. 43. pp. 129-135.

Naylor, T.H. and J.M. Finger. (1971). Validation in Computer Simulation Experiments with Models of Economic Systems. T.H. Naylor, Ed. (New York: John Wieley & son, Inc. pp. 153-164.

Neu, H.J.A. (1971). Wave climate of the Canadian Atlantic Coast and Continental Shelf - 1970. Atlantic Oceanographic Laboratory (Bedford Institute) Report Series 1971-10.

Nielson (1987) Puff and particle dispersion models effluent dispersion in coastal waters.Modelling of Marine Systems, Elsevier Pub. Com., Amsterdam.

Nihoul, J.C., (1975) (Modelling of Marine Systems, Elsevier Pub. Com., Amsterdam.

Nihoul, J.C., (1977) Three dimensional model of tides and storm surges in a shallow well-mixed continental sea, Dyn. Atmos. Ocean, 2, 29-47 .

Nihoul, J.C.J. and Jamart, B.M. (eds.), (1987) Three Dimensional Models of Marine and Estuarine Dynamics. Elsevier Oceanography Series. New York.

Okereke, V. et al. (1988). Midwest (USA) Reservoir water quality modification. II. Oxygen demanding parameters. Water, Air, Soil Pollt. 37, 325.

Pearson, C.E. and Winter, D.F., (1977). On the calculation of tidal currents in homogeneous estuaries, J. Phys. Ocean. 7, pp. 520-531.

Paul, J. (1994). Observations related to the use of the sigma coordinate transformation for estuarine and coastal ocean studies. Proc., 3rd Conf. On Estuarine and Costal Modelling, ASCE. New York.

Pelletier, C.A.(1982). Environmental data handling and long-term trend monitoring at Island Copper Mine, In: Marine Tailings Disposal, D.V. Ellis (ed.), pp 197-239.

Pinhey and Waller (1984). Personal communication.

Pinder, G.F. and Gray, W.G., (1977). Finite Element Simulation in Surface and Subsurface Hydrology, Academic Press.

Prandle, D., (1982) The vertical structure of tidal currents, Geophys. Astrophys, Fluid Dyn., 22, pp. 29-49.

Reckhow K.H., Clements J.T., and Dodd R.C. (1990). Statistical evaluation of mechanistic water quality models. Journal of Environmental Engineering, ASCE, Vol. 116, No. 2.

Richardson, W.L. (1976) An evaluation of the transport characteristics of Saginav Bay using a mathematical model of chloride, Arbour Science Publishers Inc., Ann Arbor, Mich., pp 113-139.

Rorslett, B. (1982). An integrated approach to hydropower impact assessment. I. environmental features of some Norwegian Hydroelectric Lakes. Hydrobiologia (Den), 164, 39

Rowney A. C. (1984) Preliminary application of CONHYMO to Halifax Urban Watersheds, CWRS contribution no. 84-14.

Salah, M.A. (1986). Application of the Computer Model "QUALHYMO" to the Halifax Urban Watersheds. M.A.Sc. Thesis. Department of Civil Engineering, Technical University of Nova Scotia, Halifax, N.S

Scott, R. 1984. Personal Communication.

Sehgal H. and Jyoti M. Dissolved oxygen regimes and the level of eutrophication in Surinsar, a sub-tropical freshwater lake in Jammu, India. Limnologica (ger.), 18, 359.

Seibert, G.H. (1968). Mean Sea Level Fluctuations in the Gulf of St. Lawrence. M.Sc. Thesis, McGill University.

Sengupta, S., Lee, S.S. and Miller, H.P., (1978) Three dimensional numerical investigations of tide and wind-induced transport processes in Biscayne Bay, Sea Grant Technical Bulletin No. 39, Uni. of Miami.

Shaeffer, D.L. (1980). A model evaluation methodology applicable to environmental assessment models. Ecological Modelling. 8:275-295.

Shanahan, P. and Harleman, D.R.F. (1982) Linked hydrodynamic and biogeochemical models of water quality in shallow lakes. R.M. Parsons Lab. Report 268, M.I.T., Cambridge, Ma.

Sheppard, W. J. (1982). Hydrology of the Halifax Urban Watershed data sources, Center for Water Resources Studies, Contribution No. 82-4, Technical University of Nova Scotia, Halifax, N.S.

Simons, T.J., (1974) Verification of numerical models of Lake Ontario, Part I, J. Phys.

Oceanog. 4, 507-519, 1975, Part II, J. Phys. Oceanogr., 5, 98-110.

Simons, T.J., (1980) Circulation models of lakes and inland seas, Can. Bull. Fish. Aquat. Sc. 203, pp. 146.

Simons, T.J. (1973) Development of three-dimensional numerical models of the Great Lakes, Inland Waters Directorate, Canada Canter for Inland Waters, Burlington, Ontario.

Simons, T.J. and Jordan, D.E. (1971) Computed water circulation of Lake Ontario for observed winds, 20 April - 14 May 1971, Canada Centre for Inland Waters.

Simons, T.J. (1976). Analysis and simulation of spatial variations of physical and biochemical processes in Lake Ontario, Jour. of Great Lakes Research, Vol.2, No. 2, 215-233.

Simon, T.J. and Lam, D.C.L. (1982) Personal Communication.

Stebbing, A.R.D. and J.J Cleary (1989). The problem of relating toxic effects to their chemical causes in waters receiving wastes and effluents, Inst. for Mar. Environ. Res., plymouth, U.K., In: Oceanic Process. in Mar. Poll., vol.4, pp. 127-137.

Sunderland, Preston & Simrad Assoc., (1975). Halifax Watershed Development Feasibility Study. Report to Halifax Metropolitan Area Planning Committee, 149 pp.

Sundermann, J (1979) Numerical modelling of circulation in lakes. In Hydrodynamics of Lakes (eds W.H. Graf and C.H. Mortimer) pp. 1-30, Elsevier, Amsterdam.

Sundermann, J., (1974) A three dimensional model of a homogeneous estuary, Proc. Conf.

Coastal Engrg. (A.S.C.E.) pp. 2337-2390.

Tetra Tech Inc. (1975). A comprehensive water quality ecological model for Lake Ontario, Prepared for National Oceanic and Atmospheric Administration, Ann Arbor, Michigan.

Taylor, G. and Davies, J.M., (1975) Tidal propagation and dispersion in estuaries, in Finite Elements in Fluids (ed. by R.H. Gallagher, J.T. Oden, C. Taylor & O.C. Zienkiewics, Wiley), Vol. 1, Chapter 5.

Tee, K.T., (1979) The structure of three dimensional tide generating currents, I, oscillating currents, J. Phys. Oceanogr., 9, pp.930-944.

Townson, J.M., (1974) An application of the method of characteristics to tidal calculations in x-y-t space, J. Hydraul. Res. 12, pp. 499-523.

Thomann, R.V. (1972). Systems Analysis and Water Quality Management. New York: McGraw-Hill Book Company.

Thomann, R.V., and J.S. Segna. (1980). Dynamic phytoplankton-phosphorous model of Lake Ontario: Ten year verification and simulations. R.C. Loehr, Ed. Ann Arbor Science Publishers. pp 153-205.

Thomann, R.V. , R.P. Windfield and J.J. Segna (1979) Verification analysis of Lake Ontario and Rochester Embayment three dimensional eutrophication models., Report No. EPA-600/3-79-094, USEPA.

Tolmazini, D. (1983). Some estimates of transport processes in Long Island Sound, Dept. Mar. Sci., U.Conn., J. Geophys. Res., vol. 88, no. c4, pp. 2633-2641.

Trimbee A. and Prepas E. (1988). Dependence of lake oxygen depletion rates on maximum oxygen storage in a partially meromictic lake in Alberta. Can. J. Fish. Aquat. Sci., 45, 571.

Uchrin, C.G. (1980). Mathematical Modelling of Suspended Solids and Associated Pollutant Transport. Ph.D. thesis. The University of Michigan. 339pp

Uchrin, C.G. and W.J. Weber, Jr. (1982). Real time simulation of conductivity in river-lake systems. Journal of the Environmntal Engineering Division. ASCE. 198(EE5): 1027-1044.

Waller, D.H., Hart, W.C., and Thirumurthi, D. (1983). Halifax Urban watersheds program-a case study in urban storm water quality management, Contribution No. 83-1, Centre for water resources Studies, Technical University of Nova Scotia, Canada

Waller, D.H., W.C. Hart and R.S. Scott. (1984). Preliminary Water and Chemical Mass Balances for lakes in Halifax Urban Watershed Program, Proc. of the CSCE, II: 905-915.

Waldichuk,M. (1975). points on aquatic toxicity and bioassays, In: Proc. Second Ann. Aquat. Tox. Workshop, G.R. Craig (ed.), Ont. Ministry of the Environ., Tor., pp. 337-339.

Waldichuk,M. (1985). Methods for measuring the effects of chemicals on aquatic animals as indicators of ecological damage, In: Methods for Estimating Risk of Chemical Injury: Human and Non-human Biota and Ecosystems, V.B.Vouk et al (eds), pp. 493-535.

Wang, John (1980) Analysis of tide and current meter data for model verification. In "Mathematical Modeling of Estuarine Physics" (J. Sundermann and K. P. Holz, eds) Lecture Notes on Coastal and Estuarine Studies. Springer-Verlag, New York.

Wang, J.D., (1978). Real time flow in unstratified shallow water, J. Waterway Port, Coastal and Ocean Div., A.S.C.E. 104, pp. 53-68.

Appendix A

Solution Scheme for the Vertical Momentum Equations

Solution Scheme for the Vertical Momentum Equations

The finite difference scheme for the solution of equations (4.34) and (4.35) is presented below. The methodology used is a generalization of the Crank-Nicholson scheme used for the heat equation (Nihoul and Jamart 1987, Pinter and Gray 1977). The time-step size (τ) and the vertical grid spacing (k) are notations used. The grid point (i,j) corresponds to the i^{th} time step and the j^{th} vertical grid level. The bottom z = -h is assumed to correspond to j = 1 while the free surface z = ζ is assumed to be at j = 1 while the free surface z = ζ is assumed to be at j = J + ½. Therefore, k = H / (J - ½).

The finite difference approximation to equation (4.34) is as follows:

$$\frac{1}{\tau}(u_{i+1,j} - u_{i,j}) - \frac{\lambda}{k^2}\left[\frac{1}{2}(N_{j-1}+N_j)(u_{i+1,j+1} - u_{i+1,j}) - \frac{1}{2}(N_j+N_{j-1})(u_{i+1,j} - u_{i+1,j-1})\right]$$

$$- \frac{1-\lambda}{k^2}\left[\frac{1}{2}(N_{j-1}+N_j)(u_{i,j+1} - u_{i,j})\right]\frac{1}{2}(N_j+N_{j-1})(u_{i,j} - u_{i,j-1}) - f(\mu(v_{i+1,j} + (1-\mu)v_{i,j}) = \frac{1}{2}(A_{i+1,j} + A_{i,j}) \quad (A.1)$$

Here, N_j represents the eddy viscosity at the j^{th} grid point, assumed to be independent of time, and $u_{i,j}$, $v_{i,j}$ are the velocity components at the jth grid point and the ith time step. The parameters
λ and (1 - λ) give the respective weighting of the second derivative term given to the time step i+1 and i; λ = 0 would be a fully explicit scheme, while λ = ½ corresponds to the Crank-Nicholson scheme. Similarly, μ and (1 - μ) give the two weights for the Coriolis term. It is necessary for numerical stability to take such weighted averages, but no such weighting is necessary for the right-hand side of equation (4.34) and a simple centered average is taken.

Because the surface height ζ changes from a time step to time step, the j node is not fixed in space and the left side of equation (A.1) is not a precise approximation to $\partial u/\partial t$ at node j. However, the error term can be estimated as 1 or 2 % of the terms retained in equation (44) for the problems investigated. In situations where there is rapid flow of very shallow water, however, it would be necessary to retain the additional terms.

At each time step we must solve the following equations:

$$P'_j u_{j-1} + Q_j u_j + P_j u_{j+1} - \nu v_j = b_j \qquad (A.2)$$

$$P'_j v_{j-1} + Q_j v_j + P_j v_{j+1} - \nu u_j = c_j \qquad (A.3)$$

where

$u_j \equiv u_{i+1,j}$

$v_j \equiv v_{i+1,j}$

$P_j = -\tfrac{1}{2}\, r\lambda\,(N_{j+1} + N_j)$

$P'_j = -\tfrac{1}{2}\, r\lambda\,(N_j + N_{j-1})$

$Q_j = 1 + \tfrac{1}{2}\, r\lambda\,(N_{j+1} + 2N_j + N_{j-1})$ (A.4)

$\nu = \tau f \mu$

$r = \dfrac{\tau}{k^2}$

$$b_j = \tfrac{1}{2}r(1-\lambda)(N_{j+1}+N_j)\,u_{i,j+1} + [1 - \tfrac{1}{2}r(1-\lambda)(N_{j+1} + 2N_j + N_{j-1})]\,u_{i,j}$$

$$+ \frac{1}{2} r(1-\lambda)(N_j+N_{j-1})\,(u_{i,j-1} + rf(1-\mu)v_{i,j} + \frac{1}{2}\tau(u_{i+1,j} + u_{i,j}) \qquad (A\text{-}5)$$

$$+ \frac{1}{2} r(1-\lambda)(N_j+N_{j-1})\,(v_{i,j-1} + rf(1-\mu)u_{i,j} + \frac{1}{2}\tau(v_{i+1,j} + v_{i,j}) \qquad (A\text{-}6)$$

At each time step we must solve equations (A.2) and (A.3) for [u_j, v_j], with the right sides .[b_j, c_j] being known from the preceding time step.

$$c_j = \frac{1}{2}r(1 - \lambda)(N_{j+1}+N_j)\, v_{i,j+1} + [1 - \frac{1}{2}r(1 - \lambda)(N_{j+1} + 2N_j + N_{j-1})]\, v_{i,j}$$

The solution can be found as a pair of recursion formulae of the form

$$u_{j+1} = R_j u_j + S_j v_j + T_j \tag{A.7}$$

.

$$v_{j+1} = S'_j u_j + R'_j v_j + T'_j \tag{A.8}$$

Substituting equation (A.7) into equation (A.2), the following is obtained:

.

$$P'_j u_{j-1} + (Q_j + P_j R_j) u_j + (P_j S_j - v) v_j = b_j - P_j T_j$$

On the other hand, eliminating v_j between equations (A.7) and (A.8) and replacing j by j-1, results in .

$$(S_{j-1} S'_{j-1} - R_{j-1} R'_{j-1}) u_{j-1} + R'_{j-1} u_j - S_{j-1} v_j = T_{j-1} R'_{j-1} - T'_{j-1} S_{j-1}$$

A comparison of these two results then gives that, for some K,

$$S_{j-1} S'_{j-1} - R_{j-1} R'_{j-1} = K P'_j \tag{A.9}$$

$$R'_{j-1} = K (Q_j + P_j R_j) \tag{A.10}$$

$$S_{j-1} = - K (P_j S_j - v) \tag{A.11}$$

.

$$T_{j-1} R'_{j-1} - T'_{j-1} S_{j-1} = K (b_j - P_j T_j) \tag{A.12}$$

Similarly, the following is obtained:

$$P'_j v_{j-1} + (P_j S'_j + v) u_j + (Q_j + P_j R'_j) v_j = c_j - P_j T'_j$$

And eliminating u_j between equations (A.7) and (A.8) and replacing j by j-1, results in:

$$(S_{j-1} S'_{j-1} - R_{j-1} R'_{j-1}) v_{j-1} - S'_{j-1} u_j + R_{j-1} v_j = R_{j-1} T'_{j-1} - S'_{j-1} T_{j-1}$$

Comparison of these two then gives, for some K',

$$S_{j-1} S'_{j-1} - R_{j-1} R'_{j-1} = K' P'_j \qquad \text{(A.13)}$$

$$S'_{j-1} = - K' (P_j S'_j + v) \qquad \text{(A.14)}$$

$$R_{j-1} = K' (Q_j + P_j R'_j) \qquad \text{(A.15)}$$

$$R_{j-1} T'_{j-1} - S'_{j-1} T_{j-1} = K' (c_j - Pj T' j) \qquad \text{(A.16)}$$

From equations (A.9) and (A.13) it follows that K' = K. Then substituting equations (A.10), (A.11), (A.14), and (A.15) into equation (A.9), the following is obtained:

$$K = \frac{P_j}{(P_j S_j - v)(P_j S_j + v) - (Q_j + P_j R_j)(Q_j + P_j R_j)} \qquad \text{(A.17)}$$

Finally, making similar substitutions into equations (A.12) and (A.16) and then solving for T_{j-1} and T'_{j-1}, results in:

$$T_{j-1} = \frac{[-(Q_j + P_j \acute{R}_j)(b_j - P_j T_j) + (P_j S_j - v)(c_j - P_j \acute{T}_j)]}{(P_j S_j - v)(P_j \acute{S}_j + v) - (Q_j + P_j \acute{R}_j)(Q_j + P_j R_j)} \qquad \text{(A.18)}$$

$$\acute{T}_{j-1}=\frac{(P_j\acute{S}_j+\nu)\ (b_j-P_jT_j)\ -\ (Q_j+P_jR_j)\ (c_j\ -\ P_j\acute{T}_j)}{(P_jS_j\ -\ \nu)\ (P_j\acute{S}_j+\nu)\ -\ (Q_j\ +\ P_j\acute{R}_j)\ (Q_j\ +\ P_jR_j)} \tag{A.19}$$

The quantities [R j, R' j , Sj, S'j , Tj, T'j] can now be calculated recursively downwards. For, if they are known for a particular j, then for j-1 they are given by equations (A.18), (A.19), and

$$R_{j-1}=\frac{\acute{P}_j\ (Q_j\ +\ P_j\acute{R}_j)}{(P_jS_j\ -\ \nu)\ (P_j\acute{S}_j+\nu)\ -\ (Q_j\ +\ P_j\acute{R}_j)\ (Q_j\ +\ P_jR_j)} \tag{A.20}$$

$$\acute{R}_{j-1}=\frac{\acute{P}_j\ (Q_j\ +\ P_jR_j)}{(P_jS_j\ -\ \nu)\ (P_j\acute{S}_j+\nu)\ -\ (Q_j\ +\ P_j\acute{R}_j)\ (Q_j\ +\ P_jR_j)} \tag{A.21}$$

$$S_{j-1}=\frac{-\acute{P}_j\ (P_jS_j-\nu)}{(P_jS_j\ -\ \nu)\ (P_j\acute{S}_j+\nu)\ -\ (Q_j\ +\ P_j\acute{R}_j)\ (Q_j\ +\ P_jR_j)} \tag{A.22}$$

$$\acute{S}_{j-1}=\frac{-\acute{P}_j\ (P_jS_j+\nu)}{(P_jS_j\ -\ \nu)\ (P_j\acute{S}_j+\nu)\ -\ (Q_j\ +\ P_j\acute{R}_j)\ (Q_j\ +\ P_jR_j)} \tag{A.23}$$

The starting values for this recursive calculation can be obtained from the surface boundary condition (4.23). Assuming the free surface to be midway between j = J and J+1, the finite difference approximation is:

$$\rho N \frac{\partial u}{\partial z}\Big|_{z=\zeta} = \frac{\rho}{2k} (N_{j+1} + N_j) \quad (u_{j+1} - u_j) = \tau^s_x$$

and similarly for the y-component. Thus:

$$u_{j+1} - u_j = \frac{2\ k\ \tau^s_x}{\rho\ (N_{j+1} + N_j)}$$

$$v_{j+1} - v_j = \frac{2\ k\ \tau^s_y}{\rho\ (N_{j+1} + N_j)}$$

Comparing these with the general relations, (A.7) and (A.8):

$$R_j = R'_j;\ S_j = S'_j = 0 \qquad \text{(A.21)}$$

$$T_j\ ,\ T'_j = \frac{2\ k\ (\tau^s_x, \tau^s_y)}{\rho\ (N_{j+1} + N_j)}$$

which provide the necessary starting values.

With these starting values, equation (A.23) can easily be seen to imply that R' j = R j , S' j = S j
for all j. The recurrence formulae (A.23) then reduce to

$$R_{j-1}=\frac{\acute{P}_j\,(Q_j + P_jR_j)}{(P_jS_j - \nu)\,(P_j\acute{S}_j+\nu) - (Q_j + P_j\acute{R}_j)\,(Q_j + P_jR_j)} \qquad \text{(A.25)}$$

$$S_{j-1}=\frac{-\acute{P}_j\,(P_jS_j-\nu)}{(P_jS_j - \nu)\,(P_j\acute{S}_j+\nu) - (Q_j + P_j\acute{R}_j)\,(Q_j + P_jR_j)} \qquad \text{(A.26)}$$

Simplifications also occur in equations (A.18) and (A.19) while equations (A.26) and (A.27) become:

$$u_{j+1} = R_j u_j + S_j v_j + T_j \qquad \text{(A.27)}$$

$$v_{j+1} = - S_j u_j + R_j v_j + T'_j \qquad \text{(A.27)}$$

Having computed $\{R_j, S_j, T_j, T'_j\}$ recursively downwards from j = J-1 to j = 1, equation (A.27) can now be used to compute {u j, vj} recursively upwards, provided that the starting values u_1 and v_1 are given.

APPENDIX B

MASS BALANCE IN STRATIFIED LAKE

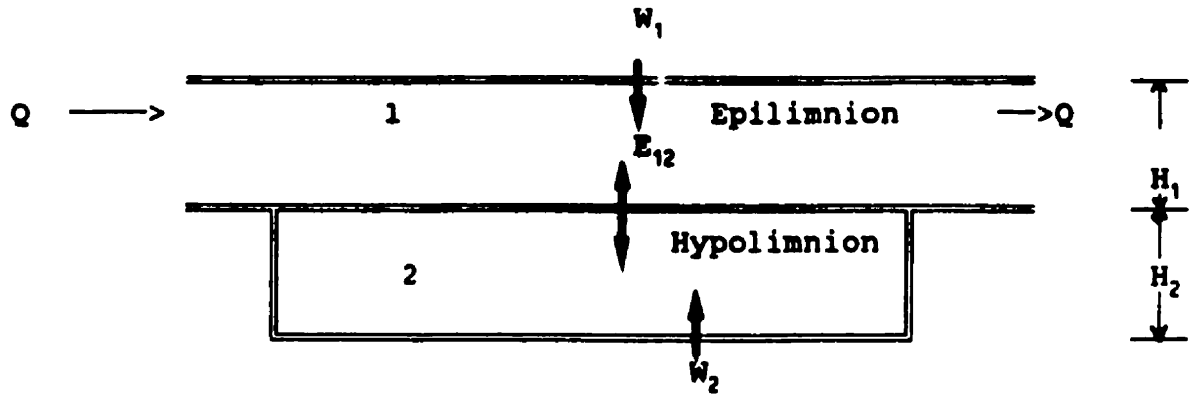

The mass balance equations for epilimnion (layer 1) and hypolimnion (layer 2) are:

$$V_1 \frac{ds_1}{dt} = W_1 - Qs_1 + E_{12}(s_2 - s_1) - V_1 K_1 s_1 \qquad (1)$$

$$V_2 \frac{ds_2}{dt} = W_2 + E_{12}(s_1 - s_2) - V_2 K_2 s_2 \qquad (2)$$

W = Load
Q = Flow
E = Vertical dispersion coefficient (L^2/T)
A = Interfacial area (L^2)
s = Concentration
K = first order decay rate
V = Volume of the layer

For steady state, the concentrations in the epilimnion and hypolimnion can be determined as:

$$S_1 = \frac{(W_1 + \beta W_2)/Q}{1 + (1-\beta) E_{12}/Q + V_1 K_1/Q} \qquad (3)$$

$$S_2 = \beta \left(s_1 + \frac{W_2}{E_{12}} \right) \qquad (4)$$

$$\beta = \frac{E_{12}}{E_{12} + V_2 K_2} \quad (5)$$

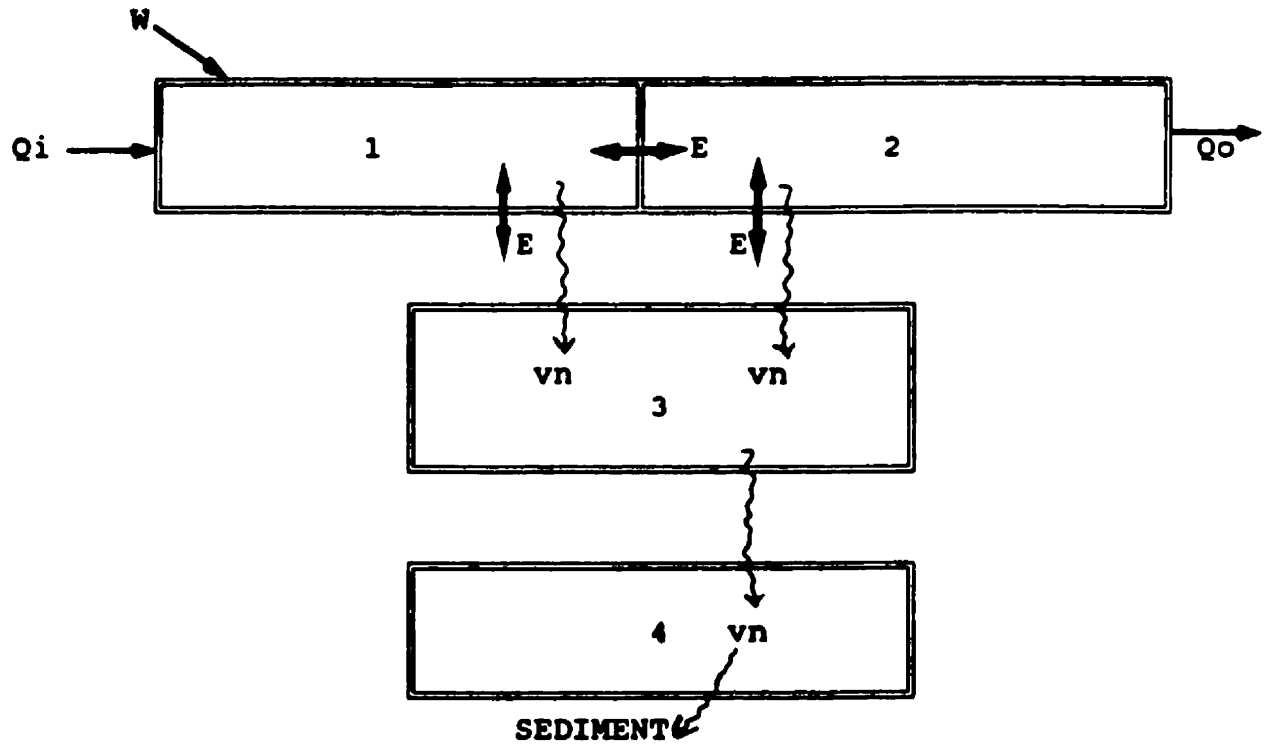

ASSUMPTION

No flow in and out of segment 3

Settling velocity = 0.2 m/day

$$F_s = v_n A s$$

Fs = Mass rate of deposition of particles (M/T)
vn = Net settling velocity of solids (M/L3) **A = Cross sectional area (L2)**
s = Concentration (M/L3)

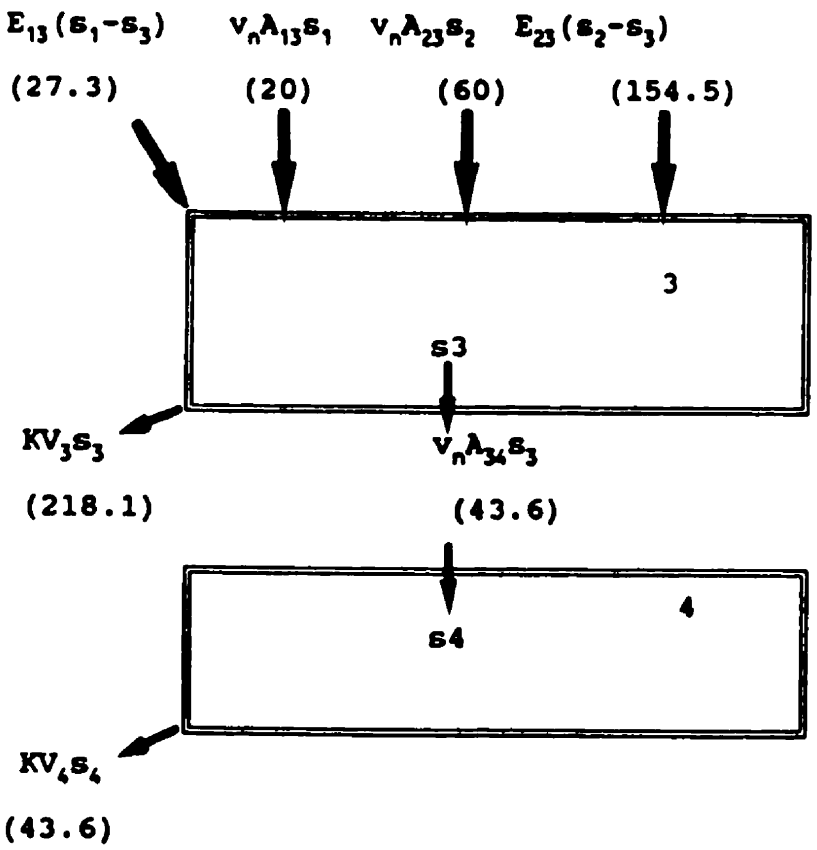
$E_{13}(\varepsilon_1-\varepsilon_3)$
(27.3)
$v_n\lambda_{13}\varepsilon_1$
(20)
$v_n\lambda_{23}\varepsilon_2$
(60)
$E_{23}(\varepsilon_2-\varepsilon_3)$
(154.5)
3
$\varepsilon 3$
$KV_3\varepsilon_3$
(218.1)
$v_n\lambda_{34}\varepsilon_3$
(43.6)
4
$\varepsilon 4$
$KV_4\varepsilon_4$
(43.6)

APPENDIX C

LISTING OF PLUME MODEL RESULTS

PLUME GEOMETRY AND TRAJECTORY

Plume Centerline Position			Dilution Ratio	Conc.	Vertical plume depth	Horizontal plume half width	Plume upper boundary	Plume lower boundary
X (m)	Y (m)	Z (m)						
.00	.00	.50	1.0	.500E+04	.10			
.00	.00	.50	1.0	.500E+04	.08			
.00	.00	.50	1.0	.497E+04	.08			
.00	.00	.50	1.0	.494E+04	.08			
.01	.00	.50	1.0	.491E+04	.08			
.01	.00	.50	1.0	.488E+04	.08			
.01	.00	.50	1.0	.486E+04	.08			
.01	.00	.50	1.0	.483E+04	.08			
.02	.00	.50	1.0	.480E+04	.08			
.02	.01	.50	1.0	.477E+04	.08			
.02	.01	.50	1.1	.475E+04	.08			
.02	.01	.50	1.1	.472E+04	.08			
.03	.01	.50	1.1	.470E+04	.08			
.03	.01	.50	1.1	.467E+04	.08			
.03	.01	.51	1.1	.465E+04	.08			
.03	.01	.51	1.1	.462E+04	.08			
.04	.01	.51	1.1	.460E+04	.08			
.04	.01	.51	1.1	.457E+04	.08			
.04	.01	.51	1.1	.455E+04	.08			
.04	.01	.51	1.1	.453E+04	.08			
.05	.01	.51	1.1	.450E+04	.08			
.05	.01	.51	1.1	.448E+04	.08			
.05	.01	.51	1.1	.446E+04	.08			
.05	.01	.51	1.1	.443E+04	.08			
.06	.01	.51	1.1	.441E+04	.08			
.06	.01	.51	1.1	.439E+04	.08			
.06	.02	.51	1.1	.437E+04	.08			
.06	.02	.51	1.2	.435E+04	.08			
.06	.02	.51	1.2	.433E+04	.08			
.07	.02	.51	1.2	.431E+04	.08			
.07	.02	.51	1.2	.428E+04	.08			
.07	.02	.51	1.2	.426E+04	.08			
.07	.02	.51	1.2	.424E+04	.08			

.08	.02	.51	1.2	.422E+04	.08
.08	.02	.51	1.2	.420E+04	.08
.08	.02	.51	1.2	.418E+04	.08
.08	.02	.51	1.2	.417E+04	.08
.09	.02	.51	1.2	.415E+04	.08
.09	.02	.51	1.2	.413E+04	.08
.09	.02	.51	1.2	.411E+04	.08
.09	.02	.51	1.2	.409E+04	.08
.10	.02	.52	1.2	.407E+04	.08
.10	.02	.52	1.2	.405E+04	.08
.10	.02	.52	1.2	.403E+04	.08
.10	.03	.52	1.2	.402E+04	.08
.11	.03	.52	1.3	.400E+04	.08
.11	.03	.52	1.3	.398E+04	.08
.11	.03	.52	1.3	.396E+04	.09
.11	.03	.52	1.3	.395E+04	.09
.11	.03	.52	1.3	.393E+04	.09
.12	.03	.52	1.3	.391E+04	.09
.12	.03	.52	1.3	.390E+04	.09
.12	.03	.52	1.3	.390E+04	.08
.55	.08	.62	2.5	.203E+04	.11
.98	.13	.71	3.8	.131E+04	.14
1.41	.16	.78	5.3	.936E+03	.16
1.84	.19	.86	7.0	.717E+03	.18
2.27	.22	.93	8.7	.574E+03	.20
2.70	.25	.99	10.5	.475E+03	.22
3.14	.27	1.06	12.4	.402E+03	.24
3.57	.29	1.12	14.4	.347E+03	.26
4.00	.31	1.18	16.5	.304E+03	.28
4.43	.33	1.23	18.6	.269E+03	.29
4.86	.34	1.29	20.7	.241E+03	.31
5.29	.36	1.34	23.0	.217E+03	.33
5.72	.38	1.40	25.3	.198E+03	.34
6.15	.39	1.45	27.6	.181E+03	.36
6.58	.41	1.50	30.0	.167E+03	.37
7.01	.42	1.55	32.4	.154E+03	.39
7.44	.43	1.60	34.9	.143E+03	.40
7.87	.45	1.64	37.4	.133E+03	.42
8.30	.46	1.69	40.0	.125E+03	.43
8.74	.47	1.74	42.6	.117E+03	.44
9.17	.48	1.78	45.2	.110E+03	.46
9.60	.49	1.83	47.9	.104E+03	.47
10.03	.50	1.87	50.7	.986E+02	.48
10.46	.51	1.91	53.4	.935E+02	.50
10.89	.52	1.96	56.2	.888E+02	.51
11.32	.53	2.00	59.0	.846E+02	.52

11.75	.54	2.04	61.9	.807E+02	.54			
12.18	.55	2.08	64.8	.771E+02	.55			
12.61	.56	2.12	67.7	.737E+02	.56			
13.04	.57	2.16	70.7	.706E+02	.57			
13.47	.58	2.20	73.7	.678E+02	.58			
13.90	.59	2.24	76.7	.651E+02	.60			
14.34	.60	2.28	79.7	.626E+02	.61			
14.77	.61	2.32	82.8	.603E+02	.62			
15.20	.62	2.36	85.9	.581E+02	.63			
15.63	.62	2.40	89.0	.560E+02	.64			
16.06	.63	2.43	92.2	.541E+02	.65			
16.49	.64	2.47	95.4	.523E+02	.67			
16.92	.65	2.51	98.6	.506E+02	.68			
17.35	.66	2.55	101.8	.490E+02	.69			
17.78	.66	2.58	105.1	.475E+02	.70			
18.21	.67	2.62	108.4	.460E+02	.71			
18.64	.68	2.65	111.7	.447E+02	.72			
19.07	.68	2.69	115.0	.434E+02	.73			
19.50	.69	2.73	118.4	.421E+02	.74			
19.94	.70	2.76	121.8	.410E+02	.75			
20.37	.71	2.80	125.2	.398E+02	.76			
20.80	.71	2.83	128.6	.388E+02	.77			
21.23	.72	2.87	132.1	.378E+02	.78			
21.66	.73	2.90	135.5	.368E+02	.79			
21.66	.73	2.90	135.5	.368E+02	.79			
23.25	.73	3.50	230.4	.216E+02	1.48	1.48	3.51	2.02
23.25	.73	3.50	230.4	.216E+02	1.48	1.48	3.51	2.02
24.11	.73	3.50	233.8	.213E+02	1.44	1.55	3.51	2.07
24.98	.73	3.50	237.1	.210E+02	1.40	1.62	3.51	2.10
25.84	.73	3.50	240.4	.207E+02	1.37	1.68	3.51	2.14
26.71	.73	3.50	243.6	.205E+02	1.34	1.74	3.51	2.17
27.57	.73	3.50	246.9	.202E+02	1.31	1.80	3.51	2.20
28.44	.73	3.50	250.1	.199E+02	1.28	1.87	3.51	2.22
29.30	.73	3.50	253.4	.197E+02	1.26	1.93	3.51	2.25
30.17	.73	3.50	256.6	.194E+02	1.24	1.98	3.51	2.27
31.03	.73	3.50	259.9	.192E+02	1.22	2.04	3.51	2.29
31.90	.73	3.50	263.3	.189E+02	1.20	2.10	3.51	2.31
32.76	.73	3.50	266.6	.187E+02	1.18	2.16	3.51	2.32
33.63	.73	3.50	270.0	.184E+02	1.17	2.21	3.51	2.34
34.49	.73	3.50	273.4	.182E+02	1.15	2.27	3.51	2.35
35.36	.73	3.50	276.9	.180E+02	1.14	2.32	3.50	2.36
36.23	.73	3.50	280.4	.177E+02	1.13	2.37	3.50	2.38
37.09	.73	3.50	284.0	.175E+02	1.12	2.43	3.50	2.39
37.96	.73	3.50	287.7	.173E+02	1.11	2.48	3.50	2.40
38.82	.73	3.50	291.4	.171E+02	1.10	2.53	3.50	2.40
39.69	.73	3.50	295.2	.169E+02	1.09	2.58	3.50	2.41

40.55	.73	3.50	299.0	.166E+02	1.09	2.63	3.50	2.42
41.42	.73	3.50	302.9	.164E+02	1.08	2.68	3.50	2.43
42.28	.73	3.50	306.9	.162E+02	1.07	2.73	3.50	2.43
43.15	.73	3.50	311.0	.160E+02	1.07	2.78	3.50	2.44
44.01	.73	3.50	315.2	.158E+02	1.06	2.83	3.50	2.44
44.88	.73	3.50	319.4	.156E+02	1.06	2.88	3.50	2.45
45.74	.73	3.50	323.7	.154E+02	1.06	2.93	3.50	2.45
46.61	.73	3.50	328.1	.152E+02	1.05	2.98	3.50	2.45
47.47	.73	3.50	332.6	.149E+02	1.05	3.03	3.50	2.45
48.34	.73	3.50	337.1	.147E+02	1.05	3.07	3.50	2.46
49.20	.73	3.50	341.8	.145E+02	1.05	3.12	3.50	2.46
50.07	.73	3.50	346.5	.143E+02	1.05	3.17	3.50	2.46
50.93	.73	3.50	351.4	.141E+02	1.05	3.21	3.50	2.46
51.80	.73	3.50	356.3	.139E+02	1.05	3.26	3.50	2.46
52.67	.73	3.50	361.3	.137E+02	1.05	3.30	3.50	2.46
53.53	.73	3.50	366.5	.136E+02	1.05	3.35	3.50	2.46
54.40	.73	3.50	371.7	.134E+02	1.05	3.39	3.50	2.46
55.26	.73	3.50	377.0	.132E+02	1.05	3.44	3.50	2.46
56.13	.73	3.50	382.5	.130E+02	1.05	3.48	3.50	2.45
56.99	.73	3.50	388.0	.128E+02	1.05	3.52	3.50	2.45
57.86	.73	3.50	393.6	.126E+02	1.05	3.57	3.50	2.45
58.72	.73	3.50	399.4	.124E+02	1.06	3.61	3.50	2.45
59.59	.73	3.50	405.2	.122E+02	1.06	3.65	3.50	2.44
60.45	.73	3.50	411.2	.121E+02	1.06	3.70	3.50	2.44
61.32	.73	3.50	417.2	.119E+02	1.07	3.74	3.50	2.44
62.18	.73	3.50	423.4	.117E+02	1.07	3.78	3.50	2.43
63.05	.73	3.50	429.7	.115E+02	1.07	3.82	3.50	2.43
63.91	.73	3.50	436.1	.114E+02	1.08	3.87	3.50	2.43
64.78	.73	3.50	442.6	.112E+02	1.08	3.91	3.50	2.42
65.64	.73	3.50	449.2	.110E+02	1.09	3.95	3.50	2.42
66.51	.73	3.50	455.9	.109E+02	1.09	3.99	3.50	2.41
66.51	.73	3.50	455.9	.109E+02	1.09	3.99	3.50	2.41
190.18	.73	3.50	897.6	.544E+01	1.09	7.86	3.50	2.41
313.85	.73	3.50	1184.8	.406E+01	1.09	10.37	3.50	2.41
437.52	.73	3.50	1415.0	.335E+01	1.09	12.38	3.50	2.41

APPENDIX D

STATISTICAL ANALYSIS OF MODEL RESULTS AND MEASURED DATA

```
> with(linalg):
> with(stats):
> #procedure to compute the mean error, absolute mean error, RMSE..
> calculation := proc(X, Y)
>   local i, n, meanE, absmean, RMSE, SI_X, SI_Y, mean_x, mean_y, sd_x, sd_y, lco
> rr;
>   n := nops(X);
> meanE:= 0;
> absmean := 0;
> RMSE := 0;
> mean_x := describe[mean](X);
> mean_y := describe[mean](Y);
> sd_x := describe[standarddeviation](X);
> sd_y:= describe[standarddeviation](Y);
> for i from 1 to n do
>   meanE := meanE + ((X[i]- Y[i])/n);
>   absmean := absmean +(abs(X[i] - Y[i])/n);
>   RMSE := RMSE + (((X[i] - Y[i])^2)/n);
> od;
> RMSE := sqrt(RMSE);
> SI_X := (RMSE / mean_x)*100;
> SI_Y := (RMSE/mean_y)*100;
> lcorr := describe[linearcorrelation](X, Y);
> print(`mean of X =`, mean_x, `mean of Y`, mean_y);
```

```
> print (`standard deviation of X =`,sd_x, `standard deviation of Y =`, sd_y);

> print(`mean error =`, meanE, `absolutemean error =`, absmean);

> print(`RMSE =`, RMSE, `SI of X =`, SI_X, `SI of Y =`, SI_Y);

> print(`linear correalation = `, lcorr);

> end:

> X:= [1.009, 2];
```

$$X := [1.009, 2]$$

```
> Y := [3.079,8.4];
```

$$Y := [3.079, 8.4]$$

```
> calculation(X, Y);
```

mean of X =, 1.504500000, *mean of Y*, 5.739500000

standard deviation of X =, .4955000000, *standard deviation of Y* =, 2.660500000

mean error =, -4.235000000, *absolutemean error* =, 4.235000000

RMSE =, 4.756306340, *SI of X* =, 316.1386733, *SI of Y* =, 82.86969841

linear correalation = , 1.000000000

```
> V_meas := [7.26, 5.65, 2.62, -1.06, -4.47, -6.77, -7.37, -6.12, -3.34, 0.27, 3.82, 6.71, 7.
> 4, 6.53, 4.03, .51, -3.13, -5.99, -7.34, -6.86, -4.66, -1.29, 2.4];
```

V_meas := [7.26, 5.65, 2.62, -1.06, -4.47, -6.77, -7.37, -6.12, -3.34, .27, 3.82, 6.71, 7.4, 6.53, 4.03, .51, -3.13, -5.99, -7.34, -6.86, -4.66, -1.29, 2.4]

```
> V_pred := [4, 3, 2, 0, -3, -4, -5.1, -4, -2, -1, 3, 4, 5.2, 4, 2, 1, -3, -4, -5, -3, -2, 0, 3];
```

V pred := [4, 3, 2, 0, -3, -4, -5.1, -4, -2, -1, 3, 4, 5.2, 4, 2, 1, -3, -4, -5, -3, -2, 0, 3]

```
> calculation(V_meas, V_pred);
```

mean of X =, -.4869565217, *mean of Y*, -.2130434783

standard deviation of X =, 5.129827894, *standard deviation of Y* =, 3.263807373

mean error =, -.2739130434, *absolutemean error* =, 1.846956523

RMSE =, 2.075928289, *SI of X* =, -426.3067022, *SI of Y* =, -974.4153191

linear correalation = , .9775300827

```
> statplots[scatter2d](V_meas, V_pred):
```

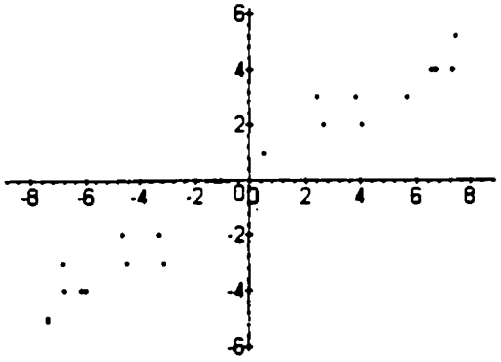

> U_meas := [-4.82, -3.95, -2.09, 0.29, 2.6, 4.26, 4.85, 4.23, 2.55, 0.23, -2.15, -3.99, -4.8
> 3, -4.46, -2.97, -0.74, 1.68, 3.67, 4.75, 4.63, 3.36, 1.24, -1.18];

U_meas := [-4.82, -3.95, -2.09, .29, 2.6, 4.26, 4.85, 4.23, 2.55, .23, -2.15, -3.99, -4.83, -4.46, -2.97, -.74, 1.68, 3.67, 4.75, 4.63, 3.36, 1.24, -1.18]

> U_pred:=[-4.4, -4, -2, 0, 3, 4.5, 5, 4, 2, 0, -3, -4.4, -5, -4, -2, 0, 3, 4.3, 5, 4, 2, 0, -3];

U pred := [-4.4, -4, -2, 0, 3, 4.5, 5, 4, 2, 0, -3, -4.4, -5, -4, -2, 0, 3, 4.3, 5, 4, 2, 0, -3]

> calculation(U_meas, U_pred);

mean of X =, .3113043478, *mean of Y*, .2173913044

standard deviation of X =, 3.372384403, *standard deviation of Y* =, 3.409532950

mean error =, .09391304349, *absolutemean error* =, .5869565218

RMSE =, .7470929166, *SI of X* =, 239.9879481, *SI of Y* =, 343.6627416

linear correalation = , .9761725529

> statplots[scatter2d](U_meas, U_pred):

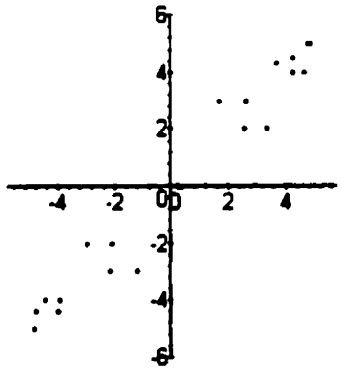

> Cl_meas :=[95.9, 57, 50.6, 50.9, 50.8, 50.4, 43.5, 60.9, 56.9, 48.5, 48.6, 48.9, 48.4, 43.
> 5];

Cl_meas := [95.9, 57, 50.6, 50.9, 50.8, 50.4, 43.5, 60.9, 56.9, 48.5, 48.6, 48.9, 48.4, 43.5]

> Cl_pred := [110.3, 58.4, 39.2, 43.2, 59.7, 34.5, 38.9, 69.2, 57.5, 38.8, 41.3, 56.6, 33.2,
> 37.8];

Cl_pred := [110.3, 58.4, 39.2, 43.2, 59.7, 34.5, 38.9, 69.2, 57.5, 38.8, 41.3, 56.6, 33.2, 37.8]

> calculation(Cl_meas, Cl_pred);

mean of X =, 53.91428572, *mean of Y*, 51.32857143

standard deviation of X =, 12.54186459, *standard deviation of Y* =, 19.64511675

mean error =, 2.585714285, *absolutemean error* =, 8.485714287

RMSE =, 9.603570765, *SI of X* =, 17.81266437, *SI of Y* =, 18.70999036

linear correalation = , .9287978910

> statplots[scatter2d](Cl_meas, Cl_pred):

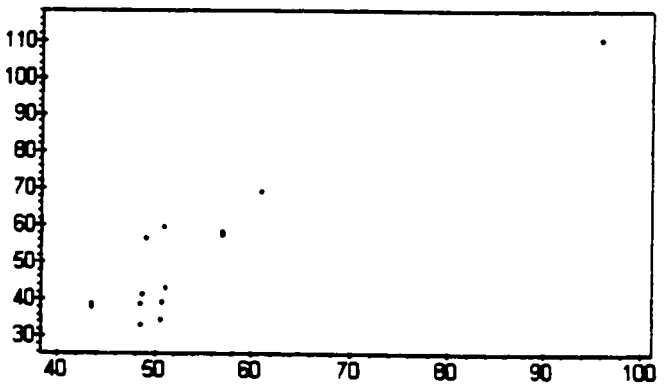

> Dr_meas := [2.8, 5.4, 6.4, 8.0, 10.0, 9.4, 16.6];

Dr meas := [2.8, 5.4, 6.4, 8.0, 10.0, 9.4, 16.6]

>

> Dr_pred:= [2.5, 6.5, 7.2, 7.2, 6.8, 7.9, 9.9];

Dr pred := [2.5, 6.5, 7.2, 7.2, 6.8, 7.9, 9.9]

> calculation (Dr_meas, Dr_pred);

mean of X =, 8.371428574, *mean of Y*, 6.857142859

standard deviation of X =, 4.058752196, *standard deviation of Y* =, 2.059720608

mean error =, 1.514285715, *absolutemean error* =, 2.057142857

RMSE =, 2.926724157, *SI of X* =, 34.96086876, *SI of Y* =, 42.68139394

linear correalation = , .8638424514

> statplots[scatter2d](Dr_pred, Dr_meas):

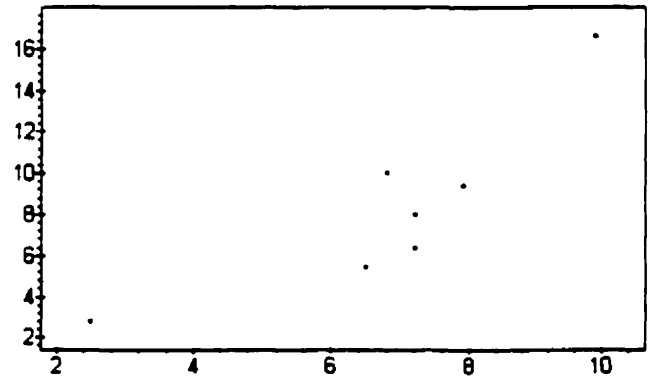

> ilx := [1.158, 1.154, 1.150, 1.146, 1.142, 1.138, 1.134, 1.130, 1.126, 1.122, 1.118, 1.11
> 4, 1.111, 1.107, 1.103, 1.099, 1.095, 1.091, 1.088, 1.084, 1.080, 1.076, 1.073, 1.069,1.
> 065];

ilx := [1.158, 1.154, 1.150, 1.146, 1.142, 1.138, 1.134, 1.130, 1.126, 1.122, 1.118, 1.114, 1.111, 1.107, 1.103, 1.099, 1.095, 1.091, 1.088, 1.084, 1.080, 1.076, 1.073, 1.069, 1.065]

> ily := [1.158, 1.158, 1.157, 1.157, 1.156, 1.156, 1.155, 1.153, 1.152, 1.150, 1.149, 1.14
> 7, 1.145, 1.143, 1.140, 1.138, 1.135, 1.133, 1.130, 1.127, 1.124, 1.121, 1.117, 1.114, 1.
> 110];

ily := [1.158, 1.158, 1.157, 1.157, 1.156, 1.156, 1.155, 1.153, 1.152, 1.150, 1.149, 1.147, 1.145, 1.143, 1.140, 1.138, 1.135, 1.133, 1.130, 1.127, 1.124, 1.121, 1.117, 1.114, 1.110]

> calculation(ilx, ily);

mean of X =, 1.110920000, *mean of Y*, 1.141000000

standard deviation of X =, .02788249630, *standard deviation of Y* =, .01494523335

mean error =, -.03008000000, *absolutemean error* =, .03008000000

RMSE =, .03313729017, *SI of X* =, 2.982869169, *SI of Y* =, 2.904232267

linear correalation = , .9689222701

> statplots[scatter2d](ilx, ily):

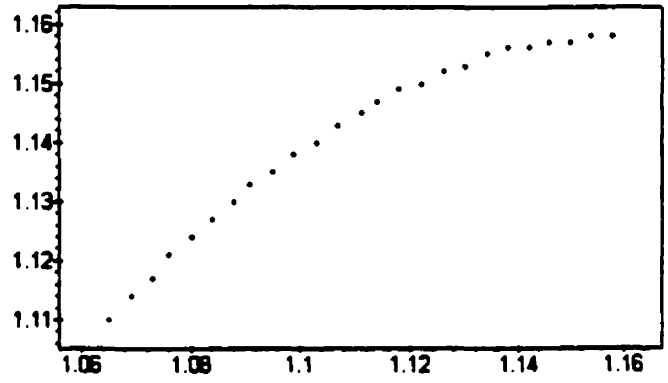

> sl1x := [0,.332,.655,.97,1.275,1.572,1.861,2.143,2.416,2.682,2.941,3.192,3.437,3.675,

> 3.906, 4.131];

sl1x := [0, .332, .655, .97, 1.275, 1.572, 1.861, 2.143, 2.416, 2.682, 2.941, 3.192, 3.437, 3.675, 3.906, 4.131]

> sl1y := [0, .332, .653, .966, 1.270, 1.566, 1.854, 2.134, 2.407, 2.672, 2.930, 3.180, 3.42
> 4, 3.661, 3.892, 4.117];

sl1y := [0, .332, .653, .966, 1.270, 1.566, 1.854, 2.134, 2.407, 2.672, 2.930, 3.180, 3.424, 3.661, 3.892, 4.117]

> calculation(sl1x, sl1y);

mean of X =, 2.199250000, *mean of Y*, 2.191125000

standard deviation of X =, 1.268725615, *standard deviation of Y* =, 1.264032234

mean error =, .008125000000, *absolutemean error* =, .008125000000

RMSE =, .009400797838, *SI of X* =, .4274547158, *SI of Y* =, .4290397781

linear correalation = , .9999998965

> statplots[scatter2d](sl1x, sl1y);

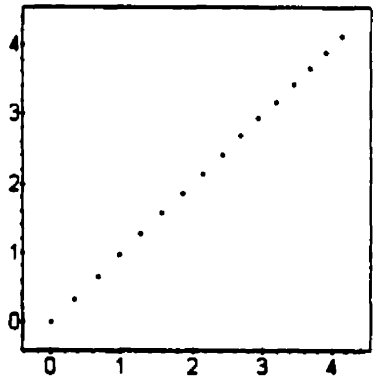

> sl2x := [12.1, 11.77, 11.45, 11.13, 10.83, 10.53, 10.24, 9.96, 9.69, 9.42, 9.16, 8.91, 8.6
> 7, 8.43, 8.20, 7.98];

sl2x := [12.1, 11.77, 11.45, 11.13, 10.83, 10.53, 10.24, 9.96, 9.69, 9.42, 9.16, 8.91, 8.67, 8.43, 8.20, 7.98]

> sl2y := [12.1, 11.77, 11.45, 11.14, 10.83, 10.54, 10.25, 9.97, 9.70, 9.43, 9.18, 8.92, 8.6
> 8, 8.44, 8.21, 7.99];

sl2y := [12.1, 11.77, 11.45, 11.14, 10.83, 10.54, 10.25, 9.97, 9.70, 9.43, 9.18, 8.92, 8.68, 8.44, 8.21, 7.99]

> calculation (sl2x, sl2y);

mean of X =, 9.904375000, *mean of Y*, 9.912500000

standard deviation of X =, 1.267018985, *standard deviation of Y* =, 1.263435297

mean error =, -.008125000000, *absolutemean error* =, .008125000000

RMSE =, .009682458366, *SI of X* =, .09775940800, *SI of Y* =, .09767927734

linear correalation = , .9999953498

```
> statplots[scatter2d](sl2x, sl2y):

>
```

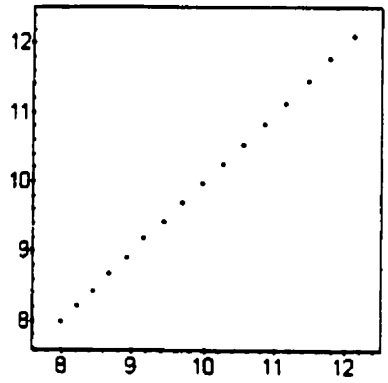

IMAGE EVALUATION
TEST TARGET (QA-3)

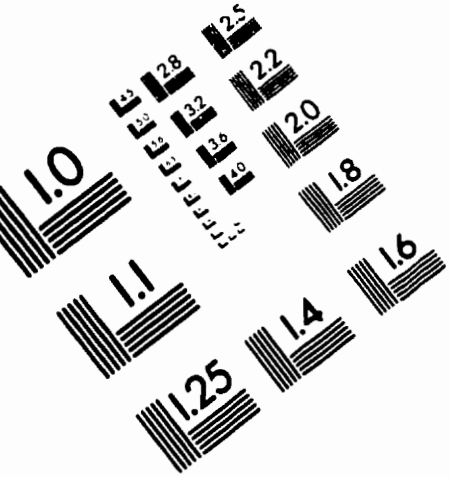

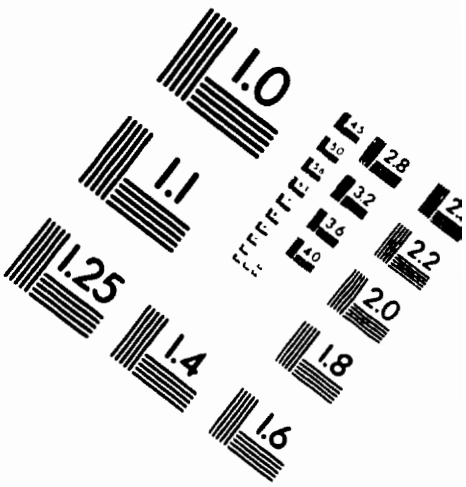

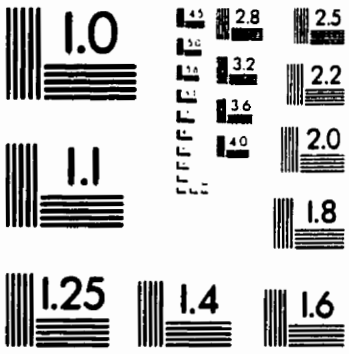

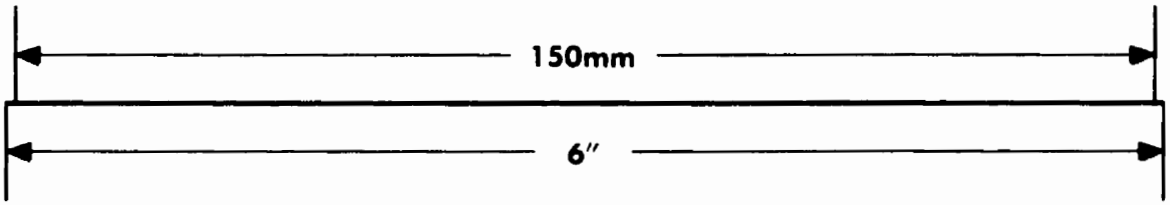

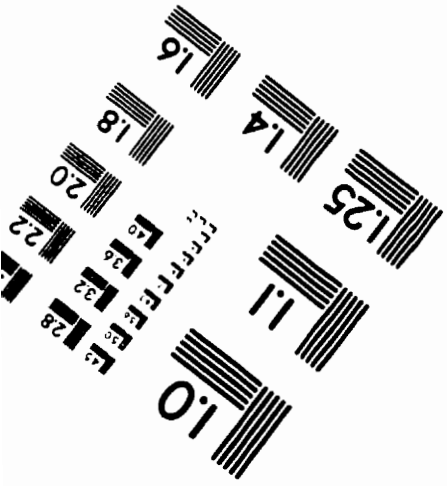

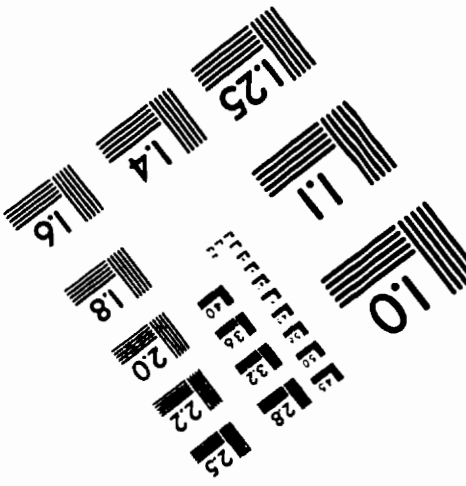

APPLIED IMAGE, Inc
1653 East Main Street
Rochester, NY 14609 USA
Phone: 716/482-0300
Fax: 716/288-5989